

Chemical and Protein Engineering of Nature's Living Light: Bioluminescence

Hsien-Wei Yeh
Taiwan

Master of Science (M.S.), National Taiwan University, 2012

A Dissertation Presented to the Graduate Faculty
of the University of Virginia in Candidacy for the Degree of
Doctor of Philosophy

Department of Chemistry

University of Virginia
May, 2019

Copyright

Chapter 1 was modified in part from *Annual Review of Analytical Chemistry*, 2019, Vol. 12 (DOI: 10.1146/annurev-anchem-061318-115027). Chapter 2 was reproduced from a research paper published on *Nature Methods*, 2017, 14, 971-974. The work described in Chapter 3 has been published on *ACS Chemical Biology* (DOI: 10.1021/acscchembio.9b00150). The work described in Chapter 4 will be submitted to *Analytical Chemistry*. All reuse permissions are automatically granted by individual publisher, all of which having me as the first author. All material in this dissertation is protected by U.S. and foreign copyright and trademark laws. All copyrights are reserved by the authors, Springer Nature, and American Chemical Society publications. Reproduced in part with permission from *Biochemistry*, *ACS Chemical Biology*, and *Analytical Chemistry*, in press or submitted for publication. Unpublished work copyright 2019 American Chemical Society.

Acknowledgement

There are many people I want to give my gratitude for their contributions to my time in graduate school. I am specifically indebted to my Ph.D. advisor, Dr. Huiwang Ai, who has been providing his trust and endless support to my research, ushering the kind of scientist I am today.

Many others have contributions to this dissertation. Omran Karmach performed animal imaging experiments in the work described in Chapter 2. Xiong Ying contributed his effort, in part, of chemical synthesis and NMR acquisition to the work described in Chapter 3 and Chapter 4. Tianchen Wu assisted handling of animal and *in vivo* bioluminescence imaging in the work described in Chapter 3.

Nobody has been more important to keep myself persistent and passionate in science than my family – my wife, my two wonderful children, and my mom. During my entire life, I am grateful to always feel the spirit from heavenly father.

Abstract

The bioluminescence imaging toolkit has continuously evolved biomedical research. Due to the fact that fluorescence measurements require external excitation light, the uses of fluorescence in thick tissues and live animals are limited. Bioluminescence imaging, on the other hand, overcomes this hurdle since they use enzyme-catalyzed exothermic biochemical reactions to generate excited-state emitters. However, the *in vivo* performance of ATP-independent marine luciferases is relatively poor due to their blue emission. Therefore, the development of red-shifted bioluminescent reporters is especially desirable for highly sensitive *in vivo* bioluminescence imaging (BLI). We integrated several approaches, including the chemical synthesis of red-shifted substrates, protein engineering of luciferases *via* directed evolution, and bioluminescence resonance energy transfer (BRET) with red fluorescent proteins. Our engineered luciferase-luciferin pairs emit bright and red-shifted bioluminescence to achieve superior *in vitro* and *in vivo* sensitivity over commonly used bioluminescent reporters.

To further expand the color palette and improve biocompatibility, we developed a family of pyridyl coelenterazine analogs that exhibit different colors of emission and enhanced water solubility. We paired them with our further evolved luciferase, and the resultant luciferase-luciferin pair can highlight early tumors in xenograft models. Furthermore, we demonstrated that it is possible to evolve multiple spectrally resolved and orthogonal luciferase-luciferin pairs for multiplexed bioassays. Our new tools offer new opportunities for designing bioluminescent biosensors to non-invasively uncover complex signaling in live cells and live animals.

Table of Contents

Chapter 1 – General Introduction

1.1. Overview of bioluminescence	1
1.2. Bioluminescent reporters	
1.2.1. Development of D-luciferin-consuming luciferases	2
1.2.2. Development and applications of CTZ-consuming luciferases	5
1.2.3. <i>Renilla</i> luciferase (RLuc) and its derivatives	6
1.2.4. <i>Gaussia</i> luciferase (GLuc) and its derivatives	8
1.2.5. <i>Oplophorus</i> luciferase (OLuc) and its derivatives	9
1.2.6. Artificial luciferase (ALuc)	11
1.2.7. Development and applications of bacterial luciferase	12
1.2.8. Other miscellaneous luciferases	12
1.3. <i>in vivo</i> Bioluminescence imaging (BLI)	14
1.4. Cell-based reporter assay in drug discovery	15
1.5. Design of BRET-based biosensors	16
1.5.1. Firefly luciferase-based BRET biosensors	16
1.5.2. <i>Renilla</i> luciferase-based BRET biosensors	18
1.5.3. NanoLuc-based BRET biosensors	21
References	25

Chapter 2 – Engineering of Red-shifted Luciferase-luciferin pairs for Enhanced Bioluminescence Imaging

2.1. Introduction	34
2.2. Experimental section	
2.2.1. Material and methods	36
2.2.2. Synthesis of diphenylterazine and selenoterazine	37
2.2.3. Construction of plasmids and libraries	41
2.2.4. Library screening	42
2.2.5. Luciferase expression and purification	43
2.2.6. Bioluminescence characterization <i>in vitro</i>	44
2.2.7. Mammalian cell culture and transfection	45

2.2.8. Bioluminescence measurements in HEK293T cells	45
2.2.9. Bioluminescence imaging at superficial sites of live mice	46
2.2.10. Bioluminescence imaging in deep tissue of live mice	46
2.3. Results	
2.3.1. The design and synthesis of CTZ analogs	47
2.3.2. Engineering of NanoLuc mutants and <i>in vitro</i> characterization	50
2.3.3. Further red-shifting the emission of teLuc/DTZ by BRET	55
2.3.4. Improved bioluminescence in mammalian cells and lysates	56
2.3.5. Enhanced bioluminescence imaging <i>in vivo</i>	61
2.4. Discussion	64
2.5. Appendix	67
References	72

Chapter 3 – A New Palette of ATP-independent Bioluminescence Reporters for Superior Biocompatibility and *in vivo* Sensitivity

3.1. Introduction	76
3.2. Experimental section	
3.2.1. Material and methods	78
3.2.2. Chemical synthesis	79
3.2.3. Construction of plasmids and libraries	88
3.2.4. Library screening	89
3.2.5. Chemiluminescence measurement	90
3.2.6. Mammalian cell culture, transfection, and imaging	90
3.2.7. <i>in vitro</i> Bioluminescence characterization	91
3.2.8. Generation of luciferase-expressing stable cell lines	91
3.2.9. Xenograft mouse model	92
3.2.10. Deep-tissue BLI mouse model	93
3.3. Results	
3.3.1. Design and synthesis of pyridyl CTZ and DTZ analogs	93
3.3.2. Directed evolution of teLuc luciferase for improved brightness	96
3.3.3. LumiLuc-8pyDTZ in cultured mammalian cells	100
3.3.4. LumiLuc-8pyDTZ to track tumor growth in a xenograft model	103
3.3.5. Engineering of BRET-based LumiScarlet for deep-tissue BLI	105

3.4. Discussion	109
3.5. Appendix	112
References	127

Chapter 4 – Development of Spectral-resolved and Orthogonal Triple Luciferase System to Enable Multiplexed Bioluminescence Assays

4.1. Introduction	130
4.2. Experimental section	
4.2.1. Material and methods	132
4.2.2. Chemical synthesis	133
4.2.3. Plasmid construction	135
4.2.4. Library screening	136
4.2.5. Mammalian cell culture, transfection, and imaging	137
4.2.6. <i>in vitro</i> Bioluminescence characterization	137
4.2.7. Activation of signaling pathways in HEK293T cells	138
4.3. Results and discussion	
4.3.1. Design of triple luciferase system	139
4.3.2. Directed evolution of luciferase to improve pyDTZ selectivity	140
4.3.3. Triple luciferase system can produce orthogonal BL signals	143
4.3.4. Monitor SRE, ARE, and NF- κ B promotor activities in HEK293T	147
4.3.5. Akaluc-AkaLumine pair is more suitable as an internal control	152
4.4. Conclusion	154
4.5. Appendix	155
References	159

Chapter 5 – General Conclusions and Perspectives

160

Chapter 1

General Introduction

1.1. Overview of bioluminescence

Bioluminescence is a light-producing phenomenon occurring in natural organisms for communication, prey, or defense.¹ The light production mechanism of bioluminescence involves a biochemical reaction relying on the oxidation of a substrate (*a.k.a.*, luciferin) by an enzyme (*a.k.a.*, luciferase). Unlike fluorescence, bioluminescence measurements do not require incident radiation. The signal glows essentially on a dark background that offers excellent sensitivity over fluorescence where phototoxicity and autofluorescence are usually problematic during sampling. Additionally, fluorescence is not ideally suited for *in vivo* imaging when scattering and absorbing of excitation photons are serious hurdles. Although it is possible to gain high spatiotemporal resolution with *in vivo* fluorescence endoscopy, this procedure is often invasive and requires high levels of expertise. Bioluminescence, on the other hand, circumvents most of these issues, acting as an excellent candidate to achieve noninvasive imaging in live animals. Moreover, optogenetic tools, which have been widely used to manipulate or control biological systems, are not always compatible with common fluorescent probes due to spectral overlaps. In this context, bioluminescence has become a highly intensive area of research and bioluminescent reporters have been employed by biomedical researchers in a wide range of applications, including gene regulation and signaling, protein-protein interactions, drug screening, molecular imaging, cell-based assays, and noninvasive *in vivo* imaging.²⁻⁶

Bioluminescence suffers from its low-brightness nature, as a result, largely caused by the slow turnover of luciferases. Bioluminescence reporters are mostly used in macroscopic imaging with limited spatiotemporal resolution; however, recent studies have produced brighter bioluminescent tools that have enabled microscopic imaging

at a single cell resolution. To further alter colors of emission while keeping high photon flux, recent advances in engineered bioluminescent reporters start to mirror the development of fluorescent proteins. Compared to the engineering of fluorescent proteins, engineering of novel bioluminescence reporters usually requires expertise in synthetic chemistry, protein engineering, and animal studies, and therefore, this type of work is highly challenging, but there are many strategies to gain improvement. In addition, the recent development of bioluminescent biosensors have enabled a wide range of bioanalytical and diagnostic applications.

1.2. Bioluminescent reporters

1.2.1. Development of D-luciferin-consuming luciferases

In 1957, the mystery of light emission from the North American firefly *Photinus pyralis* (**Figure. 1**) was uncovered by McElroy.⁷ The enzyme responsible for bioluminescence, Firefly luciferase (FLuc), is the most widely used luciferase for biological and biotechnological applications. FLuc catalyzes a reaction between its native D-luciferin substrate and adenosine-5'-triphosphate (ATP), yielding AMP-luciferin which is further oxidized by molecular oxygen (O₂) to form an excited state (**Figure. 2a**). This high-energy intermediate releases energy in the form of yellow-green light that peaks at 560 nm, leading to a ground-state product, oxyluciferin.⁸ FLuc was further codon-optimized for mammalian expression (a.k.a., the *luc2* gene). Recently, consecutive single amino acid deletion mutants of FLuc, ΔFLucs, have been reported with higher activities, altered kinetic, and lower K_M toward D-luciferin.⁹ To further improve the thermal and pH stability of FLuc, a chimeric luciferase was developed by fusing the N-terminal domain of FLuc and the C-terminal domain of *Luciola italica* luciferase, thereby resulting in a codon-optimized PLG2 that shows ~ 3-fold higher activity than the original FLuc.¹⁰

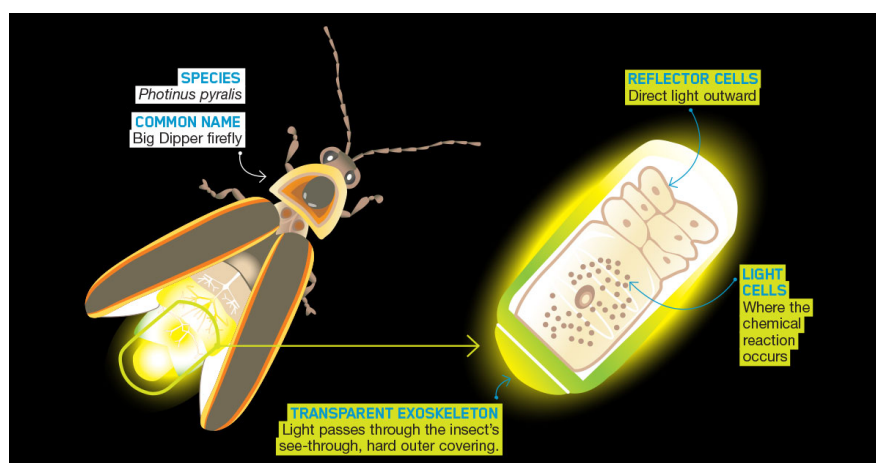


Figure 1. North American firefly *Photinus pyralis* and its light producing tissue. Picture was reprinted with permission from Scholastic of the Science World article “Gone in a Flash”.

Chemists have spent enormous efforts on developing synthetic D-luciferin analogs. For *in vivo* bioluminescence imaging (BLI), an ideal luciferin should emit near-infrared (NIR) photons to maximize tissue penetration by minimizing tissue absorption and scattering. Despite the fact that many D-luciferin analogs have been synthesized,¹¹ most red-shifted analogs do not increase photon fluxes. In one study, Moerner *et al.* replaced the sulphur atom in 6-amino-D-luciferin with a selenium atom, leading to 6-aminoseleno-D-luciferin with red-shifted emission at 600 nm and *in vivo* brightness comparable or slightly higher than that of 6-amino-D-luciferin.¹² A few other D-luciferin analogs, such as CycLuc1,¹³ AkaLumine,¹⁴ and CybLuc (**Figure. 2b**),¹⁵ improved the *in vivo* performance of FLuc. Recently, a re-engineered FLuc variant–Akaluc, in the presence of its synthetic AkaLumine substrate and a sensitive electron-multiplying CCD (EMCCD) camera, was able to highlight single cells in mice.¹⁶ Furthermore, Akaluc-AkaLumine has been demonstrated for the labeling of neurons in the brains of freely moving mice and a common marmoset.¹⁶

Effort has also gone to the development of luciferase-luciferin pairs orthogonal to FLuc and D-luciferin. Miller *et al.* identified a FLuc mutant (R218K, L286M, and S347A) that has abolished activity toward D-luciferin but remains active toward CycLuc analogs.¹⁷ These pairs were further demonstrated for mouse brain imaging.¹⁸ In addition, Prescher *et al.* synthesized a series of sterically modified D-luciferin analogs and screened for FLuc mutants that can discriminate these analogs, resulting in a set of FLuc-derived orthogonal luciferase-luciferin pairs.¹⁹ These new tools enabled sequentially multiplexed BLI in the same live animals.²⁰

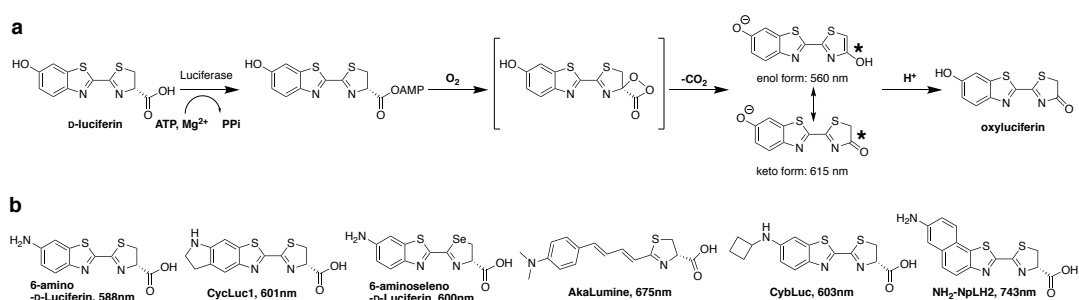


Figure 2. (a) Mechanism for bioluminescence emission generated by luciferase-catalyzed oxidation of D-luciferin. (b) Representative D-luciferin analogs and their peak emission wavelengths in the presence of firefly luciferase (FLuc).

To date, more than thirty D-luciferin-consuming luciferases have been discovered from diverse species. In addition to FLuc, click beetle luciferases from *Pyrophorus plagiophthalmus* and *Pyrearinus termitilluminans*, such as CBR and ELuc, are also popular reporters due to their excellent thermal stability and ability to emit different colors of bioluminescence from 538 nm to 615 nm in the presence of D-luciferin.²¹ In particular, codon-optimized ELuc from *Pyrearinus termitilluminans* exhibits ~ 10-fold stronger signals than FLuc.²² These click beetle luciferases variants

together can achieve spectra-resolved multicolor assay²³ and multiplexed *in vivo* BLI²⁴ (e.g., monitoring the expression of two genes simultaneously or labeling two different cell types in individual animals). Recently, Hall *et al.* reported an engineered click beetle luciferase mutant, CBR2opt, which shows maximal emission at 743 nm when paired with NH₂-NpLH2, a synthetic naphthyl-luciferin analog.²⁵ However, despite the dramatic red-shift, CBR2opt still displayed better *in vivo* sensitivity in the presence of D-luciferin than NH₂-NpLH2.

1.2.2. Development and applications of CTZ-consuming luciferases

Coelenterazine (CTZ), harboring a imidazopyrazinone core structure, is the most widely presented luciferin in luminous marine organisms, including sea pansy, copepods, squids, shrimps, and jelly fishes.¹ The light production mechanism has been proposed. Briefly, the C-2 position of CTZ first interacts with molecular oxygen (O₂) to form a dioxetanone intermediate. Next, the intermediate loses CO₂ to give a high-energy, excited-state coelenteramide, from which photons are produced (**Figure. 3a**). It has been suggested that photons may be emitted from different chemical forms of coelenteramide within the enzyme active site.²⁶ For example, the presence of phenolate anion in the excited state may be responsible for emission at ~ 480 nm.

Unlike FLuc, most CTZ-consuming luciferases do not require additional cofactors, such as ATP and Mg²⁺. Since the chemical structure of CTZ was identified and CTZ was confirmed as a shared substrate of various marine luciferases, many CTZ analogs have been synthesized.²⁷ Some representative synthetic CTZ analogs, which may lead to unique reactivity, higher brightness, red-shifted emission, or better *in vivo* performance are shown in **Figure. 3b**. Generally speaking, CTZ-consuming bioluminescent reporters commonly used in laboratories are derived from the sea pansy *Renilla reniformis*, the marine copepod *Gaussia princeps*, or the deep-sea

shrimp *Oplophorus gracilirostris*. In the following sections, we will describe various options that are currently available in the BLI toolbox.

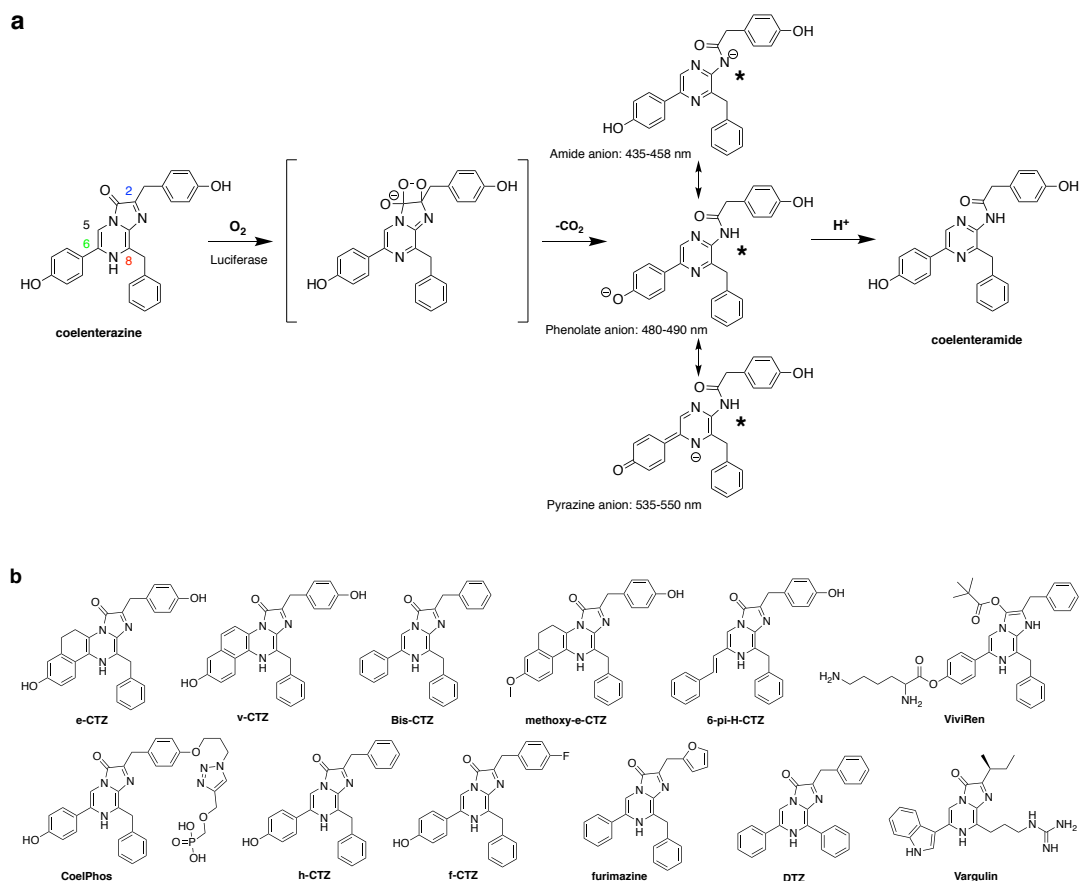


Figure 3. (a) Mechanism for luciferase-catalyzed oxidation of coelenterazine (CTZ) and proposed excited-state emitters. (b) Representative CTZ analogs, which lead to unique reactivity, higher brightness, red-shifted emission, or better *in vivo* performance.

1.2.3. *Renilla* luciferase (RLuc) and its derivatives

Renilla luciferase (RLuc) was cloned from *Renilla reniformis*, which emits at 480 nm in the presence of CTZ.²⁸ Loening *et al* reported a RLuc8 variant, which harbors eight amino acid substitutions from RLuc and shows a 4-fold enhancement in brightness and a 200-fold enhancement in serum stability.²⁹ To shift the emission of

RLuc, its active site was re-engineered, leading to a number of new variants with bioluminescence emission spanning from 475 nm to 547 nm in the presence of CTZ.³⁰ In particular, several red-shifted variants, such as RLuc7-521 and RLuc8.6-535, which have emission peaks at 521 nm and 535 nm respectively, were demonstrated for improved *in vitro* and *in vivo* brightness over native RLuc.³¹ More recently, a “super RLuc” mutant was reported for improved thermostability and emission at 540 nm when paired with CTZ.³²

Numerous CTZ analogs bearing diverse substitutions at the C-2, C-5, C-6, or C-8 positions have been synthesized mainly to enhance bioluminescence brightness and to red-shift emitting photons (**Figure. 3b**)²⁷. In particular, the RLuc and e-CTZ pair displays dual emission peaks at 418 nm and 475 nm and is 7-fold brighter than the RLuc and CTZ pair.³³ Also, the RLuc8.6 and v-CTZ pair gives red-shifted emission peaking at 588 nm.³⁰ On the other hand, Bis-CTZ could blue-shift the bioluminescence of RLuc8 to ~ 405 nm.³³ Similarly, methoxy-e-CTZ and several recently reported π -conjugated substitutions (e.g., 6- π -H-CTZ, **Figure. 3b**) at the C-6 position cause similar hypsochromic shifts but are approximately 10-fold brighter than Bis-CTZ.³⁴ Since the violet emission of RLuc8 paired with methoxy-e-CTZ is well overlapped with the second absorption peak (Soret band) of near-infrared (NIR) fluorescent iRFPs, fusion proteins between RLuc8 and iRFPs have been generated for NIR emission *via* bioluminescence resonance energy transfer (BRET).³⁵

To gain sustained light output *in vivo*, CTZ was chemically modified into temporarily inactive forms. For example, ViviRen (**Figure. 3b**) have two ester protection groups on the C-3 and C-6 positions, respectively; after entering cells, they are slowly de-esterified by endogenous esterases. This strategy not only greatly reduces the auto-oxidation of these substrates and slows down their consumption *in vivo*, but also leads to improved signals in mouse brains as demonstrated in an RLuc-labeled brain tumor model.³⁶

It can be concluded that several RLuc-derived luciferase-luciferin pairs are now available with emission spanning from ~ 400 nm to ~ 590 nm. RLuc has been a very popular bioluminescence reporter in protein- and cell-based assays. Moreover, since the blue emission of RLuc is overlapped with the excitation of bright green fluorescent fluorophores, such as enhanced green fluorescent protein (EGFP), RLuc has been widely used as a BRET donor in biosensor development.³⁷

1.2.4. *Gaussia* luciferase (GLuc) and its derivatives

The cDNA of *Gaussia* luciferase (GLuc) was cloned from the marine copepod *Gaussia princeps* in 2002.³⁸ GLuc, which is a naturally secreted luciferase, emits flash-type bioluminescence at ~ 473 nm in the presence of CTZ. Under similar experimental conditions, GLuc is ~100 times brighter than RLuc in mammalian cells.³⁹ To date, a number of GLuc variants have been reported. For example, GLuc4 shows stable light output suitable for high throughput screening.⁴⁰ GLuc8990 is ~ 10-fold brighter than GLuc and Monsta (a red-shifted mutant of GLuc) and produced a wavelength peak at 503 nm.⁴¹ Recently, GLuc has been fused with multiple repeats of an endoplasmic reticulum targeting sequence, resulting in intracellular retention of GLuc for biosensing and imaging applications.⁴²

Its high brightness and naturally secreted features make GLuc an attractive reporter for real-time *ex vivo* monitoring of biological processes in cultured cells, or in blood or urine from animals.⁴³ Interestingly, bright GLuc variants have been used to excite channelrhodopsins and proton pumps to initiate or inhibit neuronal activity.⁴⁴ The resulting fusions, Luminopsins, integrates both chemogenetic and optogenetic concepts, are becoming useful research tools for the interrogation of neuronal circuits and brain functions.⁴⁵

Different from RLuc, GLuc is not very reactive toward typical synthetic CTZ analogs. Only a cell-impermeable CTZ analog, CoelPhos (**Figure. 3b**), was reported to light up GLuc localized on cell surface.⁴⁶ Expanding the substrate scope of GLuc via protein engineering may lead to more bioluminescence colors and a broader range of applications.

1.2.5. *Oplophorus* luciferase (OLuc) and its derivatives

Oplophorus luciferase (OLuc) was isolated from deep-sea shrimp *Oplophorus gracilirostris* in 1978.⁴⁷ A key 19 kDa subunit of OLuc was later cloned, overexpressed, and confirmed for enzymatic activity toward CTZ.⁴⁸ Recently, Promega Corporation converted this 19 kDa subunit into NanoLuc, which has 16 additional mutations and in the presence of a synthetic CTZ analog, furimazine (**Figure. 4**), is ~ two orders of magnitude brighter *in vitro* than FLuc-D-luciferin.⁴⁹ Furthermore, Inouye *et al.* reported that three known CTZ analogs including h-CTZ, f-CTZ, and bis-CTZ (**Figure. 3b**), when paired with NanoLuc, can generate 2 to 3-fold stronger bioluminescence than furimazine.⁵⁰ The same research group also reported eKAZ, which has three additional mutations (V44I, A54I, Y138I) from NanoLuc; when CTZ served as the substrate of eKAZ, the bioluminescence brightness was comparable to that of the NanoLuc-furimazine pair.⁵¹

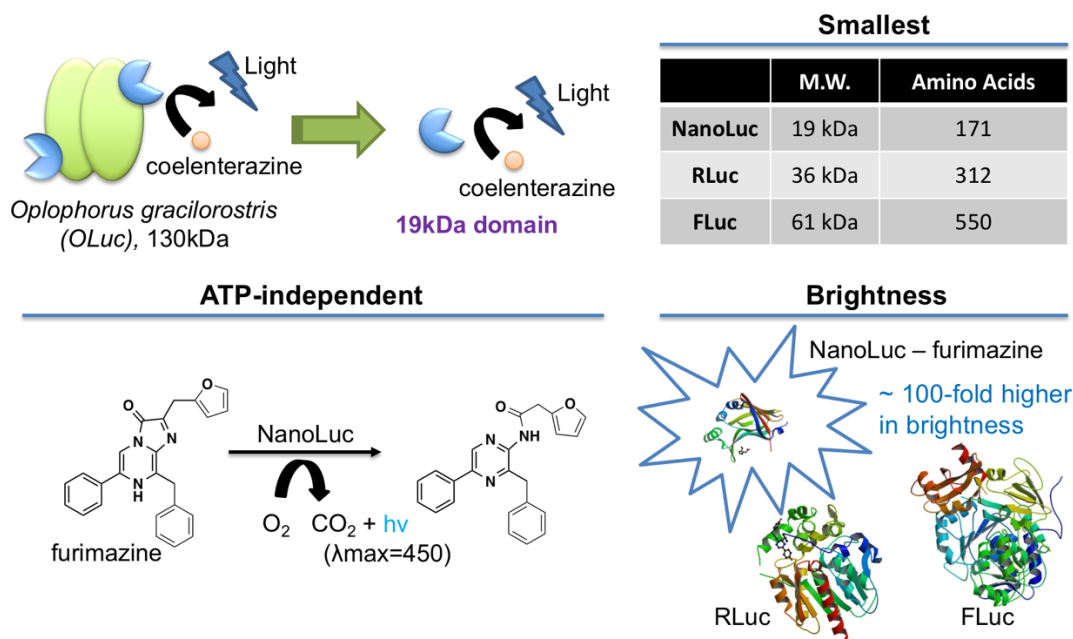


Figure 4. The development of NanoLuc provides ideal bioluminescence properties such as small size, stability, ATP-independency, and high brightness. Figure was, in part, reproduced from reference 49. Protein structures were obtained from Protein Data Bank (PDB) – NanoLuc: 5IBO, RLuc: 2PSJ, and FLuc: 1LCI.

Because of its small size, high brightness, and high stability, NanoLuc has been quickly adapted by a large number of biomedical researchers,⁵² outperforming RLuc and FLuc in many aspects.⁵³ NanoLuc have been successfully used to track virus spread *in vivo*, and the small NanoLuc gene, but not the large FLuc gene, could be integrated into the genome of influenza virus.⁵⁴ However, a major drawback of NanoLuc is its blue emission peaking at ~ 460 nm, resulting in limited tissue penetration due to strong absorption and scattering of blue photons by biological tissues. A recent study has reported novel CTZ analogs that can red-shift the emission of NanoLuc to nearly 600 nm, although their bioluminescence intensities were low and there remains a question whether NanoLuc could be further engineered to rescue bioluminescence for these new substrates.⁵⁵ Another strategy to red-shift NanoLuc uses BRET. Lin *et al.* fused NanoLuc with a CyOFP fluorescent protein, resulting in a

construct named Antares showing much improved *in vivo* bioluminescence.⁵⁶ Similarly, Nagai *et al* genetically fused NanoLuc with a number of fluorescent proteins to generate five different bioluminescence colors for multicolor cellular imaging.⁵⁷ Furthermore, NanoLuc has been fused to SNAP- or Halo-tag and further labeled with various fluorescent dyes.^{55, 58} Despite that this semisynthetic strategy could red-shifted NanoLuc for far-red or even NIR emission, it requires an additional dye conjugation step, thereby limiting its uses *in vivo*.

Split luciferases are ideal tools for studying protein-protein interactions *via* complementary assays. NanoLuc was split into a 1.3-kDa C-terminal fragment and a 18-kDa N-terminal fragment with 190 μ M affinity.⁵⁹ This NanoBiT technology has been utilized to detect the activities of GPCRs.⁶⁰ Furthermore, taking advantage of this small C-terminal fragment (11 amino acid residues), researchers have integrated the DNA sequence into genomes to label specific genes of interest by using CRISPR/Cas9 without disturbing the functions of endogenous genes.⁶¹ When the corresponding 18-kDa N-terminal fragment was co-expressed, a complete NanoLuc could form on tagged proteins to generate bioluminescence signals. NanoLuc has further been split into three fragments, which were individually fused to two antibody variable domain fragments (V_H and V_L) for a sandwich bioluminescence immunoassay.⁶²

1.2.6. Artificial luciferases (ALucs)

Kim *et al.* created a series of artificial luciferases (ALucs) based on a sequence alignment of several CTZ-consuming copepod luciferases. The resultant ALucs exhibited high thermostability and prolonged emission kinetic.⁶³ Moreover, different lineages of ALucs were evolved, giving unique substrate preferences⁶⁴ and enhanced brightness.⁶⁵ Recently, Kim *et al.* further reported a group of dye-conjugated CTZ analogs.⁶⁶ In particular, ALuc16 showed a minor, far-red emission peak in the

presence of a 6-Nile-R-CTZ substrate, and under this condition, ~ 11% of the total emission was at the wavelengths longer than 600 nm.

1.2.7. Development and applications of bacterial luciferase

Photons from naturally bioluminescent bacteria are caused by a *luxCDABE* operon that encodes a heterodimeric luciferase (*luxA* and *luxB*) and three biosynthetic enzymes (*luxC*, *luxD* and *luxE*) responsible for the production of a long-chain aldehyde substrate. This bioluminescent system can be fully genetically expressed and can glow without addition of exogenous luciferins. However, it is limited by low brightness, blue emission (490 nm), and dependence of reduced riboflavin phosphate (FMNH₂) and long-chain aldehydes. Optimizations have been done to enable heterologous expression of bacterial luciferase (Lux) to label other bacteria in infectious animal models⁶⁷ or to directly label mammalian cells.⁶⁸ Since the availability of FMNH₂ could be limited in cells, an enhanced system, iLux, has been recently reported by co-expressing of a FMN reductase and introducing additional mutations across the *luxCDABE* operon.⁶⁹ The resultant bioluminescent system was ~ 6- to 8- fold brighter than FLuc in single bacterial cells. Furthermore, long-chain aldehydes may be potentially toxic to heterologous hosts, limiting the use of Lux as a common bioluminescent reporter.

1.2.8. Other miscellaneous luciferases

To date, more than a thousand species have been observed for bioluminescence, but most have not been well-studied. For example, luciferases cloned from luminous ostracod, *Cypridina noctiluca* (CLuc) and *Vargula hilgendorffii* (VLuc) use Vargulin (**Figure. 3b**) as their substrate,⁷⁰ which shares a core imidazopyrazinone structure with CTZ but different substitutions on the C-6 and C-8

positions. This makes CLuc and VLuc evolutionarily unique. Since they do not cross-react with CTZ or D-luciferin, they are suitable for simultaneous dual-luciferase assays and multiplex imaging.⁷¹

Fungi have long been observed to emit light during night. Although fungal luciferases have not yet been cloned, research on the chemical basis of fungal bioluminescence suggests that this light production process involves two steps.⁷² The precursor luciferin is firstly reduced by an NAD(P)H-dependent enzyme, and next, oxidized by the luciferase. Recent studies demonstrated that the oxidation could yield a high-energy endoperoxide intermediate and the emission could be tuned from 480 nm to 564 nm by modulating the chemical structures of their substrates.⁷³ And later its luciferin biosynthetic pathway was identified and the whole fungal bioluminescence system was successfully genetically encoded in eukaryotes, indicating that fungal bioluminescence may have a great potential as a practical self-glow bioluminescent reporter.⁷⁴

Table 1. Common luciferase-luciferin pairs.

Original Species	Luciferase	Luciferin	Size, (kDa)	λ_{\max} (nm)	Ref.
<i>Photinus pyralis</i>	FLuc	D-luciferin	61	560	7
	Akaluc	AkaLumine	61	650	16
<i>Pyrophorus plagiophthalmus</i>	CBR	D-luciferin	61	615	21
<i>Pyrearinus termitilluminans</i>	ELuc	D-luciferin	61	538	22
<i>Renilla reniformis</i>	RLuc8	CTZ	36	480	29
	RLuc8.6	CTZ	36	535	30
<i>Gaussia princeps</i>	GLuc	CTZ	20	473	38

<i>Oplophorus gracilinostris</i>	NanoLuc	furimazine	19	460	49
	teLuc	DTZ	19	502	75
<i>Photorhabdus luminescens</i>	iLux	fatty aldehyde and FMNH ₂	>200 ^a	490	69

Note: ^athe total size of luxA, luxB, luxC, luxD, and luxE.

1.3. *in vivo* Bioluminescence imaging (BLI)

As mentioned previously, bioluminescent reporters have been widely used for live animal imaging. Bioluminescence is a superior optical imaging modality than fluorescence at macro-scale, especially for whole-body imaging. Due to the fact that bioluminescence imaging does not require incident light for chromophore excitation, the dark background gives BLI much higher signal-to-noise ratio, leading to high sensitivity and dynamic range (**Figure 5**). However, some factors, such as the emission wavelength of bioluminescence, the photon flux of bioluminescence, and tissue scattering & absorption, can significantly affect the *in vivo* BLI sensitivity.⁷⁶ Thanks to the discovery of tissue-specific promoters and response element sequences, luciferase gene expression can be controlled at transcriptional level under selected physiological and pathological conditions. Therefore, BLI has become a popular imaging modality for non-invasively tracking tumor burden and metastasis. The xenograft luciferase-expressed tumor models provide a robust preclinical strategy to evaluate the effectiveness of anti-tumor therapeutics *in vivo* in a timely manner.⁷⁷ Beyond oncology and angiogenesis fields, a growing number of luciferase expressing animal models are also available to toxicology, inflammation, metabolic diseases, and neurodegenerative diseases.⁷⁸⁻⁷⁹

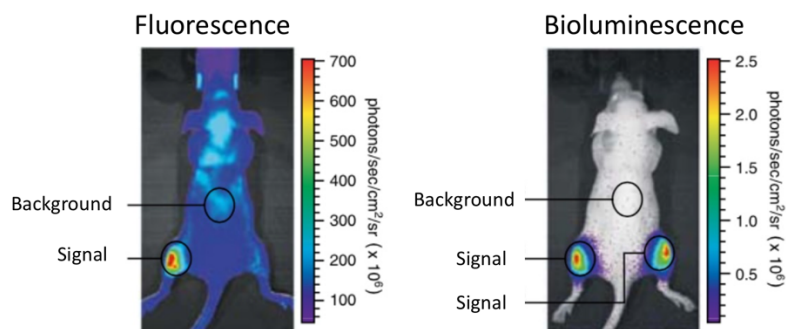


Figure 5. Comparison of live animal fluorescence and bioluminescence imaging. Bioluminescence imaging modality shows low background from non-labeled area than fluorescence imaging mode. Picture was reproduced from reference 76 with permission of SAGE Publications.

1.4. Cell-based reporter assay in drug discovery

Bioluminescence reporters have been utilized in a variety of assays to measure cell viability, toxicity, activation of signaling cascades, and production of biomarkers in high-throughput (HTS) formats.⁸⁰ Reporter assays based on the activation of luciferase expression require long response times from hours to days. To facilitate high-content screening that involves assays of more complex cellular phenotypes as outputs, the development of bioluminescent biosensors by integrating fluorescence or bioluminescence resonance energy transfer (FRET or BRET) or split complementation approach provides instant biological response of the desired biological activation. The improved optical instrumentation along with modern biosensor design described in the following paragraphs can further facilitate the early phase of the drug discovery and development with favorable features such as high-throughput, automation, cost-effectiveness, and multiplexing.

1.5. Design of BRET-based biosensors

Resonance energy transfer (RET) is a photophysical phenomenon describing a donor chromophore at its excited state may transfer energy to an acceptor chromophore via a non-radiative dipole-dipole coupling process. The RET efficiency (E) is described by Förster equation where the Förster distance (R_0) is depended on quantum yield (Q_D), spectral overlap (J), extinction coefficient of the acceptor (ϵ_A), and the dipole orientation factor (κ^2). When the donor is excited by bioluminescent reactions, this phenomenon is called bioluminescence resonance energy transfer (BRET). The BRET efficiency is inversely proportional to the sixth power of the distance between the donor and the acceptor.

$$E = \frac{R_0^6}{R_0^6 + r^6}; \text{ where the Förster distance is given by } R_0 = (2.8 \times 10^{17} Q_D J \epsilon_A \kappa^2)^{1/6}$$

Therefore, BRET is a useful method for monitoring subtle distance changes between donors and acceptors,⁸¹ leading to a large array of applications in monitoring protein-protein interactions, biosensing, and functional imaging.⁸²⁻⁸⁴ Previous studies mostly used luciferases as BRET donors and fluorescent proteins as BRET acceptors and fused them with various sensory elements to create diverse bioluminescent biosensors. We below highlight some examples with a focus on applications in *in vitro* assays, live cells, and animals.

1.5.1. Firefly luciferase-based BRET biosensors

Although FLuc is a widely used bioluminescent reporter, it is not a popular choice for the development of BRET-based biosensors. First, FLuc is ATP-dependent, making it a natural ATP sensor. For other live-cell or *in vivo* applications, the variations

in the ATP level might be a problem. Moreover, consumption of cellular ATP by this bioluminescence-generating process would definitely perturb cell physiology, since ATP is not only the most important energy currency in living cells, but also a key molecule connecting metabolism to signaling. Furthermore, the bulky size of FLuc (61 kDa) makes the designing of FLuc-based BRET biosensors difficult, because it is hard to predict donor-acceptor distances and relative orientations. Finally, fluorescent proteins that are suitable as BRET acceptors for FLuc are typically not bright,⁸⁵ and therefore, it is hard to gain sensitized emission from the acceptors. An early study made a GST (glutathione S-transferase)-FLuc fusion and a PG (Protein G)-DsRed fusion (**Figure. 6a**). The presence of an anti-GST antibody can bring these two fusion proteins in close proximity, leading to increased BRET. This system was used to measure the concentrations of the anti-GST antibody.⁸⁶ However, the emission overlap between FLuc (Em: 560 nm) and DsRed (Ex: 558 nm; Em: 583 nm) is problematic. To address this issue, another study further tagged cysteine residues on DsRed with an Alexa Fluor 680 dye (Ex: 680 nm; Em: 705 nm), resulting in sequential resonance energy transfer (SRET) for improved spectral separation.⁸⁷ This strategy has been further developed for probing caspase-3, thrombin, and factor Xa activities.⁸⁷ In another study, FLuc was combined with quantum dots to form BRET pairs and used to develop protease assays.⁸⁸

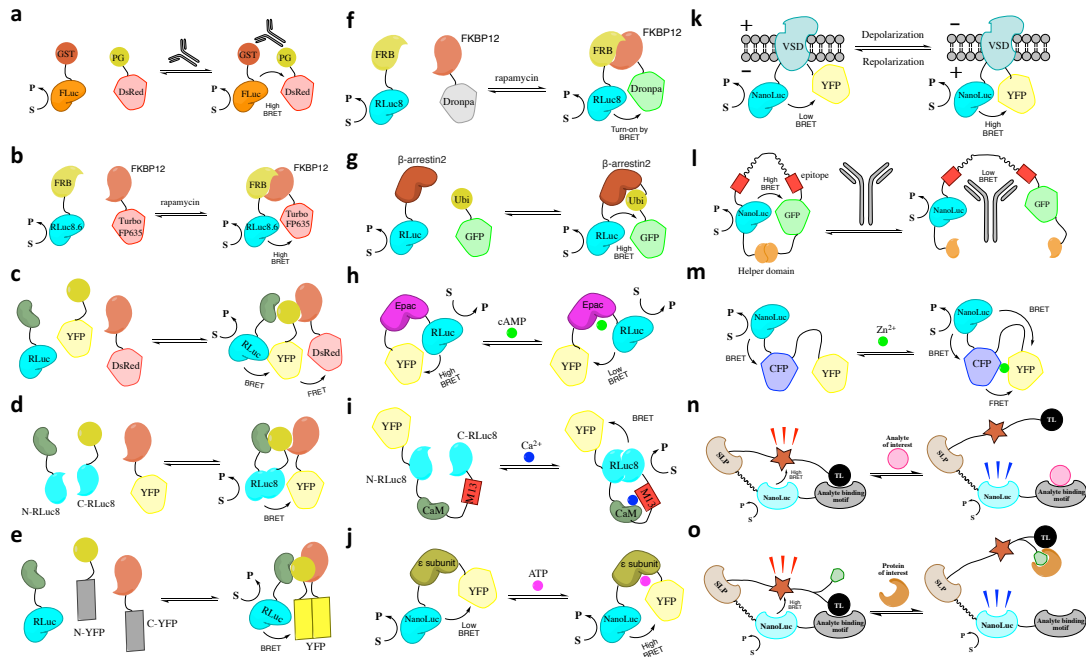


Figure 6. Representative BRET-based biosensors and their response mechanism.

(a) An immunoassay based on FLuc and DsRed to detect antibody concentrations. (b) Monitoring of rapamycin-induced FRB-FKBP12 association with the RLuc8.6 and TurboFP635 pair. (c) Sequential resonance energy transfer (SRET) to detect the interactions of three proteins. (d) BRET from a donor luciferase to complementary acceptor fragments (a.k.a., BiFC-BRET) to detect the interactions of three proteins, and (e) BRET from two complementary luciferase fragments to an acceptor fluorescent protein (a.k.a., CODA-RET) to detect the interactions of three proteins. (f) Bioluminescence-assisted switching-on of Dronpa and BRET (a.k.a., BASFI) to monitor the rapamycin-induced FRB-FKBP12 interaction in both bioluminescence and fluorescence modes. (g) Monitoring of β -arrestin2 ubiquitination by using RLuc- β -arrestin2 and GFP-ubiquitin fusion proteins. (h) An RLuc-YFP BRET-based cAMP biosensor, CAMYEL. (i) A BRET-based Ca^{2+} biosensor, Nano-lantern (Ca^{2+}), via Ca^{2+} -induced reconstitution of RLuc8. (j) A NanoLuc-YFP BRET-based ATP biosensor, BTeam. (k) A NanoLuc-YFP BRET-based voltage sensor, LOTUS-V. (l) LUMinescent AntiBody Sensors (LUMABS) for highly sensitive detection of

antibodies down to the picomolar range. (m) A bioluminescent Zn^{2+} biosensor, BLZinCh-3, based on BRET from NanoLuc to CFP and YFP of an existing fluorescent Zn^{2+} biosensor. (n) Semisynthetic LUCiferase-based Indicators of Drugs, LUCIDs and (o) Chemical Ligand-Associated Steric Hindrance, CLASH sensors for the detection of therapeutic drugs and protein effectors. Abbreviations in this Figure: GST: glutathione S-transferase; PG: IgG-binding protein G; GFP: green fluorescent protein; YFP: yellow fluorescent protein; Ubi: ubiquitin; Epac: exchange protein activated by cAMP; CaM: calmodulin; VSD: voltage sensing domain; CFP: cyan fluorescent protein; TL: tethered ligand; SLP: self-labeling protein, such as SNAP-, Halo- and CLIP-tags.

1.5.2 *Renilla* luciferase-based BRET biosensors

RLuc and its mutants have been widely used as the BRET donor, resulting in diverse BRET pairs such as RLuc-CTZ and YFP, RLuc-bis-CTZ and GFP, RLuc8-CTZ and mOrange, and RLuc8.6-CTZ and TurboFP635.⁸⁹⁻⁹⁰ In one example, a caspase-1 substrate sequence was inserted between RLuc8 and YFP. Therefore, upon caspase cleavage, BRET is disrupted. This sensor has been used as a ratiometric indicator for pro-IL-1 β processing.⁹¹ Another successful example demonstrated the monitoring of rapamycin-induced FRB-FKBP12 association by fusing RLuc8.6 to FRB and TurboFP635 to FKBP12 (**Figure. 6b**). Rapamycin induces the dimerization of FRB and FKBP12, and subsequently brings RLuc8.6 and TurboFP635 together for increased BRET. Furthermore, the system was used to monitor FRB-FKBP12 dimerization in HT1080 cells trapped in the lungs of living mice by measuring emission at 535 and 635 nm.⁹⁰

RLuc has also been used to monitor the interactions of three proteins. In one study, an SRET system based on RLuc-bis-CTZ, YFP, and DsRed (**Figure. 6c**)

enabled the BRET-FRET monitoring of three-protein interactions. Moreover, this method has been applied to the identification of neurotransmitter receptor complexes in live cells.⁹² In another study, RLuc and two complementary fragments of a split YFP were individually fused to partner proteins, leading to a BiFC-BRET method that can also detect the interactions of three proteins (**Figure. 6d**).⁹³ Similarly, RLuc has been split into two complementary fragments and used for BRET with YFP (**Figure. 6e**).⁹⁴ This so called “complemented donor-acceptor RET” (CODA-RET) method, which also allowed the identification of heteromeric complexes of three different proteins, have been used to investigate dynamic G-protein-associated signaling cascades.⁹⁴

To take advantage of both BRET and high-intensity fluorescence imaging, RLuc8 was paired with photoactivable fluorescent protein, Dronpa, to achieve bioluminescence-assisted switching and fluorescence imaging (BASFI).⁹⁵ When RLuc8 and Dronpa were brought into close proximity, Dronpa was photoswitched to a fluorescence state by the luminescence generated from RLuc8 in the presence of its substrate (**Figure. 6f**). This process can be detected as increased BRET and the fluorescence turn-on of Dronpa.

Understanding extracellular and intracellular signal transduction is key to unlock the mystery of cell biology. Ubiquitination is a type of post-translational modification (PTM) controlling protein degradation, function, localization, and interaction. Perroy *et al.* fused RLuc to β -arrestin2 and GFP to ubiquitin to study the ubiquitination dynamics of arrestin2 triggered by G protein-coupled receptors (GPCRs) (**Figure. 6g**).⁹⁶ The ubiquitination of arrestin2 brings RLuc and GFP in close proximity, and thus, increases BRET from RLuc to GFP. Monitoring the ratiometric emission of RLuc and GFP enables real-time measurement of ubiquitination in live cells. In another study, a BRET sensor was developed to measure intracellular cAMP, a cyclic nucleotide and an intracellular second messenger.⁹⁷ In the resultant cAMP sensor (CAMYEL), a cAMP-binding Epac (exchange protein activated by cAMP) domain was

inserted between RLuc and YFP (**Figure. 6h**). cAMP binds to Epac and triggers a conformational change to modulate the BRET from RLuc to YFP, and thus, the determined BRET ratios can be used as optical readouts for live-cell cAMP levels. The similar approach has been applied to create BRET-based biosensors for cGMP,⁹⁸ Ca²⁺,⁹⁹ and ATP.¹⁰⁰ In 2012, Nagai *et al.* reported a chimera of RLuc8 and Venus, named Nano-lantern, which exhibited 10-fold increased brightness than RLuc8 alone and allowed the real-time BLI of tumors in freely moving mice.¹⁰¹ By inserting different sensory domains into the N- and C-terminal domains of a split RLuc8 in Nano-lantern, three sensors for Ca²⁺, ATP, or cAMP were derived (**Figure. 6i**). These sensors were combined with optogenetic tools, such as halorhodopsin and channelrhodopsin2 for live-cell imaging of rat hippocampal neurons.¹⁰¹

1.5.3. NanoLuc-based BRET biosensors

Since the invention of NanoLuc which is much brighter than RLuc, many NanoLuc-based biosensors have been developed, mirroring the development processes of RLuc-based biosensors. For example, following the design of CAMYEL, NanoLuc-based Ca²⁺ and ATP sensors have been created. In particular, a Ca²⁺ sensor, CalfluxVTN, exhibits a larger dynamic range than Nano-lantern (Ca²⁺) and can work compatibly with optogenetic actuators in rat hippocampal neurons.¹⁰² Furthermore, an ATP sensor, BTeam (**Figure. 6j**), which is a fusion protein of NanoLuc, an ATP-binding- ϵ subunit, and YFP, was developed and used to determine intracellular ATP concentrations.¹⁰⁰ Moreover, NanoLuc replaced RLuc8 in Nano-lantern, followed by linker optimization, yielding a number of BRET-based, high-affinity Ca²⁺ indicators for multicolor BLI of Ca²⁺ in multiple subcellular organelles of living cells.¹⁰³ In addition, a BRET-based ratiometric voltage indicator, LOTUS-V (**Figure. 6k**), was reported showing robust signal-to-noise ratios. In its design, NanoLuc and YFP were fused to the two termini of a voltage-sensing domain (VSD), and voltage-induced structural

changes in VSD alter the BRET from NanoLuc to YFP. LOTUS-V is free from external excitation, and thus, provides an excellent way to monitor neuronal activities in combination with optogenetic actuators that typically overlap with GFP-based voltage sensors.¹⁰⁴ The low phototoxicity of bioluminescent indicators also makes them ideal for long-term imaging.

Antibodies are important immunological markers for infectious and immunological diseases.¹⁰⁵ A series of NanoLuc-based biosensors, called LUMABS, were developed for fast detection of antibodies in blood plasma.¹⁰⁶ All LUMABS sensors share the similar design that comprises NanoLuc, mNeonGreen, two antibody-binding epitopes, and a pair of weakly dimerizing helper domains that bring NanoLuc and mNeonGreen close for high BRET (**Figure. 6I**). Upon the binding of an antibody to the epitopes, the interaction between the two helper domains is disrupted, resulting in a large decrease of BRET and a color change from green to blue. This sensor has been demonstrated for the detection of picomolar antibodies in blood plasma. This general strategy have been adapted for the detection of other antibodies, such as trastuzumab (anti-HER2), obinutuzumab, rituximab (anti-CD20), and cetuximab (anti-EGFR), providing an potential, alternative assay for monitoring therapeutic drugs in patients.¹⁰⁷ Another strategy introduced unnatural amino acid, *p*-azidophenylalanine, via genetic code expansion to replace the epitope of the original LUMABS. The incorporated *p*-azidophenylalanine can be further site-specifically coupled with dinitrophenol or creatinine through click chemistry, and become small molecule epitopes to detect dinitrophenol or creatinine recognized antibodies.¹⁰⁸

Despite that many biosensors based on Förster resonance energy transfer (FRET) have been developed,¹⁰⁹ it is typically not possible to gain responsive BRET sensors by simply replacing FRET donors with luciferases. Fortunately, additional strategies have been developed to simplify the conversion of existing FRET biosensors into BRET biosensors.¹¹⁰ In one example, NanoLuc was fused to existing, FRET-based

Zn²⁺ biosensors, eCALWY¹¹¹ and eZinCh-2,¹¹² leading to dual BRET and FRET sensors for quantitative detection of intracellular Zn²⁺ (**Figure. 6m**).¹¹³ The bioluminescent reaction of NanoLuc was used to excite CFP and YFP while the efficiencies of the RET processes were Zn²⁺-dependent. Since the sensors have two chromophores competing with the bioluminescent light source, introducing a chromophore-silencing mutation into CFP yielded a BRET biosensor with improved responsiveness. Similarly, NanoLuc has been fused to GCaMP6s and thus gives LUCI-GECO1 for monitoring Ca²⁺ dynamics in live cells in the bioluminescence mode.¹¹⁴

In addition to biosensors that are based on BRET between luciferases and fluorescent proteins, Johnsson *et al.* developed a series of semisynthetic biosensors that are based on BRET between luciferases and synthetic dyes (**Figure. 6n**). These so-called LUCiferase-based Indicators of Drugs (LUCIDs) generally comprise of a BRET donor luciferase (e.g., NanoLuc paired with furimazine), an analyte-binding domain, and a self-labeling protein (SLP) through which a synthetic, fluorophore-containing intramolecular tether could be linked.¹¹⁵ The corresponding intramolecular tethers contain a motif for selective labeling reactions with SLPs, such as SNAP,¹¹⁶ Halo,¹¹⁷ and CLIP tags,¹¹⁸ a competitive ligand for the analyte-binding domain, and a RET acceptor fluorophore (e.g., Cy3). Initially, the competitive ligand would interact with the analyte-binding domain to form a closed state that keeps the RET acceptor in close proximity to the RET donor, leading to high BRET. In the presence of an analyte of interest, the analyte would compete with the tethered competitive ligand, leading to an open state in which BRET from the acceptor to the donor becomes low. By monitoring BRET, the concentration of the analyte can be quantitatively determined.

To date, a number of LUCIDs have been reported, showing excellent dynamic range and sensitivity toward various therapeutic drugs,¹¹⁹ such as methotrexate (MTX), tacrolimus, sirolimus, cyclosporine A, topiramate, and digoxin. For this application,

bioluminescence-based biosensors outperformed similar fluorescence-based biosensors because blood serum is highly absorptive and autofluorescent. LUCIDs can be readily modified and tuned for quantitative measurements of molecules other than drugs. In one example, the analyte-binding domain of LUCIDs was substituted with antigen-binding fragments of antibodies.¹²⁰ This strategy provides a shortcut to make bioluminescent biosensors for diverse antigens and its potential application could lead to point-of-care diagnostics. In another study, LUCIDs were modified into the so-called CLASH (Chemical Ligand-Associated Steric Hindrance) biosensors,¹²¹ which contained two exclusive ligands on the intramolecular tether (**Figure. 6o**). One ligand still has affinity with the analyte-binding domain, but the other ligand can bind to a specific effector protein, which increases the overall steric hindrance and prevent the interaction of the first ligand with the analyte-binding domain. CLASH allows an unrelated effector to control the function of a designed protein and demonstrates a general approach to the analysis of protein targets. Recently, a LUCID variant, LUPIN (luciferase-based photocatalysis induced *via* nucleic acid template) has been demonstrated to promote photocatalysis and facilitate a ruthenium-based uncaging reaction, and thus, release a specific inhibitor to control enzyme function.¹²² Overall, bioluminescent sensors have started to expand its applications to the point-of-care testing for fast monitoring of clinically related metabolites.¹²³

References

1. Haddock, S. H.; Moline, M. A.; Case, J. F., Bioluminescence in the sea. *Ann Rev Mar Sci* **2010**, *2*, 443-93.
2. Pflieger, K. D. G.; Seeber, R. M.; Eidne, K. A., Bioluminescence resonance energy transfer (BRET) for the real-time detection of protein-protein interactions. *Nat Protoc* **2006**, *1* (1), 337-345.
3. Suzuki, K.; Nagai, T., Recent progress in expanding the chemiluminescent toolbox for bioimaging. *Curr Opin Biotech* **2017**, *48*, 135-141.
4. Mezzanotte, L.; van 't Root, M.; Karatas, H.; Goun, E. A.; Lowik, C., In Vivo Molecular Bioluminescence Imaging: New Tools and Applications. *Trends Biotechnol* **2017**, *35* (7), 640-652.
5. Sun, S.; Yang, X.; Wang, Y.; Shen, X., In Vivo Analysis of Protein-Protein Interactions with Bioluminescence Resonance Energy Transfer (BRET): Progress and Prospects. *Int J Mol Sci* **2016**, *17* (10).
6. Yao, Z.; Zhang, B. S.; Prescher, J. A., Advances in bioluminescence imaging: new probes from old recipes. *Curr Opin Chem Biol* **2018**, *45*, 148-156.
7. de Wet, J. R.; Wood, K. V.; DeLuca, M.; Helinski, D. R.; Subramani, S., Firefly luciferase gene: structure and expression in mammalian cells. *Mol Cell Biol* **1987**, *7* (2), 725-37.
8. Vieira, J.; Pinto da Silva, L.; Esteves da Silva, J. C., Advances in the knowledge of light emission by firefly luciferin and oxyluciferin. *J Photochem Photobiol B* **2012**, *117*, 33-9.
9. Halliwell, L. M.; Jathoul, A. P.; Bate, J. P.; Worthy, H. L.; Anderson, J. C.; Jones, D. D.; Murray, J. A. H., Delta Flucs: Brighter Photinus pyralis firefly luciferases identified by surveying consecutive single amino acid deletion mutations in a thermostable variant. *Biotechnology and Bioengineering* **2018**, *115* (1), 50-59.
10. Branchini, B. R.; Southworth, T. L.; Fontaine, D. M.; Kohrt, D.; Talukder, M.; Michelini, E.; Cevenini, L.; Roda, A.; Grossel, M. J., An enhanced chimeric firefly luciferase-inspired enzyme for ATP detection and bioluminescence reporter and imaging applications. *Anal Biochem* **2015**, *484*, 148-153.
11. Kaskova, Z. M.; Tsarkova, A. S.; Yampolsky, I. V., 1001 lights: luciferins, luciferases, their mechanisms of action and applications in chemical analysis, biology and medicine. *Chemical Society reviews* **2016**, *45* (21), 6048-6077.
12. Conley, N. R.; Dragulescu-Andrasi, A.; Rao, J. H.; Moerner, W. E., A Selenium Analogue of Firefly D-Luciferin with Red-Shifted Bioluminescence Emission. *Angew Chem Int Edit* **2012**, *51* (14), 3350-3353.
13. Evans, M. S.; Chaurette, J. P.; Adams, S. T., Jr.; Reddy, G. R.; Paley, M. A.; Aronin, N.; Prescher, J. A.; Miller, S. C., A synthetic luciferin improves bioluminescence imaging in live mice. *Nat Methods* **2014**, *11* (4), 393-5.
14. Kuchimaru, T.; Iwano, S.; Kiyama, M.; Mitsumata, S.; Kadonosono, T.; Niwa, H.; Maki, S.; Kizaka-Kondoh, S., A luciferin analogue generating near-infrared bioluminescence achieves highly sensitive deep-tissue imaging. *Nat Commun* **2016**, *7*, 11856.
15. Wu, W.; Su, J.; Tang, C.; Bai, H.; Ma, Z.; Zhang, T.; Yuan, Z.; Li, Z.; Zhou, W.; Zhang, H.; Liu, Z.; Wang, Y.; Zhou, Y.; Du, L.; Gu, L.; Li, M., cybLuc: An Effective Aminoluciferin Derivative for Deep Bioluminescence Imaging. *Anal Chem* **2017**, *89* (9), 4808-4816.
16. Iwano, S.; Sugiyama, M.; Hama, H.; Watakabe, A.; Hasegawa, N.; Kuchimaru, T.; Tanaka, K. Z.; Takahashi, M.; Ishida, Y.; Hata, J.; Shimozone, S.; Namiki, K.; Fukano, T.; Kiyama, M.; Okano, H.; Kizaka-Kondoh, S.; McHugh, T. J.; Yamamori, T.; Hioki, H.; Maki, S.; Miyawaki, A., Single-cell bioluminescence imaging of deep tissue in freely moving animals. *Science* **2018**, *359* (6378), 935-939.

17. Mofford, D. M.; Reddy, G. R.; Miller, S. C., Aminoluciferins Extend Firefly Luciferase Bioluminescence into the Near-Infrared and Can Be Preferred Substrates over D-Luciferin. *Journal of the American Chemical Society* **2014**, *136* (38), 13277-13282.
18. Adams, S. T., Jr.; Mofford, D. M.; Reddy, G. S.; Miller, S. C., Firefly Luciferase Mutants Allow Substrate-Selective Bioluminescence Imaging in the Mouse Brain. *Angew Chem Int Ed Engl* **2016**.
19. Jones, K. A.; Porterfield, W. B.; Rathbun, C. M.; McCutcheon, D. C.; Paley, M. A.; Prescher, J. A., Orthogonal luciferase-luciferin pairs for bioluminescence imaging. *Journal of the American Chemical Society* **2017**.
20. Rathbun, C. M.; Porterfield, W. B.; Jones, K. A.; Sagoe, M. J.; Reyes, M. R.; Hua, C. T.; Prescher, J. A., Parallel Screening for Rapid Identification of Orthogonal Bioluminescent Tools. *ACS Cent Sci* **2017**, *3* (12), 1254-1261.
21. Wood, K. V.; Lam, Y. A.; Mcelroy, W. D., Introduction to Beetle Luciferases and Their Applications. *J Biolum Chemilum* **1989**, *4* (1), 289-301.
22. Nakajima, Y.; Yamazaki, T.; Nishii, S.; Noguchi, T.; Hoshino, H.; Niwa, K.; Viviani, V. R.; Ohmiya, Y., Enhanced Beetle Luciferase for High-Resolution Bioluminescence Imaging. *Plos One* **2010**, *5* (3).
23. Michelini, E.; Cevenini, L.; Mezzanotte, L.; Ablamsky, D.; Southworth, T.; Branchini, B.; Roda, A., Spectral-resolved gene technology for multiplexed bioluminescence and high-content screening. *Anal Chem* **2008**, *80* (1), 260-267.
24. Nakajima, Y.; Kimura, T.; Sugata, K.; Enomoto, T.; Asakawa, A.; Kubota, H.; Ikeda, M.; Ohmiya, Y., Multicolor luciferase assay system: one-step monitoring of multiple gene expressions with a single substrate. *Biotechniques* **2005**, *38* (6), 891-894.
25. Hall, M. P.; Woodroffe, C. C.; Wood, M. G.; Que, I.; Van't Root, M.; Ridwan, Y.; Shi, C.; Kirkland, T. A.; Encell, L. P.; Wood, K. V.; Lowik, C.; Mezzanotte, L., Click beetle luciferase mutant and near infrared naphthyl-luciferins for improved bioluminescence imaging. *Nat Commun* **2018**, *9* (1), 132.
26. Shimomura, O.; Teranishi, K., Light-emitters involved in the luminescence of coelenterazine. *Luminescence* **2000**, *15* (1), 51-8.
27. Jiang, T.; Du, L.; Li, M., Lighting up bioluminescence with coelenterazine: strategies and applications. *Photochem Photobiol Sci* **2016**, *15* (4), 466-80.
28. Lorenz, W. W.; McCann, R. O.; Longiaru, M.; Cormier, M. J., Isolation and expression of a cDNA encoding Renilla reniformis luciferase. *Proceedings of the National Academy of Sciences of the United States of America* **1991**, *88* (10), 4438-42.
29. Loening, A. M.; Fenn, T. D.; Wu, A. M.; Gambhir, S. S., Consensus guided mutagenesis of Renilla luciferase yields enhanced stability and light output. *Protein Eng Des Sel* **2006**, *19* (9), 391-400.
30. Loening, A. M.; Wu, A. M.; Gambhir, S. S., Red-shifted Renilla reniformis luciferase variants for imaging in living subjects. *Nat Methods* **2007**, *4* (8), 641-643.
31. Loening, A. M.; Dragulescu-Andrasi, A.; Gambhir, S. S., A red-shifted Renilla luciferase for transient reporter-gene expression. *Nat Methods* **2010**, *7* (1), 5-6.
32. Rahnama, S.; Saffar, B.; Kahrani, Z. F.; Nazari, M.; Emamzadeh, R., Super RLuc8: A novel engineered Renilla luciferase with a red-shifted spectrum and stable light emission. *Enzyme Microb Technol* **2017**, *96*, 60-66.
33. Inouye, S.; Shimomura, O., The use of Renilla luciferase, Oplophorus luciferase, and apoaequorin as bioluminescent reporter protein in the presence of coelenterazine analogues as substrate. *Biochem Bioph Res Co* **1997**, *233* (2), 349-353.
34. Nishihara, R.; Suzuki, H.; Hoshino, E.; Suganuma, S.; Sato, M.; Saitoh, T.; Nishiyama, S.; Iwasawa, N.; Citterio, D.; Suzuki, K., Bioluminescent coelenterazine derivatives with imidazopyrazinone C-6 extended substitution. *Chem Commun* **2015**, *51* (2), 391-394.

35. Rumyantsev, K. A.; Turoverov, K. K.; Verkhusha, V. V., Near-infrared bioluminescent proteins for two-color multimodal imaging. *Sci Rep* **2016**, *6*, 36588.
36. Otto-Duessel, M.; Khankaldyyan, V.; Gonzalez-Gomez, I.; Jensen, M. C.; Laug, W. E.; Rosol, M., In vivo testing of Renilla luciferase substrate analogs in an orthotopic murine model of human glioblastoma. *Mol Imaging* **2006**, *5* (2), 57-64.
37. Namkung, Y.; Le Gouill, C.; Lukashova, V.; Kobayashi, H.; Hogue, M.; Khoury, E.; Song, M.; Bouvier, M.; Laporte, S. A., Monitoring G protein-coupled receptor and beta-arrestin trafficking in live cells using enhanced bystander BRET. *Nat Commun* **2016**, *7*, 12178.
38. Verhaegent, M.; Christopoulos, T. K., Recombinant Gaussia luciferase. Overexpression, purification, and analytical application of a bioluminescent reporter for DNA hybridization. *Anal Chem* **2002**, *74* (17), 4378-85.
39. Tannous, B. A.; Kim, D. E.; Fernandez, J. L.; Weissleder, R.; Breakefield, X. O., Codon-optimized Gaussia luciferase cDNA for mammalian gene expression in culture and in vivo. *Mol Ther* **2005**, *11* (3), 435-43.
40. Degeling, M. H.; Bovenberg, M. S.; Lewandrowski, G. K.; de Gooijer, M. C.; Vleggeert-Lankamp, C. L.; Tannous, M.; Maguire, C. A.; Tannous, B. A., Directed molecular evolution reveals Gaussia luciferase variants with enhanced light output stability. *Anal Chem* **2013**, *85* (5), 3006-12.
41. Kim, S. B.; Suzuki, H.; Sato, M.; Tao, H., Superluminescent variants of marine luciferases for bioassays. *Anal Chem* **2011**, *83* (22), 8732-40.
42. Gaur, S.; Bhargava-Shah, A.; Hori, S.; Afjei, R.; Sekar, T. V.; Gambhir, S. S.; Massoud, T. F.; Paulmurugan, R., Engineering Intracellularly Retained Gaussia Luciferase Reporters for Improved Biosensing and Molecular Imaging Applications. *Acs Chem Biol* **2017**, *12* (9), 2345-2353.
43. Wurdinger, T.; Badr, C.; Pike, L.; de Kleine, R.; Weissleder, R.; Breakefield, X. O.; Tannous, B. A., A secreted luciferase for ex vivo monitoring of in vivo processes. *Nat Methods* **2008**, *5* (2), 171-3.
44. Park, S. Y.; Song, S. H.; Palmateer, B.; Pal, A.; Petersen, E. D.; Shall, G. P.; Welchko, R. M.; Ibata, K.; Miyawaki, A.; Augustine, G. J.; Hochgeschwender, U., Novel luciferase-opsin combinations for improved luminopsins. *J Neurosci Res* **2017**.
45. Berglund, K.; Clissold, K.; Li, H. F. E.; Wen, L.; Park, S. Y.; Gleixner, J.; Klein, M. E.; Lu, D. Y.; Barter, J. W.; Rossi, M. A.; Augustine, G. J.; Yin, H. H.; Hochgeschwender, U., Luminopsins integrate opto- and chemogenetics by using physical and biological light sources for opsin activation. *Proceedings of the National Academy of Sciences of the United States of America* **2016**, *113* (3), E358-E367.
46. Lindberg, E.; Mizukami, S.; Ibata, K.; Fukano, T.; Miyawaki, A.; Kikuchi, K., Development of cell-impermeable coelenterazine derivatives. *Chem Sci* **2013**, *4* (12), 4395-4400.
47. Shimomura, O.; Masugi, T.; Johnson, F. H.; Haneda, Y., Properties and reaction mechanism of the bioluminescence system of the deep-sea shrimp *Oplophorus gracilirostris*. *Biochemistry-U.S.* **1978**, *17* (6), 994-8.
48. Inouye, S.; Sasaki, S., Overexpression, purification and characterization of the catalytic component of *Oplophorus* luciferase in the deep-sea shrimp, *Oplophorus gracilirostris*. *Protein Expr Purif* **2007**, *56* (2), 261-8.
49. Hall, M. P.; Unch, J.; Binkowski, B. F.; Valley, M. P.; Butler, B. L.; Wood, M. G.; Otto, P.; Zimmerman, K.; Vidugiris, G.; Machleidt, T.; Robers, M. B.; Benink, H. A.; Eggers, C. T.; Slater, M. R.; Meisenheimer, P. L.; Klaubert, D. H.; Fan, F.; Encell, L. P.; Wood, K. V., Engineered Luciferase Reporter from a Deep Sea Shrimp Utilizing a Novel Imidazopyrazinone Substrate. *Acs Chem Biol* **2012**, *7* (11), 1848-1857.
50. Inouye, S.; Sato, J.; Sahara-Miura, Y.; Yoshida, S.; Kurakata, H.; Hosoya, T., C6-Deoxy coelenterazine analogues as an efficient substrate for glow luminescence reaction of nanoKAZ: The mutated catalytic 19 kDa component of *Oplophorus* luciferase. *Biochem Bioph Res Co* **2013**, *437* (1), 23-28.

51. Inouye, S.; Sato, J.; Sahara-Miura, Y.; Yoshida, S.; Hosoya, T., Luminescence enhancement of the catalytic 19 kDa protein (KAZ) of *Oplophorus* luciferase by three amino acid substitutions. *Biochem Biophys Res Commun* **2014**, *445* (1), 157-62.
52. England, C. G.; Ehlerding, E. B.; Cai, W. B., NanoLuc: A Small Luciferase Is Brightening Up the Field of Bioluminescence. *Bioconjugate Chem* **2016**, *27* (5), 1175-1187.
53. Goyet, E.; Bouquier, N.; Ollendorff, V.; Perroy, J., Fast and high resolution single-cell BRET imaging. *Sci Rep* **2016**, *6*, 28231.
54. Karlsson, E. A.; Meliopoulos, V. A.; Savage, C.; Livingston, B.; Mehle, A.; Schultz-Cherry, S., Visualizing real-time influenza virus infection, transmission and protection in ferrets. *Nat Commun* **2015**, *6*, 6378.
55. Shakhmin, A.; Hall, M. P.; Machleidt, T.; Walker, J. R.; Wood, K. V.; Kirkland, T. A., Coelenterazine analogues emit red-shifted bioluminescence with NanoLuc. *Org Biomol Chem* **2017**.
56. Chu, J.; Oh, Y.; Sens, A.; Ataie, N.; Dana, H.; Macklin, J. J.; Laviv, T.; Welf, E. S.; Dean, K. M.; Zhang, F.; Kim, B. B.; Tang, C. T.; Hu, M.; Baird, M. A.; Davidson, M. W.; Kay, M. A.; Fiolka, R.; Yasuda, R.; Kim, D. S.; Ng, H. L.; Lin, M. Z., A bright cyan-excitable orange fluorescent protein facilitates dual-emission microscopy and enhances bioluminescence imaging in vivo. *Nat Biotechnol* **2016**.
57. Suzuki, K.; Kimura, T.; Shinoda, H.; Bai, G.; Daniels, M. J.; Arai, Y.; Nakano, M.; Nagai, T., Five colour variants of bright luminescent protein for real-time multicolour bioimaging. *Nat Commun* **2016**, *7*, 13718.
58. Hiblot, J.; Yu, Q.; Sabbadini, M. D. B.; Reymond, L.; Xue, L.; Schena, A.; Sallin, O.; Hill, N.; Griss, R.; Johnsson, K., Luciferases with Tunable Emission Wavelengths. *Angew Chem Int Ed Engl* **2017**.
59. Dixon, A. S.; Schwinn, M. K.; Hall, M. P.; Zimmerman, K.; Otto, P.; Lubben, T. H.; Butler, B. L.; Binkowski, B. F.; Machleidt, T.; Kirkland, T. A.; Wood, M. G.; Eggers, C. T.; Encell, L. P.; Wood, K. V., NanoLuc Complementation Reporter Optimized for Accurate Measurement of Protein Interactions in Cells. *Acs Chem Biol* **2016**, *11* (2), 400-8.
60. Yano, H.; Cai, N. S.; Javitch, J. A.; Ferre, S., Luciferase complementation based-detection of G-protein-coupled receptor activity. *Biotechniques* **2018**, *65* (1), 9-14.
61. Schwinn, M. K.; Machleidt, T.; Zimmerman, K.; Eggers, C. T.; Dixon, A. S.; Hurst, R.; Hall, M. P.; Encell, L. P.; Binkowski, B. F.; Wood, K. V., CRISPR-Mediated Tagging of Endogenous Proteins with a Luminescent Peptide. *Acs Chem Biol* **2017**.
62. Ohmuro-Matsuyama, Y.; Ueda, H., Homogeneous Noncompetitive Luminescent Immunodetection of Small Molecules by Ternary Protein Fragment Complementation. *Anal Chem* **2018**, *90* (5), 3001-3004.
63. Kim, S. B.; Torimura, M.; Tao, H., Creation of Artificial Luciferases for Bioassays. *Bioconjugate Chem* **2013**, *24* (12), 2067-2075.
64. Nishihara, R.; Abe, M.; Nishiyama, S.; Citterio, D.; Suzuki, K.; Kim, S. B., Luciferase-Specific Coelenterazine Analogues for Optical Contamination-Free Bioassays. *Sci Rep* **2017**, *7* (1), 908.
65. Kim, S. B.; Nishihara, R.; Citterio, D.; Suzuki, K., Fabrication of a New Lineage of Artificial Luciferases from Natural Luciferase Pools. *Acs Combinatorial Science* **2017**, *19* (9), 594-599.
66. Nishihara, R.; Hoshino, E.; Kakudate, Y.; Kishigami, S.; Iwasawa, N.; Sasaki, S. I.; Nakajima, T.; Sato, M.; Nishiyama, S.; Citterio, D.; Suzuki, K.; Kim, S. B., Azide- and Dye-Conjugated Coelenterazine Analogues for a Multiplex Molecular Imaging Platform. *Bioconjug Chem* **2018**.
67. Andreu, N.; Zelmer, A.; Wiles, S., Noninvasive biophotonic imaging for studies of infectious disease. *FEMS Microbiol Rev* **2011**, *35* (2), 360-94.

68. Close, D. M.; Patterson, S. S.; Ripp, S.; Baek, S. J.; Sanseverino, J.; Saylor, G. S., Autonomous bioluminescent expression of the bacterial luciferase gene cassette (*lux*) in a mammalian cell line. *Plos One* **2010**, 5 (8), e12441.
69. Gregor, C.; Gwosch, K. C.; Sahl, S. J.; Hell, S. W., Strongly enhanced bacterial bioluminescence with the *ilux* operon for single-cell imaging. *Proceedings of the National Academy of Sciences of the United States of America* **2018**, 115 (5), 962-967.
70. Thompson, E. M.; Nagata, S.; Tsuji, F. I., Cloning and expression of cDNA for the luciferase from the marine ostracod *Vargula hilgendorfii*. *Proceedings of the National Academy of Sciences of the United States of America* **1989**, 86 (17), 6567-71.
71. Maguire, C. A.; Bovenberg, M. S.; Crommentuijn, M. H.; Niers, J. M.; Kerami, M.; Teng, J.; Sena-Esteves, M.; Badr, C. E.; Tannous, B. A., Triple bioluminescence imaging for in vivo monitoring of cellular processes. *Mol Ther Nucleic Acids* **2013**, 2, e99.
72. Purtov, K. V.; Petushkov, V. N.; Baranov, M. S.; Mineev, K. S.; Rodionova, N. S.; Kaskova, Z. M.; Tsarkova, A. S.; Petunin, A. I.; Bondar, V. S.; Rodicheva, E. K.; Medvedeva, S. E.; Oba, Y.; Oba, Y.; Arseniev, A. S.; Lukyanov, S.; Gitelson, J. I.; Yampolsky, I. V., The Chemical Basis of Fungal Bioluminescence. *Angew Chem Int Ed Engl* **2015**, 54 (28), 8124-8.
73. Kaskova, Z. M.; Dorr, F. A.; Petushkov, V. N.; Purtov, K. V.; Tsarkova, A. S.; Rodionova, N. S.; Mineev, K. S.; Guglya, E. B.; Kotlobay, A.; Baleeva, N. S.; Baranov, M. S.; Arseniev, A. S.; Gitelson, J. I.; Lukyanov, S.; Suzuki, Y.; Kanie, S.; Pinto, E.; Di Mascio, P.; Waldenmaier, H. E.; Pereira, T. A.; Carvalho, R. P.; Oliveira, A. G.; Oba, Y.; Bastos, E. L.; Stevani, C. V.; Yampolsky, I. V., Mechanism and color modulation of fungal bioluminescence. *Sci Adv* **2017**, 3 (4), e1602847.
74. Kotlobay, A. A.; Sarkisyan, K. S.; Mokrushina, Y. A.; Marcet-Houben, M.; Serebrovskaya, E. O.; Markina, N. M.; Gonzalez Somermeyer, L.; Gorokhovatsky, A. Y.; Vvedensky, A.; Purtov, K. V.; Petushkov, V. N.; Rodionova, N. S.; Chepurnyh, T. V.; Fakhranurova, L. I.; Guglya, E. B.; Ziganshin, R.; Tsarkova, A. S.; Kaskova, Z. M.; Shender, V.; Abakumov, M.; Abakumova, T. O.; Povolotskaya, I. S.; Eroshkin, F. M.; Zaraisky, A. G.; Mishin, A. S.; Dolgov, S. V.; Mitiouchkina, T. Y.; Kopantzev, E. P.; Waldenmaier, H. E.; Oliveira, A. G.; Oba, Y.; Barsova, E.; Bogdanova, E. A.; Gabaldon, T.; Stevani, C. V.; Lukyanov, S.; Smirnov, I. V.; Gitelson, J. I.; Kondrashov, F. A.; Yampolsky, I. V., Genetically encodable bioluminescent system from fungi. *Proceedings of the National Academy of Sciences of the United States of America* **2018**, 115 (50), 12728-12732.
75. Yeh, H. W.; Karmach, O.; Ji, A.; Carter, D.; Martins-Green, M. M.; Ai, H. W., Red-shifted luciferase-luciferin pairs for enhanced bioluminescence imaging. *Nat Methods* **2017**, 14 (10), 971-974.
76. Troy, T.; Jekic-McMullen, D.; Sambucetti, L.; Rice, B., Quantitative comparison of the sensitivity of detection of fluorescent and bioluminescent reporters in animal models. *Mol Imaging* **2004**, 3 (1), 9-23.
77. Morton, C. L.; Houghton, P. J., Establishment of human tumor xenografts in immunodeficient mice. *Nat Protoc* **2007**, 2 (2), 247-250.
78. Luo, J.; Lin, A. H.; Masliah, E.; Wyss-Coray, T., Bioluminescence imaging of Smad signaling in living mice shows correlation with excitotoxic neurodegeneration. *Proceedings of the National Academy of Sciences of the United States of America* **2006**, 103 (48), 18326-18331.
79. Kuchimaru, T.; Kataoka, N.; Nakagawa, K.; Isozaki, T.; Miyabara, H.; Minegishi, M.; Kadonosono, T.; Kizaka-Kondoh, S., A reliable murine model of bone metastasis by injecting cancer cells through caudal arteries. *Nat Commun* **2018**, 9 (1), 2981.
80. Fan, F.; Wood, K. V., Bioluminescent assays for high-throughput screening. *Assay Drug Dev Techn* **2007**, 5 (1), 127-136.

81. Dacres, H.; Wang, J.; Dumancic, M. M.; Trowell, S. C., Experimental Determination of the Forster Distance for Two Commonly Used Bioluminescent Resonance Energy Transfer Pairs. *Anal Chem* **2010**, *82* (1), 432-435.
82. Sun, S. H.; Yang, X. B.; Wang, Y.; Shen, X. H., In Vivo Analysis of Protein-Protein Interactions with Bioluminescence Resonance Energy Transfer (BRET): Progress and Prospects. *Int J Mol Sci* **2016**, *17* (10).
83. De, A., The new era of bioluminescence resonance energy transfer technology. *Curr Pharm Biotechnol* **2011**, *12* (4), 558-68.
84. Binkowski, B.; Fan, F.; Wood, K., Engineered luciferases for molecular sensing in living cells. *Curr Opin Biotechnol* **2009**, *20* (1), 14-8.
85. Rodriguez, E. A.; Campbell, R. E.; Lin, J. Y.; Lin, M. Z.; Miyawaki, A.; Palmer, A. E.; Shu, X.; Zhang, J.; Tsien, R. Y., The Growing and Glowing Toolbox of Fluorescent and Photoactive Proteins. *Trends Biochem Sci* **2017**, *42* (2), 111-129.
86. Arai, R.; Nakagawa, H.; Kitayama, A.; Ueda, H.; Nagamune, T., Detection of protein-protein interaction by bioluminescence resonance energy transfer from firefly luciferase to red fluorescent protein. *J Biosci Bioeng* **2002**, *94* (4), 362-4.
87. Branchini, B. R.; Rosenberg, J. C.; Ablamsky, D. M.; Taylor, K. P.; Southworth, T. L.; Linder, S. J., Sequential bioluminescence resonance energy transfer-fluorescence resonance energy transfer-based ratiometric protease assays with fusion proteins of firefly luciferase and red fluorescent protein. *Anal Biochem* **2011**, *414* (2), 239-45.
88. Kim, G. B.; Kim, Y. P., Analysis of Protease Activity Using Quantum Dots and Resonance Energy Transfer. *Theranostics* **2012**, *2* (2), 127-138.
89. De, A.; Ray, P.; Loening, A. M.; Gambhir, S. S., BRET3: a red-shifted bioluminescence resonance energy transfer (BRET)-based integrated platform for imaging protein-protein interactions from single live cells and living animals. *Faseb Journal* **2009**, *23* (8), 2702-2709.
90. Dragulescu-Andrasi, A.; Chan, C. T.; De, A.; Massoud, T. F.; Gambhir, S. S., Bioluminescence resonance energy transfer (BRET) imaging of protein-protein interactions within deep tissues of living subjects. *Proceedings of the National Academy of Sciences of the United States of America* **2011**, *108* (29), 12060-5.
91. Compan, V.; Baroja-Mazo, A.; Bragg, L.; Verkhatsky, A.; Perroy, J.; Pelegrin, P., A genetically encoded IL-1 β bioluminescence resonance energy transfer sensor to monitor inflammasome activity. *J Immunol* **2012**, *189* (5), 2131-7.
92. Carriba, P.; Navarro, G.; Ciruela, F.; Ferre, S.; Casado, V.; Agnati, L.; Cortes, A.; Mallol, J.; Fuxe, K.; Canela, E. I.; Lluís, C.; Franco, R., Detection of heteromerization of more than two proteins by sequential BRET-FRET. *Nat Methods* **2008**, *5* (8), 727-733.
93. Navarro, G.; Carriba, P.; Gandia, J.; Ciruela, F.; Casado, V.; Cortes, A.; Mallol, J.; Canela, E. I.; Lluís, C.; Franco, R., Detection of heteromers formed by cannabinoid CB1, dopamine D2, and adenosine A2A G-protein-coupled receptors by combining bimolecular fluorescence complementation and bioluminescence energy transfer. *ScientificWorldJournal* **2008**, *8*, 1088-97.
94. Urizar, E.; Yano, H.; Kolster, R.; Gales, C.; Lambert, N.; Javitch, J. A., CODA-BRET reveals functional selectivity as a result of GPCR heteromerization. *Nat Chem Biol* **2011**, *7* (9), 624-630.
95. Zhang, L. Y.; Xu, F.; Chen, Z. X.; Zhu, X. X.; Min, W., Bioluminescence Assisted Switching and Fluorescence Imaging (BASFI). *J Phys Chem Lett* **2013**, *4* (22), 3897-3902.
96. Perroy, J.; Pontier, S.; Charest, P. G.; Aubry, M.; Bouvier, M., Real-time monitoring of ubiquitination in living cells by BRET. *Nat Methods* **2004**, *1* (3), 203-8.
97. Jiang, L. I.; Collins, J.; Davis, R.; Lin, K. M.; DeCamp, D.; Roach, T.; Hsueh, R.; Rebres, R. A.; Ross, E. M.; Taussig, R.; Fraser, I.; Sternweis, P. C., Use of a cAMP BRET sensor to characterize a novel regulation of cAMP by the sphingosine 1-phosphate/G(13) pathway. *J Biol Chem* **2007**, *282* (14), 10576-10584.

98. Biswas, K. H.; Sopory, S.; Visweswariah, S. S., The GAF domain of the cGMP-Binding, cGMP-specific phosphodiesterase (PDE5) is a sensor and a sink for cGMP. *Biochemistry-Ug* **2008**, *47* (11), 3534-3543.
99. Saito, K.; Hatsugai, N.; Horikawa, K.; Kobayashi, K.; Matsu-ura, T.; Mikoshiba, K.; Nagai, T., Auto-Luminescent Genetically-Encoded Ratiometric Indicator for Real-Time Ca²⁺ Imaging at the Single Cell Level. *Plos One* **2010**, *5* (3).
100. Yoshida, T.; Kakizuka, A.; Imamura, H., BTeam, a Novel BRET-based Biosensor for the Accurate Quantification of ATP Concentration within Living Cells. *Sci Rep* **2016**, *6*, 39618.
101. Saito, K.; Chang, Y. F.; Horikawa, K.; Hatsugai, N.; Higuchi, Y.; Hashida, M.; Yoshida, Y.; Matsuda, T.; Arai, Y.; Nagai, T., Luminescent proteins for high-speed single-cell and whole-body imaging. *Nat Commun* **2012**, *3*, 1262.
102. Yang, J.; Cumberbatch, D.; Centanni, S.; Shi, S. Q.; Winder, D.; Webb, D.; Johnson, C. H., Coupling optogenetic stimulation with NanoLuc-based luminescence (BRET) Ca⁺⁺ sensing. *Nat Commun* **2016**, *7*, 13268.
103. Hossain, M. N.; Suzuki, K.; Iwano, M.; Matsuda, T.; Nagai, T., Bioluminescent Low-Affinity Ca(2+) Indicator for ER with Multicolor Calcium Imaging in Single Living Cells. *Acs Chem Biol* **2018**.
104. Inagaki, S.; Tsutsui, H.; Suzuki, K.; Agetsuma, M.; Arai, Y.; Jinno, Y.; Bai, G.; Daniels, M. J.; Okamura, Y.; Matsuda, T.; Nagai, T., Genetically encoded bioluminescent voltage indicator for multi-purpose use in wide range of bioimaging. *Sci Rep-Uk* **2017**, *7*.
105. Van Gasse, A. L.; Mangodt, E. A.; Faber, M.; Sabato, V.; Bridts, C. H.; Ebo, D. G., Molecular allergy diagnosis: status anno 2015. *Clin Chim Acta* **2015**, *444*, 54-61.
106. Arts, R.; den Hartog, I.; Zijlema, S. E.; Thijssen, V.; van der Beelen, S. H. E.; Merkx, M., Detection of Antibodies in Blood Plasma Using Bioluminescent Sensor Proteins and a Smartphone. *Anal Chem* **2016**, *88* (8), 4525-4532.
107. van Rosmalen, M.; Ni, Y.; Vervoort, D. F. M.; Arts, R.; Ludwig, S. K. J.; Merkx, M., Dual-Color Bioluminescent Sensor Proteins for Therapeutic Drug Monitoring of Antitumor Antibodies. *Anal Chem* **2018**, *90* (5), 3592-3599.
108. Arts, R.; Ludwig, S. K. J.; van Gerven, B. C. B.; Estirado, E. M.; Milroy, L. G.; Merkx, M., Semisynthetic Bioluminescent Sensor Proteins for Direct Detection of Antibodies and Small Molecules in Solution. *ACS Sens* **2017**, *2* (11), 1730-1736.
109. Hochreiter, B.; Pardo-Garcia, A.; Schmid, J. A., Fluorescent Proteins as Genetically Encoded FRET Biosensors in Life Sciences (vol 15, pg 26281, 2015). *Sensors-Basel* **2015**, *15* (11), 29182-29182.
110. Komatsu, N.; Terai, K.; Imanishi, A.; Kamioka, Y.; Sumiyama, K.; Jin, T.; Okada, Y.; Nagai, T.; Matsuda, M., A platform of BRET-FRET hybrid biosensors for optogenetics, chemical screening, and in vivo imaging. *Sci Rep* **2018**, *8* (1), 8984.
111. Chabosseau, P.; Tuncay, E.; Meur, G.; Bellomo, E. A.; Hessels, A.; Hughes, S.; Johnson, P. R.; Bugliani, M.; Marchetti, P.; Turan, B.; Lyon, A. R.; Merkx, M.; Rutter, G. A., Mitochondrial and ER-targeted eCALWY probes reveal high levels of free Zn²⁺. *Acs Chem Biol* **2014**, *9* (9), 2111-20.
112. Hessels, A. M.; Chabosseau, P.; Bakker, M. H.; Engelen, W.; Rutter, G. A.; Taylor, K. M.; Merkx, M., eZinCh-2: A Versatile, Genetically Encoded FRET Sensor for Cytosolic and Intraorganelle Zn²⁺ Imaging. *Acs Chem Biol* **2015**, *10* (9), 2126-2134.
113. Aper, S. J. A.; Dierickx, P.; Merkx, M., Dual Readout BRET/FRET Sensors for Measuring Intracellular Zinc. *Acs Chem Biol* **2016**, *11* (10), 2854-2864.
114. Qian, Y.; Rancic, V.; Wu, J.; Ballanyi, K.; Campbell, R. E., A bioluminescent Ca²⁺ indicator based on a topological variant of GCaMP6s. *Chembiochem* **2018**.
115. Xue, L.; Prifti, E.; Johnsson, K., A General Strategy for the Semisynthesis of Ratiometric Fluorescent Sensor Proteins with Increased Dynamic Range. *Journal of the American Chemical Society* **2016**, *138* (16), 5258-61.

116. Keppler, A.; Gendreizig, S.; Gronemeyer, T.; Pick, H.; Vogel, H.; Johnsson, K., A general method for the covalent labeling of fusion proteins with small molecules in vivo. *Nat Biotechnol* **2003**, *21* (1), 86-9.
117. Gautier, A.; Juillerat, A.; Heinis, C.; Correa, I. R., Jr.; Kindermann, M.; Beaufils, F.; Johnsson, K., An engineered protein tag for multiprotein labeling in living cells. *Chem Biol* **2008**, *15* (2), 128-36.
118. Los, G. V.; Encell, L. P.; McDougall, M. G.; Hartzell, D. D.; Karassina, N.; Zimprich, C.; Wood, M. G.; Learish, R.; Ohana, R. F.; Urh, M.; Simpson, D.; Mendez, J.; Zimmerman, K.; Otto, P.; Vidugiris, G.; Zhu, J.; Darzins, A.; Klauert, D. H.; Bulleit, R. F.; Wood, K. V., HaloTag: a novel protein labeling technology for cell imaging and protein analysis. *Acs Chem Biol* **2008**, *3* (6), 373-82.
119. Griss, R.; Schena, A.; Reymond, L.; Patiny, L.; Werner, D.; Tinberg, C. E.; Baker, D.; Johnsson, K., Bioluminescent sensor proteins for point-of-care therapeutic drug monitoring. *Nat Chem Biol* **2014**, *10* (7), 598-603.
120. Xue, L.; Yu, Q.; Griss, R.; Schena, A.; Johnsson, K., Bioluminescent Antibodies for Point-of-Care Diagnostics. *Angew Chem Int Ed Engl* **2017**, *56* (25), 7112-7116.
121. Schena, A.; Griss, R.; Johnsson, K., Modulating protein activity using tethered ligands with mutually exclusive binding sites. *Nature Communications* **2015**, *6*.
122. Lindberg, E.; Angerani, S.; Anzola, M.; Winssinger, N., Luciferase-induced photoreductive uncaging of small-molecule effectors. *Nat Commun* **2018**, *9* (1), 3539.
123. Yu, Q. Y.; Xue, L.; Hiblot, J.; Griss, R.; Fabritz, S.; Roux, C.; Binz, P. A.; Haas, D.; Okun, J. G.; Johnsson, K., Semisynthetic sensor proteins enable metabolic assays at the point of care. *Science* **2018**, *361* (6407), 1122-1125.

Chapter 2

Engineering of Red-shifted Luciferase-luciferin pairs for Enhanced Bioluminescence Imaging

Abstract

Bioluminescence has broad applications in bioassays, optical imaging, and drug discovery. *In vitro* and *in cellulo* studies prefer luciferase-luciferin pairs with high quantum efficiencies and fast enzyme turnovers which subsequently result in high photon fluxes for optimal detection, whereas *in vivo* bioluminescence imaging further favors emission in the near-infrared (NIR) optical window because NIR photons can travel far in biological tissues. Currently, no luciferase-luciferin pair combines all these advantageous features; in order to maximize the performance, one has to use different luciferase-luciferin pairs for *in vitro* and *in vivo* studies. Herein, we report novel luciferase-luciferin pairs based on synthetic coelenterazine analogs and correspondingly re-engineered luciferases. Because of the enhanced photon flux and red-shifted emission, one of our new reporters outperforms other common bioluminescent proteins, such as firefly luciferase (FLuc) and NanoLuc, under all tested conditions from assays based on proteins, intact cells, and cell lysates to *in vivo* bioluminescence imaging at superficial sites and in deep tissues of live mice. Our work has provided a novel luciferase-luciferin pair with superior sensitivity to streamline bioluminescence applications both *in vitro* and *in vivo*.

2.1. Introduction

The process of bioluminescence involves a production of excited states for light emission *via* enzyme (luciferase)-catalyzed oxidation of small-molecule substrates (luciferins).¹ Due to the low autoluminescence of typical samples and a superior signal-to-background ratio resulting from this, there is enormous interest in harnessing bioluminescence for ultrasensitive bioassays, drug screening, and *in vivo* imaging of biological processes from molecular and cellular levels to tissue and whole-body scales.²⁻⁵ In contrast to fluorescent reporters whose emission intensities are proportional to the amplitude of incident excitation, the photon fluxes of bioluminescent reporters are determined by the quantum efficiencies and catalytic rates of bioluminescence reactions. Although the quantum efficiencies of some luciferase reactions are comparable to the quantum efficiencies of common fluorescent reporters (e.g. the *Photinus pyralis* firefly luciferase (FLuc)/D-luciferin pair has a quantum efficiency of 0.41),⁶ their slow catalytic rates often result in bioluminescence emission several orders of magnitude lower than that of fluorescence.⁷ To enhance the sensitivity and spatiotemporal resolution of bioluminescence measurements, there is an urgent need for brighter bioluminescent reporters. One of the most exciting advances in recent years was the engineering of NanoLuc luciferase from a naturally occurring, coelenterazine (CTZ, **Figure. 1a**)-utilizing, deep-sea shrimp *Oplophorus gracilirostris* luciferase (OLuc).⁸ Because of the unusually high catalytic rate of NanoLuc toward a synthetic furimazine substrate (**Figure. 1b**), the *in vitro* brightness of the blue-emitting NanoLuc is way above that of the most popular bioluminescent reporters such as FLuc and *Renilla* luciferase (RLuc).⁸

Despite excellent results gained with NanoLuc/furimazine *in vitro* and *in cellulo*, the performance of this pair *in vivo*, particularly in deep tissues, is limited compared to that of FLuc/D-luciferin, which has peak emission at 563 nm under physiological pH (7.4).⁹ For *in vivo* imaging, bioluminescence emission between 600 and 900 nm,

namely a near-infrared (NIR) optical window, are highly preferred, because mammalian tissues are minimally absorptive in this spectral region and red photons are also less likely to scatter than blue photons.¹⁰⁻¹¹ FLuc/D-luciferin, for which a significant portion of emission is above 600 nm, remains to be one of the best choices for deep-tissue bioluminescence imaging.¹² Recently, both FLuc and D-luciferin have been engineered for redder emission, but the spectral shift is often penalized by a substantially reduced total intensity.¹³⁻¹⁷ Therefore, most derivatives of FLuc and D-luciferin failed to show improvement in terms of *in vitro* or *in vivo* detection sensitivity.¹⁸ Only a very few examples, such as the synthetic D-luciferin analogues CycLuc1 and AkaLumine-HCl,¹⁹⁻²⁰ have been shown to enhance the *in vivo* bioluminescence of FLuc at certain concentration ranges, despite that the corresponding *in vitro* bioluminescence was significantly lower than that of FLuc/D-luciferin.^{17, 20-21} To date, no single bioluminescent reporter is available to give the highest sensitivity both *in vitro* and *in vivo*.

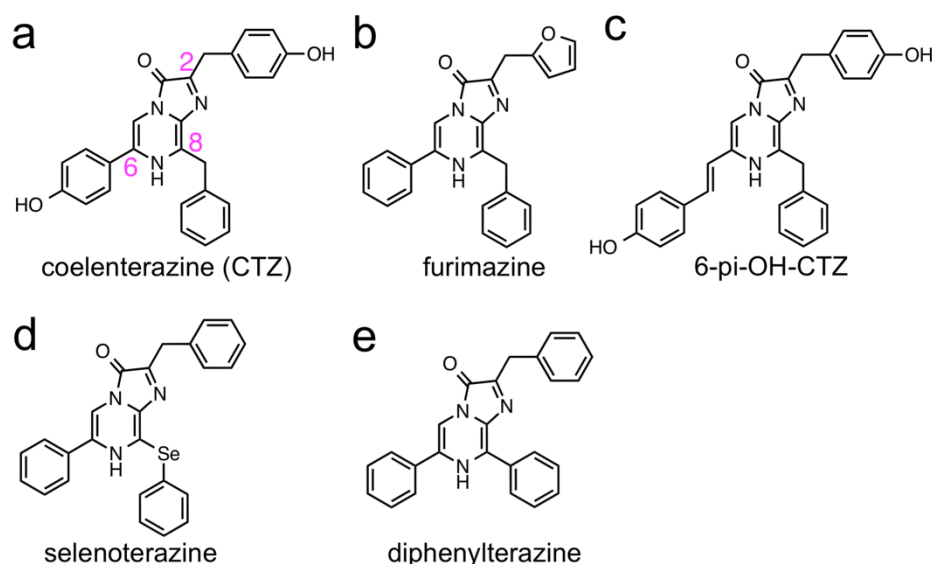


Figure 1. Chemical structures of coelenterazine (CTZ) and CTZ analogs.

It can be reasoned that an improved luciferase-luciferin pair may be derived by red-shifting the bioluminescence of NanoLuc, and at the same time, retaining its high catalytic activity and quantum efficiency. Several early studies reported red-shifted CTZ analogs for OLuc, the ancestor protein of NanoLuc²²⁻²³; however, the intensities were low and it was unknown whether the spectral shift for OLuc could be extended to NanoLuc. A few additional studies tested NanoLuc with synthetic CTZ analogs, but no significantly red-shifted bioluminescence has been noted.²⁴⁻²⁶ More recently, NanoLuc has been genetically linked to a bright cyan-excitable orange fluorescent protein for bioluminescence resonance energy transfer (BRET) and the resulting fusion protein “Antares”, in spite of its reduced overall brightness, improved bioluminescence detection in mammalian tissues.²⁷ Here we present novel luciferase-luciferin pairs based on synthetic CTZ analogs and correspondingly re-engineered NanoLuc luciferase mutants for highly bright, substantially red-shifted bioluminescence. Although the emission peaks of our new reporters are still below 600 nm, because of their high brightness, they emit considerably more photons above 600 nm than FLuc/D-luciferin.

2.2. Experimental section

2.2.1. Material and methods

Synthetic DNA oligonucleotides were purchased from Integrated DNA Technologies (San Diego, CA). Restriction endonucleases were purchased from Thermo Scientific Fermentas (Vilnius, Lithuania). Accura high-fidelity DNA polymerase and EconoTaq DNA polymerase were purchased from Lucigen (Middleton, WI). Products of PCR and restriction digestion were purified using gel electrophoresis and Syd Laboratories Gel Extraction columns (Malden, MA). Plasmid DNA was purified using Syd Laboratories Miniprep columns (Malden, MA). DNA sequences were analyzed by Retrogen (San

Diego, CA). D-Luciferin was purchased from Thermo Fisher Scientific. Furimazine was purchased from Promega. All other chemicals were purchased from Sigma-Aldrich (St. Louis, MO), Fisher Scientific (Hampton, NH), or VWR (Radnor, PA), and used without further purification. Varian Inova 500 with a 5-mm triple resonance ($^1\text{H}/^{13}\text{C}/^{15}\text{N}$) triple axis gradient probe at the UCR ACIF NMR Facility was used to record all NMR spectra. Chemical shift (δ) is given in parts per million relative to ^1H : 7.24 ppm and ^{13}C : 77.23 ppm for CDCl_3 ; and ^1H : 2.50 ppm and ^{13}C : 39.5 ppm for DMSO-d_6 . Splitting patterns are reported as s (singlet), bs (broad singlet), d (doublet), t (triplet), dd (doublet of doublets), m (multiplet). Coupling constant (J) was given in Hz. ESI-MS was run on an Agilent LC-TOF system by direct infusion. A Gilson PLC 2020 Purification System coupled with Agela Venusil XBP C18 HPLC Columns (10 μM , 100 \AA , 10*150mm) was used for preparative reverse-phase HPLC purifications. BALB/c mice obtained from the Jackson Laboratory (Cat. # 000651) were used to conduct the *in vivo* experiments.

2.2.2. Synthesis of diphenylterazine and selenoterazine

di-tert-butyl (5-bromo-3-iodopyrazin-2-yl)carbamate (2): To a solution of 2-amino-5-bromopyrazine (**1**, 5g, 28.7 mmol) in acetonitrile (50 mL) were added trifluoroacetic acid (1.1 mL, 14.3 mmol) and *N*-iodosuccinimide (NIS, 7.76g, 34.5 mmol) at 0 °C. The mixture was stirred at reflux for 18 h under N_2 . After cooling to room temperature, the solvent was removed under reduced pressure. The residue was extracted with 50 mL ethyl acetate, neutralized and washed twice with saturated aq. NaHCO_3 (50 mL), dried with anhydrous Na_2SO_4 , filtered, and concentrated to give black residue. The crude was next dissolved in dry THF (50 mL), to which was added Boc_2O (13.78g, 63.1 mmol) and triethylamine (12.1 mL, 86.2 mmol). The mixture was stirred under N_2 for additional 5 h. The progress of the reaction was monitored with TLC (hexane/ethyl acetate = 3:1). After completion of the transformation, MeOH (10 mL) was added to quench the reaction. The solvent was removed under reduced pressure. The residue was purified

using column chromatography (silica gel; gradient elution with hexane/ethyl acetate from 20:1 to 5:1) to give compound **2** as white solid (9.7 g, 85% over two steps). $^1\text{H-NMR}$ (CDCl_3 , 500 MHz): δ 8.46 (s, 1H), 1.41 (s, 18H); $^{13}\text{C-NMR}$ (CDCl_3 , 125 MHz) δ 151.3, 149.0, 144.6, 136.8, 119.0, 84.7, 28.0; ESI-MS ($\text{C}_{14}\text{H}_{19}\text{BrIN}_3\text{O}_4$): $[\text{M}+\text{Na}]^+$ calcd: 521.96, found: 521.95.

tert-butyl (5-bromo-3-(phenylselanyl)pyrazin-2-yl)carbamate (3): To a mixture of Cu_2O (155 mg, 1.08 mmol), magnesium granule (196 mg, 8.16 mmol), 2,2'-bipyridine (0.34 g, 2.2 mmol) in dry DMF (20 mL) were added compound **2** (2.7g, 5.4 mmol) and diphenyl diselenide (0.9 g, 2.9 mmol). The mixture was stirred at 85 °C under N_2 for 6 h. After removing solvent *in vacuo*, the residue was dissolved in minimum CH_2Cl_2 and next purified with column chromatography (silica gel; hexane/ethyl acetate = 4:1) to give compound **3** (1.18 g, 51%) as yellow oil. $^1\text{H-NMR}$ (CDCl_3 , 500 MHz) δ 7.95 (s, 1H), 7.49 (dd, 2H, $J = 8.0, 1.2$ Hz), 7.26 (t, 3H, $J = 8.0$ Hz), 1.47 (s, 9H); $^{13}\text{C-NMR}$ (CDCl_3 , 125 MHz) δ 151.6, 148.6, 145.0, 141.5, 135.8, 135.1, 129.7, 127.7, 127.2, 84.2, 28.3; ESI-MS ($\text{C}_{15}\text{H}_{16}\text{BrN}_3\text{O}_2\text{Se}$): $[\text{M}+\text{Na}]^+$ calcd: 451.96, found: 451.91.

5-phenyl-3-(phenylselanyl)pyrazin-2-amine (5): To a solution of compound **3** (500 mg, 1.17 mmol) in CH_2Cl_2 (5 mL) was added trifluoroacetic acid (5 mL). After stirring at RT for 30 min, the reaction was diluted with 50 mL CH_2Cl_2 , and neutralize with saturated aq. NaHCO_3 . The organic layer was isolated, washed twice with saturated aq. NaHCO_3 (30 mL) and brine (30 mL), dried over anhydrous Na_2SO_4 , filtered, and concentrated to give the crude compound **4**, which was next dissolved in 2 mL EtOH for later use without further purification. In another round-bottle flask, 1,4-bis(diphenylphosphino)butane (BDPB, 30 mg, 0.07 mmol) was added to a suspension of bis(benzonitrile)dichloro palladium (23 mg, 0.06 mmol) in toluene (3 mL), and the mixture was stirred at RT under N_2 for 30 min. Next, to the solution of compound **4** in

EtOH, phenylboronic acid (172 mg, 1.4 mmol), 1.0 M aq. Na₂CO₃ (1 mL), toluene (8 mL), and the mixture of BDPB and bis(benzonitrile)dichloro palladium in toluene were added sequentially. The mixture was maintained at reflux under N₂ for 12 h. The progress of the reaction was monitored by TLC (hexane/ethyl acetate = 2:1). Next, the mixture was cooled down to RT, and the solvent was removed *in vacuo*. The residue was extracted with ethyl acetate (30 mL), which was washed twice with water (30 mL), dried over anhydrous Na₂SO₄, and concentrated *in vacuo*. The residue was next purified with column chromatography (silica gel; gradient elution with hexane/ethyl acetate from 4:1 to 2:1) to give compound **5** (209 mg, 55%). Compound **6** (37 mg, 13%) was also isolated as a by-product. ¹H-NMR (CDCl₃, 500 MHz) δ 8.21 (s, 1H), 7.71 (dd, 2H, J = 8.5, 1.5 Hz), 7.61 (dd, 2H, J = 7.5, 1.5 Hz), 7.38-7.33 (m, 6H), 5.77 (bs, 2H); ¹³C-NMR (CDCl₃, 125 MHz) δ 151.2, 143.3, 139.2, 135.7, 134.8, 134.7, 132.61, 129.9, 129.8, 129.0, 126.8, 125.7 ppm; ESI-MS (C₁₆H₁₃N₃Se): [M+H]⁺ calcd: 328.02; found: 328.05.

selenoterazine (7): To a solution of compound **5** (50 mg, 0.153 mmol) and 1,1-diethoxy-3-phenylacetone (51 mg, 0.23 mmol) in degassed EtOH (2 mL) was added 6 N HCl (0.3 mL) under continuous N₂ flow. The reaction flask was wrapped in aluminum foil and heated to 80 °C with stirring for 12 h. The mixture was cooled down to RT. Solvent was removed *in vacuo*, and the residue was re-dissolved in 1 mL acetonitrile, which was next purified using preparative RP-HPLC (acetonitrile/water = 30:70 to 98:2, 2 mL/min, UV 254 nm). Product fractions were combined and lyophilized to give selenoterazine (15.5 mg, 22%). The compound has to be stored as solid at -80 °C for long-term stability. ¹H-NMR (DMSO-d₆, 500 MHz) δ 7.98 (s, 1H), 7.57 (d, 2H, J = 8.5 Hz), 7.41 (d, 2H, J = 7.5), 7.35-7.26 (m, 11H), 4.05 (s, 2H); ¹³C-NMR (DMSO-d₆, 125 MHz) δ 139.7, 136.0, 134.2, 132.8, 131.7, 129.3, 129.1, 128.8, 128.5,

128.3, 127.7, 126.0, 114.9, 31.9; ESI-MS ($C_{25}H_{19}N_3OSe$): $[M+H]^+$ calcd: 458.07, found: 458.08.

2-amino-3,5-diphenylpyrazine (6): 1,4-Bis(diphenylphosphino)butane (BDPB, 30 mg, 0.07 mmol) was added to a suspension of bis(benzonitrile)dichloro palladium (23 mg, 0.06 mmol) in toluene (3 mL) and the mixture was stirred at RT for 30 min under N_2 . To this mixture were sequentially added compound **9** (303 mg, 1.2 mmol) in EtOH (2 mL), phenylboronic acid (318 mg, 2.6 mmol), 1.0 M aq. Na_2CO_3 (1 mL) and toluene (8 mL). The mixture was heated under reflux for 8 h. After cooling down to RT, the solvent was removed under reduced pressure. The residue was extracted with ethyl acetate (30 mL), which was washed twice with water (30 mL), dried over Na_2SO_4 , and concentrated on rotary evaporator. The residue was purified with column chromatography (silica gel; gradient elution with hexane/ethyl acetate from 4:1 to 2:1) to give compound **6** (193mg, 66%). 1H NMR ($CDCl_3$) δ 8.55 (s, 1H), 7.95 (d, 2H, $J = 10.0$ Hz), 7.78 (m, 2H), 7.47-7.24 (m, 6H), 5.21 (s, 2H) ppm; HRMS (ESI-TOF) calcd for $C_{16}H_{13}N_3$ $[M + H]^+$: 248.11, found: m/z 248.12.

diphenylterazine (8): To a solution of compound **6** (50 mg, 0.2 mmol) and 1,1-diethoxy-3-phenylacetone (67mg, 0.3 mmol) in degassed EtOH (3 mL) was added 6 N HCl (0.3 mL) under continuous N_2 flow. The reaction flask was wrapped with aluminum foil and heated at 80 °C with stirring for 6 h. The mixture was cooled down to room temperature, before the solvent was removed *in vacuo*. The residue was re-dissolved in 1 mL acetonitrile, which was next purified with preparative RP-HPLC (acetonitrile/water = 30:70 to 98:2, 2 mL/min, UV 254 nm). Product fractions were combined and lyophilized to give diphenylterazine (26.7mg, 35%). The compound has to be stored as solid at -80 °C for long-term stability. 1H -NMR ($DMSO-d_6$, 500 MHz) δ 9.54 (s, 1H), 8.16 (d, 2H, $J = 7.0$ Hz), 7.57 (d, 2H, $J = 7.5$ Hz), 7.53 (d, 2H, $J = 7.0$

Hz), 7.33-7.24 (m, 9H), 4.17 (s, 2H) ppm; $^{13}\text{C-NMR}$ (DMSO- d_6 , 125 MHz) δ 139.9, 136.0, 134.0, 130.5, 130.2, 129.8, 129.3, 128.8, 128.5, 128.3, 128.2, 127.8, 127.3, 126.3, 125.9, 32.0 ppm; HRMS (ESI-TOF) calcd for $\text{C}_{25}\text{H}_{19}\text{N}_3\text{O}$ [$M - H$] $^-$: 376.15, found: m/z 376.14.

2.2.3 Construction of plasmids and libraries.

Polymerase chain reactions (PCR) were used to amplify all genetic elements with various synthetic oligonucleotide pairs (see **Table 2**). The gene for NanoLuc was purchased from Integrated DNA Technologies as a gBlock, and further amplified with oligos XhoI-NL-F and NL-R-HindIII. To create a gene library with randomization at residues 44, 45 and 138, oligo pairs XhoI-NL-F and I44I54-NNK-R, I44I54-NNK-F and I138-NNK-R, and I138-NNK-F and NL-R-HindIII were utilized to amplify three individual fragments from NanoLuc. The resultant three fragments were purified by agarose gel electrophoresis and utilized as templates for assembly in subsequent PCR reactions by using oligos XhoI-NL-F and NL-R-HindIII. The assembled full-length fragment was next digested with Xho I and Hind III restriction enzymes, and ligated into a predigested compatible pBAD/His B plasmid (Life Technologies, Carlsbad, CA). To create a library with randomization at residues 18, 19, 162 and 164, a similar multi-step overlap PCR strategy was used. XhoI-NL-F and L18D19-NNK-R, L18D19-NNK-F and R162C164-NNK-R were utilized to create two fragments, which were next assembled by using XhoI-NL-F and NL-R-HindIII. The resultant gene fragment was also treated with Xho I and Hind III, and ligated into a predigested compatible pBAD/His B plasmid. To introduce random mutations across the NanoLuc gene, Taq DNA polymerase was used in all reactions and 0.2 mM MnCl_2 was also added into reaction mixtures to promote amplification errors. To create mammalian expression plasmids, HindIII-NL-F-Koz and NL-R-XhoI (or NL-R-164H and NL-R-164S) were used to amplify NanoLuc and NanoLuc mutants. The products were treated with Hind III and Xho I

restriction enzymes and ligated into a predigested compatible pcDNA3 plasmid (Life Technologies, Carlsbad, CA). The Firefly luciferase (FLuc) gene was amplified from a pGL2-GAL4-UAS-Luc plasmid by using Fluc-F and Fluc-R, and inserted into pcDNA3 between Hind III and Xho I sites. Ant-HindIII-F-koz and Ant-XhoI-R were used to amplify a fragment contains Antares gene from pNCS-Antares (Addgene Cat # 74279). The product was digested with Hind III and Xho I and then ligated into a predigested pcDNA3 plasmid as mentioned above. To replace the NanoLuc fragment in Antares with our new teLuc, oligo pairs Ant-HindIII-F-koz and Te19DtoS_R, Te19DtoS_F and Te85DtoN_R, Te85DtoN_F and Te164CtoH_R, Te164CtoH_F and Antares_R_HindIII were utilized to amplify four individual fragments from pNCS-Antares. The resultant four fragments were used as templates and assembled *via* PCR reactions by using oligo pairs Ant-HindIII-F-koz and Ant-XhoI-R. The product was digested with Hind III and Xho I, purified by agarose gel electrophoresis, and ligated into a predigested pcDNA3 plasmid to give pcDNA3-Antares2. To construct a bacterial expression plasmid for Antares2, oligo pairs Antares_F_XhoI and Antares_R_HindIII were used to amplify the whole gene from pcDNA3-Antares2, which was subsequently digested with Xho I and Hind III and inserted into a compatible, predigested pBAD/HisB plasmid. All ligation products were used to transform *Escherichia coli* DH10B electrocompetent cells, which were next plated on LB agar plates supplemented with ampicillin (100 µg/mL). Additional L-arabinose (0.02%, w/v%) was supplemented to induce protein expression for direct bioluminescence imaging of bacterial colonies.

2.2.4 Library screening

DH10B cells containing NanoLuc mutants were plated on LB agar plates supplemented with ampicillin (100 µg/mL) and L-arabinose (0.02%, w/v%) and incubated at 37 °C overnight to form bacterial colonies. Agar plates were left at room

temperature for another 6 hours, followed by bioluminescence imaging using a luminescence dark box (Stanford Photonics) equipped with a Pixis 1024B CCD camera (Princeton Instruments). Digital images were acquired after spraying ~ 100 μ L of 200 μ M substrates to each agar plate, and next processed with the Fiji image analysis software²⁸ to derive bioluminescence intensities of individual colonies. For each compound, the brightest ten colonies from a total of ~ 20,000 colonies were chosen and inoculated in 5 mL liquid LB broth containing ampicillin (100 μ g/mL) and L-arabinose (0.02%, w/v%). After overnight growth at 37 °C and 250 rpm, the cultures were moved onto a shaker at room temperature for another 6 h. Cells were next diluted with the assay buffer (1 mM CDTA, 0.5% Tergitol NP-40, 0.05% Antifoam 204, 150 mM KCl, 100 mM MES, pH 6.0, 1 mM DTT, and 35 mM thiourea) to $OD_{600} = 0.1$. Next, bioluminescence activities of individual samples were measured in white 96-well plates (Costar 3912) on a Synergy Mx Microplate Reader (BioTek, Winooski, VT) after directly injecting substrates (final concentration of 30 μ M). Kinetics were followed for 1-s signal integration every 60 s for a total of 40 min. Mutants showing exceptional high bioluminescence activities were chosen for sequencing, protein preparation, and other additional characterization.

2.2.5 Luciferase expression and purification

Luciferases were expressed and purified as His₆-tagged fusion proteins. DH10B cells containing corresponding pBAD plasmids were grown in a starter culture of 5 mL of LB broth containing ampicillin (100 μ g/mL) at 37 °C and 250 rpm overnight. Next, the saturated starter culture was diluted 100-fold into 2YT medium containing the appropriate antibiotics and grown under the same conditions. When OD_{600} reached 0.7-0.9, the expression culture was induced with L-arabinose (0.2%, w/v%) and incubated at room temperature with shaking at 250 rpm for another 16 h. Cells were

harvested by centrifugation at 4700 rpm for 15 min and lysed by sonication. The resulting cell lysate was clarified by centrifugation at 18,000 rpm for 30 min at 4 °C. The supernatant was incubated with Ni-NTA agarose beads (Pierce, Rockford, IL) at 4 °C for 2 h. Agarose beads loaded to a plastic column were sequentially washed with 20 mL of wash buffer 1 (pH 8.0, 50 mM Tris HCl, 20 mM Imidazole, 300 mM NaCl, 1 mM DTT) and 3 ml of wash buffer 2 (pH 8.0, 50 mM Tris HCl, 50 mM Imidazole, 300 mM NaCl, 1 mM DTT), followed by elution with an elution buffer (pH 8.0, 50 mM Tris HCl, 300 mM Imidazole, 300 mM NaCl, 1 mM DTT). Proteins were buffer-exchanged into Tris HCl (50 mM, pH 7.4) containing 1mM DTT using Thermo Scientific Snakeskin dialysis tubing, and next concentrated using 3-kDa Amicon Ultra Centrifugal Filters (EMD Millipore). Protein concentrations were determined using the Pierce Coomassie Bradford Protein Assay Kit (Thermo Fisher). For storage, glycerol was added to a final concentration of 50% (v/v) and the resultant mixtures were kept at -20 °C.

2.2.6 Bioluminescence characterization *in vitro*

A Synergy Mx Microplate Reader (BioTek) was used for all *in vitro* bioluminescence characterizations. For kinetics measurements, no emission filter or monochromator was used. 50 μ L of luciferin substrates in the assay buffer (1 mM CDTA, 0.5% Tergitol NP-40, 0.05% Antifoam 204, 150 mM KCl, 100 mM MES pH 6.0, 1 mM DTT, and 35 mM thiourea) was injected into wells of white 96-well plates containing 50 μ L of pure enzymes also in the same assay buffer. The final concentrations of all enzymes and substrates were 100 pM and 30 μ M, respectively. Measurements were taken every 60 s after injection (1-s integration and 10-s shaking during intervals). FLuc bioluminescence assays were performed similarly, except for that its assay buffer contains 30 mM MOPS, pH 7.0, 1.5 mM ATP, and 5 mM MgSO₄. To derive values for apparent Michaelis constants (K_m), substrate concentrations varied from 0.78 to 50 μ M

and peak bioluminescence intensities at individual substrate concentrations were used to fit the Michaelis-Menten equation. The Synergy Mx Microplate Reader is also equipped with a monochromator for scanning of emission wavelengths. 50 μL of individual substrates (60 μM) in assay buffers were injected into 50 μL of 2 nM pure enzymes, and bioluminescence spectra were collected with 0.1-s integration and 1-nm increments from 400 to 750 nm.

2.2.7 Mammalian cell culture and transfection

We utilized HEK 293T (purchased from ATCC and tested for mycoplasma by PCR), which is one of the most widely used and readily transfectable cell lines. HEK 293T cells were cultured at 37 °C with 5% CO_2 in Dulbecco's Modified Eagle's Medium (DMEM) supplemented with 10% fetal bovine serum (FBS). Transfection mixtures were prepared with 3 μg of plasmid DNA and 9 μg of PEI (polyethylenimine, linear, MW 25 kDa) in DMEM and incubated for 20 min at room temperature. The medium was first aspirated, and the transfection mixtures were added to cells at 70% confluency on 35-mm culture dishes seeded the day before transfection. Incubation lasted for 3 h at 37 °C. Fresh DMEM containing 10% FBS was next utilized to replace the transfection mixtures. After incubation for another 24 hours at 37 °C in a CO_2 incubator, the medium was removed and cells were collected and resuspended in Dulbecco's phosphate-buffered saline (DPBS).

2.2.8 Bioluminescence measurements in HEK 293T cells

The number and density of cells in DPBS suspension were determined using a hemocytometer. Cells were next diluted with DPBS to gain the needed numbers in each 100 μL solution. To use the luminescence dark box to directly image cells, we

added luciferase-expressing HEK293T cells (5000 cells per well with ~70% transfection efficiency) and the corresponding luciferin substrates into wells of a white 96-well plate. Bioluminescence was imaged using a Pixis 1024B cooled CCD camera equipped with a 50-mm f/0.95 lens at one min post substrate addition. The camera exposure time was 1 s, and the field of view was 6x6 inches. A 695BP50 (Omega Optical) filter was utilized to acquire NIR emission. All images were analyzed using the Fiji image analysis software²⁸. To prepare cell lysates, cell suspensions were subjected to 10-s sonication. Without further separation, substrates and 100 μ L of additional assay buffers were added to initiate bioluminescence reactions.

2.2.9 Bioluminescence imaging at superficial sites of live mice

BALB/c mice on a 37 °C electronic heat pad were anesthetized using 2% isoflurane in 100% oxygen with a flow of 0.5 L/min. We subcutaneously injected 2 million HEK 293T cells transfected with luciferase genes and resuspended in 100 μ L PBS to the upper right back of each mouse, and another 2 million cells transfected with an empty vehicle vector and also resuspended in 100 μ L PBS to the lower left back of the same mouse. After cells were settled for 5 min, the corresponding luciferase substrates with indicated concentrations in 100 μ L PBS were also subcutaneously injected to each site. Mice were next imaged continuously with 30-s exposure time per frame for a total of 5 min using a luminescence dark box (Stanford Photonics) equipped with a Pixis 1024B cooled CCD camera. The Fiji image analysis software²⁸ was used to analyze images and integrate bioluminescence intensities over common regions of interest encompassing all injected cells.

2.2.10 Bioluminescence imaging in deep tissue of live mice

We followed a published procedure to hydrodynamically transfect BALB/c mice²⁹. Briefly, 20 µg of each luciferase-expressing plasmid in sterilized saline (volume equivalent to 9% bodyweight of the treated mouse) was injected into individual mice placed in a restrainer *via* tail vein in 4-8 sec. Mice were allowed to recover on the heat pad and monitored until breathing resumed to a normal speed. Bioluminescent images were acquired at 12 h post injection. D-luciferin at the indicated dose was dissolved in 100 µL PBS and intraperitoneally injected into FLuc-transfected mice. Prior to the intraperitoneal injection of CTZ analogs to teLuc or yeLuc transfected mice, DTZ or STZ at the indicated dose was dissolved in a 100 µL solution containing 8% glycerol, 10% ethanol, 10% hydroxypropyl-β-cyclodextrin, 35% PEG 400 in water. To inject 3.3 µmol DTZ, the total volume was increased to 500 µL. The luminescence dark box (Stanford Photonics) equipped with a Pixis 1024B cooled CCD camera was again used to image anesthetized mice with 1-min exposure time per frame for a total of 10 min. The Fiji image analysis software²⁸ was used to process images and derive integrated intensities.

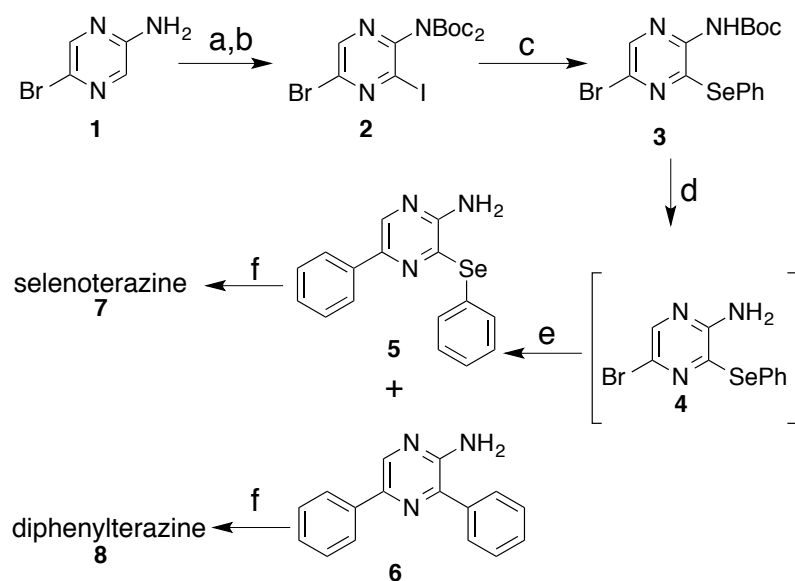
Statistical analysis. The two-tailed t-test was used to determine all P values. No statistical method was used to pre-determine the sample size. No sample was excluded from data analysis, and no blinding was employed. Animals were randomly assigned to receive various treatments. Unless otherwise indicated, data are shown as mean ± s.d., and error bars in figures represent s.d..

2.3. Results

2.3.1 The design and synthesis of CTZ analogs

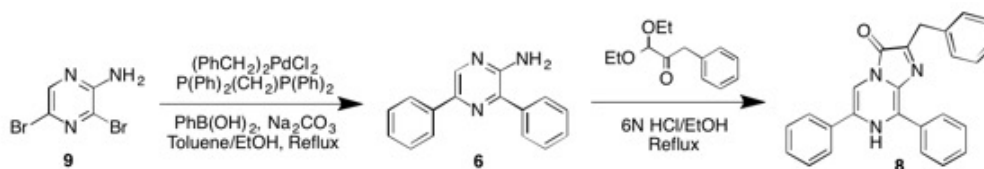
A few CTZ analogs have previously been prepared for red-shifted bioluminescence²⁵, although they typically give low emission with their tested luciferases.^{22, 30-31} They have not been directly tested with NanoLuc, and their impact

on the bioluminescence of NanoLuc is still unknown because the spectral shift observed for one CTZ-utilizing luciferase may not be transferable to another CTZ-utilizing luciferase.²⁵ In a recent report, 6-*pi*-OH-CTZ (**Figure. 1c**), which has an extended conjugation at the C-6 position, was shown to red-shifted the bioluminescence of an RLuc mutant, RLuc8, by 41 nm, but almost no bioluminescence was observed for NanoLuc.²⁶ We reasoned that NanoLuc might not well tolerate substrate with structural changes at the C-6 position, so we mainly focused our effort on the derivatization of CTZ at the C-8 position. Introducing heteroatoms, such as selenium, into fluorescent dyes or D-luciferin, is a proven strategy via heavy atom effect to red-shift fluorescence or bioluminescence emission.³²⁻³⁴ Oxygen and sulfur atoms haven also been introduced to the C-8 position of CTZ to shift the bioluminescence of RLuc to longer wavelengths.³⁰⁻³¹ On the basis of these results, we hypothesized that introducing selenium to the C-8 position of CTZ could be effective to red-shift the bioluminescence of NanoLuc. We therefore designed selenoterazine (STZ, **Figure. 1d**) and developed a synthetic route (**Scheme. 1**) for this molecule. To build the carbon-selenium bond in a chemoselective manner (**Step c, Scheme 1**), we identified an optimal condition based on magnesium-induced Cu(I) catalysis at 85 °C.³⁵ After removing the *t*-Boc group from the resultant intermediate, we utilized Suzuki coupling to introduce a phenyl group to the C-6 position,³⁶ followed by acid-catalyzed condensation with 1,1-diethoxy-3-phenylacetone to afford the final product selenoterazine from inexpensive, commercially available chemicals in six steps with 5.2% overall yield.



Scheme 1. The synthetic route to prepare selenoterazine (and diphenylterazine as a minor product): (a) TFA, NIS, ACN, Reflux; (b) (Boc)₂O, NEt₃, THF, RT, 85% from **1**; (c) PhSe₂, Cu₂O, bpy, Mg, DMF, 85°C, 51%; (d) TFA, CH₂Cl₂, RT; (e) (C₆H₅CN)₂PdCl₂, (C₆H₅)₂P(CH₂)₄P(C₆H₅)₂, PhB(OH)₂, Na₂CO₃, toluene, EtOH, Reflux, 55% for **5** and 13% for **6** from **3**; (f) PhCH₂COC(OEt)₂, 6N HCl, EtOH, Reflux, 22% for **7** and 35% for **8**.

We also serendipitously prepared another CTZ analog, diphenylterazine (DTZ, **Figure. 1e**), which extends conjugation at C-8 through an aromatic ring. The precursor of DTZ was initially derived as a side-product during the synthesis of STZ. We later tested DTZ with NanoLuc and fortunately found it to be one of the most useful CTZ analogs to enhance and red-shift the bioluminescence of NanoLuc. Because DTZ exhibits red-shifted emission and maintain reasonable brightness over STZ, we revised a reported procedure³⁷ and prepare diphenylterazine in large quantities from commercially available chemicals in two steps with 23.1% overall yield (**Scheme. 2**).



Scheme 2. The synthetic route to prepare diphenylterazine as the major product.

2.3.2 Engineering of NanoLuc mutants and *in vitro* characterization

With selenoterazine (STZ) and diphenylterazine (DTZ) in hand, we next determined their bioluminescence in the presence of the freshly purified NanoLuc protein. Under our condition, the peak emission of NanoLuc/furimazine was at 450 nm, whereas NanoLuc/DTZ and NanoLuc/DTZ emitted maximally at 527 nm and 498 nm, respectively (**Table 1**). We want to note that our determined emission maximum for NanoLuc/furimazine is close to that reported by Hosoya *et al.*,²⁴ but 10-nm blue-shifted from that reported by Wood *et al.*⁸ Nevertheless, DTZ and DTZ caused 77- and 48-nm red-shifts from furimazine, respectively. Interestingly, DTZ is a better substrate for NanoLuc than CTZ. The NanoLuc/DTZ pair retained ~ 44% of the intensity of NanoLuc/furimazine, whereas the maximal bioluminescence intensity of NanoLuc/DTZ was only 3.3% of NanoLuc/furimazine.

Table 1. Photoluminescence properties of various luciferase/luciferin pairs.

	λ_{\max} (nm)	Reporter size (kDa)	Relative intensity ^a							
			Protein ^b		HEK 293T Cells ^c			Mice		
			Total	> 600 nm	Intact (Total)	Intact (695/50)	Lysate	Subcutaneously injected cells ^d	Hydrodynamic transfection ^e	
									0.3 μ mol	3 μ mol
NanoLuc + furimazine	450	19	43.5	0.66	307	7.4	167	7.2	ND ^f	ND ^f
teLuc + DTZ	500	19	113	13	793	56	317	54	53	119
yeLuc + STZ	527	19	13	4.3	89	21	6.5	1.8	3.5	ND ^f
FLuc + D-luciferin	563	61	1	1	1	1	1	1	1	3.7
FLuc + AkaLumine- HCl	677	61	3.4	6	5.6	22	11	1.3	ND ^f	8.2
Antares + furimazine	450, 582	70.5	30	19	180	165	112	26	49	78
Antares2 + DTZ	500, 582	70.5	79	76	636	275	252	57	86	155

a. Intensity values normalized to FLuc/D-luciferin under comparable experimental conditions;

b. 30 μ M substrate and 1 nM proteins. Values are based on intensities integrated over the first 10 min post substrate injection;

c. 50 μ M substrates and 5000 cells with an average transfection efficiency of \sim 70%;

d. Subcutaneous injection of 2 million HEK 293T cells and 100 μ L of 100 μ M each substrate;

e. Intraperitoneal injection of each substrate. All intensity values normalized to FLuc and 0.3 μ mol D-luciferin;

f. Not determined.

We next engineered NanoLuc for enhanced activities toward either DTZ or STZ (**Figure 2a**). We simultaneously randomized residues 44, 54 and 138 (numbered according to Protein Data Bank (PDB) ID 5B0U), since they have previously been reported to modulate the substrate preference of NanoLuc.³⁸ Unfortunately, screening of this library did not give us any NanoLuc mutant showing improved activities. We subsequently fully randomized residues 18, 19, 162, and 164, because they are close to a putative substrate-binding site based on our analysis of a recently reported X-ray crystal structure of the apo-form of NanoLuc.³⁹ In the meanwhile, we also introduced random mutations across the gene under an error-prone PCR condition. We next introduced the resultant gene library into DH10B *E. coli* cells and imaged bacterial colonies for bioluminescence by directly spaying either DTZ or STZ. We examined \sim 20,000 individual colonies for each substrate, and selected ten top clones for each substrate for further investigation. Pure proteins for each clone were prepared and

tested against DTZ or STZ. To our delight, we identified a mutant showing exceptional activity toward DTZ (**Figure 2b**).

This mutant (NanoLuc-D19S/D85N/C164H), which enhanced the NanoLuc-catalyzed bioluminescence of DTZ by 5.7-fold, was designated teLuc for its teal bioluminescence (emission max: 500 nm) in the presence of DTZ. The bioluminescence intensity of teLuc/DTZ is ~ 34-fold and ~ 2.5-fold of the intensities of NanoLuc/CTZ and NanoLuc/furimazine, respectively (**Table 1**), making teLuc/DTZ one of the brightest luciferase-luciferin pairs to date.

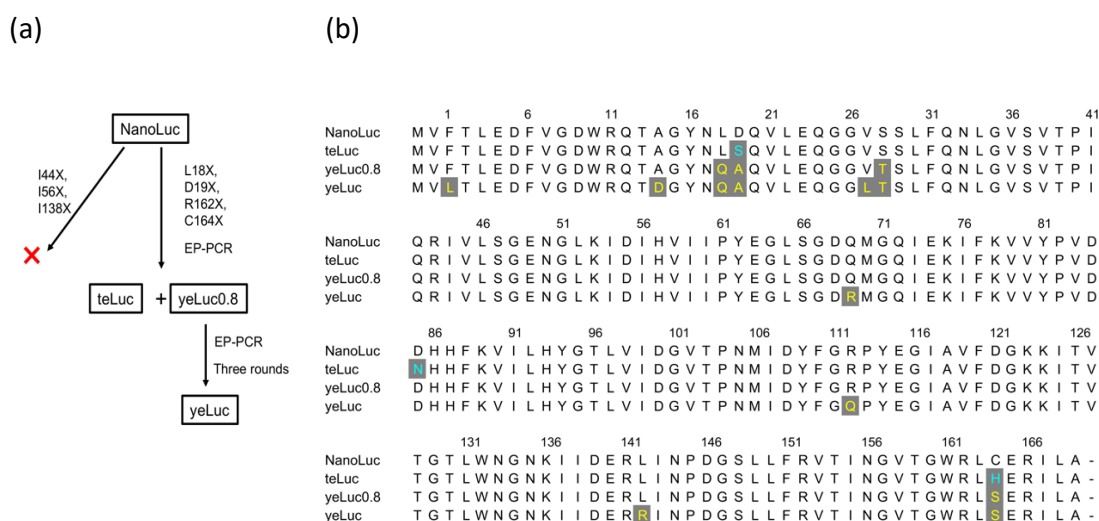


Figure 2. (a) Illustration of the process to engineer teLuc and yeLuc. (b) Sequence alignment between NanoLuc and NanoLuc mutants described in this work. teLuc mutations are highlighted in teal fonts and gray background, whereas all yeLuc mutations are highlighted in yellow fonts and gray background. Residues in this figure are numbered according to Protein Data Bank (PDB) ID 5B0U.

Due to its red-shifted spectrum, teLuc/DTZ can partially emit photons at wavelengths above 600 nm, the NIR optical window suited for mammalian tissue imaging. In comparison, NanoLuc/furimazine has little emission in this region. Because

the total intensity of teLuc/DTZ is much higher than that of FLuc/D-luciferin, teLuc/DTZ can emit 13-fold more photons than FLuc/D-luciferin in this NIR optical window (**Table 1**). In the meanwhile, we identified another NanoLuc mutant (designated yeLuc0.8; NanoLuc-L18Q/D19A/S28T/C164S) showing enhanced activity toward STZ. To further increase the brightness of the yeLuc0.8/STZ pair, we performed three additional rounds of random mutagenesis and bacterial colony-based screening. We arrived at a further enhanced variant which has 6 additional mutations and is ~ 51% brighter than yeLuc0.8. This new mutant (**Figure. 2a** and **2b**), which provides an overall 11.5-fold enhancement of STZ bioluminescence from NanoLuc, was named yeLuc (NanoLuc-F1L/A14D/L18Q/D19A/V27L/S28T/Q69R/R112Q/L142R /C164S). The peak intensity of yeLuc/STZ is ~ 17-fold higher than that of FLuc/D-luciferin, with ~ 4.2-fold more emission in the spectral region above 600 nm than FLuc/D-luciferin during a 10-min integration (**Table 1**).

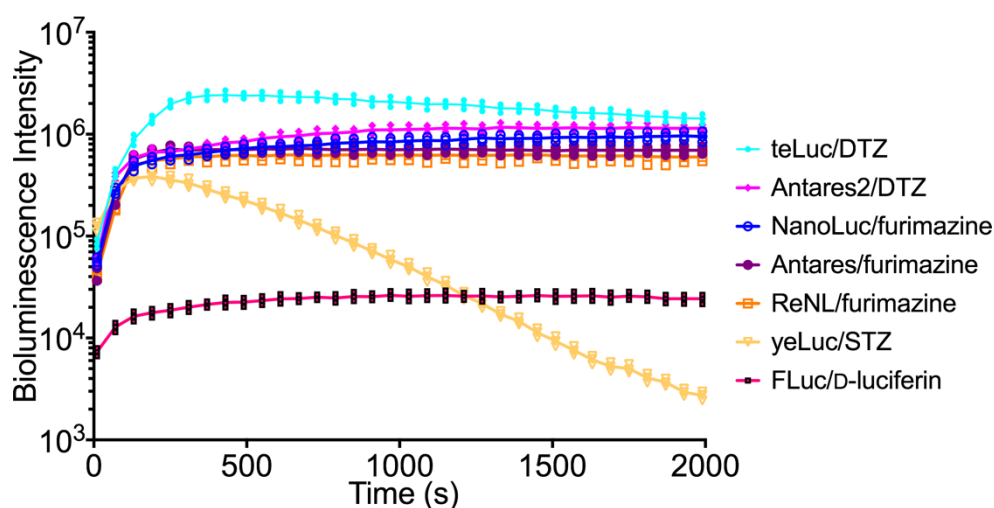


Figure 3. Bioluminescence decay kinetics for pure enzymes. The final concentrations of all enzymes and substrates were 100 pM and 30 μ M, respectively. Measurements were taken every 60 s after substrate addition. Individual data points from three independent measurements are presented.

We utilized the buffer previously reported for NanoLuc⁸ in our protein-based bioluminescence assays. Under this condition, teLuc/DTZ displayed sustained bioluminescence with a half-life of ~ 40 min, whereas the decay of yeLuc/STZ bioluminescent was fast with a half-life of ~ 5 min (**Figure. 3**). The relative intensities (including peak intensities and integrated intensities) of various luciferase-luciferin pairs, as compared to NanoLuc/furimazine, are reported in **Table 1**. We also determined apparent Michaelis constants (K_m) for these luciferase-luciferin pairs, and the K_m values of teLuc and yeLuc were 10.6 μM and 11.8 μM for DTZ and STZ, respectively (**Figure. 4a** and **Table 1**). These values are close to that of NanoLuc/furimazine, suggesting that the enzyme-substrate affinity was not significantly altered during our engineering process.

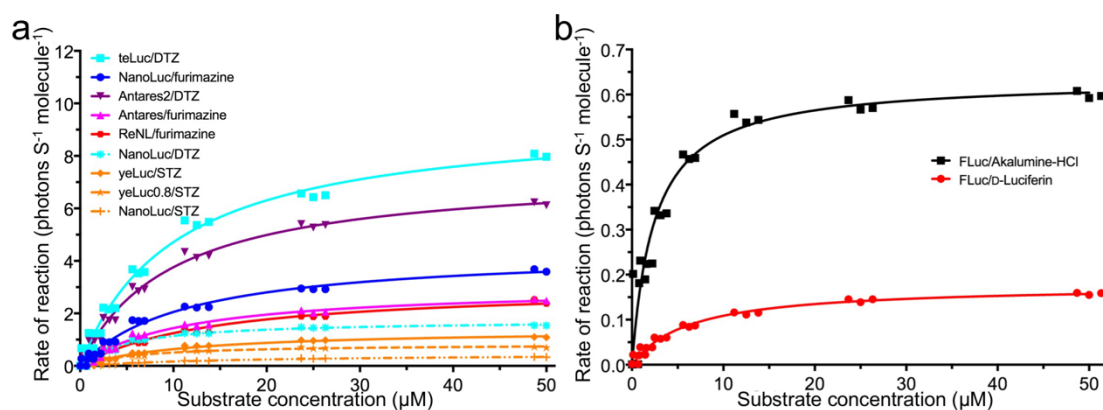


Figure 4. Substrate titrations with pure enzymes to determine apparent Michaelis constants (K_m). The final concentrations of all enzymes were 100 pM. Substrate concentrations varied from 0.78 to 50 μM , and peak bioluminescence intensities at individual substrate concentrations were used to fit the Michaelis-Menten equation. Individual data points from three independent measurements at each substrate concentration are presented.

2.3.3 Further red-shifting the emission of teLuc/DTZ by BRET

Even though the NIR emission of teLuc has been improved comparing to NanoLuc, the emission maximum is still far away from ideal NIR transparent window. We next fused teLuc to two copies of cyan-excitable orange fluorescent protein (CyOFP) to further red-shifting the emission by bioluminescence resonance electron transfer (BRET) mechanism (**Figure. 5a**). The emission of teLuc/DTZ overlaps better with the absorbance of CyOFP1 (**Figure. 5b**) and teLuc/DTZ is brighter than NanoLuc/furimazine. Therefore, replacing NanoLuc in Antares with teLuc resulted in a BRET-based Antares2 reporter emitting 76-fold more photons above 600 nm than FLuc/D-luciferin (**Table 1**).

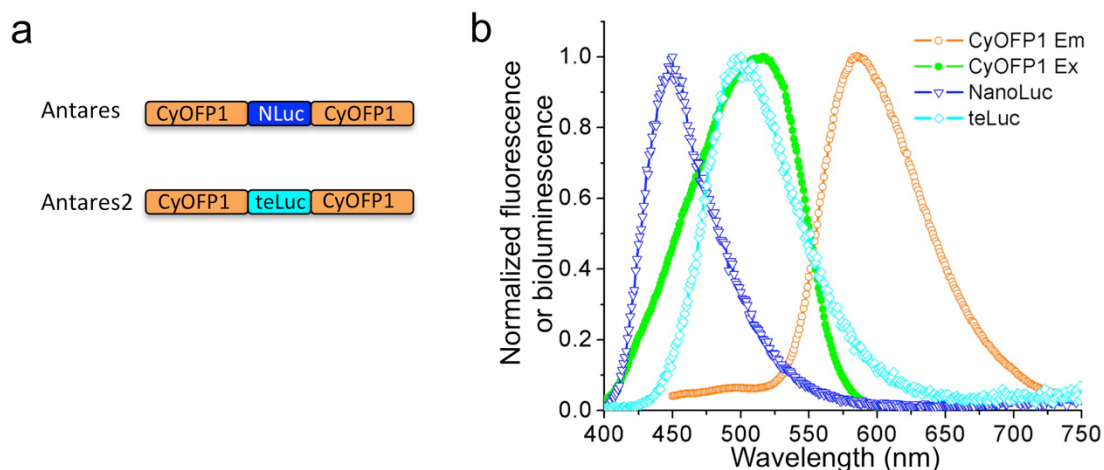


Figure 5. Domain arrangement and spectral overlap of Antares2. (a) Primary structural arrangement of Antares and Antares2. (b) Fluorescence and bioluminescence profiles of CyOFP1, NanoLuc, and teLuc, showing a better BRET spectral overlap between teLuc and CyOFP1 than between NanoLuc and CyOFP1. Two copies of CyOFP1 give higher BRET efficiency. The BRET efficiency increased from 67% in Antares to 71% Antares2 by comparing the intensities of Antares, Antares2, NanoLuc, and teLuc at the same concentrations.

2.3.4 Improved bioluminescence in mammalian cells and lysates

To evaluate the performance of newly engineered luciferase-luciferin pairs in mammalian cell-based bioluminescence assays, we expressed our luciferase mutants in Human Embryonic Kidney (HEK) 293T cells. Utilizing the same number of cells, we determined bioluminescence intensities in the presence of their corresponding luciferin substrates (30 μ M). The peak intensities of bioluminescence generated by teLuc and yeLuc were \sim 480-fold and \sim 56-fold, respectively, higher than that of FLuc/D-luciferin in intact HEK 293T cells (**Table 1** and **Figure. 6b**). These enhancements are even more dramatic than the results observed in protein-based assays, suggesting that our synthetic substrates have excellent cell permeability (**Table 1**). Moreover, teLuc/DTZ displayed 2.4-fold higher bioluminescence than NanoLuc/furimazine. To the best of our knowledge, among all bioluminescent reporters that have been tested in live mammalian cells, teLuc/DTZ is currently the brightest option. We next sonicated HEK 293T cells to disrupt cell membrane and determined bioluminescence activities in cell lysates. We observed the same trend for their relative brightness (**Table 1**).

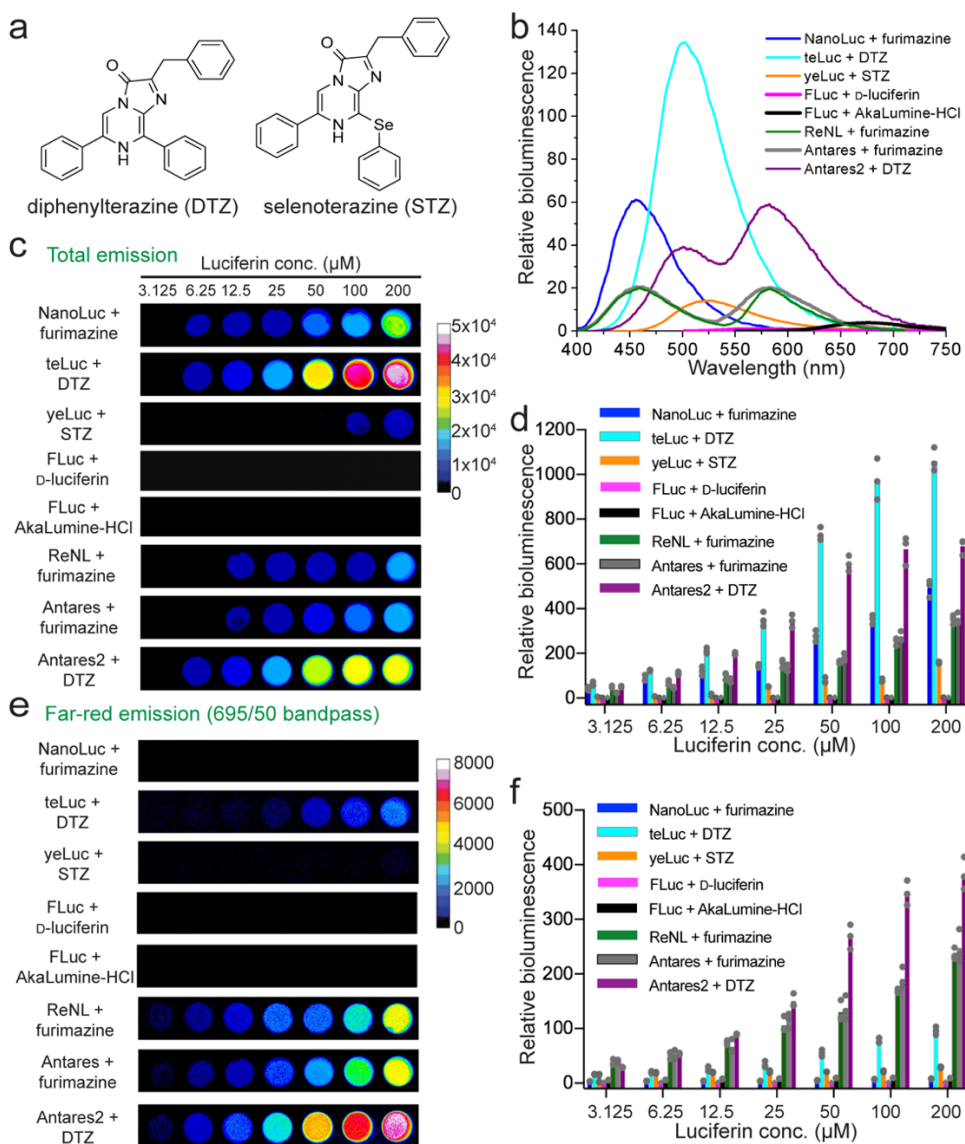


Figure 6. (a) Chemical structures of diphenylterazine (DTZ) and selenoterazine (STZ). (b) Bioluminescence emission of purified luciferases (1 nM) with their corresponding luciferin substrates (30 μ M). The spectra were normalized to peak emission of FLuc–D-luciferin. (c–f) Representative pseudocolored images (c,e) and quantifications (d,f) of luciferase-expressing HEK 293T cells in the presence of various luciferins. Images were acquired without a filter (c) or with a 695 ± 25 -nm NIR emission filter (e). Panels d and f are quantification results for panels c and e, respectively. All values were normalized to the intensities of FLuc–D-luciferin (50 μ M) under the same imaging conditions. The graphs show mean values and individual data points of three independent measurements.

To evaluate the substrate dependency of the bioluminescence reactions in live cells, we next imaged HEK 293T cells transfected with each luciferase gene in the presence of various concentrations of substrates (**Figure. 6c and 6d**). As the concentrations increased from 3.125 μM to 200 μM , the bioluminescence intensities also increased for all groups. In particular, teLuc/DTZ were several hundred times brighter than FLuc/D-luciferin. This new pair also generated consistent improvement from NanoLuc/furimazine at all tested concentrations. The improvement was even more dramatic when cells were imaged with a NIR emission filter (**Figure. 6e and 6f**), because the bioluminescence profile of teLuc/DTZ and Antares2/DTZ is more red-shifted than that of NanoLuc/furimazine.

We also monitored bioluminescence decay kinetics for various luciferase-luciferin pairs. Similar to NanoLuc/furimazine, both teLuc/DTZ and Antares2/DTZ showed sustained bioluminescence with a half-life of > 2 h in both intact cells and cell lysates (**Figure. 7**). In contrast, the bioluminescence of yeLuc/STZ and FLuc/D-luciferin decayed quickly to show flash-type kinetics. Moreover, DTZ alone yielded very little background and thus exhibited excellent signal-to-background ratios (**Figure. 8**). Furthermore, DTZ elicited minimal cell toxicity at millimolar concentrations (**Figure. 9**). In contrast, AkaLumine-HCl, furimazine, and STZ induced cell death within the tested substrate concentration range.

Both teLuc/DTZ and Antares2/DTZ pairs showed robust, red-shifted bioluminescence in protein and cell based assays. More importantly, these two new pairs give enhanced signals in the NIR spectral range, strongly suggesting their usefulness for *in vivo* bioluminescent imaging.

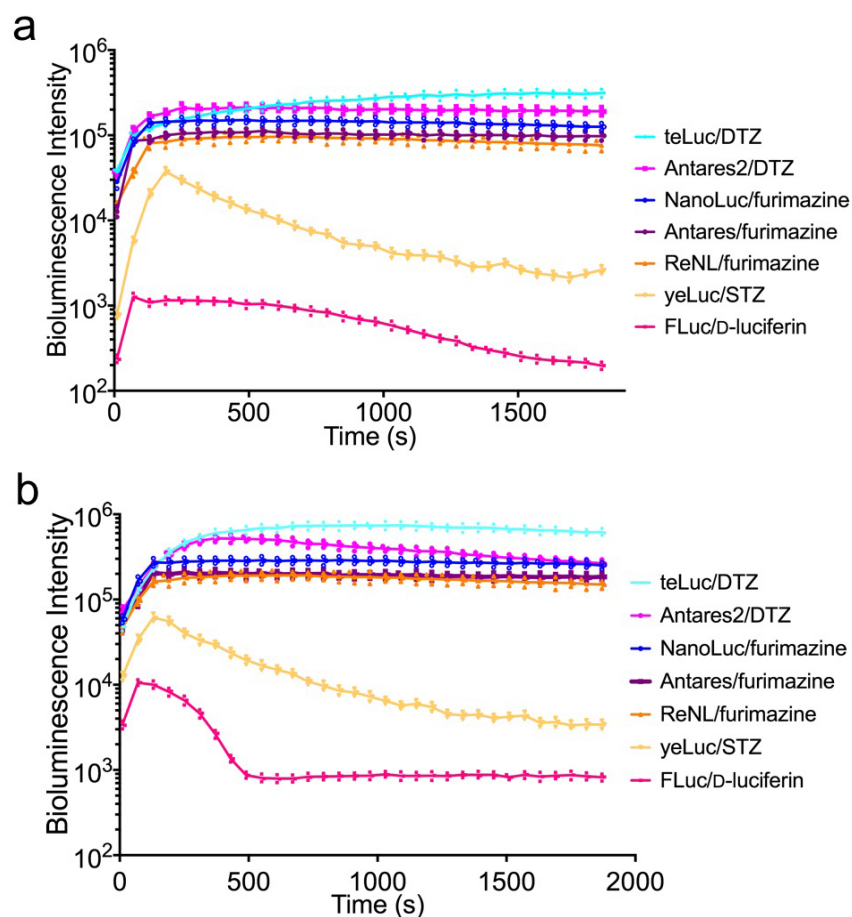


Figure 7. Bioluminescence decay kinetics in intact HEK 293T cells (a) and HEK 293T cell lysates (b). The assay was performed with 30 μ M substrates in a 96-well plate format containing \sim 5000 luciferase-expressing HEK 293T cells or cell lysates. Bioluminescence intensities were measured at 60 s intervals after substrate addition. Individual data points from three independent measurements are presented.

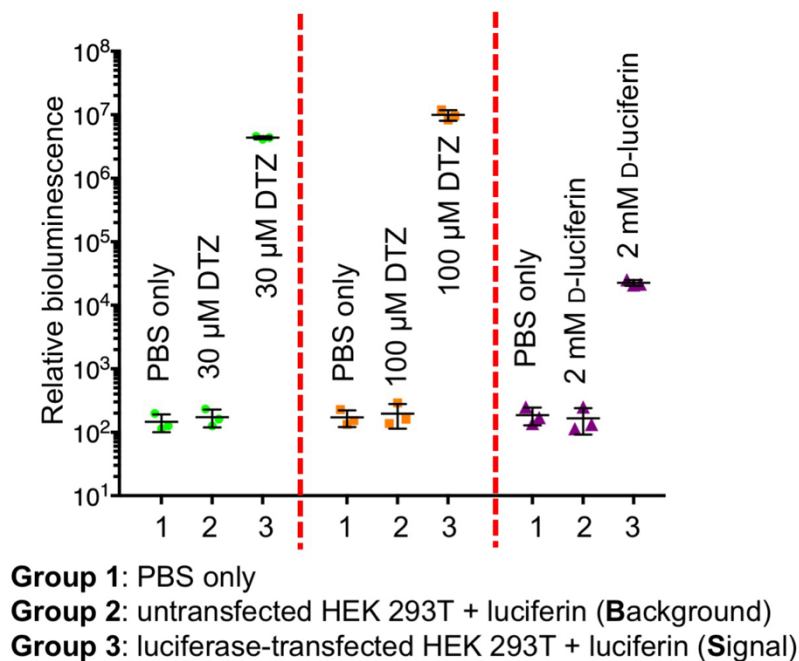


Figure 8. Evaluation of signal-to-background ratios (S/B) of various luciferase-luciferin pairs in HEK 293T cell based assays. The addition of DTZ to untransfected HEK 293T cells generated signals close to instrumental noises. S/B ratios were 2.5×10^4 for 30 μM DTZ and 5.0×10^4 for 100 μM DTZ in the presence or absence of teLuc, and 136 for 2 mM D-luciferin in the presence or absence of FLuc. Individual data points and mean with s.d. from three independent experiments are presented.

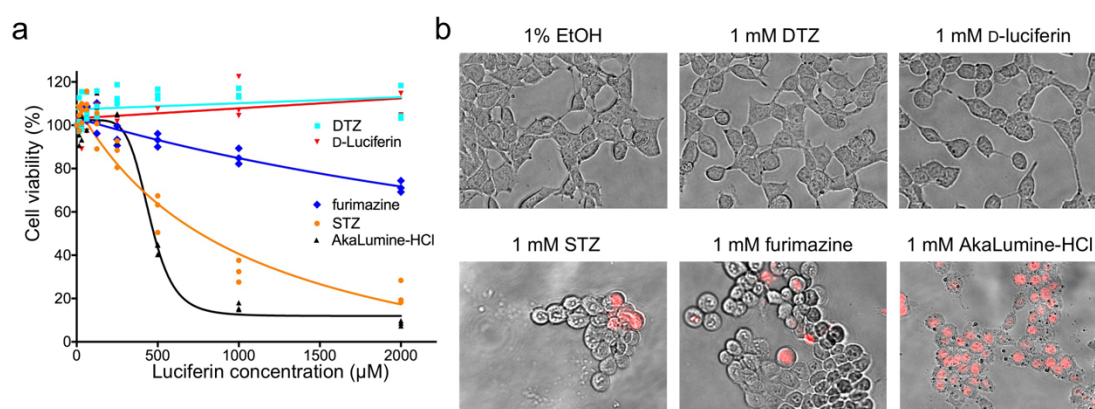


Figure 9. Evaluation of the cytotoxicity of various luciferins. (a) Viability of HEK 293T cells determined using RealTime-Glo™ MT Cell Viability Assay (Promega) after

incubation with individual luciferin substrates for 24 h at 37°C. Individual data points from three independent measurements are presented. Lines were drawn to emphasize the trends. (b) Evaluation of cell morphology and staining of dead cells. Cells incubated with the indicated luciferins for 24 h at 37°C were stained with propidium iodide (PI), a fluorescent dye for dead cells. The cytotoxicity of STZ, furimazine, and AkaLumine was further confirmed by the red fluorescence of PI. These experiments were independently repeated three times.

2.3.5 Enhanced bioluminescence imaging *in vivo*

We next explored the use of our new reporters for *in vivo* bioluminescence imaging. To compare bioluminescence at superficial sites, we subcutaneously injected HEK 293T cells expressing individual luciferases to the upper right back of BALB/c mice with hair unremoved. For comparison, we also administered cells transfected with an empty vehicle vector to the same mice at the lower left back. After cells were settled down, we subcutaneously injected luciferin substrates to both sites of each mouse. No background bioluminescence was observed from sites injected with vehicle-transfected cells. At the same substrate concentration (0.1 mM), teLuc/DTZ was ~ 54-fold brighter than FLuc/D-luciferin and ~ 7.5-fold brighter than NanoLuc/furimazine (**Figure. 10a** and **10b** and **Table 1**), while the brightness of Antares2 was comparable to that of teLuc. Very dim bioluminescence was observed for yeLuc/STZ at this substrate concentration. However, when the STZ concentration increased from 0.1 mM to 0.5 mM, yeLuc/STZ emitted more robustly than FLuc in the presence of 1 mM D-luciferin. NanoLuc/furimazine was still quite bright at the superficial sites, suggesting that tissue absorption and scattering had less impact on photons from the body surface.

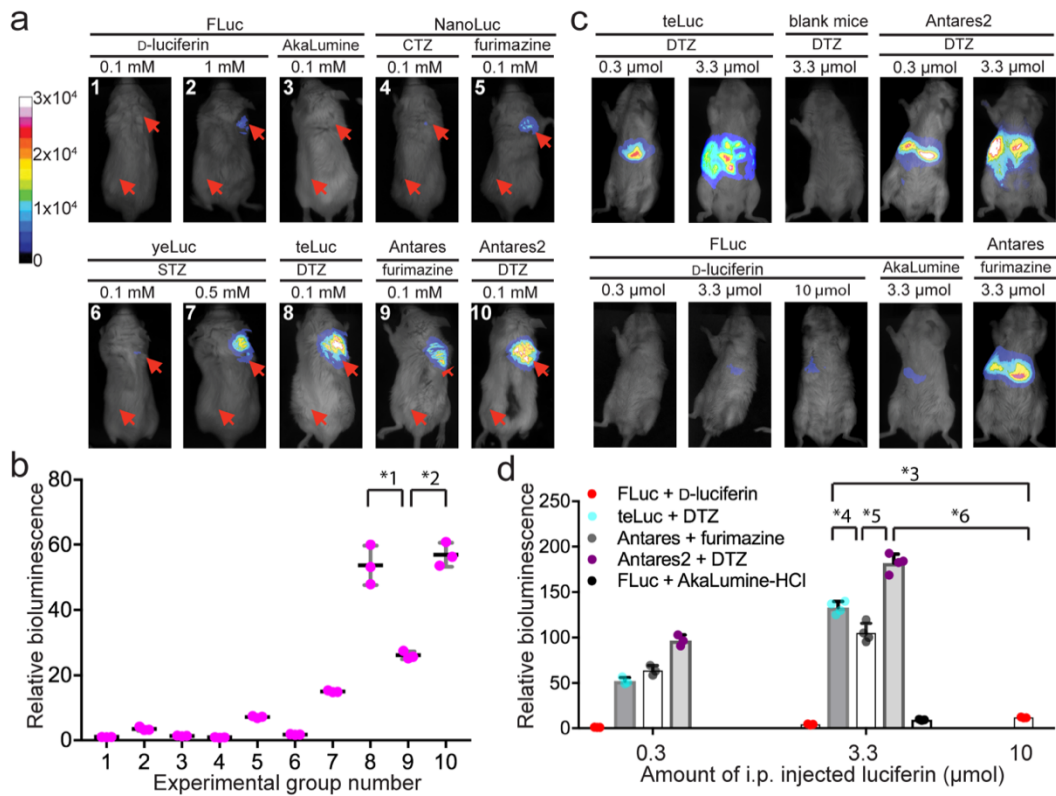


Figure 10. Bioluminescence imaging of luciferase-luciferin pairs at superficial sites and in deep tissues of live mice. (a,b) Representative bioluminescence images (a) and quantitative analysis (b) of BALB/c mice with subcutaneously injected luciferase-expressing HEK 293T cells and 100 μL luciferin substrates at the indicated concentrations. The group numbers in panel b are aligned with these in panel a. Two injection sites (one for luciferase-expressing cells and one for empty-vector controls) of each mouse are illustrated with red arrows. Intensity values were normalized to the intensity of FLuc/D-luciferin (0.1 mM) acquired under the same condition. (c,d) Representative bioluminescence images (c) and quantitative analysis (d) of BALB/c mice to which luciferase-coding plasmids were hydrodynamically delivered through tail vein and luciferase substrates were intraperitoneally delivered at 12 h post plasmid injection (n = 3). Intensity values were normalized to the intensity of FLuc/D-luciferin (0.3 μmol) acquired under the same condition. Two-tailed t-tests were used to compare values for teLuc/DTZ, Antares/furimazine, and Antares2/DTZ (**P* < 0.05), indicating the existence of significant enhancement of bioluminescence by teLuc or Antares2.

To further evaluate the reporters for imaging deep-tissue targets, we utilized hydrodynamic transfection to express exogenous luciferase genes in internal organs of mice.²⁹ This procedure is known to lead to efficient expression of exogenous genes in internal organs, such as the lung, heart, liver, spleen and kidney. After transgene expression, we intraperitoneally injected various luciferin substrates of 0.3 μmol individual luciferin substrates into mice. Compared to FLuc/D-luciferin, teLuc/DTZ displayed significantly enhanced bioluminescence signals. Injection of 0.01 μmol and 0.1 μmol D-luciferin into FLuc-expressing mice did not produce noticeable bioluminescence, whereas signals were detected for DTZ-expressing mice injected with the same amounts of DTZ. teLuc/DTZ generated ~ 53 -fold higher emission than FLuc/D-luciferin (**Figure. 10c** and **10d**). We further intraperitoneal injected 3.3 μmol substrates, a dose used in many D-luciferin imaging experiments (~ 50 mg/kg) and recommended for the use of AkaLumine-HCl²⁰. teLuc/DTZ was still ~ 32 -fold brighter than FLuc/D-luciferin and ~ 14.5 -fold brighter than FLuc/AkaLumine-HCl. When 10 μmol D-luciferin was utilized, the emission of FLuc-expressing mice increased by ~ 7.8 -fold. Despite that, the bioluminescence of teLuc-expressing mice in the presence of 10-fold less substrate was still ~ 2.7 -fold higher than FLuc/D-luciferin. Injection of DTZ into untransfected blank mice did not cause any background emission (**Figure 10c**). When Antares2 was utilized for deep-tissue imaging, an additional 30%-60% increase of signal was detected since its emission profile is more red-shifted than teLuc. Furthermore, the bioluminescence resulting from intraperitoneal injected DTZ displayed extended kinetics (**Figure. 11**), supporting that teLuc and Antares2 are suitable for time-lapse bioluminescence imaging.

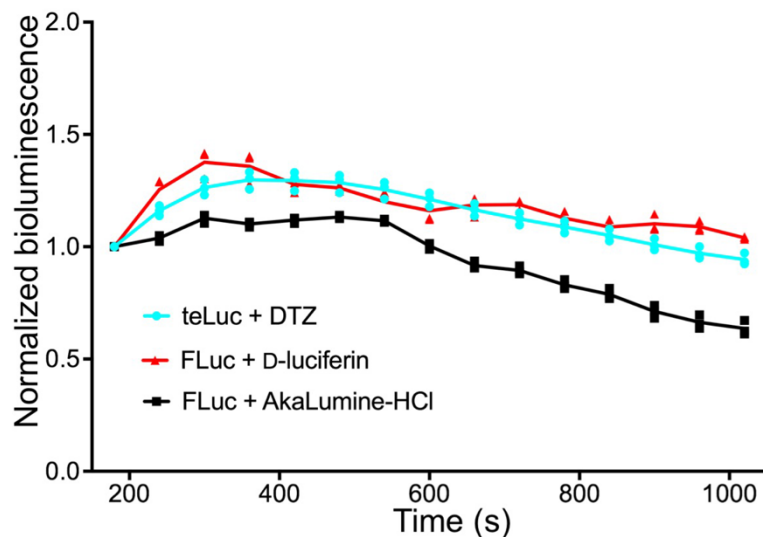


Figure 11. Bioluminescence kinetics of IP injected luciferins (3.3 μmol each) in hydrodynamically transfected mice. Values are normalized to the starting intensities ($t = 180$ s post-injection) and shown as individual data points of three independent experiments.

2.4. Discussion

Bioluminescence have been harnessed for a large array of applications in biotechnology, drug discovery, and imaging of biological processes. Although several luciferase-luciferin pairs are being broadly utilized, the NanoLuc/furimazine and FLuc/D-luciferin pairs are among the brightest and most popular ones for *in vitro* and *in vivo* bioluminescence measurements, respectively. NanoLuc/furimazine is highly attractive because of its substantially high overall brightness. However, despite that it improves *in vitro* and *in cellulo* detection limit, FLuc/D-luciferin remains as a better option for *in vivo* imaging, in particular, for imaging targets in deep tissues.⁹ Our studies advanced the status quo by providing a new luciferase-luciferin pair, teLuc/DTZ, which surpasses NanoLuc/furimazine and FLuc/D-luciferin under all tested conditions,

including protein-based assays and bioluminescence measurements using live cells and cell lysates and in surface and deep tissues of live mice.

We derived this new luciferase-luciferin pair by chemically synthesizing CTZ analogs and re-engineering NanoLuc to accommodate the new substrates. In particular, DTZ has previously been reported to red-shift the bioluminescence of OLuc to 483 nm but with very low emission;²³ we were able to generate bioluminescence at 500 nm and when paired with our further engineered teLuc luciferase, DTZ resulted in the highest photon flux *in vitro* and *in cellulo* among all luciferase-luciferin pairs. Moreover, it further improved bioluminescence detection *in vivo*. Even when D-luciferin was used at a 10-fold higher concentration, teLuc/DTZ and Antares2/DTZ was still significantly brighter than FLuc/D-luciferin *in vivo*. Therefore, we provided novel luciferase-luciferin pairs with benefits for both *in vitro* and *in vivo* applications.

In summary, we have synthesized CTZ analogues with modifications at the C-8 position and re-engineered NanoLuc luciferase for the new substrates, resulting in bright, red-shifted bioluminescence. In particular, teLuc/DTZ is one of the brightest bioluminescent systems showing robust performance for applications *in vitro*, *in cellulo* and in live mice. This will streamline a variety of applications for high sensitivity and consistency, enable new measurements in the bioluminescence mode, or improve measurements *in vitro* and *in vivo* to allow the use of less demanding instrumentation to track less abundant targets with higher spatiotemporal resolution. Our study suggests that modification of CTZ at the C-8 position may be a viable way to red-shift the bioluminescence of CTZ-utilizing enzymes. Moreover, it demonstrates the general feasibility of co-engineering CTZ-utilizing luciferases and substrates for improved bioluminescence.

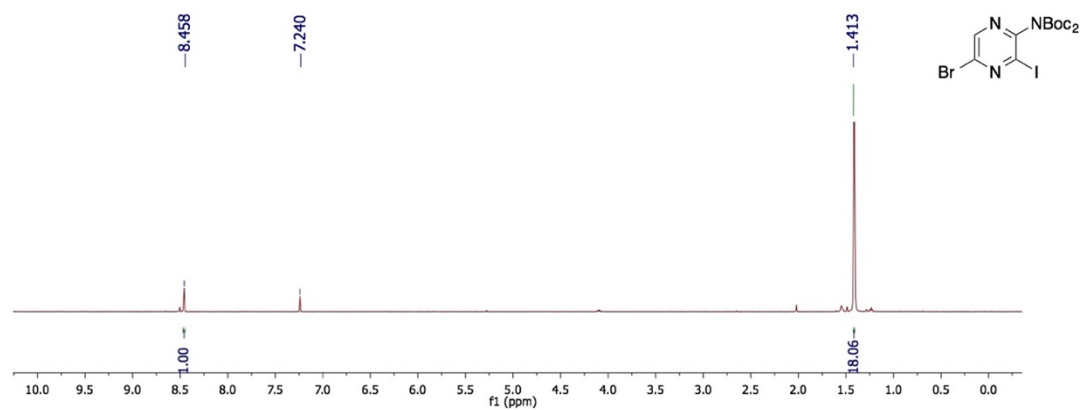
The increased detection sensitivity is not the only benefit of teLuc/DTZ. Compared to FLuc (61 kDa) and several other luciferases, NanoLuc and its derived

teLuc and yeLuc (19 kDa) are small proteins. It is advantageous to use them to create fusion proteins to track protein dynamics, or to construct viral vectors which may have limited packing capacity. Furthermore, NanoLuc forms a β -barrel structure amenable to various genetic and structural manipulations such as split and fragment complementation. The bioluminescence is independent of ATP, Mg^{2+} , or Ca^{2+} . All these suggest that teLuc may be an excellent scaffold for the development of bioluminescent reporters and biosensors that will be well-compatible with popular optogenetic tools. Fusing luciferases to fluorescent proteins is a widely-used method to further enhance and red-shift bioluminescence. We fused teLuc with CyOFP1 to derive Antares2, which improved detection in deep tissues. Antares2 is an optimal bioluminescent reporter when the molecular size of the reporter does not matter and there is no spectral crosstalk with CyOFP1. Overall, our work provides several robust bioluminescent reporters, including teLuc and Antares2, which will have broad applications *in vitro* and *in vivo*.

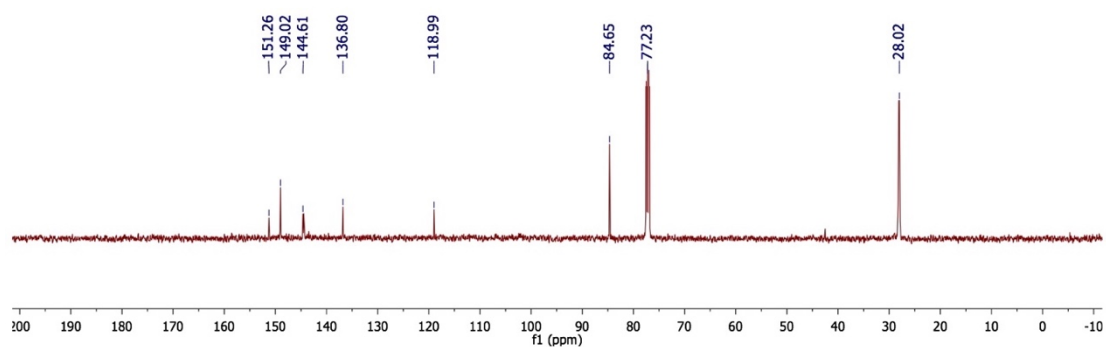
2.5. Appendix

NMR and MS characterization of
di-*tert*-butyl (5-bromo-3-iodopyrazin-2-yl)carbamate (**2**)

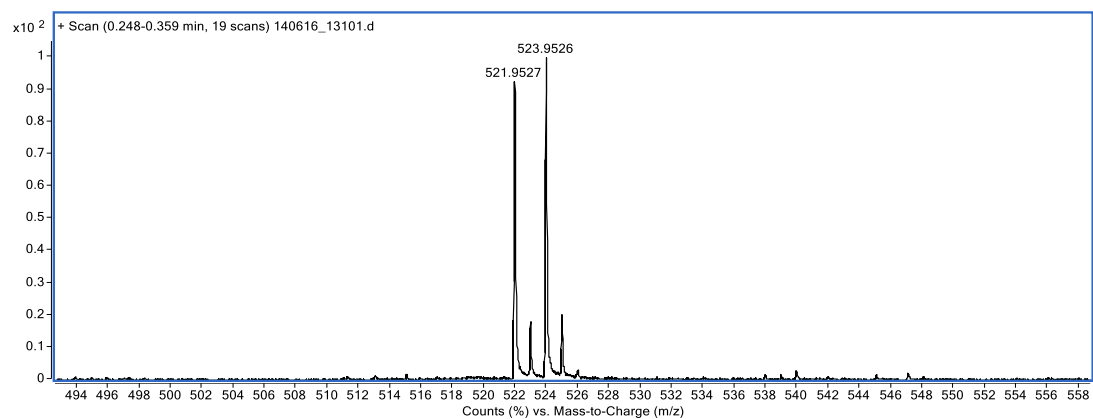
^1H NMR



^{13}C NMR

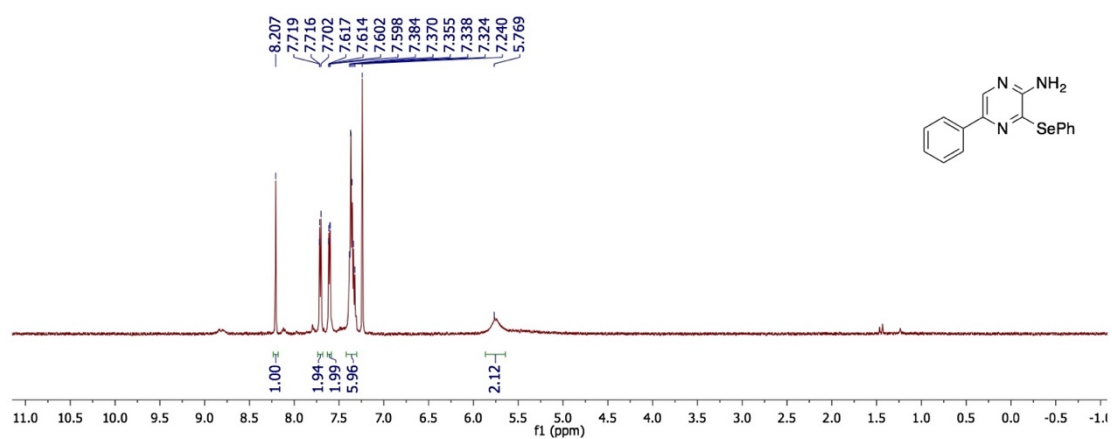


ESI-MS

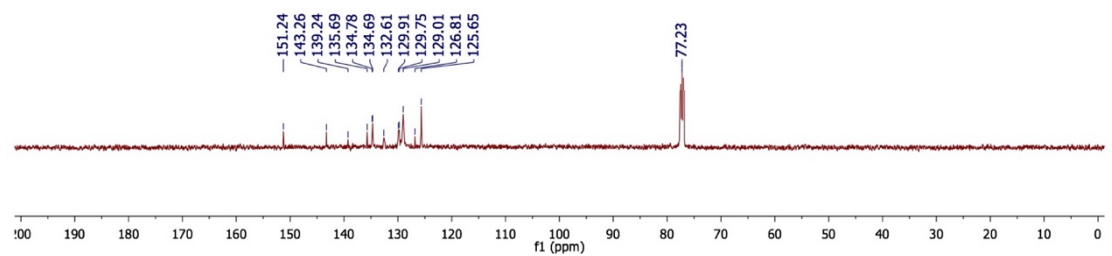


NMR and MS characterization of
5-phenyl-3-(phenylselanyl)pyrazin-2-amine (**5**)

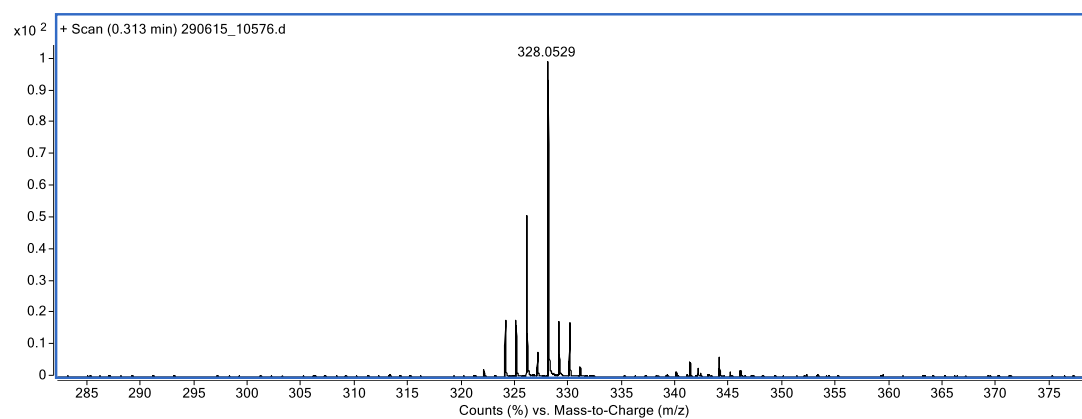
^1H NMR



^{13}C NMR

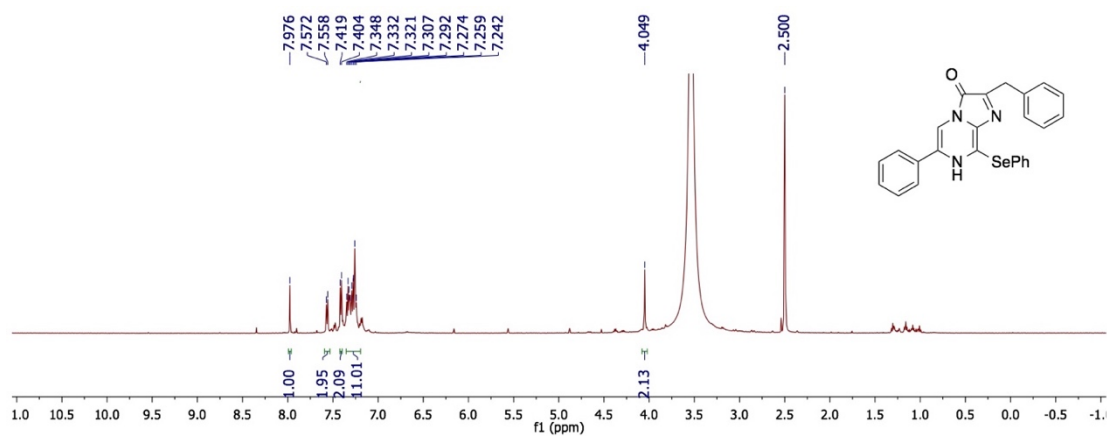


ESI-MS

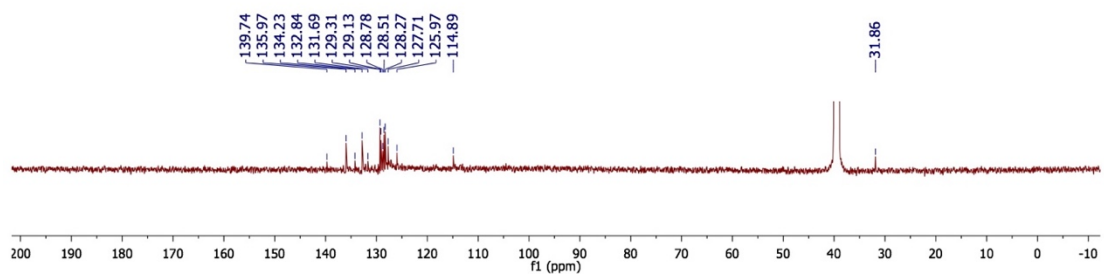


NMR and MS characterization of selenoterazine (**7**)

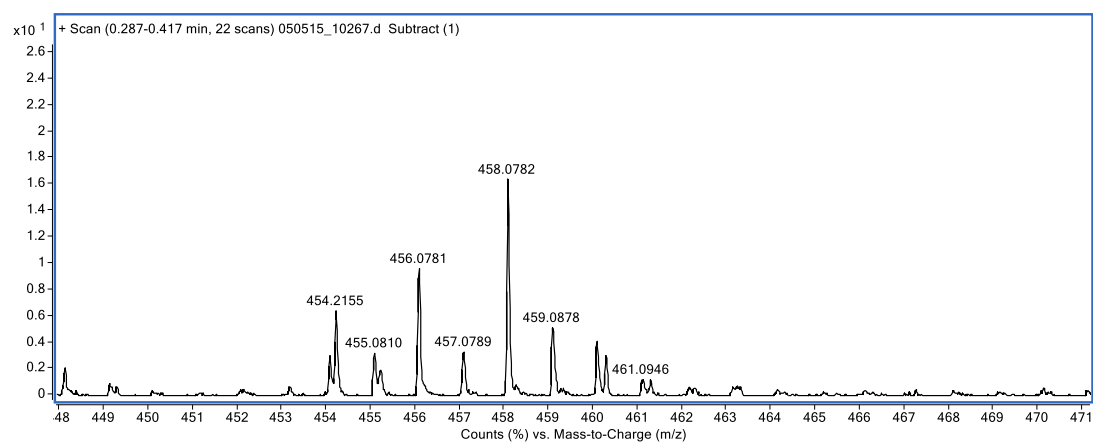
^1H NMR



^{13}C NMR

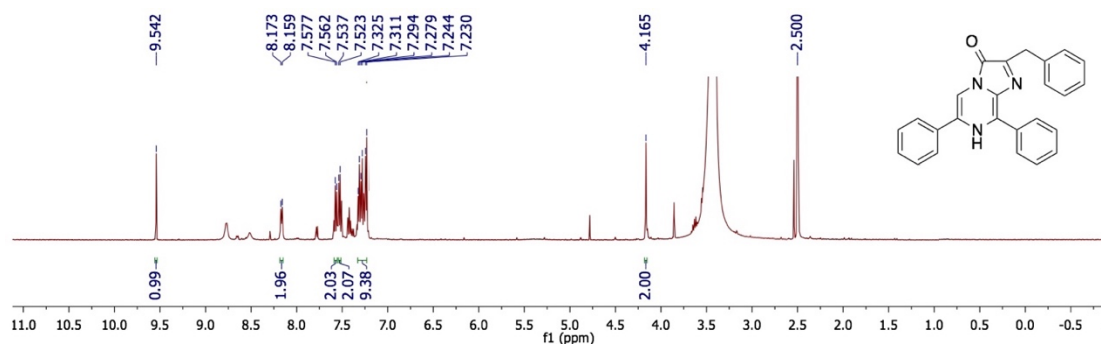


ESI-MS

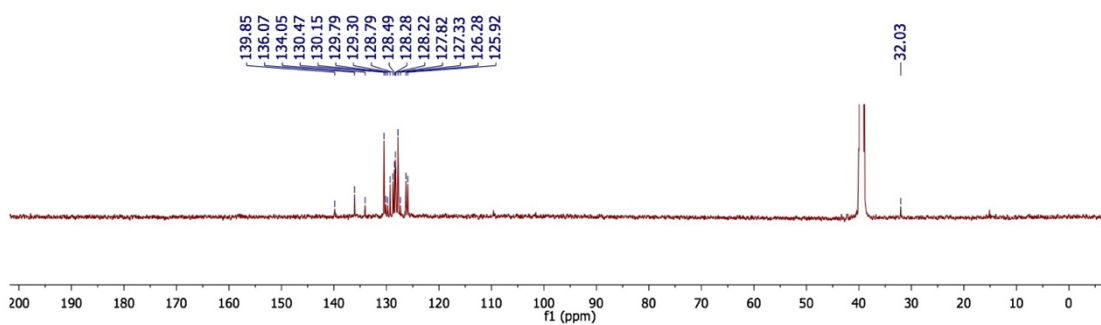


NMR and MS characterization of diphenylterazine (8)

^1H NMR



^{13}C NMR



ESI-MS

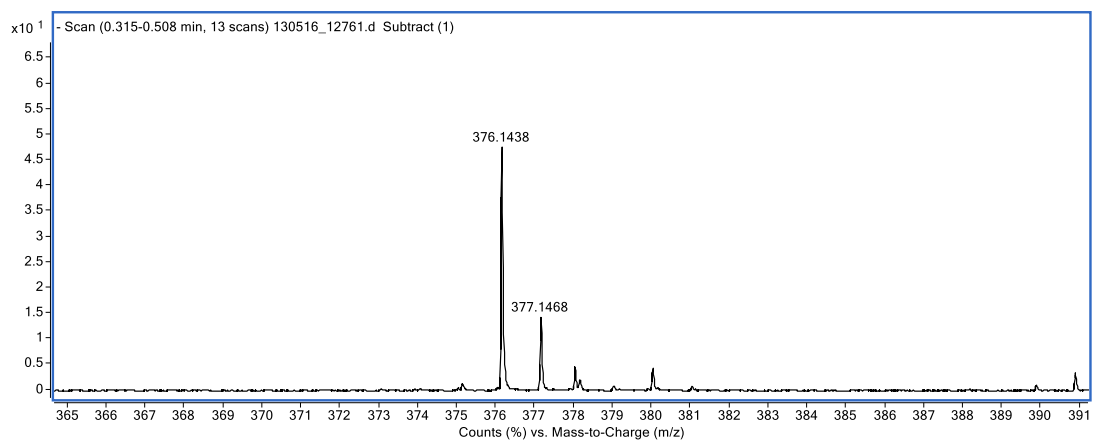


Table 2. Oligonucleotides used in this study.

Oligo name	Nucleotide sequence
XhoI-NL-F	GCAACTCGAGCATGGTCTTCACACTCGAAGATTTGTTGG
NL-R-HindIII	TTGCCAAGCTTACGCCAGAATGCGTTTCGACAGCCGC
I44I54NNK-F	CCGATCCAAAGGNNKGTCTGAGCGGTGAAAATGGGCTGAAGNNKGACATCCATGTC
I44I54NNK-R	GACATGGATGTCMNNCTTCAGCCATTTTCACCGCTCAGGACMNNCTTTGGATCGG
I138NNK-F	TGGAACGGCAACAAAATTNNKGACGAGCGCTGATCAAC
I138NNK-R	GTTGATCAGGCGCTCGTCMNNAAATTTGTGCCGTTCCA
L18D19NNK-F	CAGACAGCCGGCTACAACNNKNNKCAAGTC CTTGAACAGGGAGGTGTG
L18D19NNK-R	CACACCTCCCTGTTCAAG GACTTGMNNMNNGTGTAGCCGGCTGTCTG
R162C164NNK-R	TTGCCAAGCTTACGCCAGAATGCGTTMNNCAGMNN CCAGCCGGTCACTCCGTT
HindIII-NL-F-Koz	AATAAAGCTTGCCGCCACCATGGTCTTCACACTCGAAGATTTGTTGG
NL-R-XhoI	TAATCTCGAGTTACGCCAGAATGCGTTCGCA
NL-R-164H	TAATCTCGAGTTACGCCAGAATGCGTTCATG
NL-R-164S	TAATCTCGAGTTACGCCAGAATGCGTTCACT
FLuc-F	ATTATAAAGCTTGCCGCCACCATGGAAGACGCCAAAAACATAAAGAAAG
FLuc-R	TTATTCTCGAGTTACAATTTGGACTTTCCGCCCTTCTTGG
Ant-HindIII-F-koz	ATTATAAAGCTTGCCGCCACCATGGTGAGCAAGGGCGAGGAG
Ant-XhoI-R	TTATTCTCGAGTTACTTGTACAGCTCGTCCAT
Te19DtoS_F	GGCTACAACCTTGAGTCAAGTCCTGAA
Te19DtoS_R	TTCAAGGACTTGACTCAAGTTGTAGCC
Te85DtoN_F	TACCCTGTGGATAATCATCACTTTA
Te85DtoN_R	TAAAGTGATGATTATCCACAGGGTA
Te164CtoH_F	TGACCGGCTGGCGTCTGCATGAACGCATTCTGG
Te164CtoH_R	CCAGAATGCGTTTACATGCAGACGCCAGCCGGTCA
Antares_F_XhoI	ATAACTCGAGCATGGTGAGCAAGGGCGAGGAG
Antares_R_HindIII	TTGCCAAGCTTACTTGTACAGCTCGTCCAT
NL-Myc-R	TGAGTTTTTGTTCGCCGGAGCCCGCCAGAATGCGTTCGCACAGCCGC
teLuc-Myc-R	TGAGTTTTTGTTCGCCGGAGCCCGCCAGAATGCGTTCATGCAGACGC
yeLuc-Myc-R	TGAGTTTTTGTTCGCCGGAGCCCGCCAGAATGCGTTCCTCAGACGC
FLuc-Myc-R	TGAGTTTTTGTTCGCCGGAGCCCAATTTGGACTTTCCGCCCTTCTTGG
Antares-Myc-R	TGAGTTTTTGTTCGCCGGAGCCCTTGTACAGCTCGTCCATGCCTCCG
Myc-R-XhoI	TAATCTCGAGTTACAGATCCTCTTCTGAGATGAGTTTTTGTTCGCCGGAGCC
P2A-FLuc-F	GCAGGCTGGAGACGTGGAGGAGAACCCTGGACCTATGGAAGACGCCAAAAACATAAAGAA
P2A-ext-R	CCAGGGTCTCCTCCACGTCTCCAGCCTGCTTCAGCAGGCTGAAGTTAGTAGCTCCGCTT
teLuc-P2A-R	AGGCTGAAGTTAGTAGCTCCGCTTCCCGCCAGAATGCGTTCATGCAGACGC
NLuc-P2A-R	AGGCTGAAGTTAGTAGCTCCGCTTCCCGCCAGAATGCGTTCATGCAGACCCGC
Luc2-F-HindIII-Kozak	ATTATAAAGCTTGCCGCCACCATGGAAGATGCCAAAAACATTAAGA
Luc2-Myc-R	TGAGTTTTTGTTCGCCGGAGCCACGGCGATCTTGCCGCCCTTCTT

References

1. Thorne, N.; Inglese, J.; Auld, D. S., Illuminating insights into firefly luciferase and other bioluminescent reporters used in chemical biology. *Chem. Biol.* **2010**, *17* (6), 646-57.
2. Zinn, K. R.; Chaudhuri, T. R.; Szafran, A. A.; O'Quinn, D.; Weaver, C.; Dugger, K.; Lamar, D.; Kesterson, R. A.; Wang, X.; Frank, S. J., Noninvasive bioluminescence imaging in small animals. *ILAR J.* **2008**, *49* (1), 103-15.
3. Negrin, R. S.; Contag, C. H., In vivo imaging using bioluminescence: a tool for probing graft-versus-host disease. *Nat. Rev. Immunol.* **2006**, *6* (6), 484-90.
4. Tung, J. K.; Berglund, K.; Gutekunst, C. A.; Hochgeschwender, U.; Gross, R. E., Bioluminescence imaging in live cells and animals. *Neurophotonics* **2016**, *3* (2), 025001.
5. Kelkar, M.; De, A., Bioluminescence based in vivo screening technologies. *Curr. Opin. Pharmacol.* **2012**, *12* (5), 592-600.
6. Ando, Y.; Niwa, K.; Yamada, N.; Enomoto, T.; Irie, T.; Kubota, H.; Ohmiya, Y.; Akiyama, H., Firefly bioluminescence quantum yield and colour change by pH-sensitive green emission. *Nat Photon* **2008**, *2* (1), 44-47.
7. Saito, K.; Chang, Y. F.; Horikawa, K.; Hatsugai, N.; Higuchi, Y.; Hashida, M.; Yoshida, Y.; Matsuda, T.; Arai, Y.; Nagai, T., Luminescent proteins for high-speed single-cell and whole-body imaging. *Nat. Commun.* **2012**, *3*, 1262.
8. Hall, M. P.; Unch, J.; Binkowski, B. F.; Valley, M. P.; Butler, B. L.; Wood, M. G.; Otto, P.; Zimmerman, K.; Vidugiris, G.; Machleidt, T.; Robers, M. B.; Benink, H. A.; Eggers, C. T.; Slater, M. R.; Meisenheimer, P. L.; Klaubert, D. H.; Fan, F.; Encell, L. P.; Wood, K. V., Engineered luciferase reporter from a deep sea shrimp utilizing a novel imidazopyrazinone substrate. *ACS Chem. Biol.* **2012**, *7* (11), 1848-57.
9. Stacer, A. C.; Nyati, S.; Moudgil, P.; Iyengar, R.; Luker, K. E.; Rehemtulla, A.; Luker, G. D., NanoLuc reporter for dual luciferase imaging in living animals. *Mol. Imaging* **2013**, *12* (7), 1-13.
10. Zhao, H.; Doyle, T. C.; Coquoz, O.; Kalish, F.; Rice, B. W.; Contag, C. H., Emission spectra of bioluminescent reporters and interaction with mammalian tissue determine the sensitivity of detection in vivo. *J Biomed Opt* **2005**, *10* (4), 41210.
11. Lin, M. Z.; McKeown, M. R.; Ng, H. L.; Aguilera, T. A.; Shaner, N. C.; Campbell, R. E.; Adams, S. R.; Gross, L. A.; Ma, W.; Alber, T.; Tsien, R. Y., Autofluorescent proteins with excitation in the optical window for intravital imaging in mammals. *Chem. Biol.* **2009**, *16* (11), 1169-79.
12. Mezzanotte, L.; Aswendt, M.; Tennstaedt, A.; Hoeben, R.; Hoehn, M.; Lowik, C., Evaluating reporter genes of different luciferases for optimized in vivo bioluminescence imaging of transplanted neural stem cells in the brain. *Contrast Media Mol. Imaging* **2013**, *8* (6), 505-13.
13. Mofford, D. M.; Reddy, G. R.; Miller, S. C., Aminoluciferins extend firefly luciferase bioluminescence into the near-infrared and can be preferred substrates over D-luciferin. *J. Am. Chem. Soc.* **2014**, *136* (38), 13277-82.
14. Liang, Y.; Walczak, P.; Bulte, J. W., Comparison of red-shifted firefly luciferase Ppy RE9 and conventional Luc2 as bioluminescence imaging reporter genes for in vivo imaging of stem cells. *J Biomed Opt* **2012**, *17* (1), 016004.
15. Kojima, R.; Takakura, H.; Ozawa, T.; Tada, Y.; Nagano, T.; Urano, Y., Rational design and development of near-infrared-emitting firefly luciferins available in vivo. *Angew. Chem. Int. Ed. Engl.* **2013**, *52* (4), 1175-9.
16. Jathoul, A. P.; Grounds, H.; Anderson, J. C.; Pule, M. A., A dual-color far-red to near-infrared firefly luciferin analogue designed for multiparametric bioluminescence imaging. *Angew Chem Int Ed Engl* **2014**, *53* (48), 13059-63.
17. Harwood, K. R.; Mofford, D. M.; Reddy, G. R.; Miller, S. C., Identification of mutant firefly luciferases that efficiently utilize aminoluciferins. *Chem. Biol.* **2011**, *18* (12), 1649-57.
18. Adams, S. T., Jr.; Miller, S. C., Beyond D-luciferin: expanding the scope of bioluminescence imaging in vivo. *Curr. Opin. Chem. Biol.* **2014**, *21c*, 112-120.
19. Evans, M. S.; Chaurette, J. P.; Adams, S. T., Jr.; Reddy, G. R.; Paley, M. A.; Aronin, N.; Prescher, J. A.; Miller, S. C., A synthetic luciferin improves bioluminescence imaging in live mice. *Nat Methods* **2014**, *11* (4), 393-5.

20. Kuchimaru, T.; Iwano, S.; Kiyama, M.; Mitsumata, S.; Kadonosono, T.; Niwa, H.; Maki, S.; Kizaka-Kondoh, S., A luciferin analogue generating near-infrared bioluminescence achieves highly sensitive deep-tissue imaging. *Nat Commun* **2016**, *7*, 11856.
21. Iwano, S.; Obata, R.; Miura, C.; Kiyama, M.; Hama, K.; Nakamura, M.; Amano, Y.; Kojima, S.; Hirano, T.; Maki, S.; Niwa, H., Development of simple firefly luciferin analogs emitting blue, green, red, and near-infrared biological window light. *Tetrahedron* **2013**, *69* (19), 3847-3856.
22. Inouye, S.; Shimomura, O., The use of Renilla luciferase, Oplophorus luciferase, and apoaequorin as bioluminescent reporter protein in the presence of coelenterazine analogues as substrate. *Biochem. Biophys. Res. Commun.* **1997**, *233* (2), 349-53.
23. Wu, C.; Nakamura, H.; Murai, A.; Shimomura, O., Chemi- and bioluminescence of coelenterazine analogues with a conjugated group at the C-8 position. *Tetrahedron Lett.* **2001**, *42* (16), 2997-3000.
24. Inouye, S.; Sato, J.; Sahara-Miura, Y.; Yoshida, S.; Kurakata, H.; Hosoya, T., C6-Deoxy coelenterazine analogues as an efficient substrate for glow luminescence reaction of nanoKAZ: the mutated catalytic 19 kDa component of Oplophorus luciferase. *Biochem. Biophys. Res. Commun.* **2013**, *437* (1), 23-8.
25. Jiang, T.; Du, L.; Li, M., Lighting up bioluminescence with coelenterazine: strategies and applications. *Photochem. Photobiol. Sci.* **2016**, *15* (4), 466-80.
26. Nishihara, R.; Suzuki, H.; Hoshino, E.; Suganuma, S.; Sato, M.; Saitoh, T.; Nishiyama, S.; Iwasawa, N.; Citterio, D.; Suzuki, K., Bioluminescent coelenterazine derivatives with imidazopyrazinone C-6 extended substitution. *Chem. Commun.* **2015**, *51* (2), 391-4.
27. Chu, J.; Oh, Y.; Sens, A.; Ataie, N.; Dana, H.; Macklin, J. J.; Laviv, T.; Welf, E. S.; Dean, K. M.; Zhang, F.; Kim, B. B.; Tang, C. T.; Hu, M.; Baird, M. A.; Davidson, M. W.; Kay, M. A.; Fiolka, R.; Yasuda, R.; Kim, D. S.; Ng, H. L.; Lin, M. Z., A bright cyan-excitable orange fluorescent protein facilitates dual-emission microscopy and enhances bioluminescence imaging in vivo. *Nat Biotechnol* **2016**, *34* (7), 760-7.
28. Schindelin, J.; Arganda-Carreras, I.; Frise, E.; Kaynig, V.; Longair, M.; Pietzsch, T.; Preibisch, S.; Rueden, C.; Saalfeld, S.; Schmid, B.; Tinevez, J. Y.; White, D. J.; Hartenstein, V.; Eliceiri, K.; Tomancak, P.; Cardona, A., Fiji: an open-source platform for biological-image analysis. *Nat. Methods* **2012**, *9* (7), 676-82.
29. Liu, F.; Song, Y.; Liu, D., Hydrodynamics-based transfection in animals by systemic administration of plasmid DNA. *Gene Ther* **1999**, *6* (7), 1258-66.
30. Giuliani, G.; Molinari, P.; Ferretti, G.; Cappelli, A.; Anzini, M.; Vomero, S.; Costa, T., New red-shifted coelenterazine analogues with an extended electronic conjugation. *Tetrahedron Lett.* **2012**, *53* (38), 5114-5118.
31. Yuan, M.-L.; Jiang, T.-Y.; Du, L.-P.; Li, M.-Y., Luminescence of coelenterazine derivatives with C-8 extended electronic conjugation. *Chin. Chem. Lett.* **2016**, *27* (4), 550-554.
32. Sun, Y. Q.; Liu, J.; Lv, X.; Liu, Y.; Zhao, Y.; Guo, W., Rhodamine-inspired far-red to near-infrared dyes and their application as fluorescence probes. *Angew. Chem. Int. Ed. Engl.* **2012**, *51* (31), 7634-6.
33. Yamashita, Y.; Ono, K.; Tomura, M.; Tanaka, S., Synthesis and Properties of Benzobis(thiadiazole)s with Nonclassical π -Electron Ring Systems. *Tetrahedron* **1997**, *53* (29), 10169-10178.
34. Conley, N. R.; Dragulescu-Andrasi, A.; Rao, J.; Moerner, W. E., A selenium analogue of firefly D-luciferin with red-shifted bioluminescence emission. *Angew Chem Int Ed Engl* **2012**, *51* (14), 3350-3.
35. Taniguchi, N.; Onami, T., Magnesium-Induced Copper-Catalyzed Synthesis of Unsymmetrical Diaryl Chalcogenide Compounds from Aryl Iodide via Cleavage of the Se-Se or S-S Bond. *The Journal of Organic Chemistry* **2004**, *69* (3), 915-920.
36. Miyaura, N.; Yamada, K.; Suzuki, A., A new stereospecific cross-coupling by the palladium-catalyzed reaction of 1-alkenylboranes with 1-alkenyl or 1-alkynyl halides. *Tetrahedron Lett.* **1979**, *20* (36), 3437-3440.
37. Adamczyk, M.; Akireddy, S. R.; Johnson, D. D.; Mattingly, P. G.; Pan, Y.; Reddy, R. E., Synthesis of 3,7-dihydroimidazo[1,2a]pyrazine-3-ones and their chemiluminescent properties. *Tetrahedron* **2003**, *59* (41), 8129-8142.

38. Inouye, S.; Sato, J.; Sahara-Miura, Y.; Yoshida, S.; Hosoya, T., Luminescence enhancement of the catalytic 19 kDa protein (KAZ) of *Oplophorus* luciferase by three amino acid substitutions. *Biochem Biophys Res Commun* **2014**, *445* (1), 157-62.
39. Tomabechi, Y.; Hosoya, T.; Ehara, H.; Sekine, S.; Shirouzu, M.; Inouye, S., Crystal structure of nanoKAZ: The mutated 19 kDa component of *Oplophorus* luciferase catalyzing the bioluminescent reaction with coelenterazine. *Biochem Biophys Res Commun* **2016**, *470* (1), 88-93.

Chapter 3

A New Palette of ATP-independent Bioluminescence Reporters for Superior Biocompatibility and *in vivo* Sensitivity

Abstract

Coelenterazine (CTZ)-utilizing marine luciferases and their derivatives have attracted significant attention because of their ATP-independency, fast enzymatic turnover, and high bioluminescence brightness. However, marine luciferases typically emit blue photons and their substrates, including CTZ and the recently developed diphenylterazine (DTZ), have poor water solubility, hindering their *in vivo* applications. Herein, we report a family of pyridyl CTZ and DTZ analogs that exhibit spectrally shifted emission and improved water solubility. Through directed evolution, we engineered a LumiLuc luciferase with broad substrate specificity. In the presence of corresponding pyridyl substrates (i.e., pyCTZ, 6pyDTZ, or 8pyDTZ), LumiLuc generates highly bright blue, teal, or yellow bioluminescence. We compared our LumiLuc-8pyDTZ pair with several benchmark reporters in a tumor xenograft mouse model. Our new pair, which does not need organic cosolvents for *in vivo* administration, surpasses other reporters by detecting early tumors. We further fused LumiLuc to a red fluorescent protein, resulting in a LumiScarlet reporter with further red-shifted emission and enhanced tissue penetration. LumiScarlet-8pyDTZ was comparable to Akaluc-AkaLumine, the brightest ATP-dependent luciferase-luciferin pair, for detecting cells in deep tissues of mice. In summary, we have engineered a new palette of ATP-independent bioluminescent reporters, which will have broad applications because of their ATP-independency, excellent biocompatibility, and superior *in vivo* sensitivity.

3.1. Introduction

In the past few decades, fluorescence imaging has evolved quickly and become a dominant visualization method for live-cell studies.¹ However, fluorescence imaging has several limitations, such as photobleaching, phototoxicity, and poor tissue penetration, largely due to the need for light excitation. Unlike fluorescence, bioluminescence produces photons *via* enzyme-catalyzed biochemical reactions in which luciferases oxidize their corresponding small-molecule substrates (*a.k.a.*, luciferins) to generate excited-state emitters. As a result, bioluminescence signals glow essentially on dark background, leading to excellent signal-to-background ratios. Moreover, even though the spatial resolution of bioluminescence imaging (BLI) is usually worse than that of fluorescence imaging, the emitted photons can escape through several centimeters of tissue.² BLI is thus especially suited for diverse, noninvasive *in vivo* imaging applications.³⁻⁵

Photinus pyralis firefly luciferase (FLuc) and D-luciferin (λ_{max} : 563 nm) constitute the most widely used luciferase-luciferin pair for *in vivo* BLI. Recently, research has been performed to develop FLuc and D-luciferin derivatives for brighter and more red-shifted emission. In particular, an Akaluc-AkaLumine luciferase-luciferin pair with near-infrared (NIR) emission (λ_{max} : 650 nm) was reported for highly sensitive deep-tissue *in vivo* BLI.⁶ Despite the progress, AkaLumine has been shown to induce cell morphology changes and cytotoxicity.⁷⁻⁹ Moreover, FLuc, Akaluc, and other insect luciferases consume ATP for photon production; the bioluminescence reaction between FLuc and D-luciferin reduced the intracellular ATP-to-ADP ratio of live mammalian cells from > 40:1 to ~ 20:1,⁸ suggesting metabolic disruption by all ATP-dependent luciferases. Because ATP is required for the activation of the luciferin substrates, this metabolic disruption issue cannot be addressed by simply improving insect luciferases and the corresponding substrates.

In contrast to insect luciferases, a large family of marine luciferases and photoproteins, such as *Renilla* luciferase (RLuc), *Gaussia* luciferase (GLuc), *Oplophorus* luciferase (OLuc), and aequorin, are ATP-independent and use coelenterazine (CTZ, **Figure 1**) as their native substrate for bioluminescence production.¹⁰ The 19kDa catalytic domain of OLuc¹¹ was recently engineered into NanoLuc, which has a fast enzyme turnover and produces intense blue bioluminescence (λ_{\max} : 456 nm) in the presence of a synthetic CTZ analog, furimazine (FRZ, **Figure 1**).¹² To expand the color palette, NanoLuc was further engineered into teLuc, which emits red-shifted photons (λ_{\max} : 502 nm) when paired with a synthetic substrate diphenylterazine (DTZ, **Figure 1**).⁷ Since biological tissues significantly absorb and scatter short-wavelength photons,¹³ NanoLuc and teLuc have been fused to fluorescent proteins, resulting in Antares, Antares2, and enhanced Nano-Lanterns for further red-shifted emission *via* bioluminescence resonance energy transfer (BRET).^{7, 14-15} Despite the progress, *in vivo* applications of these bioluminescent reporters are greatly hindered by the low solubility of their substrates. Typically, hydroxypropyl- β -cyclodextrin, polyethylene glycols (PEGs), or other organic cosolvents are used to formulate the substrates for *in vivo* administration.^{7, 14, 16-17} These formulation ingredients are not biologically inert and may cause irritation or biotoxicity. It is also practically difficult to handle these highly viscous solutions for *in vivo* operations. Furthermore, it is still of great interest to further red-shift marine luciferases for enhanced tissue penetration.

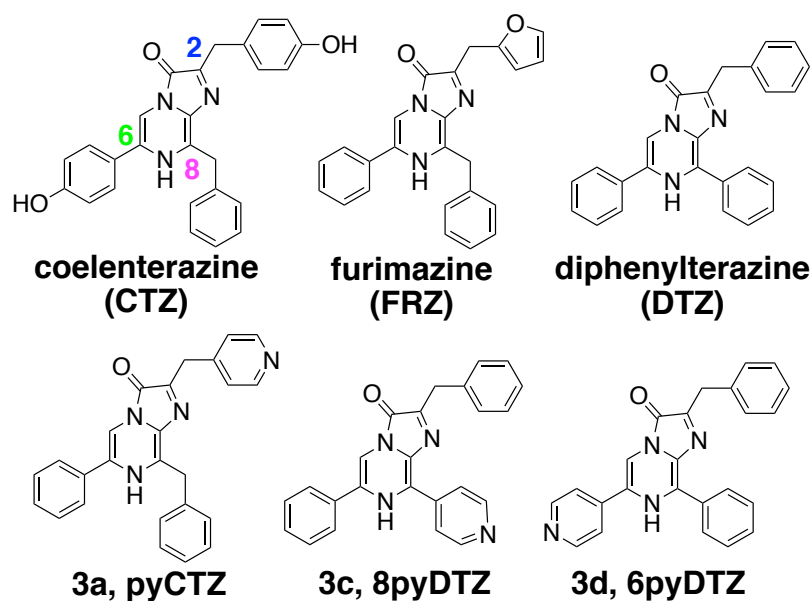


Figure 1. Chemical structures of coelenterazine (CTZ), furimazine (FRZ), diphenylterazine (DTZ), pyCTZ (**3a**), 8pyDTZ (**3c**) and 6pyDTZ (**3d**).

In this work, we chemically modified CTZ and DTZ for spectrally shifted emission and enhanced water solubility. Concurrently, we engineered teLuc into a LumiLuc luciferase, which is highly active toward the new substrates for intense blue, teal, and yellow emission. Moreover, by harnessing a recently reported high-quality red fluorescent protein, mScarlet-I, we developed a LumiScarlet reporter with significant emission longer than 600 nm. Our multipronged approach yielded a new palette of ATP-independent bioluminescent reporters, which are expected to have broad applications.

3.2. Experimental section

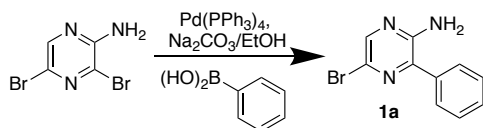
3.2.1. Material and methods

Synthetic DNA oligonucleotides were purchased from Integrated DNA Technologies. Restriction endonucleases were purchased from Thermo Fisher Scientific. Q5 high-

fidelity DNA polymerase and Taq DNA polymerase were purchased from NEB. Products of PCR and restriction digestion were purified by gel electrophoresis and Syd Laboratories Gel Extraction columns. Plasmid DNA was purified using Syd Laboratories Miniprep columns. DNA sequences were analyzed by Eurofins. Potassium D-luciferin was purchased from Thermo Fisher Scientific. Coelenterazine was purchased from Gold Biotechnology. Furimazine (Nano-Glo®) was purchased from Promega. AkaLumine-HCl was purchased from Aobious. CTZ was purchased from GOLDBIO. DTZ was obtained from Haoyuan Chemexpress Co., Ltd. All other chemicals were purchased from Sigma-Aldrich, Fisher Scientific, or VWR and used without further purification. Bruker Avance DRX 600 and Varian NMRS 600 at the UVA Biomolecular Magnetic Resonance Facility was used to record all NMR spectra. Chemical shift (δ) is given in parts per million relative to ^1H (7.24 p.p.m.) and ^{13}C (77.23 p.p.m.) for CDCl_3 ; ^1H (2.50 p.p.m.) and ^{13}C (39.5 p.p.m.) for DMSO-d_6 ; ^1H (3.31 p.p.m.) and ^{13}C (49.15 p.p.m.) for methanol- d_4 . Splitting patterns are reported as s (singlet), bs (broad singlet), d (doublet), t (triplet), dd (doublet of doublets), and m (multiplet). Coupling constant (J) is given in Hz. High resolution ESI-MS was run on an Agilent 6545 Q-TOF LC/MS system by direct infusion. A Waters Delta Prep ZQ 2000 LC-MS Purification System equipped with a XBridge BEH Amide OBD Prep Column (130Å, 5 μm , 30 mm X 150 mm) was used for preparative reverse-phase HPLC purifications. Nu/J mice were obtained from the Jackson Laboratory (Cat. # 002019) and maintained and treated in standard conditions that complied with all relevant ethical regulations. All animal procedures were approved by the UVA Institutional Animal Care and Use Committee. Images were analyzed using the Fiji image analysis software. Microsoft Excel and GraphPad Prism were used to analyze data and prepare figures.

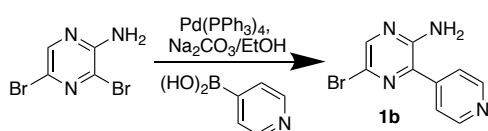
3.2.2. Chemical synthesis

5-bromo-3-phenylpyrazin-2-amine (1a):

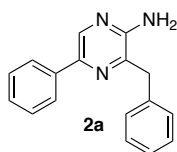


To a solution of Pd(PPh₃)₄ (460 mg, 0.4 mmol, 0.1 equiv.) in 200 mL EtOH was added 2-Amino-3,5-dibromopyrazine (1010 mg, 4 mmol, 1 equiv.), 1N Na₂CO₃ solution (8 mL, 8 mmol, 2 equiv.) and phenylboronic acid (490 mg, 4 mmol, 1 equiv.). The resultant mixture was stirred at 80 °C under argon for 12 h. The solvent was removed *in vacuo* and the residue was suspended in 200 mL ddH₂O, which was extracted twice with EtOAc (200 mL). The organic layers were combined and dried over anhydrous Na₂SO₄, filtered and removed in *vacuo*. The residue was purified by silica column chromatography with elution (DCM:MeOH = 100:1) to yield compound **1a** as yellow solid (360 mg, 36%). ¹H NMR (600 MHz, CDCl₃) δ 8.07 (s, 1H), 7.71 (d, J = 7.4 Hz, 2H), 7.50 (t, J = 7.4 Hz, 2H), 7.45 (t, J = 7.4 Hz, 1H), 4.82 (s, 2H). ¹³C NMR (151 MHz, DMSO-d₆) δ 152.4, 142.4, 139.3, 135.9, 129.2, 128.8, 128.7, 128.1, 127.9, 123.9. HRMS (ESI-TOF) calcd for C₁₀H₈BrN₃ [M + H]⁺: 249.9902, found: m/z 249.9916.

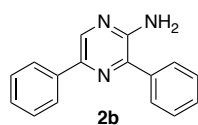
5-bromo-3-(pyridin-4-yl)pyrazin-2-amine (**1b**):



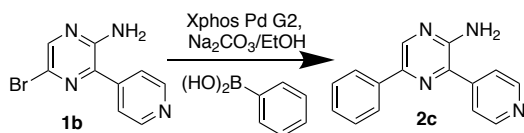
The synthesis of **1b** followed the same procedure as **1a**, whereas 4-pyridylboronic acid (492 mg, 4 mmol, 1 equiv.) was used. Crude **1b** was purified by column chromatography with elution (DCM:MeOH = 10:1) to yield **1b** as yellow solid (301 mg, 30%). ¹H NMR (600 MHz, DMSO-d₆) δ 8.69 (d, J = 6.0 Hz, 2H), 8.17 (s, 1H), 7.67 (d, J = 6.0 Hz, 2H), 6.68 (s, 2H). ¹³C NMR (151 MHz, DMSO-d₆) δ 152.6, 150.1, 144.1, 143.3, 136.1, 124.0, 122.4. HRMS (ESI-TOF) calcd for C₉H₇BrN₄ [M + H]⁺: 250.9854, found: m/z 250.9845.

3-benzyl-5-phenylpyrazin-2-amine (2a):

2a was prepared following the published synthesis methods¹⁸. ¹H NMR (600 MHz, DMSO-d₆) δ 8.41 (s, 1H), 7.89 (d, J = 7.4 Hz, 2H), 7.39 (t, J = 7.7 Hz, 2H), 7.33 (d, J = 7.6 Hz, 2H), 7.27 (q, J = 7.7, 7.1 Hz, 3H), 7.18 (t, J = 7.3 Hz, 1H), 6.39 (s, 2H), 4.07 (s, 2H). ¹³C NMR (150 MHz, DMSO-d₆) δ 153.2, 140.5, 139.2, 138.6, 137.6, 137.4, 129.4, 129.1, 128.7, 127.8, 126.6, 125.2, 39.1. HRMS (ESI-TOF) calcd for C₁₇H₁₅N₃ [M + H]⁺: 262.1266, found: m/z 262.1258.

3,5-diphenylpyrazin-2-amine (2b):

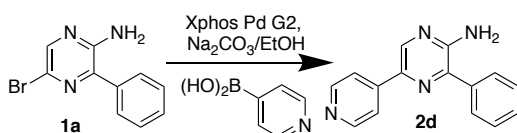
2b was reported in our previous paper.⁷

5-phenyl-3-(pyridin-4-yl)pyrazin-2-amine (2c):

The synthesis and purification of **2c** followed the same procedure as **2d**, whereas **1b** was used as the starting compound and phenylboronic acid (245 mg, 2 mmol, 2 equiv.) was used as boron reagent. Yellow solid (87 mg, 70%). ¹H NMR (600 MHz, DMSO-d₆) δ 7.88 – 7.84 (m, 2H), 7.70 (s, 1H), 7.15 (dt, J = 7.8, 1.2 Hz, 2H), 7.12 – 7.08 (m, 2H), 6.65 – 6.59 (m, 2H), 6.57 – 6.51 (m, 1H). ¹³C NMR (150 MHz, DMSO-d₆) δ 152.3,

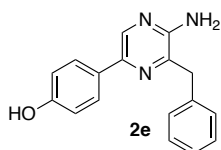
150.1, 144.9, 140.0, 139.4, 136.6, 134.7, 128.8, 127.9, 125.0, 122.7. HRMS (ESI-TOF) calcd for $C_{15}H_{12}N_4$ $[M + H]^+$: 249.1062, found: m/z 249.1059.

3-phenyl-5-(pyridin-4-yl)pyrazin-2-amine (2d):



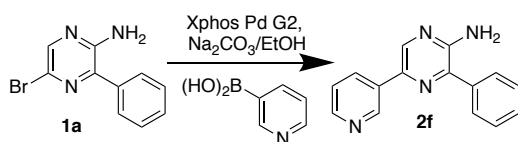
To a mixture of XPhos Pd G2 (79 mg, 0.1 mmol, 0.2 equiv.) and XPhos (24 mg, 0.05 mmol, 0.1 equiv.) in 5 mL EtOH was added **1a** (125 mg, 0.5 mmol, 1 equiv.), 1N Na₂CO₃ (1 mL, 1 mmol, 2 equiv.) and 4-pyridylboronic acid (246 mg, 2 mmol, 4 equiv.). The resulting mixture was stirred at 80 °C under argon for 12 h. The solvent was then removed *in vacuo* and the residue was dissolved in 1N HCl (30 mL) and subsequently washed with EtOAc (30 mL). The aqueous layer was collected and the pH was then adjusted to 10 by the addition of 1N NaOH. Product **2d** precipitated as yellow solid, which was filtered, washed with EtOAc and dried under reduced pressure overnight. (93 mg, 75%). ¹H NMR (600 MHz, DMSO-d₆) δ 8.71 (s, 1H), 8.58 (d, J = 6.2 Hz, 2H), 7.94 (d, J = 6.2 Hz, 2H), 7.78 (d, J = 7.2 Hz, 2H), 7.52 (t, J = 7.5 Hz, 2H), 7.46 (t, J = 7.3 Hz, 1H), 6.63 (s, 2H). ¹³C NMR (150 MHz, DMSO-d₆) δ 153.3, 150.1, 144.0, 139.2, 138.6, 137.1, 128.8, 128.2, 119.0. HRMS (ESI-TOF) calcd for $C_{15}H_{12}N_4$ $[M + H]^+$: 249.1062, found: m/z 249.1060.

4-(5-amino-6-benzylpyrazin-2-yl)phenol (2e):



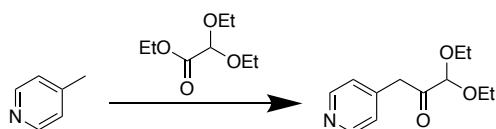
2e was prepared following the published synthesis methods¹⁹. ¹H NMR (600 MHz, DMSO-*d*₆) δ 9.49 (s, 1H), 8.29 (s, 1H), 7.72 (d, *J* = 8.6 Hz, 2H), 7.33 (d, *J* = 7.3 Hz, 2H), 7.28 (t, *J* = 7.6 Hz, 2H), 7.18 (t, *J* = 7.3 Hz, 1H), 6.79 (d, *J* = 8.6 Hz, 2H), 6.19 (s, 2H), 4.06 (s, 2H). ¹³C NMR (150 MHz, DMSO-*d*₆) δ 157.1, 152.0, 139.7, 139.5, 138.3, 135.9, 135.9, 128.9, 128.2, 126.2, 126.1, 115.5, 115.4, 38.7. HRMS (ESI-TOF) calcd for C₁₇H₁₅N₃O [M + H]⁺: 278.1215, found: m/z 278.1208.

3-phenyl-5-(pyridin-3-yl)pyrazin-2-amine (2f):



The synthesis and purification of **2f** followed the same procedure as **2d**, whereas 3-pyridylboronic acid (246 mg, 2 mmol, 4 equiv.) was used. Yellow solid (95 mg, 77%). ¹H NMR (600 MHz, DMSO-*d*₆) δ 9.19 (s, 1H), 8.64 (s, 1H), 8.54 (d, *J* = 3.9 Hz, 1H), 8.39 (d, *J* = 8.1 Hz, 1H), 7.79 (d, *J* = 7.3 Hz, 2H), 7.53 – 7.49 (m, 3H), 7.46 (t, *J* = 7.3 Hz, 1H), 6.47 (s, 2H). ¹³C NMR (151 MHz, DMSO-*d*₆) δ 152.6, 148.5, 146.3, 138.4, 138.4, 137.3, 137.2, 132.6, 132.3, 132.2, 128.8, 128.6, 128.3. HRMS (ESI-TOF) calcd for C₁₅H₁₂N₄ [M + H]⁺: 249.1062, found: m/z 249.1060.

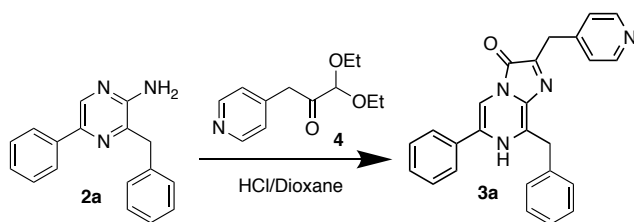
3-pyridin-4-yl-1,1-diethoxyacetone (4):



To a solution of 4-methylpyridine (931 mg, 10 mmol, 1 equiv.) in 50 mL anhydrous THF was added potassium tert-butoxide (5.6 g, 50 mmol, 5 equiv.), and the mixture was

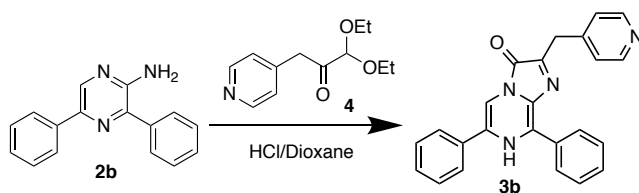
stirred at room temperature for 10 min. Ethyl diethoxyacetate (3.52 g, 20 mmol, 2 equiv.) in 20 mL THF was then added dropwise over 10 min. The resulting mixture was stirred overnight, and solvent was removed under *vacuo*. The residue was purified by silica column chromatography with elution (Hexane:EtOAc = 1:3 to 100% EtOAc) to yield product as light yellow solid (669 mg, 30%). ¹H NMR (600 MHz, DMSO-d₆) δ 8.47 (d, J = 5.8 Hz, 2H), 7.18 (d, J = 5.8 Hz, 2H), 4.81 (s, 1H), 3.91 (s, 2H), 3.63 (dq, J = 9.7, 7.1 Hz, 2H), 3.54 (dq, J = 9.7, 7.1 Hz, 2H), 1.15 (t, J = 7.1 Hz, 6H). ¹³C NMR (150 MHz, DMSO-d₆) δ 202.0, 149.3, 143.2, 125.3, 101.6, 62.8, 42.6, 15.1. HRMS (ESI-TOF) calcd for C₁₂H₁₇NO₃ [M + H]⁺: 224.1208, found: m/z 224.1195.

8-benzyl-6-phenyl-2-(pyridin-4-ylmethyl)imidazo[1,2-a]pyrazin-3(7H)-one (3a):



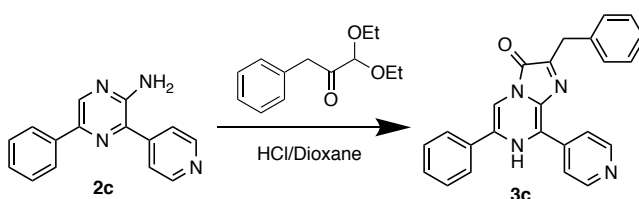
To a solution of **2a** (26 mg, 0.1 mmol, 1 equiv.) and **4** (89 mg, 0.4 mmol 4 equiv) in 5 mL degassed 1,4-dioxane was added 0.8 mL 6N HCl. The resulting mixture was stirred at 80°C in a sealed tube for 12 h. The solvent was then removed *in vacuo* and the residue was dissolved in 1 mL (ACN:H₂O = 1:1) and purified with preparative RP-HPLC. (acetonitrile/water = 1:99 to 90:10, 20 mL/min, UV 254 nm). Product fractions were combined and lyophilized to give **3a** as yellow powder (15 mg, 38%), which has to be stored as solid at -80 °C for long-term stability. ¹H NMR (600 MHz, Methanol-d₄) δ 8.43 (d, J = 6.2 Hz, 2H), 7.74 (s, 1H), 7.65 (d, J = 6.8 Hz, 2H), 7.49 – 7.38 (m, 7H), 7.29 (t, J = 7.6 Hz, 2H), 7.23 (t, J = 7.4 Hz, 1H), 4.42 (s, 2H), 4.23 (s, 2H). ¹³C NMR (150 MHz, Methanol-d₄) δ 142.6, 137.9, 131.1, 130.4, 130.0, 129.9, 129.1, 128.5, 128.3, 110.1, 49.7. HRMS (ESI-TOF) calcd for C₂₅H₂₀N₄O [M + H]⁺: 393.1637, found: m/z 393.1630.

6,8-diphenyl-2-(pyridin-4-ylmethyl)imidazo[1,2-a]pyrazin-3(7H)-one (**3b**):



The synthesis and purification of **3b** followed the same procedure as **3a**, whereas **2b** (25 mg, 0.1 mmol, 1 equiv.) was used as the starting compound. Orange powder (8 mg, 21%). ¹H NMR (600 MHz, Methanol-d₄) δ 8.79 (d, J = 6.5 Hz, 2H), 8.50 (s, 1H), 8.15 (d, J = 7.2 Hz, 2H), 8.06 (d, J = 6.5 Hz, 2H), 8.00 (d, J = 7.4 Hz, 2H), 7.69 (t, J = 7.4 Hz, 1H), 7.65 (t, J = 7.2 Hz, 2H), 7.58 (t, J = 7.2 Hz, 2H), 7.56 – 7.53 (m, 1H), 4.66 (s, 2H). ¹³C NMR (150 MHz, Methanol-d₄) δ 161.0, 146.2, 142.7, 139.3, 134.7, 133.3, 133.0, 131.3, 131.0, 130.4, 130.3, 128.8, 128.5, 112.2. HRMS (ESI-TOF) calcd for C₂₄H₁₈N₄O [M + H]⁺: 379.1481, found: m/z 379.1480.

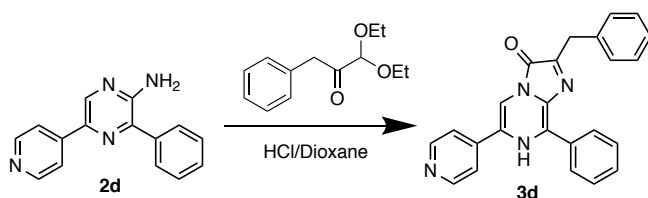
2-benzyl-6-phenyl-8-(pyridin-4-yl)imidazo[1,2-a]pyrazin-3(7H)-one (**3c**):



To a solution of **2c** (25 mg, 0.1 mmol, 1 equiv.) and 1,1-diethoxy-3-phenylpropan-2-one (89 mg, 0.4 mmol, 4 equiv.) in 5 mL degassed 1,4-dioxane was added 0.8 mL 6 N HCl, and the resulting mixture was stirred at 80°C in a sealed tube for 12 h. The solvent was then removed *in vacuo* and the residue was dissolved in 1 mL (ACN:H₂O = 1:1) and next purified with preparative RP-HPLC. (acetonitrile/water = 1:99 to 90:10, 20 mL/min, UV 254 nm). Product fractions were combined and lyophilized to give **3c**

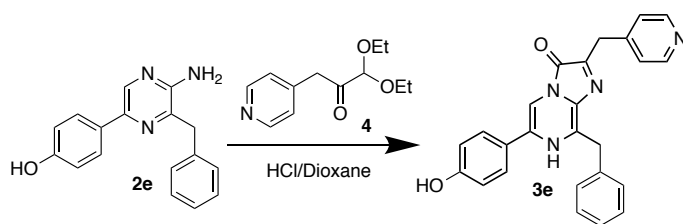
as brown powder (9 mg, 23%). ^1H NMR (600 MHz, Acetonitrile- d_3 and D_2O , ratio = 9:1) δ 9.31 (d, J = 6.8 Hz, 2H), 8.84 (d, J = 6.8 Hz, 2H), 8.54 (s, 1H), 8.09 (d, J = 8.0 Hz, 2H), 7.52 (t, J = 7.6 Hz, 2H), 7.44 (t, J = 7.3 Hz, 1H), 7.35 (d, J = 7.7 Hz, 2H), 7.28 (t, J = 7.7 Hz, 2H), 7.24 – 7.21 (m, 1H), 4.19 (s, 2H). ^{13}C NMR (150 MHz, Methanol- d_4) δ 143.0, 140.7, 140.1, 139.5, 137.5, 132.0, 130.2, 129.9, 129.6, 129.4, 127.8, 127.5, 127.4, 126.5, 113.8, 33.6. HRMS (ESI-TOF) calcd for $\text{C}_{24}\text{H}_{18}\text{N}_4\text{O}$ [$\text{M} + \text{H}$] $^+$: 379.1481, found: m/z 379.1477.

2-benzyl-8-phenyl-6-(pyridin-4-yl)imidazo[1,2-a]pyrazin-3(7H)-one (3d):



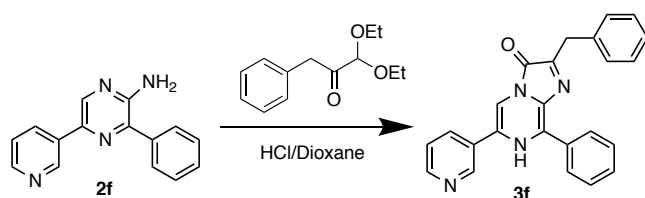
The synthesis and purification of **3d** followed the same procedure as **3c**, whereas **2d** (25 mg, 0.1 mmol, 1 equiv.) was used as the starting compound. Yellow powder (6 mg, 16%). ^1H NMR (600 MHz, Methanol- d_4) δ 9.52 (s, 1H), 9.01 (d, J = 6.8 Hz, 2H), 8.97 (d, J = 6.8 Hz, 2H), 8.15 – 8.11 (m, 2H), 7.71-7.66 (m, 3H), 7.35-7.30 (m, 7.4 Hz, 4H), 7.25 (t, J = 7.4 Hz, 1H), 4.36 (s, 2H). ^{13}C NMR (150 MHz, Methanol- d_4) δ 154.5, 148.8, 143.5, 140.4, 138.4, 137.2, 135.0, 133.1, 130.6, 130.4, 130.4, 130.1, 129.8, 129.5, 128.7, 128.3, 125.3, 117.2, 30.5. HRMS (ESI-TOF) calcd for $\text{C}_{24}\text{H}_{18}\text{N}_4\text{O}$ [$\text{M} + \text{H}$] $^+$: 379.1481, found: m/z 379.1476.

8-benzyl-6-(4-hydroxyphenyl)-2-(pyridin-4-ylmethyl)imidazo[1,2-a]pyrazin-3(7H)-one (3e):



The synthesis and purification of **3e** followed the same procedure as **3a**, whereas **2e** (28 mg, 0.1 mmol, 1 equiv.) was used as the starting compound. Yellow powder (14 mg, 34%). $^1\text{H NMR}$ (600 MHz, Methanol- d_4) δ 8.78 (d, $J = 5.2$ Hz, 2H), 8.08 (d, $J = 5.2$ Hz, 2H), 8.01 (s, 1H), 7.72 (d, $J = 7.7$ Hz, 2H), 7.53 (d, $J = 7.7$ Hz, 3H), 7.42 (d, $J = 7.4$ Hz, 2H), 7.31 (t, $J = 7.4$ Hz, 2H), 7.25 (t, $J = 7.7$ Hz, 1H), 4.58 (s, 2H), 4.52 (s, 2H). $^{13}\text{C NMR}$ (150 MHz, Methanol- d_4) δ 161.2, 142.6, 137.1, 130.3, 130.2, 130.1, 129.1, 128.7, 117.3, 111.3. HRMS (ESI-TOF) calcd for $\text{C}_{25}\text{H}_{20}\text{N}_4\text{O}_2$ $[\text{M} + \text{H}]^+$: 409.1586, found: m/z 409.1585.

2-benzyl-8-phenyl-6-(pyridin-3-yl)imidazo[1,2-a]pyrazin-3(7H)-one (**3f**):



The synthesis and purification of **3f** followed the same procedure as **3c**, whereas **2f** (25 mg, 0.1 mmol, 1 equiv.) was used as the starting compound. Orange powder (8 mg, 21%). $^1\text{H NMR}$ (600 MHz, Methanol- d_4) δ 9.73 (s, 1H), 9.47 (d, $J = 8.3$ Hz, 1H), 9.36 (s, 1H), 8.99 (d, $J = 5.6$ Hz, 1H), 8.32 – 8.27 (m, 1H), 8.09 (d, $J = 6.6$ Hz, 2H), 7.72 – 7.66 (m, 3H), 7.32 (7.67-7.30, 4H), 7.25 (t, $J = 7.0$ Hz, 1H), 4.36 (s, 2H). $^{13}\text{C NMR}$ (150 MHz, Methanol- d_4) δ 148.6, 145.3, 142.9, 141.5, 138.3, 137.4, 137.2, 134.8,

133.1, 130.5, 130.4, 130.1, 129.5, 129.1, 128.3, 128.2, 121.6, 114.8, 30.3. HRMS (ESI-TOF) calcd for $C_{24}H_{18}N_4O$ $[M + H]^+$: 379.1481, found: m/z 379.1478.

3.2.3 Construction of plasmids and libraries

Polymerase chain reactions (PCRs) with various synthetic oligonucleotide pairs (see **Table 3**) were used to amplify genetic elements. To create a gene library with randomization at residues 18 and 19, oligo pairs pBAD-F and L18D19NNK-R, L18D19NNK-F and pBAD-R, were used to amplify two individual fragments from pBAD-teLuc; the corresponding products were used for assembly in a subsequent overlap PCR reaction by using oligos pBAD-F and pBAD-R. The assembled full-length fragment was digested with Xho I and Hind III restriction enzymes and ligated into a predigested, compatible pBAD/His B plasmid. Similarly, pBAD-F, 27VSSNNK-R, 27VSSNNK-F, and pBAD-R were used to create a library with randomization at residues 27, 28, and 29. To introduce random mutations across the gene, Taq DNA polymerase was used in all reactions with 0.2 mM $MnCl_2$ along with unbalanced dNTPs to promote amplification errors. To create mammalian expression plasmids, HindIII-pyr-F-Koz and pyr-R-XhoI were used to amplify the LumiLuc gene fragment, which was further treated with Hind III and Xho I restriction enzymes and ligated into a predigested, compatible pcDNA3 plasmid. The Akaluc gene was synthesized by Eurofins, and cloned into a pBAD plasmid for bacterial expression and a pcDNA3 plasmid for mammalian expression, by using Aka-F-XhoI and Aka-R-HindIII or Aka-F-HindIII-Kozak and Aka-R-XhoI oligonucleotides. To build mScarlet-LumiLuc fusion library, mScarlet-F-XhoI and mScar-NNK-pyr-R oligonucleotides were used to amplify mScarlet-I gene, while mScar-NNK-pyr-F and pyr-R-HindIII oligonucleotides were used for LumiLuc cloning, which were subsequently assembled by overlap PCR reaction. The product was digested with Xho I and Hind III restriction enzymes and ligated into a predigested, compatible pBAD/His B plasmid. The LumiScarlet gene was

cloned into pcDNA3 for mammalian expression using HindIII-mScarlet-F-Koz and pyr-R-XhoI oligonucleotides. All ligation products were used to transform *Escherichia coli* DH10B electrocompetent cells, which were next plated on LB agar plates supplemented with ampicillin (100 µg/mL).

3.2.4 Library screening

DH10B cells containing luciferase mutants were plated on LB agar plates supplemented with ampicillin (100 µg/mL) and L-arabinose (0.02%, w/v%) and incubated at 37°C overnight to form bacterial colonies. Agar plates were left at room temperature for another 6 h, and this was followed by bioluminescence imaging using a luminescence dark box (UVP Bio Spectrum) equipped with a QSI 628 cooled CCD camera (Quantum Scientific Imaging). Digital images were acquired after spraying ~ 200 µL of 10 µM substrates to each agar plate, and next, images were processed with the Fiji image analysis software to derive bioluminescence intensities of individual colonies. For each round of selection, the brightest 20 colonies from a total of ~10,000 colonies were chosen and inoculated in 5 mL liquid LB broth containing ampicillin (100 µg/mL) and L-arabinose (0.02%, w/v%). After overnight growth at 37°C and 250 r.p.m., the cultures were moved onto a shaker at room temperature for another 6 h. 500 µL cell cultures were centrifuged and next lysed with 100 µL B-PER (Thermo Fisher Scientific). Next, to 1 µL lysate from each sample was added 100 µL substrate at a final concentration of 20 µM in assay buffer. Bioluminescence activities of individual samples were measured on a Synergy Mx Microplate Reader (BioTek). Kinetics were followed for 0.1 s signal integration every 60 s for a total of 20 min. Top three Mutants showing exceptionally high bioluminescence activities or extended kinetics were chosen for next-round selection, sequencing, and other additional characterization. mScarlet-I and LumiLuc fusion libraries were screened for high BRET efficiency using

a 600-700 nm bandpass filter. 20 colonies were picked from each library and inoculated in 5 mL liquid LB broth containing ampicillin (100 µg/mL) and L-arabinose (0.02%, w/v%). The cell lysates were prepared with B-PER and the bioluminescence emission spectra were measured by adding 20 µM 8pyDTZ. The construct showed highest BRET efficiency was designated LumiScarlet.

3.2.5 Chemiluminescence measurement

0.63 g ammonium bicarbonate was dissolved in 12 mL water and 24 mL acetonitrile containing 30% aqueous hydrogen peroxide, resulting in an active peroxymonocarbonate solution. The solution was left at room temperature for 10 min. Each stock solution containing synthetic analogues (500 µM, 100 µL) was dispensed into wells of a 96-well plate, and chemiluminescence was triggered by addition of 100 µL of the peroxymonocarbonate solution. Light emission was recorded on a Synergy Mx Microplate Reader (BioTek) with 0.1 s integration and 1 nm increments from 350 to 750 nm.

3.2.6 Mammalian cell culture, transfection, and imaging

HEK 293T cells were cultured and transfected as previously described.⁷ The number and density of cells in Dulbecco's phosphate-buffered saline (DPBS) were determined using a hemocytometer. Cells were next diluted in DPBS to gain the desired numbers in each 50 µL solution. To use the luminescence dark box to directly image cells, we added luciferase-expressing HEK 293T cells (5,000 cells per well with ~70% transfection efficiency) and the corresponding luciferin substrates into wells of a white-wall, 96-well plate. Bioluminescence was imaged using a luminescence dark box immediately after substrate addition. The camera exposure time was set at 2 s. A

Chroma Red 600-700 nm filter was used to acquire far-red emission. All images were analyzed using the Fiji image analysis software.

3.2.7 *in vitro* Bioluminescence characterization

Luciferases were expressed and purified as previously described.⁷ A Synergy Mx Microplate Reader (BioTek) was used for all *in vitro* bioluminescence characterizations. 50 μ L of luciferin substrates was injected into the wells of white 96-well plates containing 50 μ L of pure enzymes in assay buffer (1 mM CDTA, 0.5% Tergitol NP-40, 0.05% Antifoam 204, 150 mM KCl, 100 mM MES pH 6.0, 1 mM DTT, and 35 mM thiourea). The final concentrations of all enzymes were 20 pM. Measurements were taken every 30 s post injection (0.1 s integration and 10 s shaking during intervals). Akaluc bioluminescence assays were performed at final concentration of 10 nM Akaluc and 100 μ M AkaLumine in an assay buffer contained 30 mM MOPS (pH 7.0), 1.5 mM ATP, and 5 mM MgSO₄. To derive values for apparent Michaelis constants (K_m), substrate concentrations varied from 0.78 to 50 μ M, and peak bioluminescence intensities at individual substrate concentrations were used to fit the Michaelis–Menten equation. To record emission spectra, 50 μ L of 20 μ M substrates were injected into 50 μ L of 2 nM pure enzymes, and the bioluminescence spectra were collected with 0.1 s integration and 1 nm increments from 350 to 750 nm.

3.2.8 Generation of luciferase-expressing stable cell lines

HeLa cells were cultured at 37°C with 5% CO₂ in Dulbecco's Modified Eagle's Medium (DMEM) supplemented with 10% fetal bovine serum (FBS). HeLa cells were transfected with pcDNA3-teLuc, pcDNA3-Antares2, pcDNA3-LumiLuc, pcDNA3-LumiScarlet, or pcDNA3-Akaluc as previously described.⁷ 48 h after transfection, cells were passed into fresh DMEM containing 10% FBS and 1 mg/mL G418. The medium

was removed and replaced every 3 days. Stable polyclonal cell lines were generated after ~ 2 weeks of G418 selection.

3.2.9 Xenograft mouse model

HeLa cells stably expressing luciferases were dissociated with trypsin and re-suspended in 10 mL DMEM. Cell numbers were determined using a hemocytometer, and cell viability was determined using a trypan blue exclusion test. 10^4 or 10^5 cells were re-suspended in 100 μ L FBS-free DMEM containing 50% Matrigel matrix (Corning). 8-week-old female nude mice were first anesthetized using isoflurane. Cells were subcutaneously injected into the left and right dorsolateral trapezius regions or thoracolumbar regions. Mice were recovered on heat pads for 5 min while cells were allowed to settle. On day 1, 3, 5, 7, 14, and 28 post tumor implants, mice were subsequently imaged using a Caliper IVIS Spectrum (Perkin Elmer) approximately 5 min after intravenous (i.v.) administration of corresponding luciferins (100 μ L solution for indicated doses). DTZ was dissolved in a 100 μ L solution containing 8% glycerol, 10% ethanol, 10% hydroxypropyl- β -cyclodextrin, and 35% PEG 400 in water. 8pyDTZ and AkaLumine-HCl was dissolved in normal saline. All solutions were passed through 0.22 μ m pore filters before administrations. The following conditions were used for image acquisition: open filter for total bioluminescence, exposure time = 60 s (Day 1, 3, and 5); 30 s (Day 7); 10 s (Day 14); 3 s (Day 28), binning = small, field of view = 21.6 \times 21.6 cm, and f/stop = 1. Image analysis was performed using the Living Image 4.3.1 software.

3.2.10 Deep-tissue BLI mouse model

10⁶ HeLa cells stably expressing either LumiLuc, LumiScarlet or Akaluc were i.v. injected to female nude mice. After 4 h, images were acquired using a Caliper IVIS Spectrum immediately after i.v. delivery 0.2 μ mol 8pyDTZ or 1.5 μ mol AkaLumine-HCl in 100 μ L normal saline. The following conditions were used for image acquisition: open filter for total bioluminescence, exposure time = 10 s, binning = small, field of view = 21.6 \times 21.6 cm, and f/stop = 1.

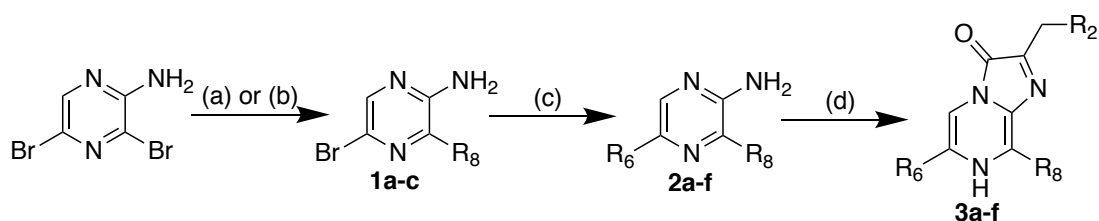
Statistical analysis. Unpaired two-tailed t-tests were used to determine all *p*-values. No statistical methods were used to predetermine the sample size. Animals were randomly assigned to receive various treatments. Unless otherwise indicated, data are shown as mean \pm s.d., and error bars in figures represent s.d.

3.3. Results

3.3.1 Design and synthesis of pyridyl CTZ and DTZ analogs

Recent studies have synthesized and tested a number of CTZ analogs with NanoLuc²⁰⁻²¹; however the luciferase has not yet been optimized to pair with these new substrates and the water solubility issue of the substrates has not yet been tackled systematically. We sought to develop CTZ and DTZ analogs with improved water solubility by using the concept of bioisostere replacements in medicinal chemistry. Pyridine is considered a biocompatible *N*-heterocycle substituent for benzene with enhanced water solubility, because pyridine-containing molecules can be readily turned into pyridinium salts. Therefore, we designed a convergent synthetic route to prepare a series of CTZ and DTZ analogs with pyridyl isomer substitutions at the C-2, C-6 and C-8 positions of the imidazopyrazinone core (**Scheme 1**). Briefly, we first used Suzuki or Negishi cross-coupling reactions to regioselectively functionalize 2-amino-

3,5-dibromopyrazine with either pyridyl, phenyl, or benzyl functional groups to give monosubstituted products (**1a-c**), which were subsequently derivatized via Suzuki cross-coupling reactions to afford disubstituted intermediates (**2a-f**, see structures and synthetic methods in the chemical synthesis section). In the second cross-coupling step, the XPhos-Pd-G2 catalyst was used to enhance reaction yields and minimize the protodeboronation of pyridyl boronic acids.²² We further used the acid-catalyzed ring closing reaction¹⁹ in dioxane to derive various pyridyl CTZ and DTZ analogs (**3a-f**, **Table 1**) from the disubstituted intermediates and corresponding α -ketoacetals.



Scheme 1. Synthesis of pyridyl CTZ and DTZ analogs. (a) Suzuki coupling: Pd(PPh₃)₄, Na₂CO₃, R₈-B(OH)₂, and EtOH; (b) Negishi coupling: PhCH₂MgCl, ZnCl₂, (PPh₃)₂PdCl₂, and THF; (c) Suzuki coupling: XPhos-Pd-G2, Na₂CO₃, R₆-B(OH)₂, and EtOH; (d) Acid-catalyzed ring closing: corresponding α -ketoacetal, HCl, and dioxane.

We next used turbidimetric solubility assays²³ to evaluate water solubility of these CTZ and DTZ analogs (**Table 1**). Our newly synthesized pyridyl analogs enhanced the solubility by 4- to 14-fold from CTZ and DTZ. We further investigated their chemiluminescence, in addition to their bioluminescence in the presence of several representative luciferases such as RLuc8, NanoLuc, teLuc, and aequorin (**Figure 1** and **Figure 2**). Although each luciferase has different substrate preferences, the compound **3a** (pyCTZ) generated strong blue bioluminescence in the presence of each of these tested luciferases. When paired with aequorin, the bioluminescence intensity of pyCTZ was comparable to native CTZ, suggesting that pyCTZ may be

directly used to replace CTZ for aequorin-based calcium sensing.²⁴ Furthermore, compared to DTZ, compounds **3c**, and **3f** were able to emit red-shifted chemiluminescence and/or bioluminescence, while **3b** and **3d** (6pyDTZ) caused hypsochromic shift (**Figures 1** and **Table 1**). Chemiluminescence spectra revealed the relaxation patterns of emitter in solution, while bioluminescence spectra indicated the overall interactions between emitter and luciferase catalytic pocket. Because **3c** (8pyDTZ) showed the most red-shifted emission and red-shifted photons can penetrate through tissue better,²⁵ we selected **3c** (8pyDTZ) as our candidate substrate for further development of an optimized, red-shifted luciferase-luciferin pair.

Table 1. Chemical and photoluminescence properties of synthetic pyridyl CTZ and DTZ analogs.

Compound	R ₆	R ₈	R ₂	Bioluminescence ^a λ_{max} (nm)	Chemiluminescence ^b λ_{max} (nm)	Water Solubility (μM)
3a				451	505	1416
3b				497	506	1813
3c				532	555	1711
3d				483	492	1736
3e				450	465	987
3f				518	503	1562
CTZ				455	461	256
DTZ				502	510	131

Note: ^a Determined with 1 nM teLuc in PBS; ^b Triggered by peroxydicarbonate formed *in situ*.

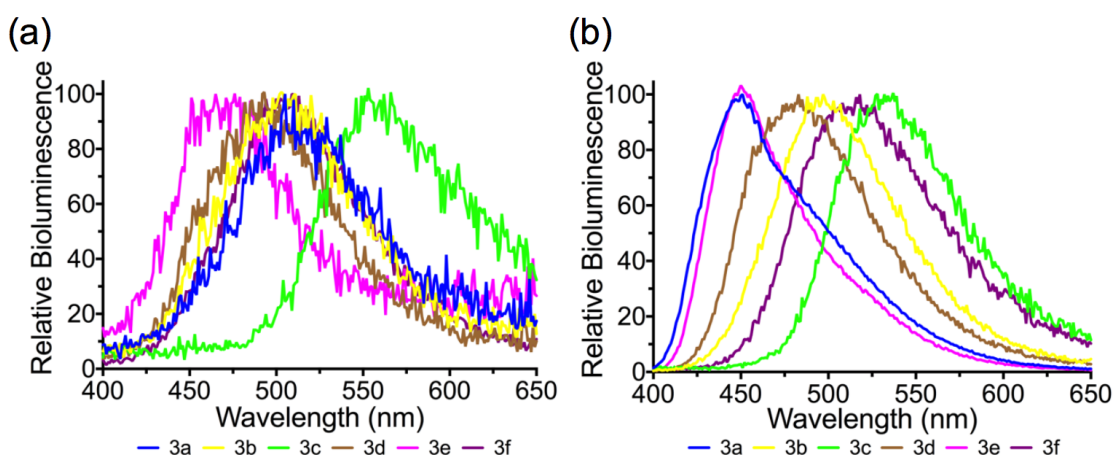


Figure 1. Chemiluminescence (a) and bioluminescence (b) spectra for synthetic CTZ and DTZ analogs described in this work. Chemiluminescence was initiated with peroxymonocarbonate generated *in situ*. Bioluminescence was determined with 1 nM teLuc in PBS.

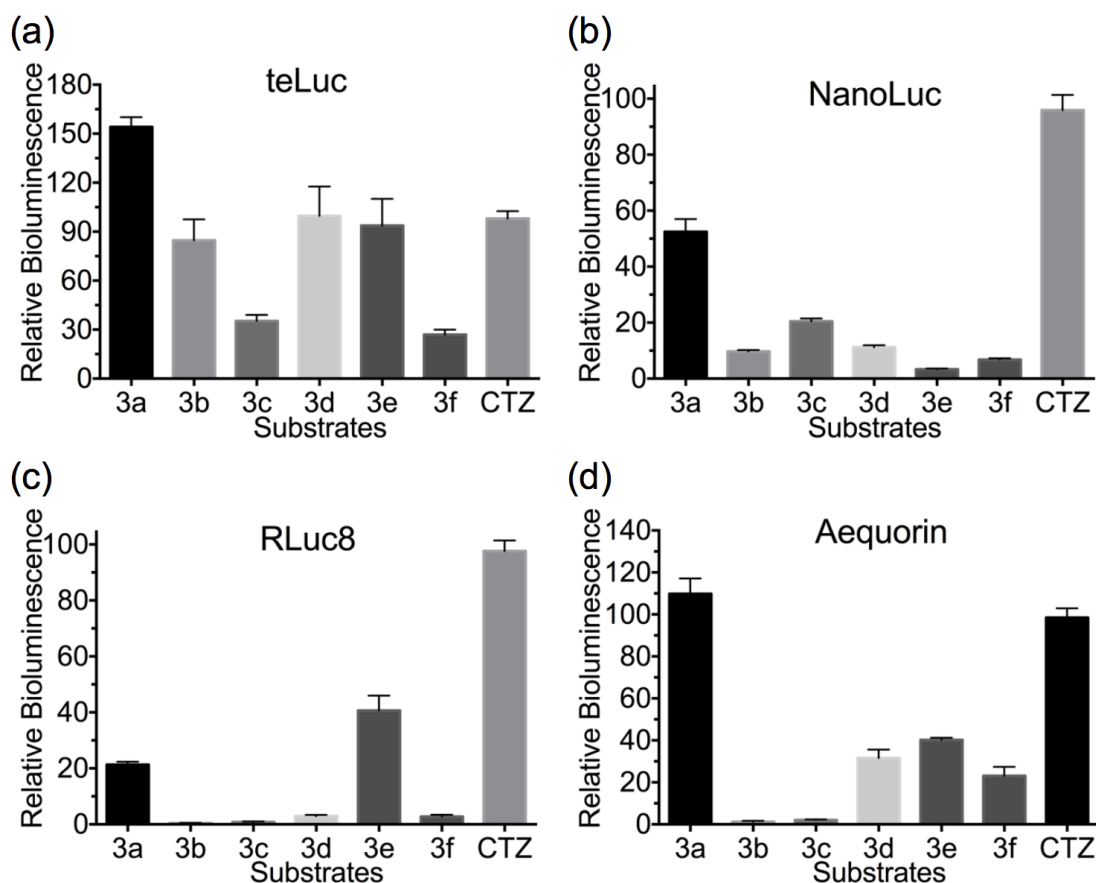


Figure 2. Relative bioluminescence intensities of various luciferases. Total signals were integrated for the first 10 min after injection of indicated substrates (the final concentrations were 25 μ M) in the presence of 1 nM purified (a) teLuc and (b) NanoLuc, or 10 nM (c) RLuc8 and (d) aequorin in PBS. Values were normalized to the intensity of CTZ in each group.

3.3.2 Directed evolution of teLuc luciferase for improved brightness

8pyDTZ exhibits ~ 30 nm red-shift but the emission of teLuc-8pyDTZ has been greatly attenuated compared to teLuc-DTZ. Since teLuc was previously engineered for

diphenyl substitutions of the imidazopyrazinone core, we next engineered teLuc for increased photon flux in the presence of 8pyDTZ. On the basis of a published apo-nanoKAZ structure²⁶ and our computational model,⁷ we first introduced random mutations to residues 18 and 19 close to a putative substrate-binding pocket (**Figure 2**). After screening for improved mutants, we further randomized residues 27, 28, and 29 located deeper in the putative catalytic site. From the first two rounds of protein engineering, a teLuc-L18Q/S19A/V27L/S28T mutant was identified, to which we further introduced random mutations using error-prone PCR. After eight additional rounds of mutagenesis and screening, we derived a LumiLuc luciferase with 12 total mutations and ~ 5-fold enhancement of 8pyDTZ bioluminescence from teLuc (**Figure 3** and **Figure 4**).

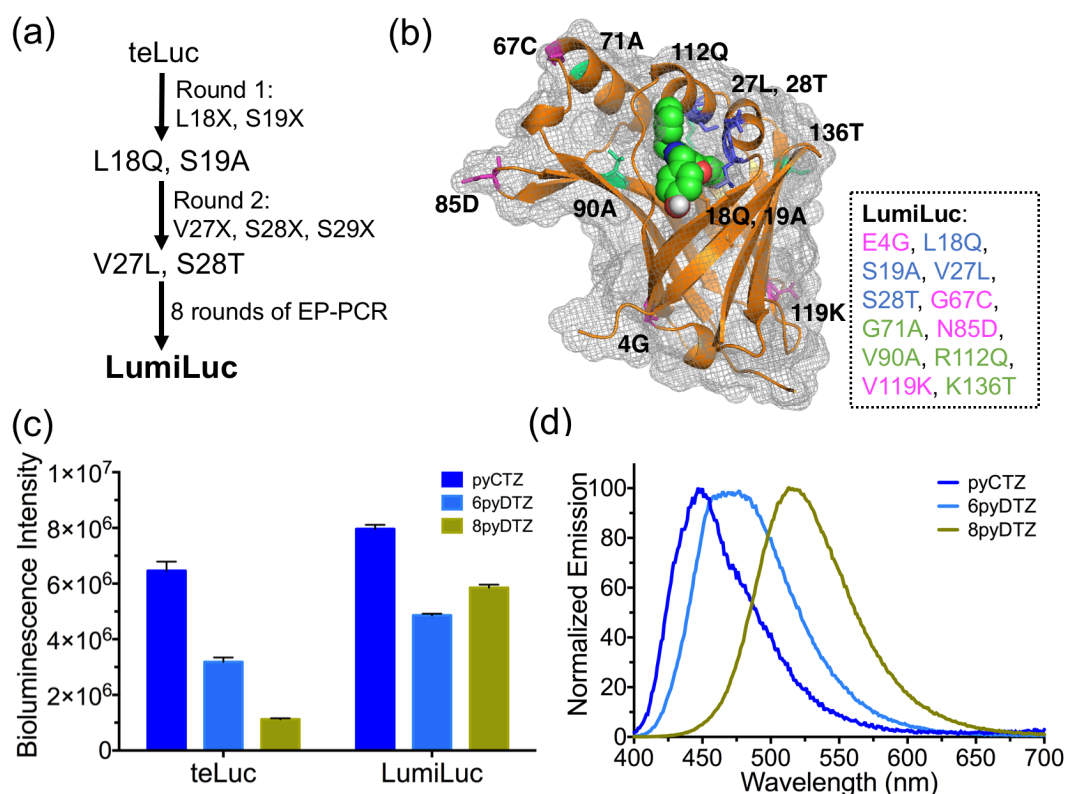


Figure 3. Engineering of a LumiLuc luciferase. (a) Procedure to derive LumiLuc from teLuc. (b) Illustration of the putative substrate-binding site and LumiLuc mutations from

teLuc. CTZ is shown as spheres and mutated residues are presented in sticks. (c) Bioluminescence of pyCTZ, 6pyDTZ, or 8pyDTZ in the presence of either teLuc or LumiLuc. (d) Normalized bioluminescence emission spectra of pyCTZ, 6pyDTZ, and 8pyDTZ in the presence of LumiLuc.



Figure 4. Alignments of primary sequences of NanoLuc, teLuc, and LumiLuc. teLuc mutations are highlighted in teal background, whereas all LumiLuc mutations are highlighted in green background. Residues in this figure are numbered according to Protein Data Bank (PDB) ID 5B0U.

LumiLuc has broad substrate specificity. It improved the photon flux of pyCTZ and 6pyDTZ from teLuc by ~ 120% and ~ 150%, respectively (**Figure 3c**). The directed evolution process to enhance photon flux of teLuc for 8pyDTZ did not preclude the luciferase from catalyzing other structurally relevant substrates. LumiLuc is capable of efficiently generating blue, teal, or yellow bioluminescence when paired with pyCTZ, 6pyDTZ or 8pyDTZ (λ_{\max} : 450, 476, and 525 nm, respectively; **Figure 3d**), thereby leading to a new palette of ATP-independent bioluminescent reporters with water-soluble substrates.

The resultant LumiLuc-8pyDTZ pair has an emission peak at 525 nm. Its *in vitro* maximal photon emission rate (V_{\max}) is $\sim 60\%$ and $\sim 36\%$ of NanoLuc-FRZ and teLuc-DTZ, respectively. The apparent Michaelis constant (K_M) of LumiLuc-8pyDTZ was $4.6 \mu\text{M}$, lower than that of teLuc-DTZ or NanoLuc-FRZ (**Figure 5a**). This reduced K_M is practically beneficial, since LumiLuc-8pyDTZ would be relatively brighter when effective substrate concentrations are limited, such as in live cells (**Figure 5b**) and *in vivo*. Similar to NanoLuc and teLuc, the bioluminescence kinetics of LumiLuc is flash-type in phosphate buffer saline (PBS) and glow-type in a specially formulated assay buffer (**Figure 5c**).¹²

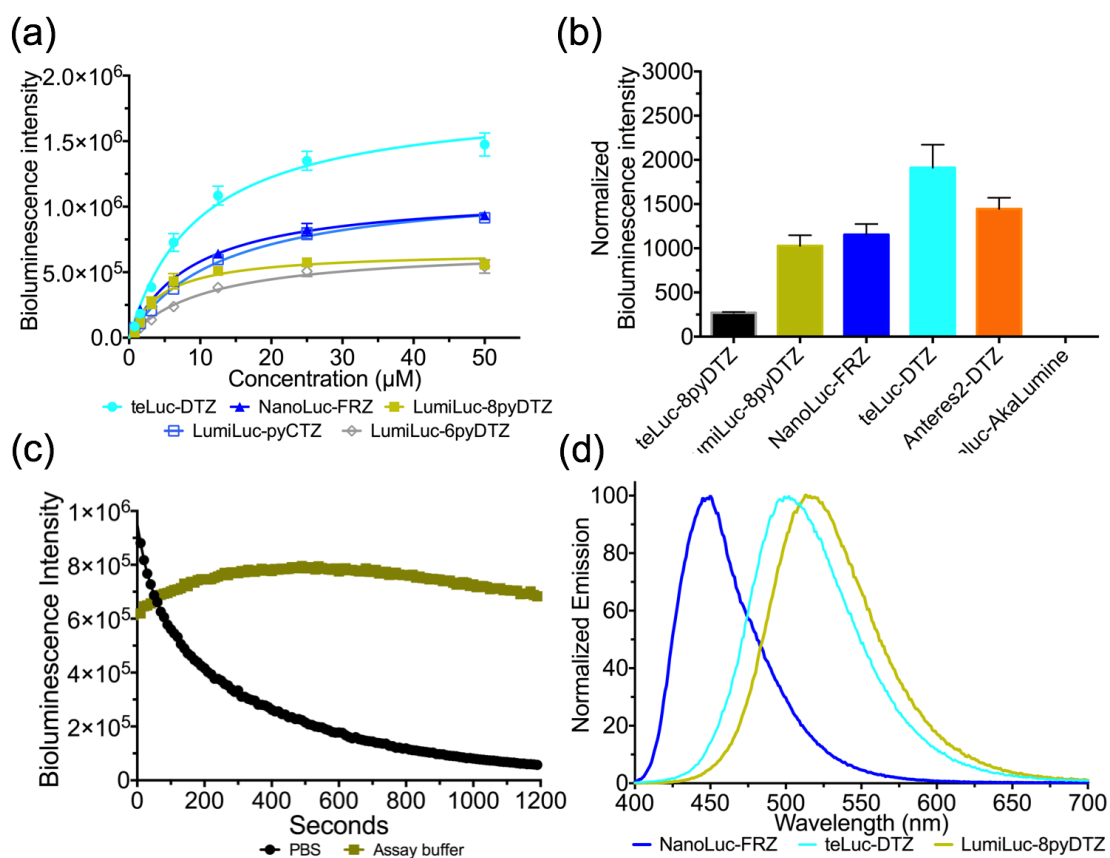


Figure 5. Comparison of luciferase-luciferin pairs in enzyme-based assays. (a) Determination of apparent Michaelis constants (K_M) by substrate titrations (teLuc-DTZ: $9.9 \pm 0.9 \mu\text{M}$; NanoLuc-FRZ: $9.1 \pm 0.6 \mu\text{M}$; LumiLuc-8pyDTZ: $4.6 \pm 0.6 \mu\text{M}$; LumiLuc-pyCTZ: $13.1 \pm 0.8 \mu\text{M}$; LumiLuc-6pyDTZ: $11.0 \pm 1.2 \mu\text{M}$). Final concentrations of all enzymes were 20 pM . Substrate concentrations varied from 0.78 to $50 \mu\text{M}$, and peak

bioluminescence intensities at individual substrate concentrations were used to fit the Michaelis-Menten equation. **(b)** Total bioluminescence over the first 10 min post addition of corresponding luciferins. Final concentrations for luciferins were 10 μ M and final concentrations for luciferases were 50 pM. Data are normalized to the intensity of Akaluc-AkaLumine and shown as mean and s.d. from three independent measurements. Under this condition, LumiLuc-8pyDTZ produced \sim 1200-fold higher photon flux than Akaluc-AkaLumine. Assays in panels **a** and **b** were all performed in PBS. **(c)** Bioluminescence kinetic of LumiLuc-8pyDTZ in PBS or in a formulated assay buffer containing 1 mM CDTA, 0.5% Tergitol NP-40, 0.05% Antifoam 204, 150 mM KCl, 100 mM MES, pH 6.0, 1 mM DTT, and 35 mM thiourea. **(d)** Normalized bioluminescence emission spectra of NanoLuc-FRZ, teLuc-DTZ, and LumiLuc-8pyDTZ. Note: the detected bioluminescence signal intensity by detector can vary from multiple factors, including but not limited to enzyme concentration, enzyme activity, substrate concentration, assay buffer pH, buffer additives and surfactants, emission kinetic, integration time, self-inhibition effect, instrument sensitivity, data processing, etc.

3.3.3 LumiLuc-8pyDTZ in cultured mammalian cells

We next evaluated LumiLuc-8pyDTZ in human embryonic kidney (HEK) 293T cells transiently expressing the luciferase (**Figure 6**). The LumiLuc-8pyDTZ pair produced \sim 3- to 5-fold more bioluminescence than teLuc-8pyDTZ at all tested substrate concentrations (**Figure 7**). Moreover, despite that LumiLuc-8pyDTZ is less bright than teLuc-DTZ at saturated substrate concentrations, LumiLuc-8pyDTZ is notably brighter than teLuc-DTZ at low substrate concentrations (from 6.25 to 25 μ M; **Figure 8a**). Far-red emission at wavelengths longer than 600 nm is more indicative of the *in vivo* performance of bioluminescent reporters, because mammalian tissue is

more transparent in this spectral region.²⁵ To compare far-red emission intensities of bioluminescent reporters, we imaged HEK 293T cells in the presence of a 600-700 nm bandpass filter. At substrate concentrations from 6.25 to 100 μ M, LumiLuc-8pyDTZ consistently produces 1.6- to 3.9-fold higher photon flux than teLuc-DTZ (**Figure 8b**).

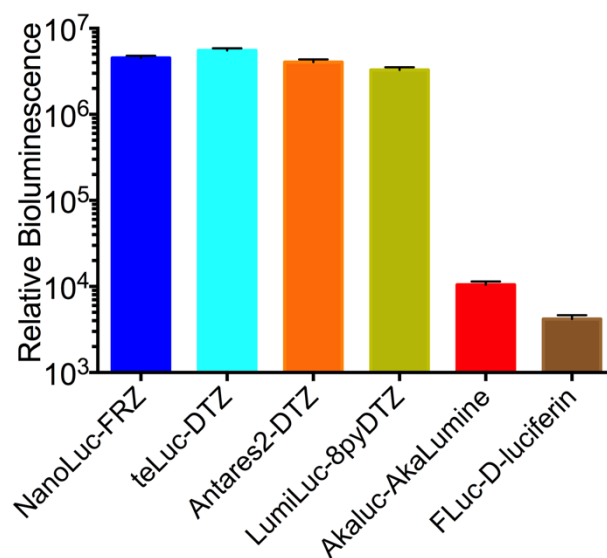


Figure 6. Comparison of luciferase-luciferin pairs in live mammalian cells. Measurements were performed with 5000 luciferase-expressing HEK 293T cells in PBS. Final concentrations for FRZ, DTZ, and 8pyDTZ were 20 μ M, and final concentrations for AkaLumine and D-luciferin were 100 μ M. Signals were integrated over the first 10 min post injection of substrates. Data are presented as mean and s.d. from three independent measurements. Under this condition, LumiLuc-8pyDTZ produced \sim 300-fold higher photon flux than Akaluc-AkaLumine.

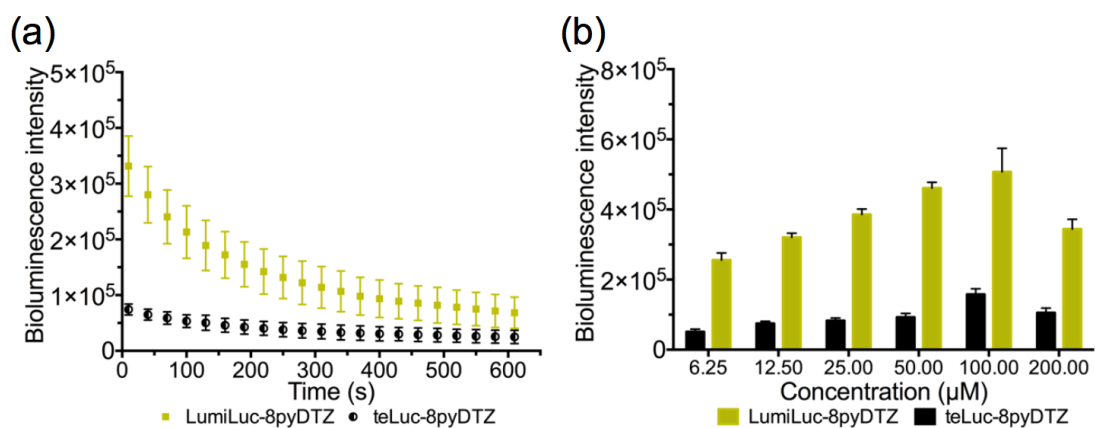


Figure 7. Bioluminescence kinetics (a) and intensities (b) of 8pyDTZ in the presence of teLuc- or LumiLuc-expressing HEK 293T cells. 20 μM 8pyDTZ and 5000 cells were used. Data are presented as mean and s.d. from three independent measurements. For panel b, signals were integrated for the first 10 min post injection of substrates.

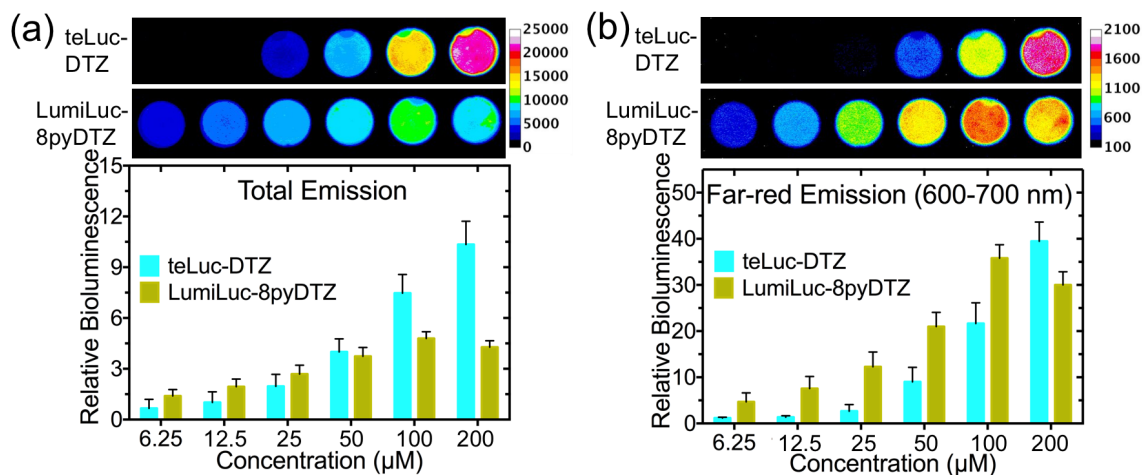


Figure 8. Bioluminescence of teLuc- and LumiLuc-expressing HEK 293T cells. Images were acquired (a) without or (b) with a 600-700 nm bandpass filter. Values for relative brightness were normalized to teLuc in the presence of 6.25 μM DTZ.

3.3.4 LumiLuc-8pyDTZ to track tumor growth in a mouse xenograft model

BLI has been a popular imaging modality for various animal models.^{13, 25} The recently reported Akaluc-AkaLumine and Antares2-DTZ pairs are two benchmark reporters for *in vivo* BLI.⁶⁻⁷ We adapted a biologically-relevant tumor xenograft mouse model²⁷ to compare these bioluminescent reporters. We first generated cervical cancer HeLa cell lines stably expressing individual luciferases, including teLuc, Antares2, LumiLuc, and Akaluc (**Figure 9**).

Next, we injected 10^4 or 10^5 luciferase-expressing HeLa cells into the left or right dorsolateral trapezius and thoracolumbar regions of immunodeficient NU/J mice (day 0) and monitored tumor growth over 4 weeks. Bioluminescence was quantified in days 1, 3, 5, 7, 14, and 28 after tail vein injection of corresponding substrates. AkaLumine-HCl was delivered at a dose of 1.5 μmol per mouse. This dosage (~ 75 nmol/g), which is normalized against the body weights of mice, is identical to the previously reported dosage.⁶ Moreover, when 3 μmol of AkaLumine-HCl per mouse (~ 150 nmol/g) was used, we observed death for 2 out of 3 mice in our pilot experiment. 8pyDTZ was dissolved in normal saline to its saturation concentration and intravenously injected, resulting in a dose of 0.2 μmol per mouse (~ 10 nmol/g). The LumiLuc-8pyDTZ pair showed detectable bioluminescence on day 1 at sites inoculated with 10^4 cells, and kept exhibiting ~ 3 -fold higher photon flux over Akaluc-AkaLumine up to day 7 (**Figures 10a** and **10b**). The signals for Akaluc-AkaLumine at sites inoculated 10^4 cells were not consistently higher than background until day 3. Furthermore, the *in vivo* brightness of LumiLuc-8pyDTZ is comparable to, if not higher than, the Antares2-DTZ pair, despite the fact that the majority of emitted photons from LumiLuc-8pyDTZ has not yet exceeded 600 nm. These data collectively support that LumiLuc-8pyDTZ is a superior bioluminescent reporter system for high-sensitivity *in vivo* BLI.

AkaLumine-HCl could be delivered into mice at a much higher dose than 8pyDTZ due to the higher solubility of AkaLumine-HCl. We thus interpret that 8pyDTZ may be a limiting reagent in large tumors. Presumably, we may further enhance the *in vivo* performance of marine luciferases and their derivatives by further increasing the water solubility and thus the administration dosage of CTZ and DTZ analogs.

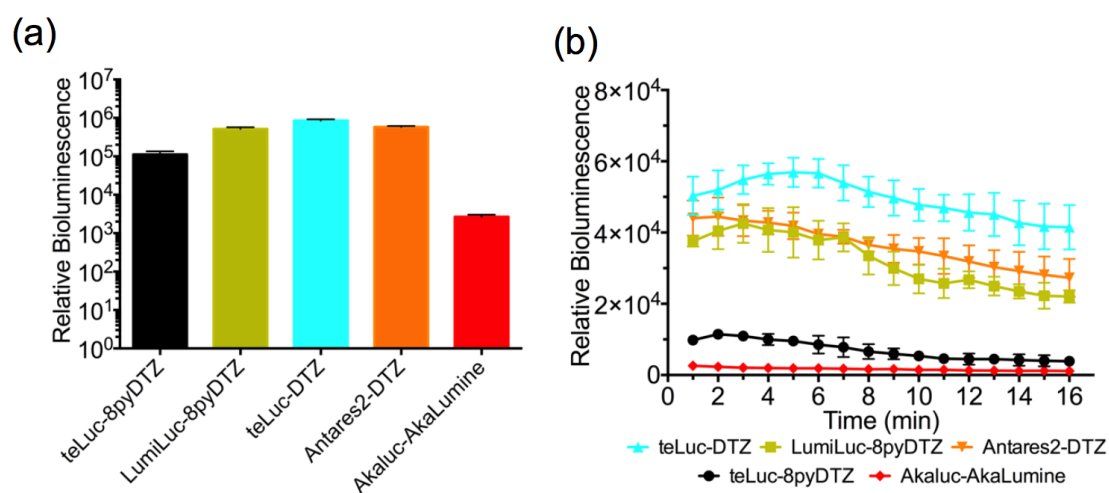


Figure 9. Bioluminescence characterizations of HeLa cells stably expressing luciferases. **(a)** Bioluminescence intensities integrated over the first 10 mins post injection of substrates in a logarithmic scale. **(b)** Decay kinetics. Assays were performed with 20 μ M substrates and 500 HeLa cells. Under this condition, LumiLuc-8pyDTZ produced \sim 190-fold higher photon flux than Akaluc-AkaLumine. Data are presented as mean and s.d. from three independent measurements.

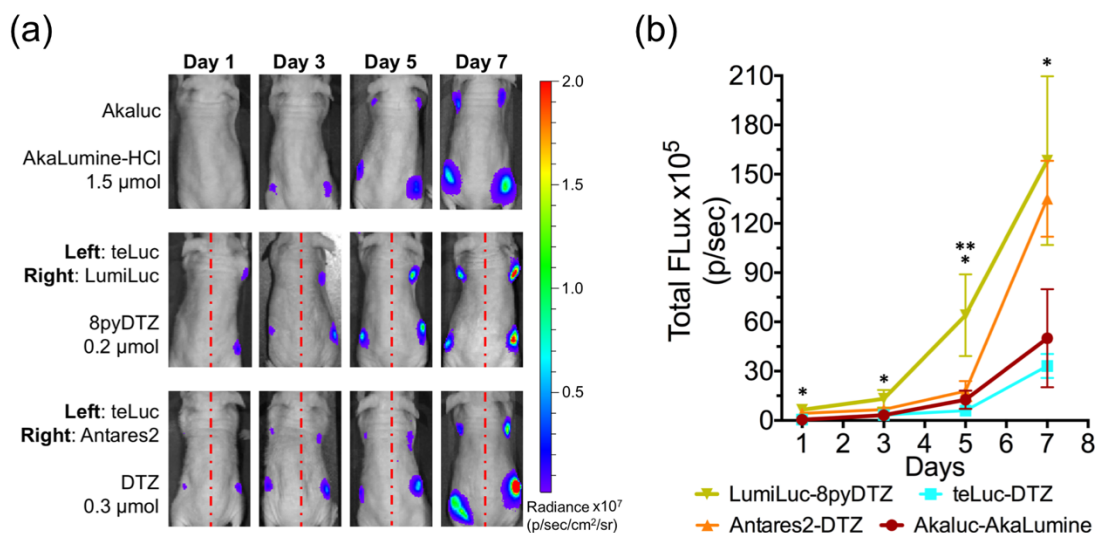


Figure 10. Tracking of tumor growth in a xenograft mouse model with various luciferase-luciferin pairs. (a) BLI ($n = 4$) on day 1, 3, 5, and day 7. 10^4 luciferase-expressing HeLa cells were injected to the left and right dorsolateral trapezius regions and 10^5 cells were injected to the left and right dorsolateral thoracolumbar regions of NU/J mice. For i.v. administration of substrates, AkaLumine-HCl and 8pyDTZ were dissolved in normal saline, and DTZ was formulated with a mixture of organic cosolvents. (b) Comparison of luciferase-luciferin pairs at tumor sites inoculated with 10^4 cells. (* $p < 0.05$ for LumiLuc-8pyDTZ and teLuc-DTZ, and for LumiLuc-8pyDTZ and Akaluc-AkaLumine; ** $p < 0.05$ for LumiLuc-8pyDTZ and Antares2-DTZ).

3.3.5 Engineering of BRET-based LumiScarlet for deep-tissue BLI

mScarlet-I is a recently reported red fluorescent protein with high quantum yield and excellent performance as a Förster resonance energy transfer (FRET) acceptor.²⁸ We thus hypothesized that LumiLuc could be genetically fused to mScarlet-I for BRET, thereby red-shifting the emission of LumiLuc. We explored three fusion strategies between LumiLuc and mScarlet-I, constructed libraries by randomizing the linkers, and screened for mutants with high BRET efficiency (**Figures 11a** and **11b**). We identified

a mutant, namely LumiScarlet (**Figure 12a**), which is a fusion protein of truncated mScarlet-I (residues 1-225) linked to the N-terminus of LumiLuc (residues 2-169) through a single-residue “Lys” linker.

High BRET efficiency was achieved with LumiScarlet in the presence of either pyCTZ, or 6pyDTZ, or 8pyDTZ (**Figure 12b**). In particular, because the emission spectrum of LumiLuc-8pyDTZ overlaps well with the excitation spectrum of mScarlet-I (**Figure 11c**), ~ 51% of the total emission of LumiScarlet, when paired with 8pyDTZ, was longer than 600 nm (**Table 2**).

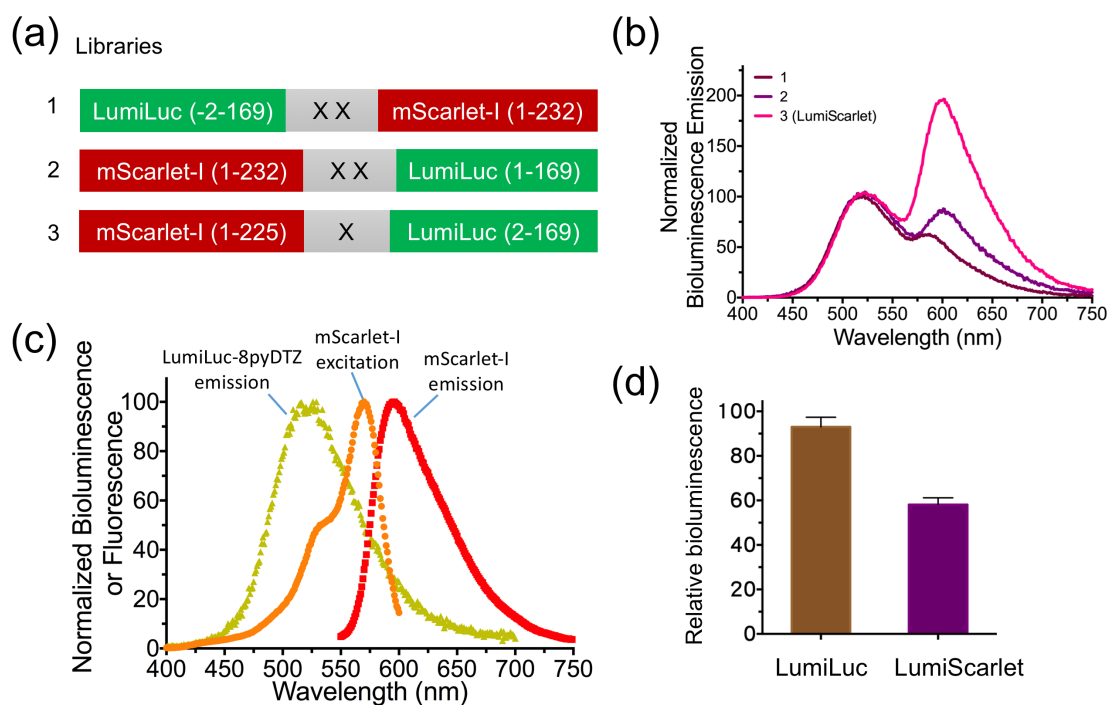


Figure 11. Engineering and characterization of BRET-based LumiScarlet. **(a)** Libraries screened for high BRET. Each “X” represents an amino acid residue randomized with the NNK codon, in which N = A/C/G/T and K = G/T. **(b)** Bioluminescence spectra of constructs selected from each library in the presence of 8pyDTZ. **(c)** Normalized fluorescence excitation and emission spectra of mScarlet-I and bioluminescence emission of LumiLuc-8pyDTZ, showing excellent spectral overlap for BRET. **(d)**

Comparison of LumiLuc and LumiScarlet (100 pM purified enzymes) for bioluminescence integrated over the first 10 min post injection of 20 μ M 8pyDTZ.

Table 2. BRET-based bioluminescent reporters that are based on NanoLuc and its derivatives.

BRET Construct	BRET Donor	BRET Acceptor	Size (kDa)	λ_{\max} (nm)	Luciferin	Photon > 600 nm (%)	Ref.
LumiScarlet	LumiLuc	mScarlet-l	44	527, 600	8pyDTZ	51	This work
	LumiLuc	mScarlet-l	44	476, 600	6pyDTZ	38	
	LumiLuc	mScarlet-l	44	450, 600	pyCTZ	26	
Antares	NanoLuc	CyOFP	70	456, 583	FRZ	23	(1)
Antares2	teLuc	CyOFP	70	501, 583	DTZ	33	(2)
ReNL	NanoLuc	tdTomato	72	459, 583	FRZ	24	(3)

We next compared our newly engineered LumiLuc-8pyDTZ and LumiScarlet-8pyDTZ with Akaluc-AkaLumine for deep-tissue BLI. We injected a million HeLa cells stably expressing corresponding luciferases into each of NU/J mice via tail vein and performed BL imaging 4 h later. Immunodeficient mice were used here to minimize immune responses to HeLa cells, so that signals will be mostly from live cells trapped in the lungs. LumiScarlet gave ~ 3-fold higher detectable signals than LumiLuc under this condition (**Figure 12c** and **12d**), even though the *in vitro* brightness of LumiScarlet is only ~ 70% of LumiLuc (**Figure 11d**). Moreover, the signals from LumiScarlet-8pyDTZ were comparable to the signals from Akaluc-AkaLumine.

We want to note that we observed some diffuse signals from areas other than just the lungs. These signals were not caused by substrate background, as injection of 8pyDTZ into blank mice resulted in only weak background much lower than what we observed in **Figure 12c**. Collectively, our deep-tissue BLI results confirm that red-shifted BRET-based LumiScarlet has better mammalian tissue penetration than LumiLuc. Moreover, LumiScarlet-8pyDTZ is a novel, ATP-independent bioluminescent

reporter with exceptional deep-tissue BLI performance comparable to ATP-dependent Akaluc-AkaLumine.

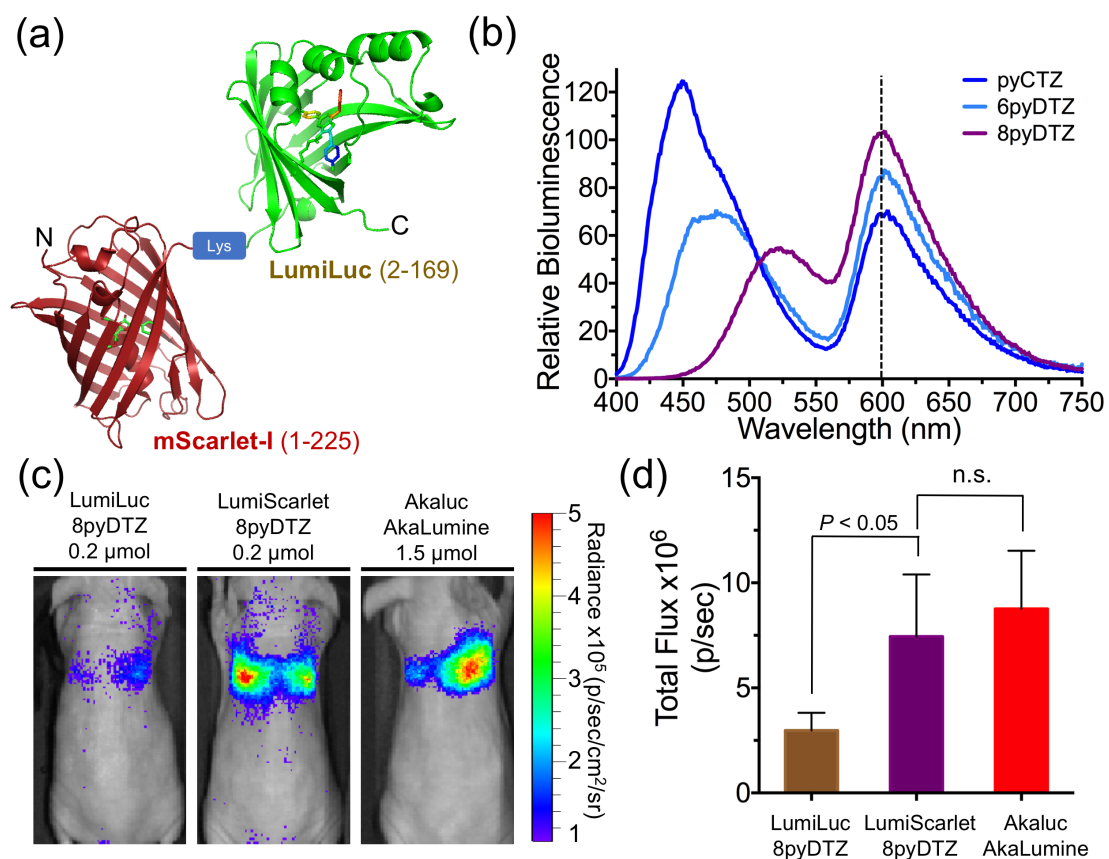


Figure 12. BRET-based LumiScarlet for deep tissue BLI. (a) Schematic diagram of LumiScarlet, a genetic fusion of mScarlet-I and LumiLuc. (b) Bioluminescence emission of LumiScarlet in the presence of pyCTZ, 6pyDTZ, or 8pyDTZ, showing significant emission longer than 600 nm. (c) Comparison of LumiLuc-8pyDTZ, LumiScarlet-8pyDTZ, and Akaluc-AkaLumine in NU/J mice ($n = 4$) at 4 h post i.v. injection of 10^6 luciferase-expressing HeLa cells. (d) Quantitative analysis of bioluminescence from the regions around the lungs in panel c (n.s.: not significant).

3.4. Discussion

Conventionally, ATP-dependent bioluminescent reporters, such as FLuc and Akaluc, are considered to be more useful for *in vivo* BLI than ATP-independent marine luciferases, because the emission of ATP-dependent insect luciferases is often at the red end of the visible spectrum where the mammalian tissue is relatively transparent. However, these insect luciferases require ATP and Mg^{2+} for bioluminescence. The ATP- and Mg^{2+} -dependency is sometimes problematic because ATP and Mg^{2+} levels may vary under different biological circumstances.²⁹ In particular, ATP-dependent luciferases are inactive in extracellular space and common biological fluids such as blood and urine, where ATP accessibility is limited.⁸ Moreover, ATP-dependent luciferases consume ATP in bioluminescence reactions and may cause concerns such as metabolic disruption.⁸ In contrast, most ATP-independent marine luciferases are enzymatically active in extracellular space and common biological fluids; they do not consume ATP for bioluminescence. Furthermore, some marine luciferase derivatives have fast catalytic turnover and thus give high photon flux. It is therefore not surprising that marine luciferase and their derivatives, such as NanoLuc and *Gaussia* luciferase, have been widely used for *in vitro* bioluminescence assays. Currently, the *in vivo* applications of marine luciferases are hindered by their blue emission and poor substrate water solubility. In this study, we combined chemical synthesis and protein engineering approaches to enhance ATP-independent marine luciferases for *in vivo* BLI by developing red-shifted colors and water-soluble substrates.

First, we prepared a series of pyridyl CTZ and DTZ analogs with diverse emission profiles. The water solubility of these synthetic analogs generally increased by ~10-fold from their ancestors. These substrate analogs can not only be paired with the new luciferases engineered here, but also existing ones, such as RLuc and aequorin.

We further engineered a luciferase for the 8pyDTZ substrate via directed protein evolution. The resultant LumiLuc-8pyDTZ bioluminescent reporter system exhibited reduced K_M and red-shifted emission. These factors favored *in vivo* BLI. As a result, LumiLuc-8pyDTZ showed high sensitivity in a mouse xenograft model. In addition, LumiLuc-8pyDTZ did not perturb the intracellular ATP/ADP level, and 8pyDTZ could be dissolved up to ~ 2 mM in low-viscosity saline without organic cosolvent. Therefore, our effort enhanced not only the biocompatibility of bioluminescent reporters, but also reproducibility for intravenous injections.

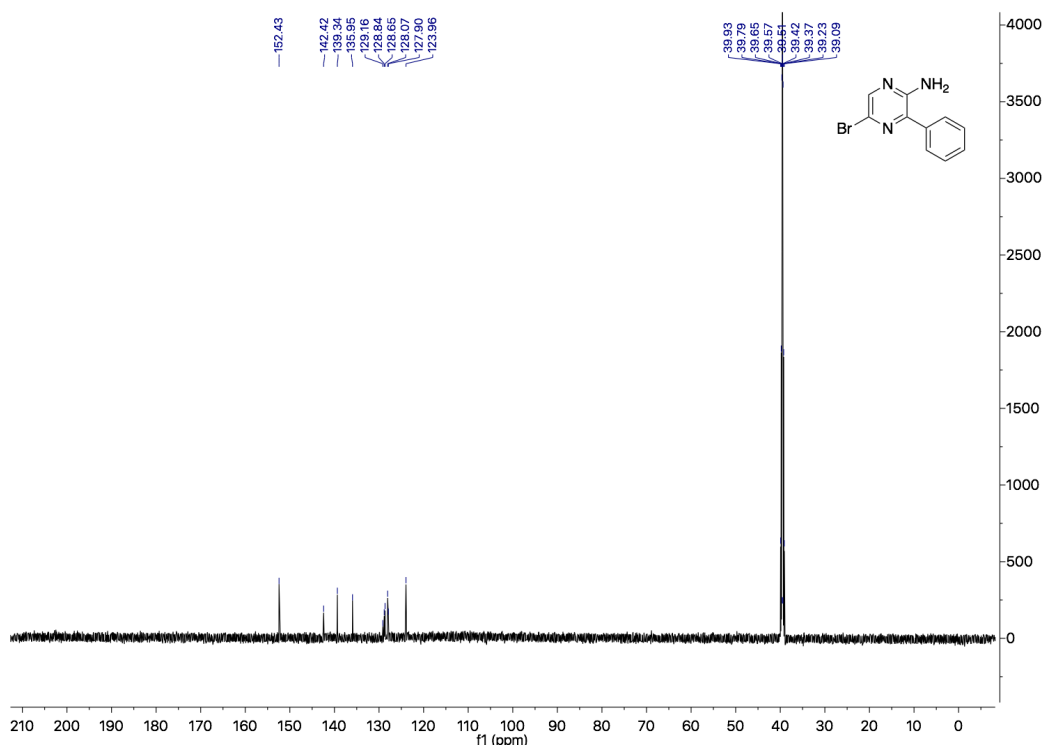
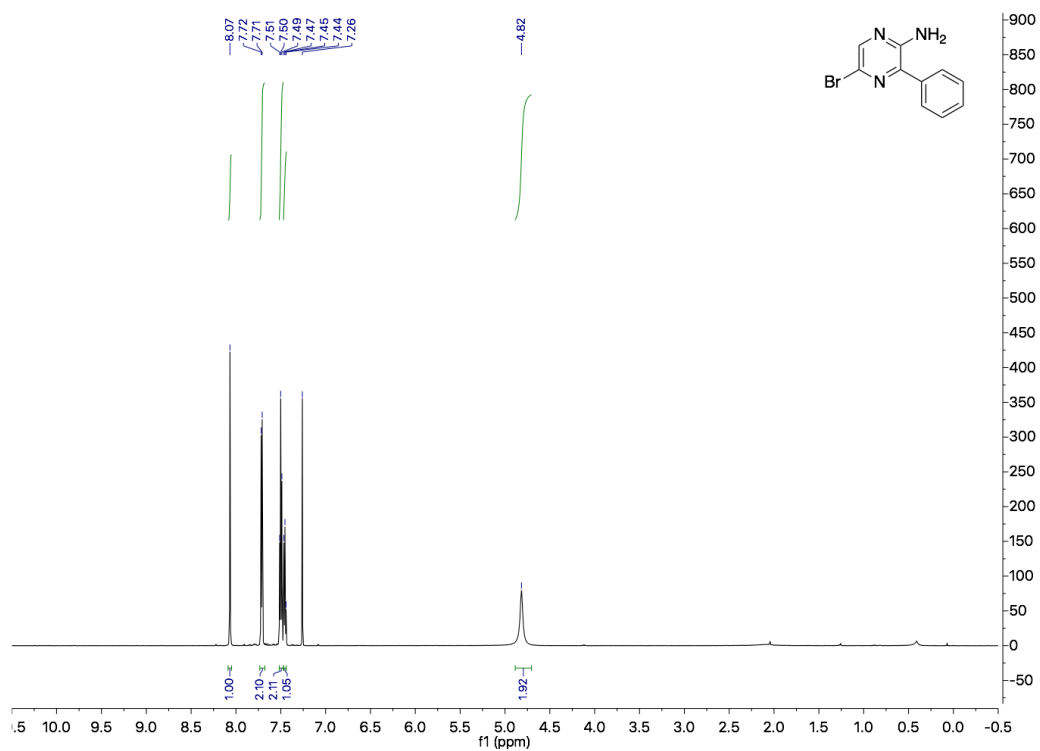
Furthermore, we developed a BRET-based LumiScarlet reporter for further red-shifted emission. The emission of LumiLuc-8pyDTZ overlaps well with the excitation of mScarlet-I, an excellent red-emitting resonance energy transfer acceptor. LumiScarlet-8pyDTZ exhibited high brightness, significant emission longer than 600 nm, and excellent tissue penetration. LumiScarlet-8pyDTZ was comparable to NIR-emitting Akaluc-AkaLumine in a mouse model for deep-tissue BLI. Moreover, because LumiScarlet is enzymatically active in blood, we envision that it would be an excellent reporter for monitoring targets of interest in the blood of *in vivo* models.

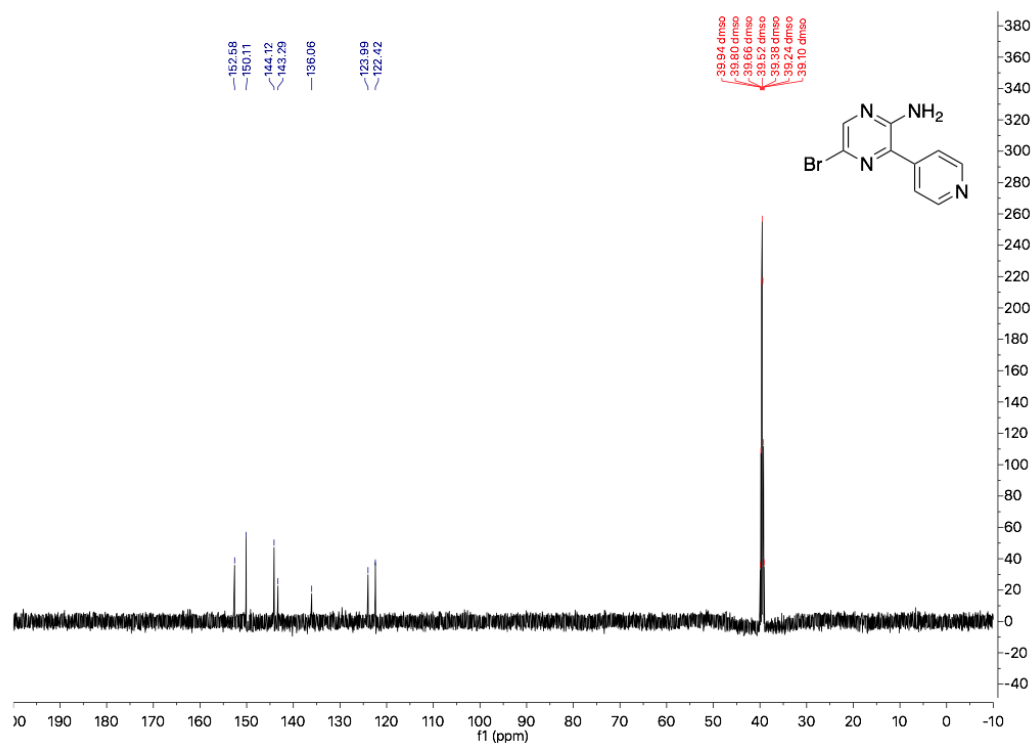
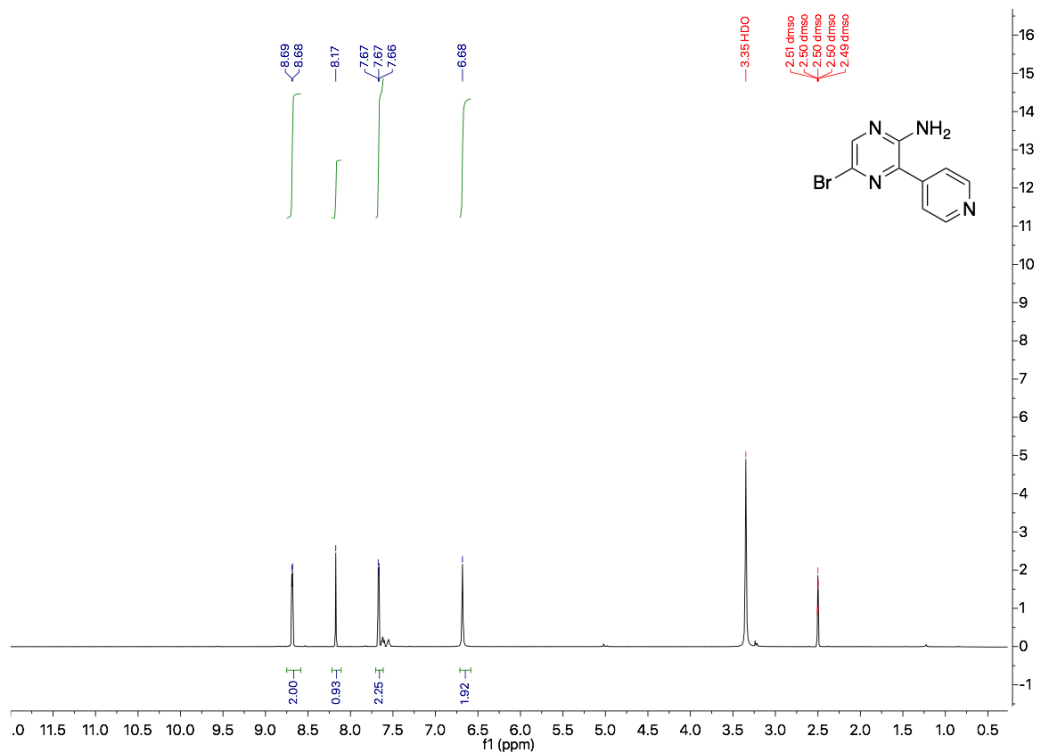
LumiLuc is a luciferase with broad substrate specificity. When it was paired with different substrates, intense blue, teal, and yellow bioluminescence was generated. Subsequently, we gained different emission profiles from LumiScarlet in the presence of different substrates. We demonstrated the use of LumiScarlet-8pyDTZ for deep-tissue imaging. In addition, because the two emission peaks of LumiScarlet-pyCTZ or LumiScarlet-6pyDTZ are more separated than LumiScarlet-8pyDTZ, we envision that LumiScarlet-pyCTZ and LumiScarlet-6pyDTZ would be useful for studying protein-protein interactions or constructing BRET-based biosensors.

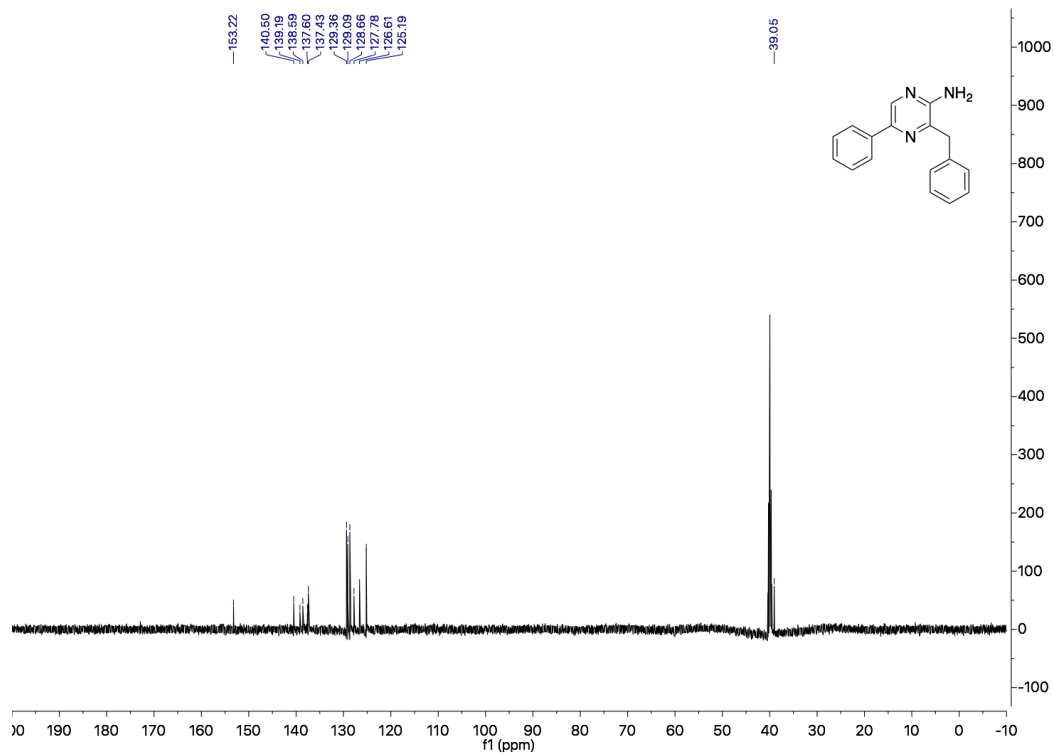
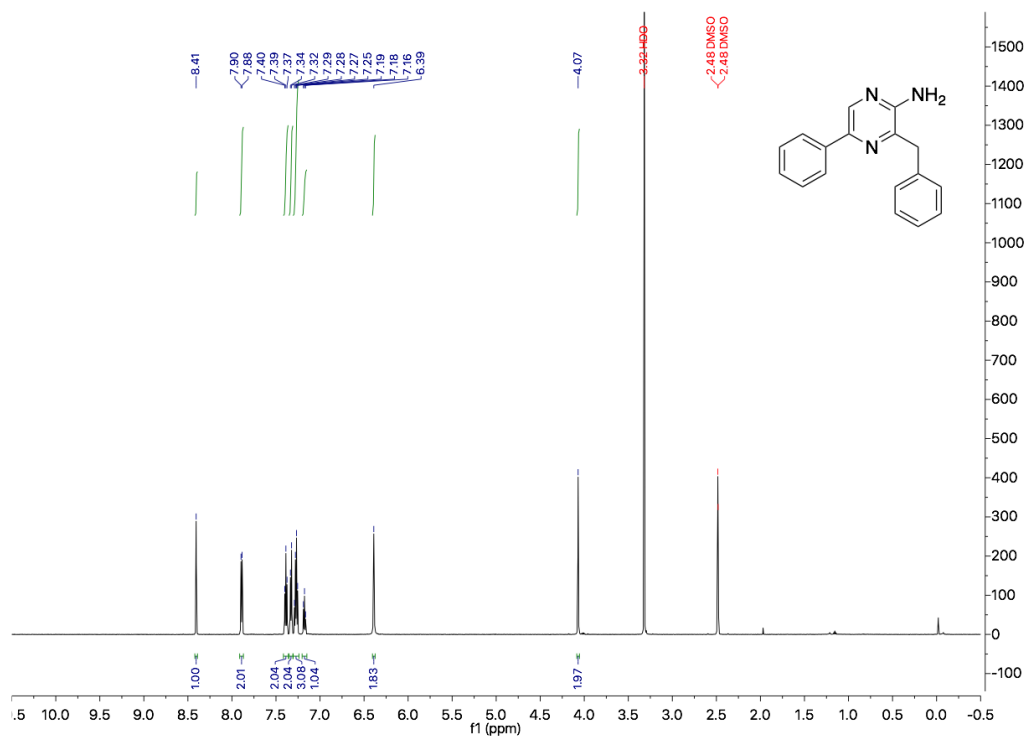
In summary, we have developed several engineered luciferase-luciferin pairs that emit photons spanning an appreciable range in the visible spectrum. Our effort has greatly enhanced the biocompatibility and sensitivity of ATP-independent

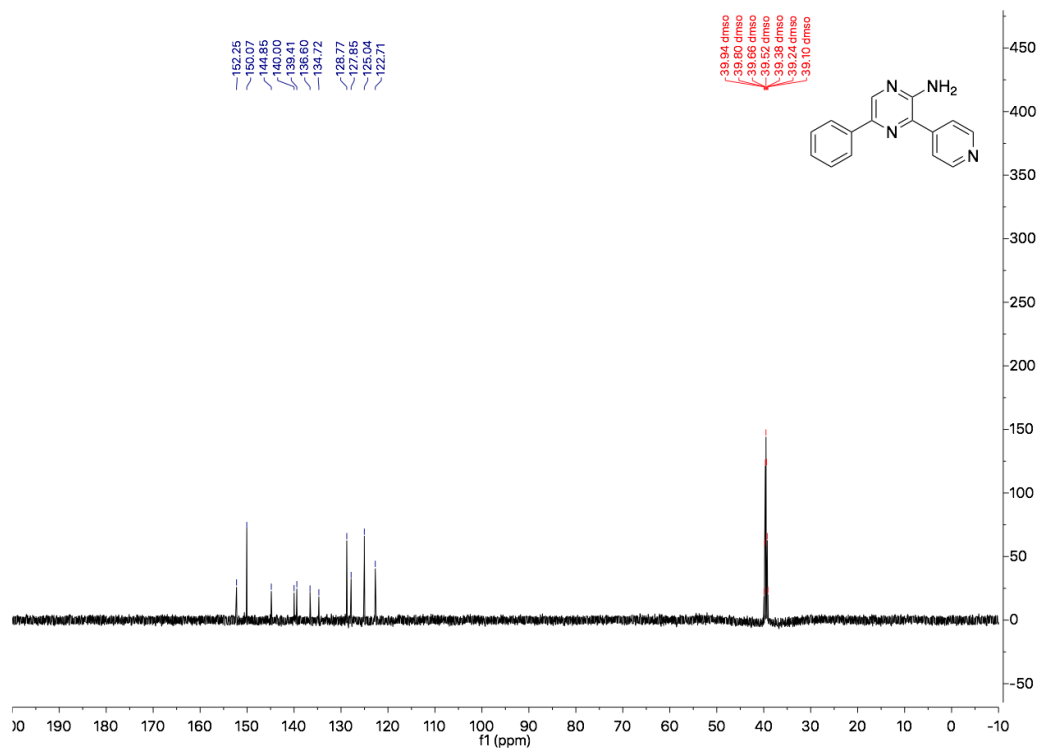
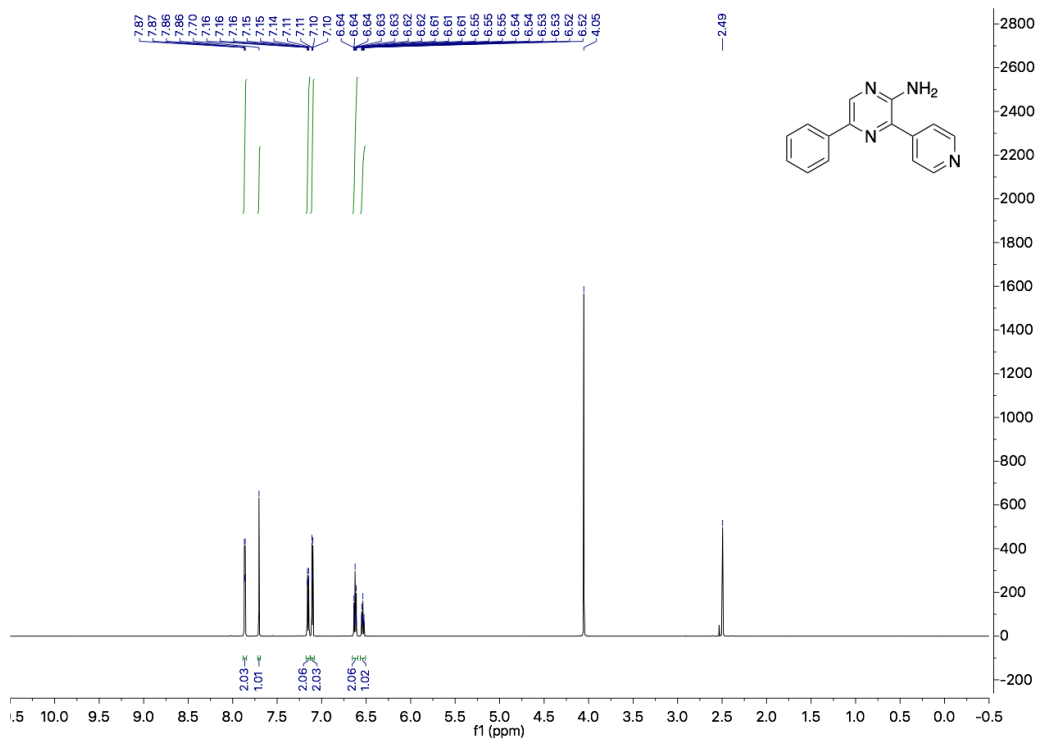
bioluminescent reporters for *in vivo* BLI while the stability of these newly synthesized analogs is moderate. We expect that future studies will continuously increase the water-solubility and biodistribution of CTZ and DTZ analogs and red-shift the emission of marine luciferases. Subsequently, we expect that a large array of bioluminescent biosensors will be developed on the basis of these bright, ATP-independent bioluminescent reporters.³⁰ The new reporters and biosensors will further ease non-invasive imaging of freely moving animals, leading to new biological insights.

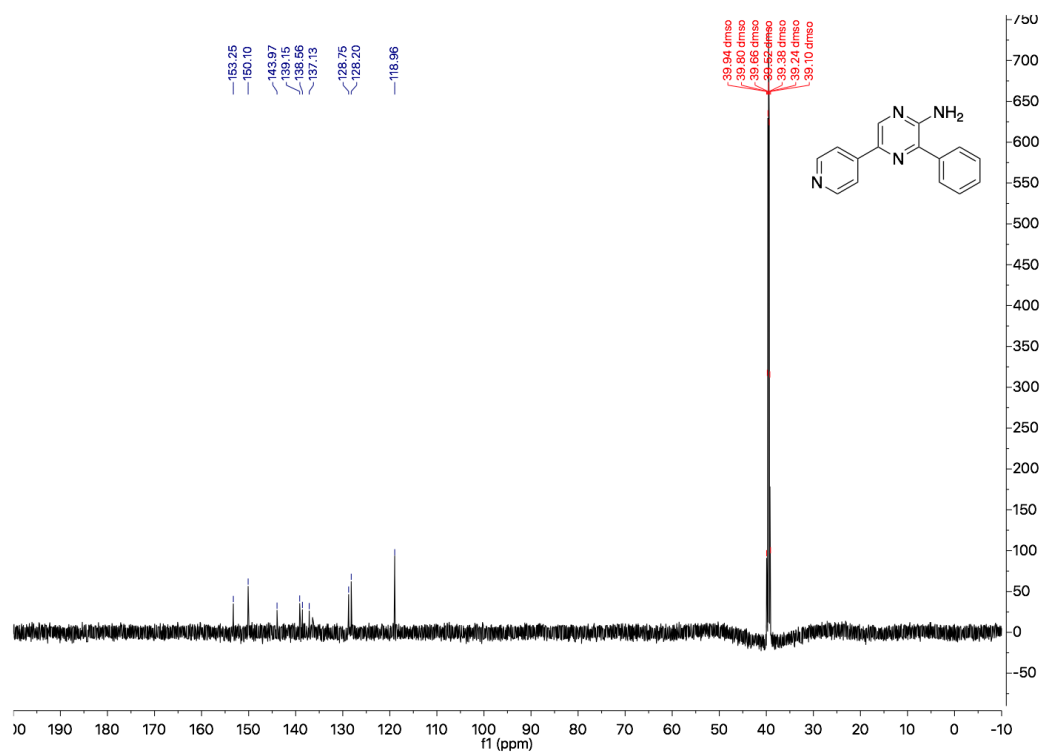
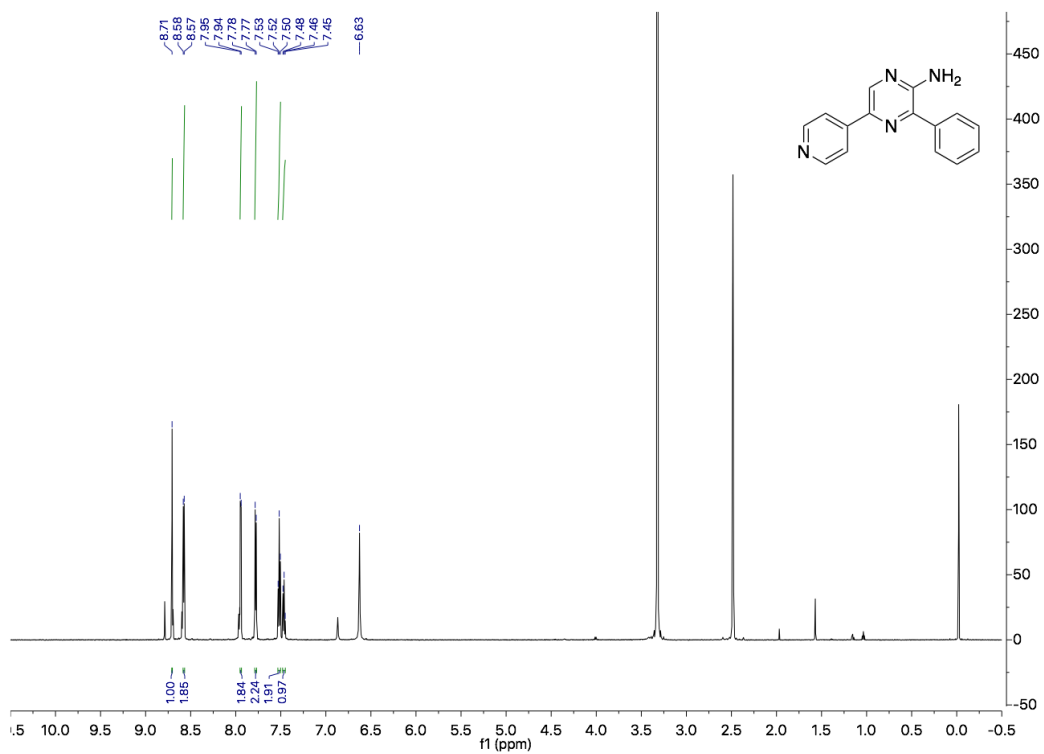
3.5. Appendix

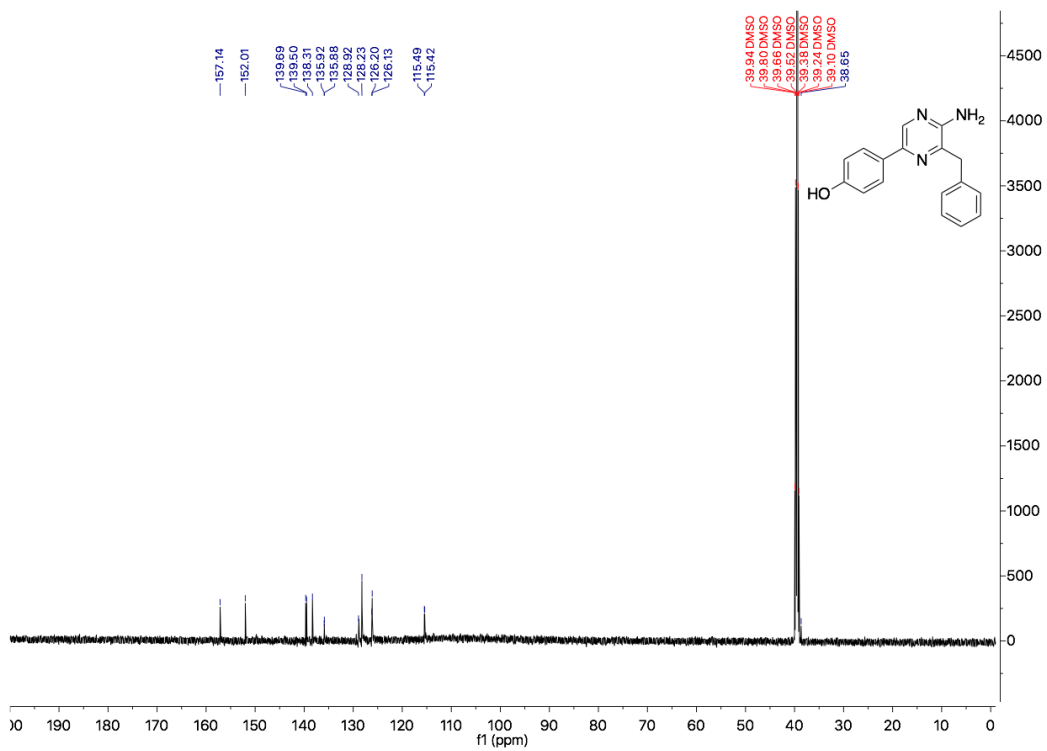
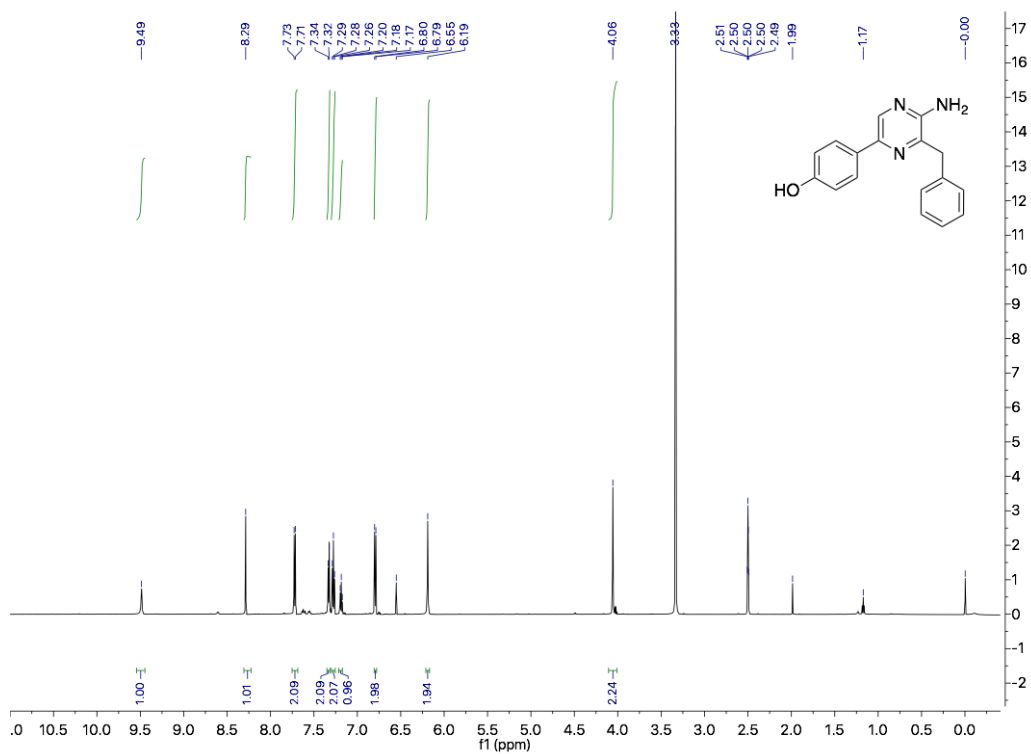


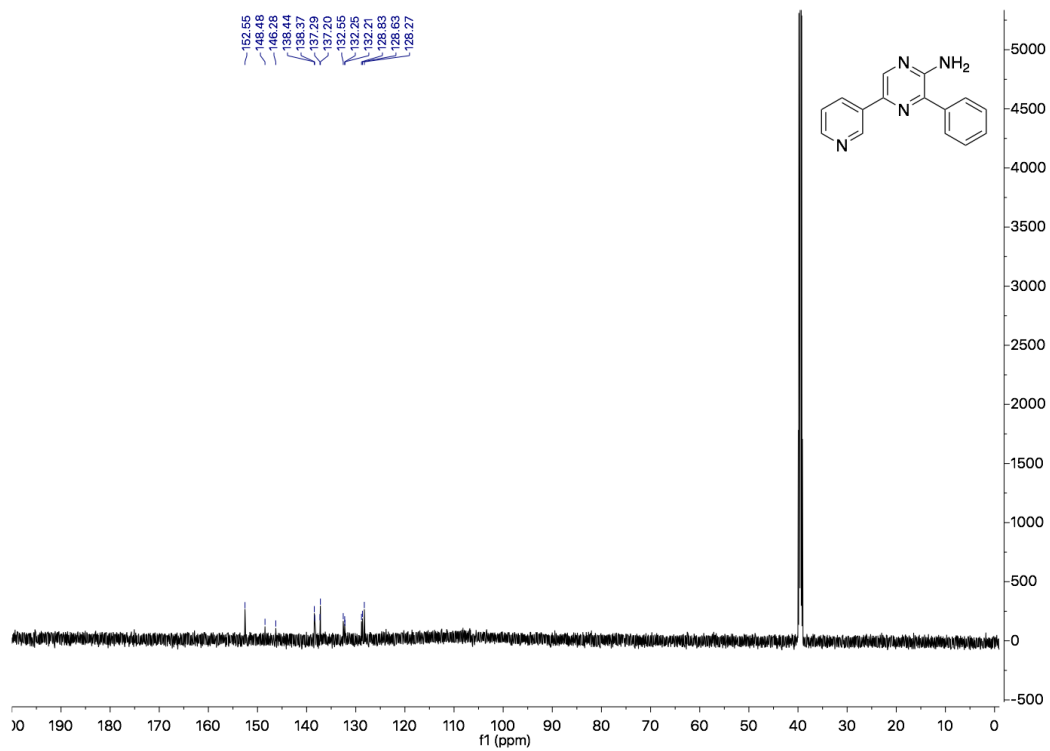
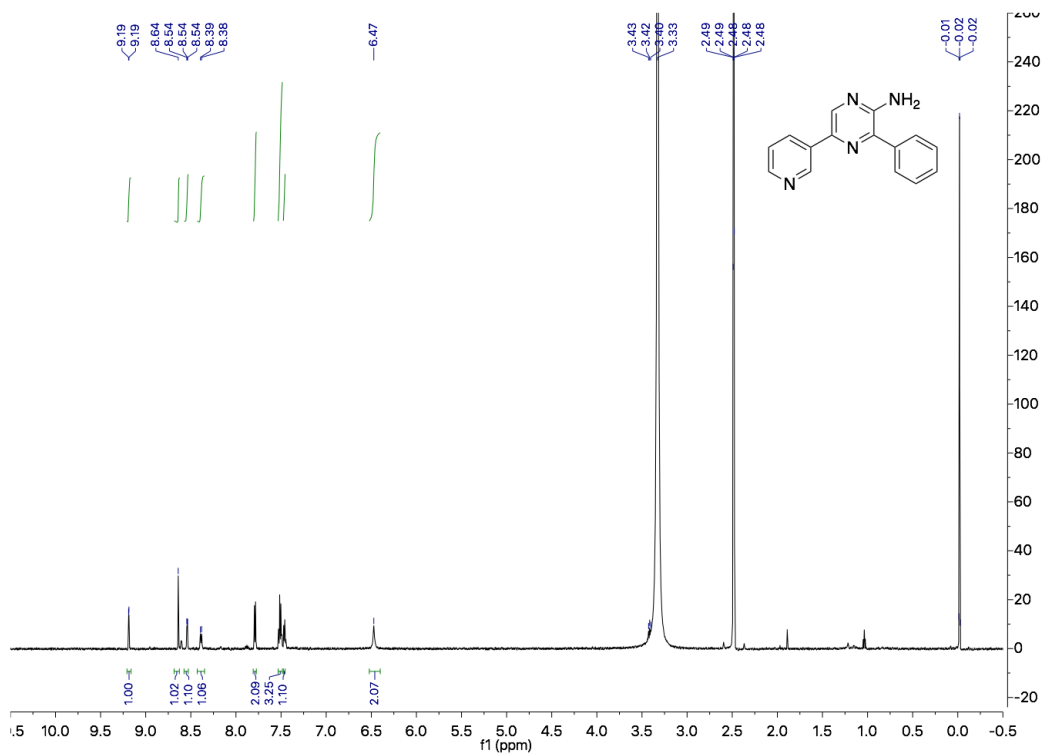


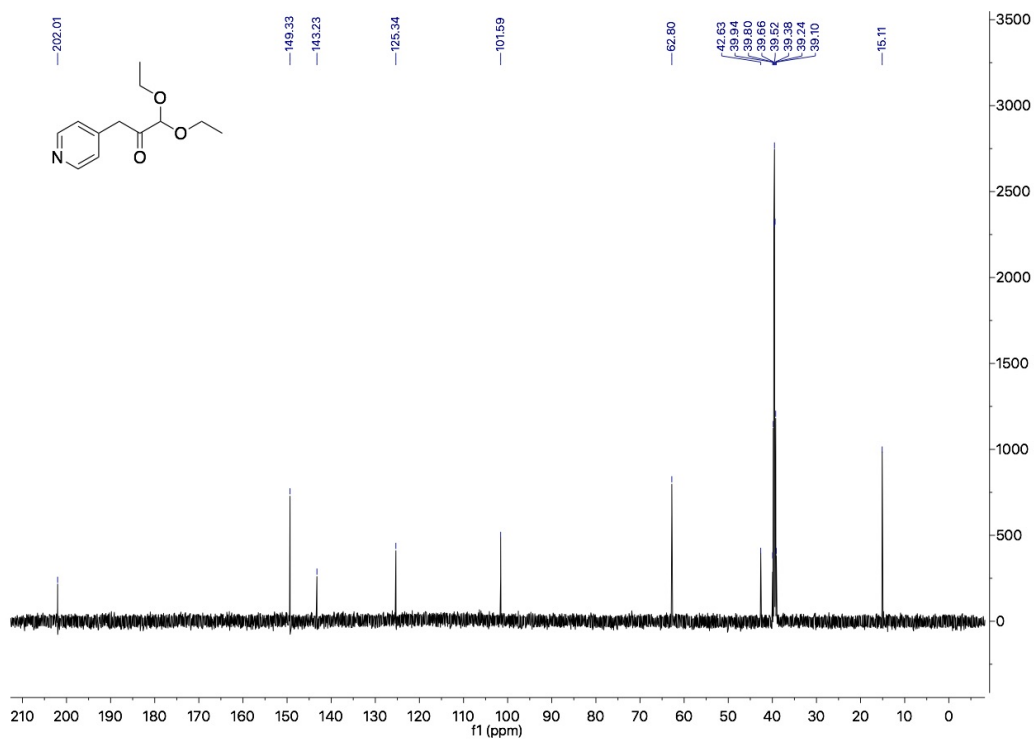
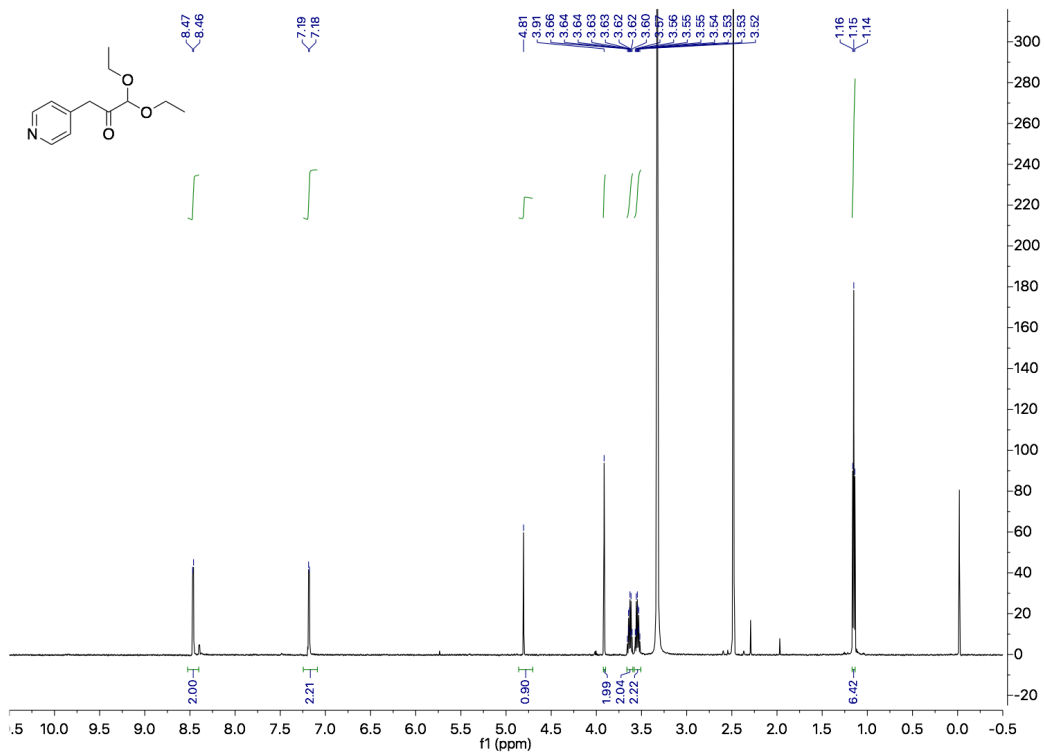


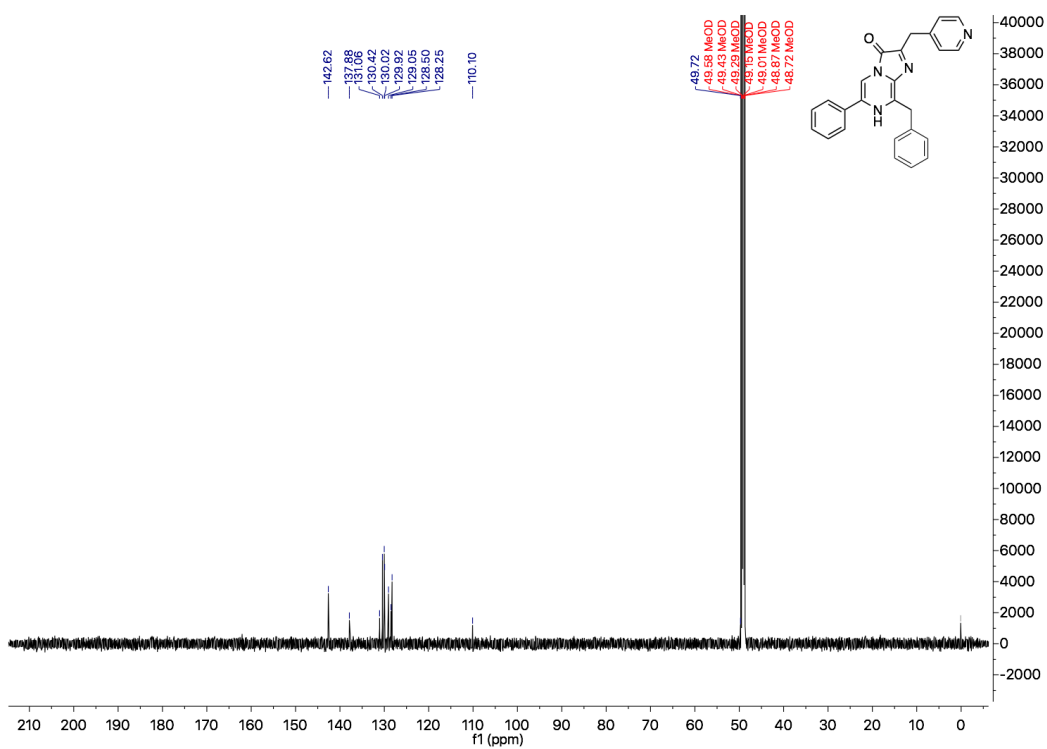
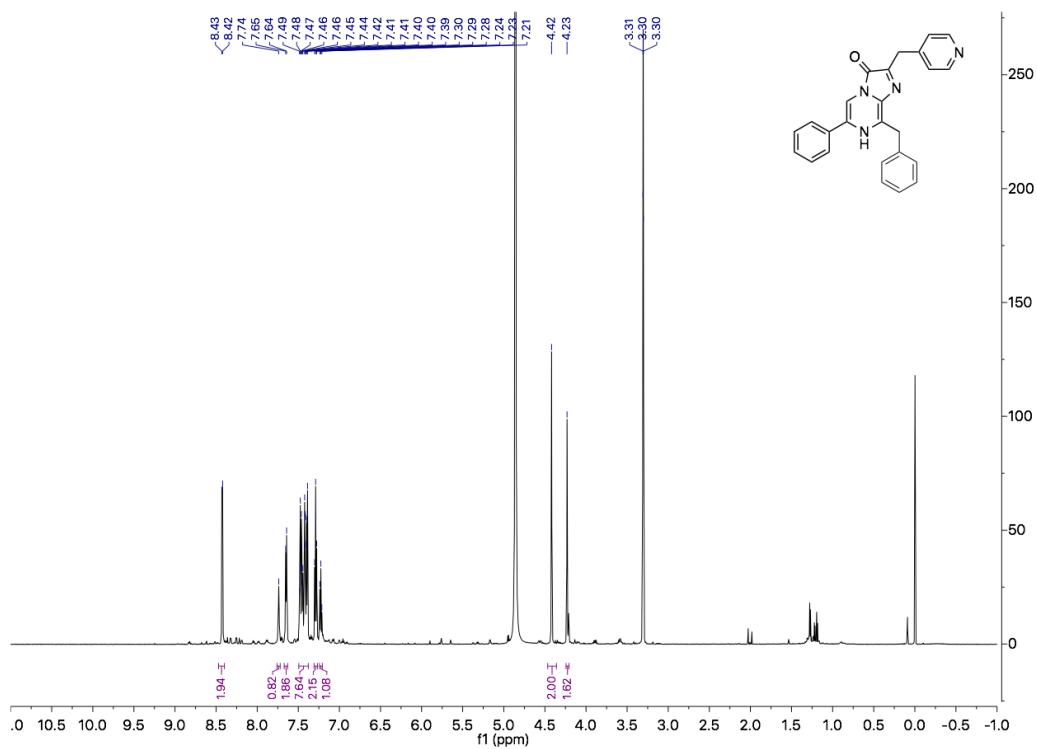


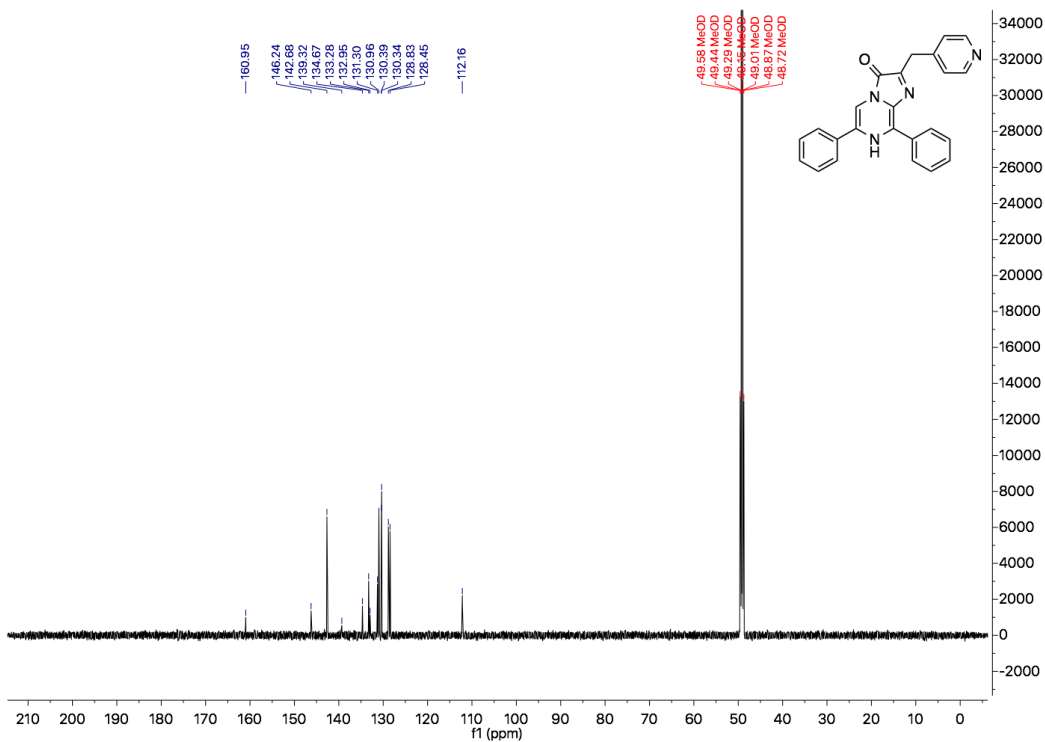
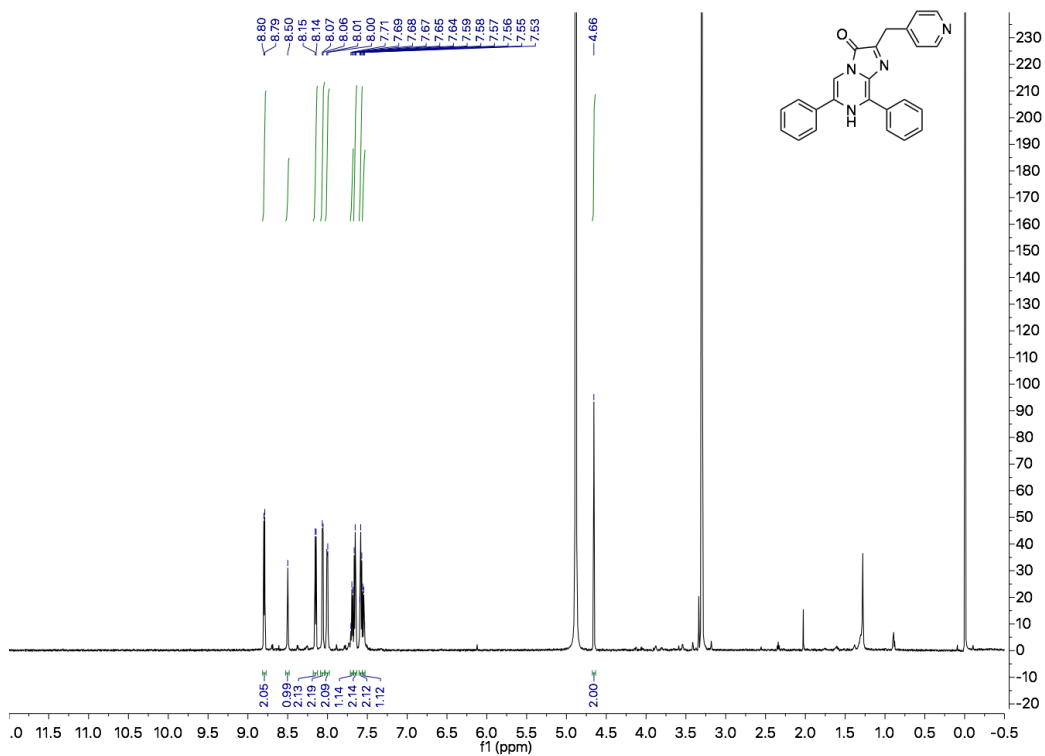


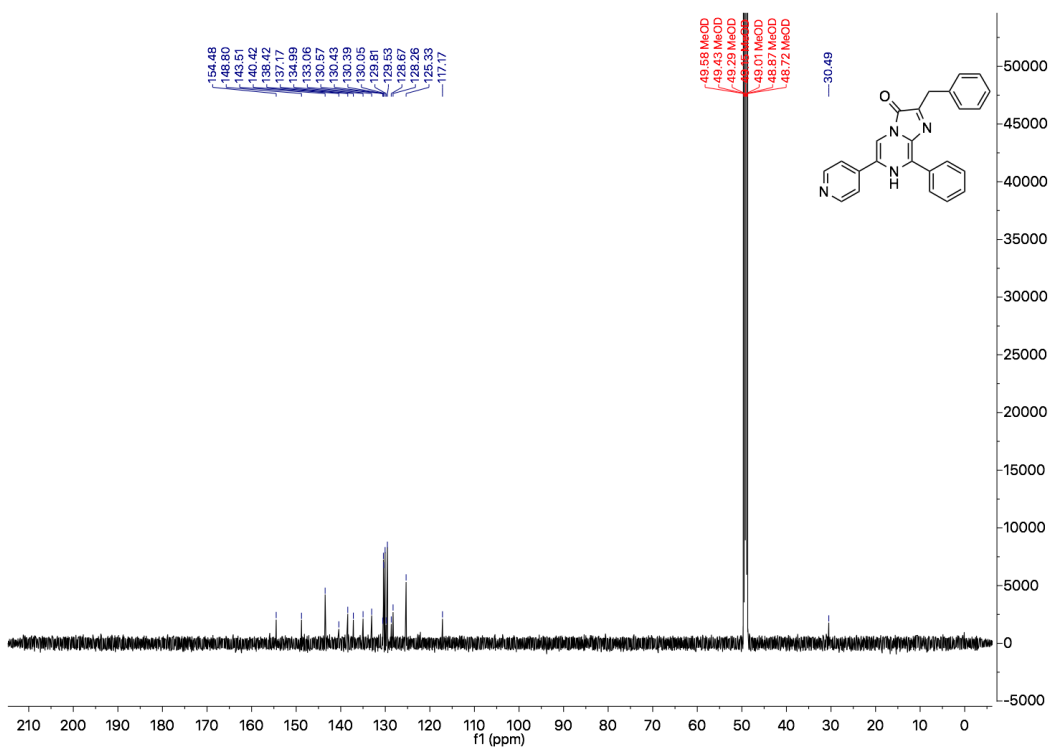
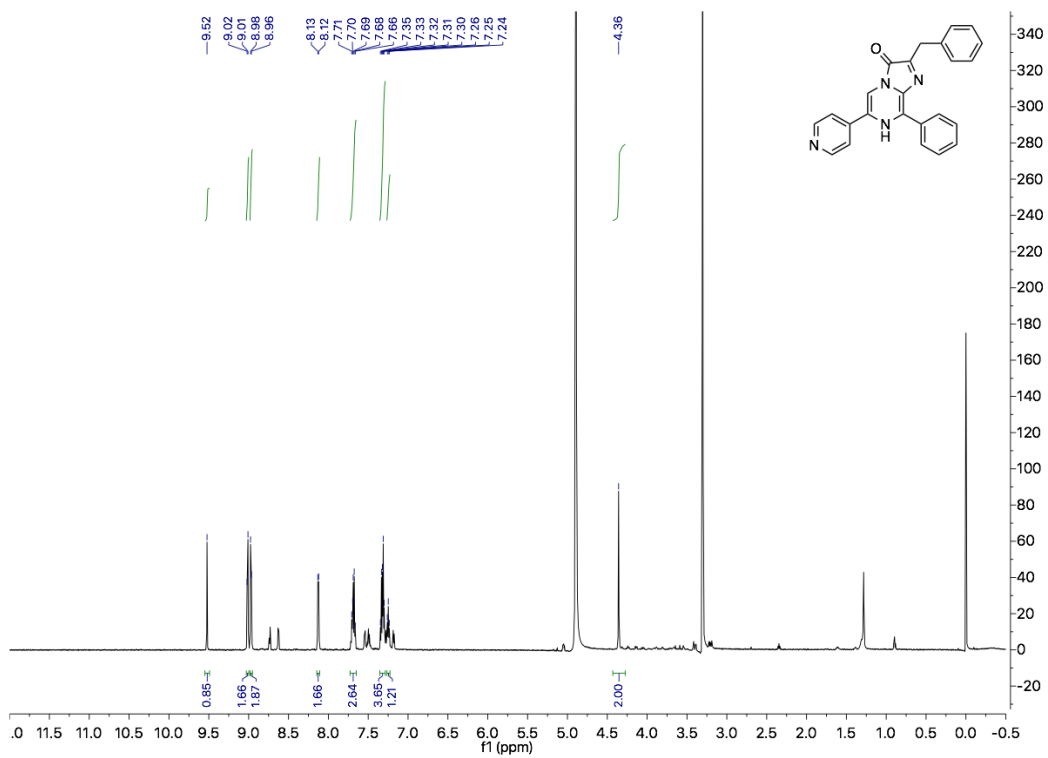


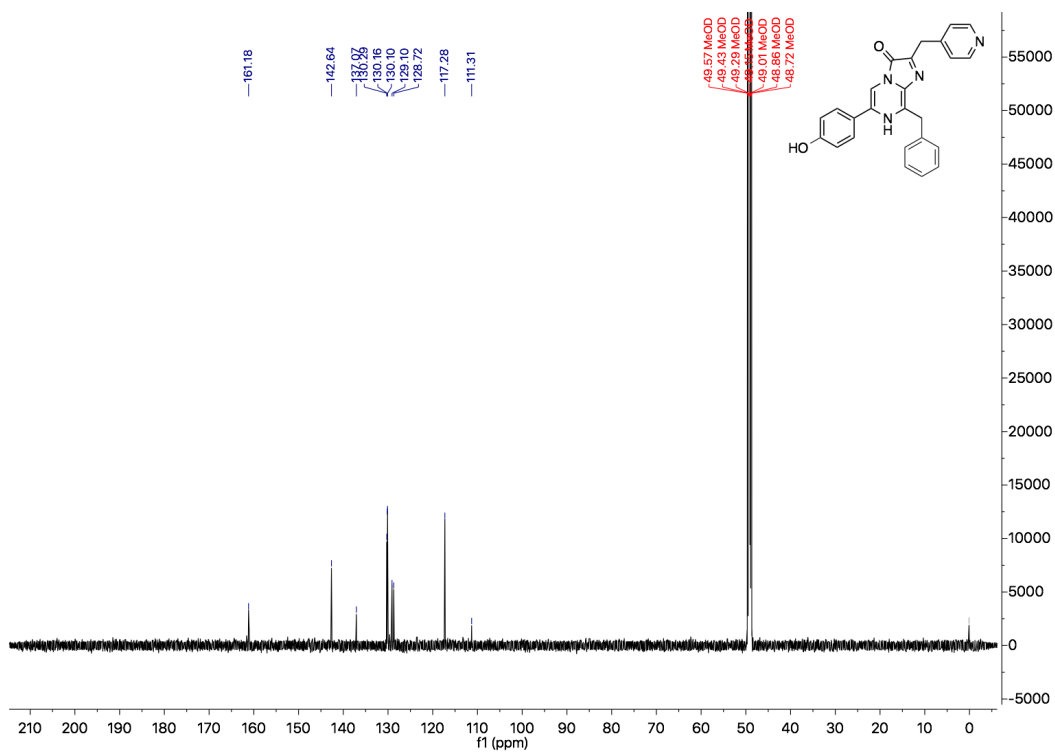
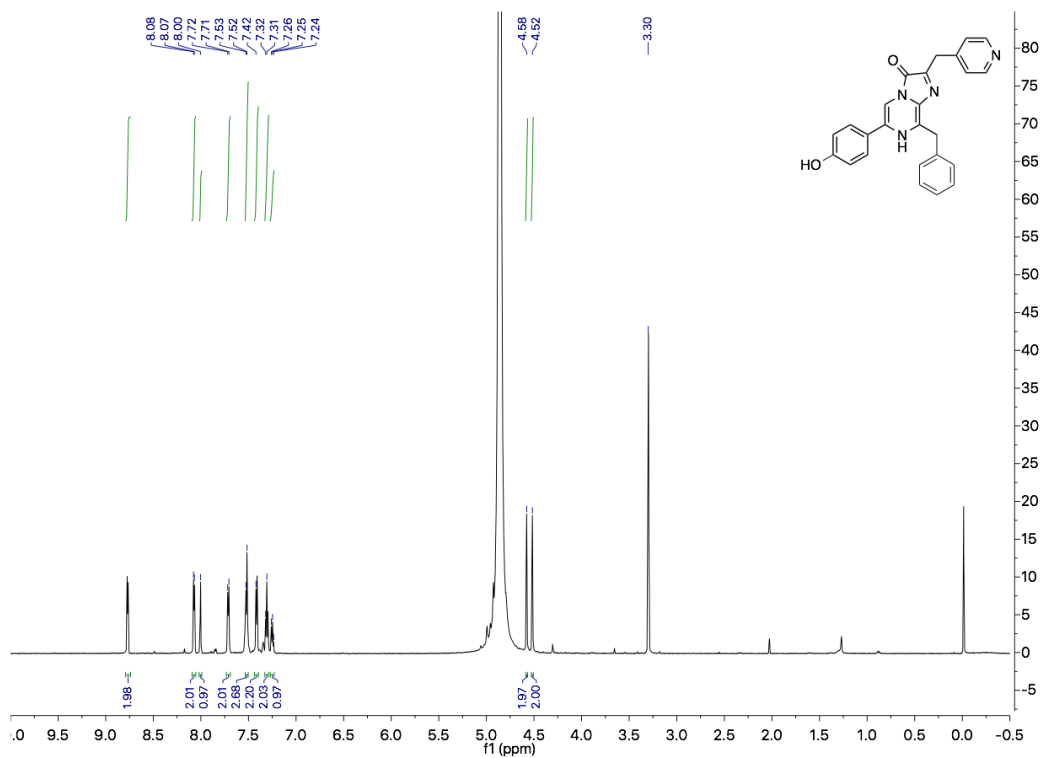












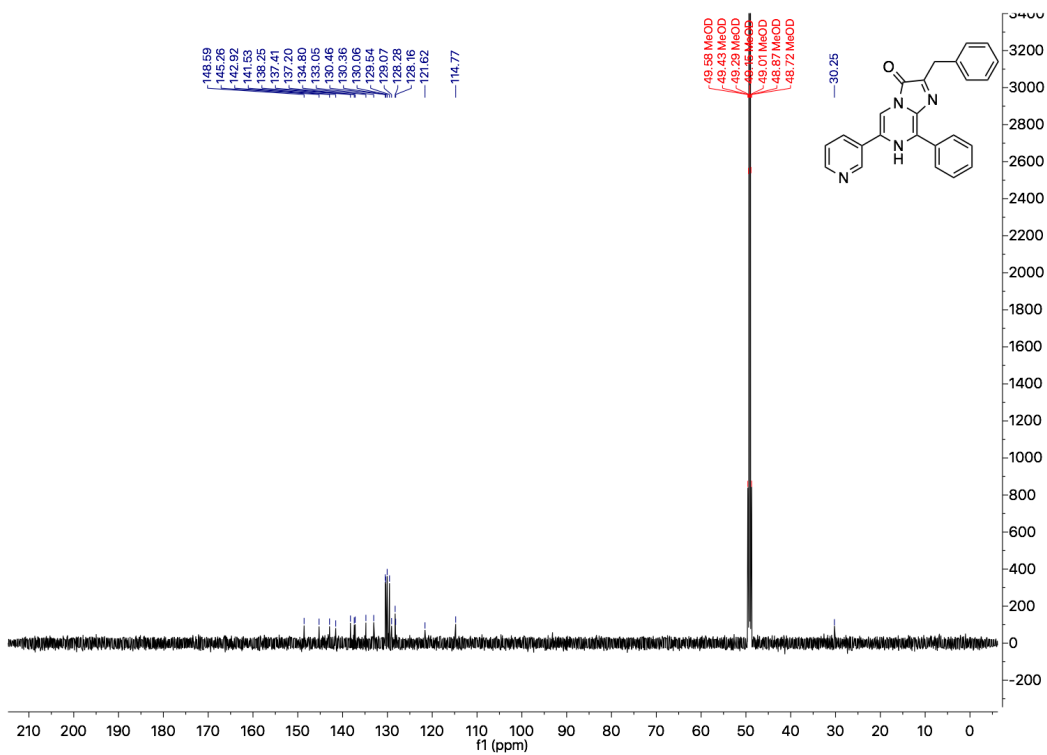
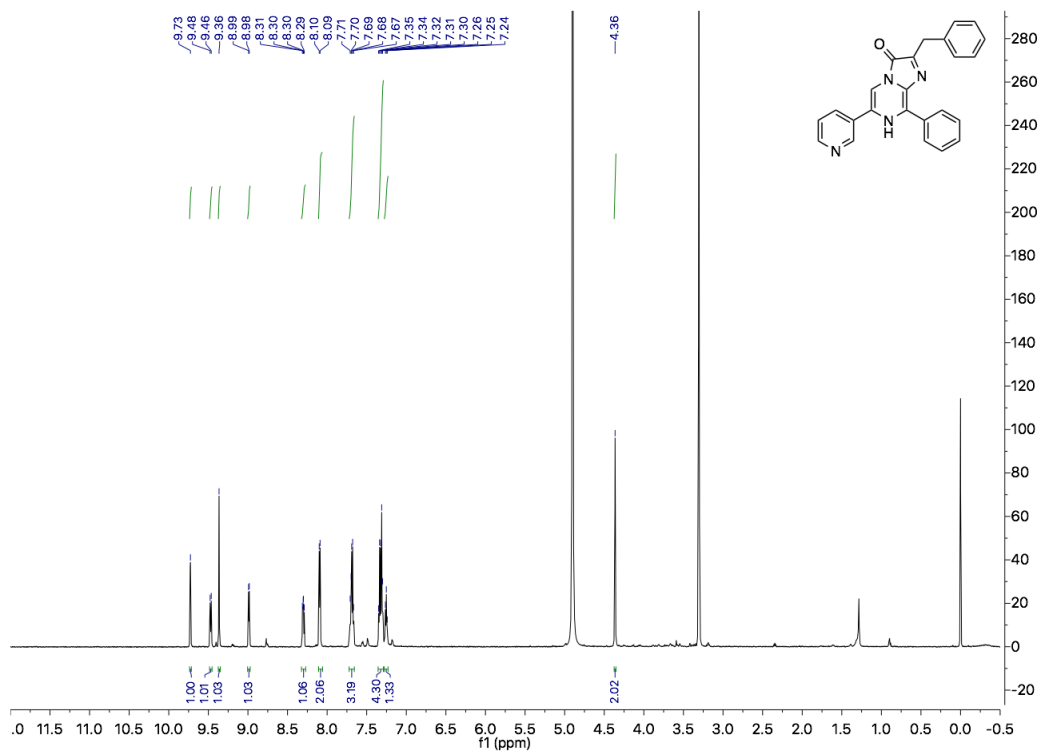


Table 3. Oligonucleotides used in this study.

Oligo name	Nucleotide sequence (5'→ 3')
L18D19NNK-F	CAGACAGCCGGCTACAACNNKNNKCAAGTC CTTGAACAGGGAGGTGTG
L18D19NNK-R	CACACCTCCCTGTTCAAG GACTTGMNNMNNGTGTAGCCGGCTGTCTG
27VSSNNK-F	CAAGTCCTTGAACAGGGAGGTNNKNNKNNKTTGTTTCAGAATCTCGGGG TG
27VSSNNK-R	CACCCCGAGATTCTGAAACAAMNNMNNMNNACCTCCCTGTTCAAGGACT TG
pBAD-F	ATGCCATAGCATTTTTATCC
pBAD-R	GATTTAATCTGTATCAGG
HindIII-pyr-F-Koz	AATAAAGCTTGCCGCCACCATGGTCTTCACTCTCGGGGATTTT
pyr-R-XhoI	TAATTCTCGAGTTACGCCAGAATGCGTTCATGCAG
Aka-F-HindIII-Kozak	ATTATAAAGCTTGCCGCCACCATGGAAGATG CCAAAAACATTAAGA
Aka-R-XhoI	TTATTCTCGAGTTACACGGCGATCTTGCCGTCCTTCTT
Aka-F-XhoI	ATAACTCGAGCATGGAAGATGCCAAAAACATTAAGA
Aka-R-HindIII	TTGCCAAGCTTACACGGCGATCTTGCCGTCCTTCTT
HindIII-mScarlet-F-Koz	ATTATAAAGCTTGCCGCCACCATGGTGAGCAAGGGCGAGGCAGT
mScarlet-F-XhoI	ATAACTCGAGCATGGTGAGCAAGGGCGAGGCAGTG
pyr-R-HindIII	TTGCCAAGCTTACGCCAGAATGCGTTCATGCA
mScar-NNK-pyr-F	GAGGGCCGCACTCCACCGGANNKACTCTCGGGGATTTTGTGGG
mScar-NNK-pyr-R	CCCAACAAAATCCCCGAGAGTMNNTCCGGTGGAGTGCGGCCCTC

References

- Rodriguez, E. A.; Campbell, R. E.; Lin, J. Y.; Lin, M. Z.; Miyawaki, A.; Palmer, A. E.; Shu, X.; Zhang, J.; Tsien, R. Y., The Growing and Glowing Toolbox of Fluorescent and Photoactive Proteins. *Trends Biochem. Sci.* **2017**, *42* (2), 111-129.
- Sadikot, R. T.; Blackwell, T. S., Bioluminescence imaging. *Proc. Am. Thorac. Soc.* **2005**, *2* (6), 537-40, 511-2.
- Mezzanotte, L.; van 't Root, M.; Karatas, H.; Goun, E. A.; Lowik, C., In Vivo Molecular Bioluminescence Imaging: New Tools and Applications. *Trends Biotechnol.* **2017**, *35* (7), 640-652.
- Yao, Z.; Zhang, B. S.; Prescher, J. A., Advances in bioluminescence imaging: new probes from old recipes. *Curr. Opin. Chem. Biol.* **2018**, *45*, 148-156.
- Adams, S. T., Jr.; Miller, S. C., Beyond D-luciferin: expanding the scope of bioluminescence imaging in vivo. *Curr. Opin. Chem. Biol.* **2014**, *21c*, 112-120.
- Iwano, S.; Sugiyama, M.; Hama, H.; Watakabe, A.; Hasegawa, N.; Kuchimaru, T.; Tanaka, K. Z.; Takahashi, M.; Ishida, Y.; Hata, J.; Shimozono, S.; Namiki, K.; Fukano, T.; Kiyama, M.; Okano, H.; Kizaka-Kondoh, S.; McHugh, T. J.; Yamamori, T.; Hioki, H.; Maki, S.; Miyawaki, A., Single-cell bioluminescence imaging of deep tissue in freely moving animals. *Science* **2018**, *359* (6378), 935-939.
- Yeh, H. W.; Karmach, O.; Ji, A.; Carter, D.; Martins-Green, M. M.; Ai, H. W., Red-shifted luciferase-luciferin pairs for enhanced bioluminescence imaging. *Nat Methods* **2017**, *14* (10), 971-974.
- Yeh, H. W.; Wu, T.; Chen, M.; Ai, H., Identification of Factors Complicating Bioluminescence Imaging. *Biochemistry* **2019**, *58* (12), 1689-1697.
- Saito, R.; Kuchimaru, T.; Higashi, S.; Lu, S. W.; Kiyama, M.; Iwano, S.; Obata, R.; Hirano, T.; Kizaka-Kondoh, S.; Maki, S. A., Synthesis and luminescence properties of near-infrared N-heterocyclic luciferin analogues for in vivo optical imaging. *B Chem Soc Jpn* **2018**.
- Haddock, S. H.; Moline, M. A.; Case, J. F., Bioluminescence in the sea. *Ann Rev Mar Sci* **2010**, *2*, 443-93.
- Inouye, S.; Sasaki, S., Overexpression, purification and characterization of the catalytic component of Oplophorus luciferase in the deep-sea shrimp, Oplophorus gracilirostris. *Protein Expr Purif* **2007**, *56* (2), 261-8.
- Hall, M. P.; Unch, J.; Binkowski, B. F.; Valley, M. P.; Butler, B. L.; Wood, M. G.; Otto, P.; Zimmerman, K.; Vidugiris, G.; Machleidt, T.; Robers, M. B.; Benink, H. A.; Eggers, C. T.; Slater, M. R.; Meisenheimer, P. L.; Klaubert, D. H.; Fan, F.; Encell, L. P.; Wood, K. V., Engineered luciferase reporter from a deep sea shrimp utilizing a novel imidazopyrazinone substrate. *ACS Chem. Biol.* **2012**, *7* (11), 1848-57.
- Weissleder, R.; Ntziachristos, V., Shedding light onto live molecular targets. *Nat Med* **2003**, *9* (1), 123-8.
- Chu, J.; Oh, Y.; Sens, A.; Ataie, N.; Dana, H.; Macklin, J. J.; Laviv, T.; Welf, E. S.; Dean, K. M.; Zhang, F.; Kim, B. B.; Tang, C. T.; Hu, M.; Baird, M. A.; Davidson, M. W.; Kay, M. A.; Fiolka, R.; Yasuda, R.; Kim, D. S.; Ng, H. L.; Lin, M. Z., A bright cyan-excitable orange fluorescent protein facilitates dual-emission microscopy and enhances bioluminescence imaging in vivo. *Nat Biotechnol* **2016**, *34* (7), 760-7.
- Suzuki, K.; Kimura, T.; Shinoda, H.; Bai, G.; Daniels, M. J.; Arai, Y.; Nakano, M.; Nagai, T., Five colour variants of bright luminescent protein for real-time multicolour bioimaging. *Nat Commun* **2016**, *7*, 13718.
- Teranishi, K.; Shimomura, O., Solubilizing coelenterazine in water with hydroxypropyl-beta-cyclodextrin. *Biosci Biotech Bioch* **1997**, *61* (7), 1219-1220.
- Morse, D.; Tannous, B. A., A water-soluble coelenterazine for sensitive in vivo imaging of coelenterate luciferases. *Mol Ther* **2012**, *20* (4), 692-3.
- Jiang, T. Y.; Yang, X. Y.; Zhou, Y. B.; Yampolsky, I.; Du, L. P.; Li, M. Y., New bioluminescent coelenterazine derivatives with various C-6 substitutions. *Org Biomol Chem* **2017**, *15* (33), 7008-7018.
- Adamczyk, M.; Akireddy, S. R.; Johnson, D. D.; Mattingly, P. G.; Pan, Y.; Reddy, R. E., Synthesis of 3,7-dihydroimidazo[1,2a]pyrazine-3-ones and their chemiluminescent properties. *Tetrahedron* **2003**, *59* (41), 8129-8142.

20. Shakhmin, A.; Hall, M. P.; Machleidt, T.; Walker, J. R.; Wood, K. V.; Kirkland, T. A., Coelenterazine analogues emit red-shifted bioluminescence with NanoLuc. *Org Biomol Chem* **2017**, 15 (40), 8559-8567.
21. Shakhmin, A.; Hall, M. P.; Walker, J. R.; Machleidt, T.; Binkowski, B. F.; Wood, K. V.; Kirkland, T. A., Three Efficient Methods for Preparation of Coelenterazine Analogues. *Chem-Eur J* **2016**, 22 (30), 10369-10375.
22. Jedinak, L.; Zatopkova, R.; Zemankova, H.; Sustkova, A.; Cankar, P., The Suzuki-Miyaura Cross-Coupling Reaction of Halogenated Aminopyrazoles: Method Development, Scope, and Mechanism of Dehalogenation Side Reaction. *The Journal of organic chemistry* **2017**, 82 (1), 157-169.
23. Kerns, E. H.; Di, L.; Carter, G. T., In vitro solubility assays in drug discovery. *Curr. Drug Metab.* **2008**, 9 (9), 879-85.
24. Rogers, K. L.; Picaud, S.; Roncali, E.; Boisgard, R.; Colasante, C.; Stinnakre, J.; Tavitian, B.; Brulet, P., Non-invasive in vivo imaging of calcium signaling in mice. *Plos One* **2007**, 2 (10), e974.
25. Zinn, K. R.; Chaudhuri, T. R.; Szafran, A. A.; O'Quinn, D.; Weaver, C.; Dugger, K.; Lamar, D.; Kesterson, R. A.; Wang, X.; Frank, S. J., Noninvasive bioluminescence imaging in small animals. *ILAR J.* **2008**, 49 (1), 103-15.
26. Inouye, S.; Sato, J.; Sahara-Miura, Y.; Yoshida, S.; Hosoya, T., Luminescence enhancement of the catalytic 19 kDa protein (KAZ) of *Oplophorus* luciferase by three amino acid substitutions. *Biochem Biophys Res Commun* **2014**, 445 (1), 157-62.
27. Morton, C. L.; Houghton, P. J., Establishment of human tumor xenografts in immunodeficient mice. *Nat Protoc* **2007**, 2 (2), 247-250.
28. Bindels, D. S.; Haarbosch, L.; van Weeren, L.; Postma, M.; Wiese, K. E.; Mastop, M.; Aumonier, S.; Gotthard, G.; Royant, A.; Hink, M. A.; Gadella, T. W., Jr., mScarlet: a bright monomeric red fluorescent protein for cellular imaging. *Nat Methods* **2017**, 14 (1), 53-56.
29. Salin, K.; Auer, S. K.; Rey, B.; Selman, C.; Metcalfe, N. B., Variation in the link between oxygen consumption and ATP production, and its relevance for animal performance. *P Roy Soc B-Biol Sci* **2015**, 282 (1812), 14-22.
30. Greenwald, E. C.; Mehta, S.; Zhang, J., Genetically Encoded Fluorescent Biosensors Illuminate the Spatiotemporal Regulation of Signaling Networks. *Chemical reviews* **2018**, 118 (24), 11707-11794.

Chapter 4

Development of Spectral-resolved and Orthogonal Triple Luciferase System to Enable Multiplexed Bioluminescence Assays

Abstract

Bioluminescent reporter assays, providing high sensitivity and high dynamic range, has become a routine method to monitor gene expression. Commercial bioluminescent reporter assays suffer from the lack of orthogonal luciferase-luciferin pairs and spectral-resolved emission, so they are limited to the monitoring of only one transcriptional event. Here, we combined both advantageous features by utilizing different colors and luciferin selectivity, meanwhile we designed a screening strategy emphasizing on substrate selectivity to engineer a luciferase (OpyLuc) that exhibits the unique preference for our synthetic luciferin analog. When pairing with *Renilla* Luciferase and Akaluc, the cross-reactivity between each luciferase-luciferin pair is minimized, while the respective emission spectra are well resolved. This work yields a triple luciferase system to monitor up to three gene expression events simultaneously. We present a proof-of-concept to engineer the orthogonality of coelenterazine-utilizing luciferase via directed evolution for the development of multiplexed bioassays.

4.1. Introduction

In the past few decades, a number of bioluminescent reporters have been discovered and further developed for a wide range of applications, such as bioassays, *in vivo* imaging, and visualizing biology at subcellular resolution.¹ Bioluminescence (BL) light is produced by an enzyme (a.k.a., luciferase) that catalyzes an oxidative reaction of a substrate (a.k.a., luciferin). The BL emission process, in contrast to fluorescence, does not require excitation light, thereby providing excellent signal-to-background ratio. As an analytical modality, bioluminescence measurement is more sensitive and exhibits wide dynamic range that gives highly compatible adaptability to high-throughput screening than other typical reporters, such as β -galactosidase and fluorescent proteins.²⁻³ Therefore, bioluminescent probes are ideally suited as genetic reporters for the biomedical research, including drug screening, cell-based assays, studying gene expression, signal transduction, and transcriptional factor-promoter interactions.⁴⁻⁵

The majority of luciferases used in laboratory are derived from insects, beetles, and marine organisms, which consume their respective luciferins to generate different colors of emission photon. Insertion of a luciferase gene at the downstream of the targeted promoter yields several commercial luciferase assays for the quantitative measurement of gene expression.⁶ However, cell signaling is a complicated network cascade. It has been increasingly demanded to monitor multiple gene regulations at once, in which multiplexed BL assay could reveal unanticipated facets of signaling from the molecular basis to various biological functions. To achieve multiplexed BL assay, the setup of a specific assay has to produce more than one distinguishable BL signal in order to report more than one gene expression. Retrospectively, several attempts to monitor multiple gene regulation have been investigated by a set of luciferases that either exhibiting mutually exclusive substrate selectivity (i.e., orthogonal) or producing distinct colors of light.⁷⁻¹⁰

For instance, Promega Dual-Luciferase Reporter Assay system utilized the firefly luciferase (FLuc, λ_{max} : 560 nm) from *Photinus pyralis* and the *Renilla* luciferase (RLuc, λ_{max} : 480 nm) from *Renilla reniformis* in combination with their corresponding substrate, D-luciferin and coelenterazine (CTZ). Nevertheless, this assay has to be performed in a sequential manner where the emission from FLuc has to be first measured and then quenched before the second acquisition of RLuc signals, thereby compromising its high-throughput capability. On the other hand, Pierce Cypridina-Firefly Luciferase Dual Assay combined the *cypridina* luciferase (CLuc, λ_{max} : ~470 nm) from *Cypridina noctiluca* and the red firefly luciferase (λ_{max} : ~610 nm) from *Luciola cruciate* with a unique substrate combination – vargulin and D-luciferin. Because the emission spectra from CLuc and red firefly luciferase are well spectrally resolved, this assay enables simultaneous monitoring of both luciferase activities in a single-read event by adding a mixture solution containing both substrates. These two commercial systems take advantage of the natural substrate preferences of two bioluminescence systems and their spectrally resolved emission, to more accurately quantify single gene expression by performing one experimental reporter and one internal control for the normalizations of cell number, transfection efficiency, and cell viability.

On the other hand, dual-color BL assay has also been developed by employing the combination of a green- and a red-emitting insect luciferase to monitor multicomponent, while the BL emission is produced by a single substrate (D-luciferin). In fact, the emission spectra of these two luciferases (λ_{max} : ~550 nm and ~610 nm) were not well-separated due to their broad bandwidths, thereby it required un-mixing calculation by considering the filter correction factors to determine the intensities of each signal.¹¹⁻¹³ Even though efforts have been devoted to monitor three genes expression, it is still unlikely to circumvent their spectral overlap because the same substrate, D-luciferin, initiates all color emission at the same time.^{7, 14} Therefore,

substrate selectivity has again attracted attention to potentially achieve truly orthogonal multicomponent BL assay.⁸⁻⁹

Substrate selectivity has been explored for some ATP-dependent insect luciferases.^{8-9, 15} However, BL assay using two marine luciferases usually do not show substrate selectivity because CTZ is the shared substrate of most marine luciferases. For example, two nonhomologous marine luciferases – NanoLuc, and *Gaussia* luciferase (GLuc) were used together in a secreted assay. The need for calculation and subtraction to determine individual luciferase activities is essential because a significant signal from NanoLuc-CTZ was also observed and equivalent to ~25% signal from GLuc-CTZ pair.¹⁰

To overcome the limitations of current reporter assay systems, we aimed to combine the pros and cons of previous BL technologies, and to engineer a triple-color BL system in which the emission spectra are well-resolved. By accessing engineered luciferase with our synthetic substrate via directed evolution, each single luciferase orthogonally processes its corresponding luciferin, providing a set of feasible toolkit to facilitate multiplexed BL assay. This system will allow unprecedented flexibility for the design of multiplexed assay to track two or more gene expression events.

4.2. Experimental section

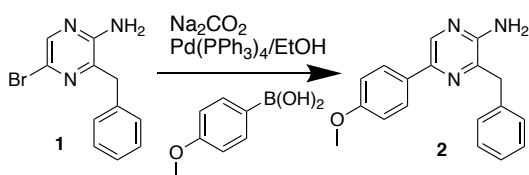
4.2.1. Material and methods

Synthetic DNA oligonucleotides were purchased from Integrated DNA Technologies. Restriction endonucleases were purchased from Thermo Fisher Scientific. Q5 high-fidelity DNA polymerase and Taq DNA polymerase were purchased from NEB. Products of PCR and restriction digestion were purified by gel electrophoresis and Syd Laboratories Gel Extraction columns. Plasmid DNA was purified using Syd Laboratories Miniprep columns. DNA sequences were analyzed by Eurofins.

AkaLumine-HCl was purchased from Aobious. All other chemicals were purchased from Sigma-Aldrich, Fisher Scientific, or VWR and used without further purification. Bruker Avance DRX 600 and Varian NMRS 600 at the UVA Biomolecular Magnetic Resonance Facility was used to record all NMR spectra. Chemical shift (δ) is given in parts per million relative to ^1H (7.24 p.p.m.) and ^{13}C (77.23 p.p.m.) for CDCl_3 ; ^1H (2.50 p.p.m.) and ^{13}C (39.5 p.p.m.) for DMSO-d_6 ; ^1H (3.31 p.p.m.) and ^{13}C (49.15 p.p.m.) for methanol- d_4 . Splitting patterns are reported as s (singlet), bs (broad singlet), d (doublet), t (triplet), dd (doublet of doublets), and m (multiplet). Coupling constant (J) is given in Hz. High resolution ESI-MS was run on an Agilent 6545 Q-TOF LC/MS system by direct infusion. A Waters Delta Prep ZQ 2000 LC-MS Purification System equipped with a XBridge BEH Amide OBD Prep Column (130Å, 5 μm , 30 mm X 150 mm) was used for preparative reverse-phase HPLC purifications. Images were analyzed using the Fiji image analysis software. Microsoft Excel and GraphPad Prism were used to analyze data and prepare figures.

4.2.2. Chemical synthesis

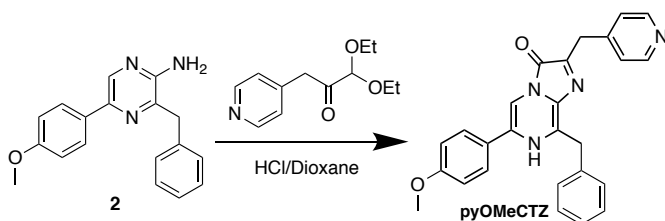
3-benzyl-5-(4-methoxyphenyl)pyrazin-2-amine (2):



1 was prepared following the published synthesis methods¹⁶. To a solution of $\text{Pd}(\text{PPh}_3)_4$ (230 mg, 0.2 mmol, 0.1 equiv.) in 50 mL EtOH was added **1** (528 mg, 2 mmol, 1 equiv.), 1N Na_2CO_3 solution (4 mL, 4 mmol, 2 equiv.) and 4-Methoxyphenylboronic acid (304 mg, 2 mmol, 1 equiv.). The resultant mixture was stirred at 80 °C under argon for 12 h. The solvent was removed *in vacuo* and the residue was suspended in 100 mL ddH₂O, which was extracted twice with EtOAc (100

mL). The organic layers were combined and dried over anhydrous Na_2SO_4 , filtered and removed in *vacuo*. The residue was purified by silica column chromatography with elution (Ethyl acetate:Hexane = 1:1) to yield compound **2** as yellow solid (413 mg, 71%). ^1H NMR (600 MHz, DMSO-d_6) δ 8.33 (s, 1H), 7.82 (d, J = 8.8 Hz, 2H), 7.32 (d, J = 6.7 Hz, 2H), 7.26 (t, J = 7.6 Hz, 2H), 7.17 (t, J = 7.4 Hz, 1H), 6.95 (d, J = 8.8 Hz, 2H), 6.26 (s, 2H), 4.05 (s, 2H), 3.76 (s, 3H). ^{13}C NMR (150 MHz, DMSO-d_6) 158.9, 152.2, 139.8, 139.0, 138.2, 136.2, 128.9, 128.2, 126.1, 126.1, 114.1, 55.1, 38.6. HRMS (ESI-TOF) calcd for $\text{C}_{18}\text{H}_{17}\text{N}_3\text{O}$ [$\text{M} + \text{H}$] $^+$: 292.1372, found: m/z 292.1369.

8-benzyl-6-(4-methoxyphenyl)-2-(pyridin-4-ylmethyl)imidazo[1,2-a]pyrazin-3(7H)-one
(pyOMeCTZ):



To a solution of **2** (29 mg, 0.1 mmol, 1 equiv.) and 3-pyridin-4-yl-1,1-diethoxyacetone (45 mg, 0.2 mmol, 2 equiv) in 2 mL degassed 1,4-dioxane was added 1 mL 6N HCl. The resulting mixture was stirred at 80°C in a sealed tube for 12 h. The solvent was then removed *in vacuo* and the residue was dissolved in 1 mL (ACN:H₂O = 1:1) and next purified with preparative RP-HPLC. (acetonitrile/water = 1:99 to 90:10, 20 mL/min, UV 254 nm). Product fractions were combined and lyophilized to give **pyOMeCTZ** as yellow powder (10 mg, 24%), which has to be stored as solid at -80 °C for long-term stability. ^1H NMR (600 MHz, Methanol- d_4) δ 8.82 (d, J = 6.4 Hz, 2H), 8.27 (s, 1H), 8.09 (d, J = 6.2 Hz, 2H), 7.73 (d, J = 8.7 Hz, 2H), 7.43 (d, J = 7.5 Hz, 2H), 7.32 (t, J = 7.6 Hz, 2H), 7.26 (t, J = 7.2 Hz, 1H), 7.10 (d, J = 8.7 Hz, 2H), 4.66 (s, 2H), 4.61 (s, 2H), 3.87 (s, 3H). ^{13}C NMR (150 MHz, Methanol- d_4) δ 142.7, 137.0,

130.2, 130.1, 129.1, 128.7, 126.5, 115.9, 56.2. HRMS (ESI-TOF) calcd for $C_{26}H_{22}N_4O_2$ [M + H]⁺: 423.1743, found: m/z 423.1740.

4.2.3 Plasmid construction

Polymerase chain reactions with various synthetic oligonucleotide pairs (see **Table 1**) were used to amplify genetic elements. Generating gene libraries with randomizations were previously described. The above-mentioned screening approach was applied to the selection process of random mutagenesis by Error prone-PCR. Oligonucleotides pBAD-F and pBAD-R were used to create a library with randomization by using Taq DNA polymerase, 0.2 mM MnCl₂, and unbalanced dNTPs to promote amplification errors. The PCR product was digested with Xho I and Hind III restriction enzymes and ligated into a predigested, compatible pBAD/His B plasmid. To create mammalian expression plasmids containing NFκB response element, NFκB_SacI_F and NFκB_BglII_R were used to amplify the fragment from pHAGE NFκB-TA-LUC-UBC-GFP-W plasmid (Addgene:49343), which was further treated with Sac I and Bgl II restriction enzymes and ligated into a predigested, compatible SRE reporter vector_559 plasmid (Addgene:82686). For Antioxidant response element, the DNA fragment was synthesized by IDT and ligated into Sac I and Bgl II predigested SRE reporter vector_559 plasmid. The OpyLuc, RLuc8, and Akaluc gene were cloned into corresponding plasmids containing desired response element by using opyluc_AscI_Kozak_F/opyluc_FseI_R, RLuc_AscI_Kozak_F/RLuc_FseI_R, or Akaluc_AscI_Kozak_F/Akaluc_FseI_R oligonucleotide pairs with Asc I and Fse I double digestion. All ligation products were used to transform *Escherichia coli* DH10B electrocompetent cells, which were next plated on LB agar plates supplemented with ampicillin (100 µg/mL).

4.2.4 Library screening

DH10B cells containing luciferase mutants were plated on LB agar plates supplemented with ampicillin (100 $\mu\text{g}/\text{mL}$) and l-arabinose (0.02%, w/v%) and incubated at 37°C overnight to form bacterial colonies. Agar plates were left at room temperature for another 6 h, and this was followed by bioluminescence imaging using a luminescence dark box (UVP Bio Spectrum) equipped with a QSI 628 cooled CCD camera (Quantum Scientific Imaging). Digital images were acquired after spraying $\sim 200 \mu\text{L}$ of 50 μM pyDTZ to each agar plate, and next, images were processed with the Fiji image analysis software to derive bioluminescence intensities of individual colonies. For each round of selection, colonies showing bright bioluminescence were chosen and inoculated in 1 mL liquid LB broth containing ampicillin (100 $\mu\text{g}/\text{mL}$) and l-arabinose (0.02%, w/v%) in 96-well deep plates. After overnight growth at 37°C and 250 r.p.m., the cultures were moved onto a shaker at room temperature for another 6 h. The 96-well plates were centrifuged and the pellet in each well was lysed with 200 μL B-PER. After 30-minute incubation, the 96-well plates were centrifuged again. Next, 2 μL lysate from each sample was transferred to the wells of new white 96-well plates where 100 μL of 20 μM pyDTZ in assay buffer was added to each well. Bioluminescence activities of individual samples were measured on a microplate reader. Kinetics were followed for 0.1 s signal integration every 30 s for a total of 10 min. Meanwhile, 2 μL lysate from each sample was added 100 μL of 20 μM pyOMeCTZ in assay buffer. The selectivity was determined by the specific activity toward pyDTZ/activity toward pyOMeCTZ. Top three mutants showing exceptionally high bioluminescence selectivity of pyDTZ over pyOMeCTZ were chosen for next-round selection, sequencing, and other additional characterization.

4.2.5 Mammalian cell culture, transfection, and imaging

HEK 293T cells were cultured and transfected as previously described.¹⁷ The number and density of cells in Dulbecco's phosphate-buffered saline (DPBS) were determined using a hemocytometer. Cells were next diluted in DPBS to gain the desired numbers in each 50 μ L solution. Cell lysates were obtained by incubating desired number of cell in a CellLytic M solution for 15 minutes and centrifuged. UVP Bio Spectrum luminescence dark box was used for all bioluminescence imaging. To record bioluminescence imaging with pure enzymes, 50 μ L of 60 μ M substrates were injected into corresponding 50 μ L pure enzymes (final concentration: 10 nM for RLuc8 and OpyLuc; 100 nM for Akaluc), and the bioluminescence imaging was collected with 10 s exposure time. A filter wheel equipped with a Chroma Blue 360-500 nm, a Chroma Green 495-580 nm, and a Chroma Red 600-700 nm filter was used to acquire emission in each channel. To use the luminescence dark box to directly image cells, we added luciferase-expressing HEK 293T cells (5,000 cells per well for RLuc8 and OpyLuc; 30,000 cells per well for Akaluc) and the indicated luciferin substrates solution were injected into wells of a white 96-well plate. Final concentration of each substrate were 25 μ M for pyOMeCTZ, 10 μ M for pyDTZ, and 100 μ M for AkaLumine-HCl. Bioluminescence was imaged in the luminescence dark box immediately after substrate addition. The camera exposure time was set at 30 s. All images were analyzed using the Fiji image analysis software.

4.2.6 *in vitro* Bioluminescence characterization

Luciferases were expressed and purified as previously described.¹⁷ A microplate reader was used for all *in vitro* bioluminescence characterizations. To record bioluminescence emission spectra, 50 μ L of luciferin substrates was injected into the wells of white 96-well plates containing 50 μ L of pure enzymes in PBS (1.5 mM ATP

and 5 mM MgSO₄ were supplemented for Akaluc). Kinetic measurements were taken every 30 s post injection with 0.1 s integration and 10 s shaking during intervals) To derive values for apparent Michaelis constants (K_m), substrate concentrations varied from 0.78 to 50 μM, and 10-min integrated bioluminescence at individual substrate concentrations were used to fit the Michaelis–Menten equation.

4.2.7 Activation of signaling pathways in HEK293T cells

HEK293T cells were transfected at ~70% confluency by using plasmid DNA : PEI = 3 : 9 mixture. Plasmids used in this study included SRE-RLuc8, ARE-OpyLuc, and NF-κB-Akaluc, NF-κB-RLuc8, SRE-OpyLuc, ARE-Akaluc and CMV-Akaluc. 3 h after transfection, the medium was removed and replaced by fresh medium. The cells were allowed to recover for another 3 h. 20% fetal bovine serum (FBS), 50 μM *tert*-butylhydroquinone (tBHQ), or 10 ng/mL tumor necrosis factor alpha (TNFα) were used to activate serum response element (SRE), antioxidant response element (ARE), or nuclear factor kappa B (NF-κB) responsive element. Bioluminescence signals were acquired 16 h post induction. An un-transfected sample was used for background subtraction and an un-induced sample was used as a negative control.

Statistical analysis. Unpaired two-tailed t-tests were used to determine all *p*-values. No statistical methods were used to predetermine the sample size. Unless otherwise indicated, data are shown as mean ± s.d., and error bars in figures represent s.d.

4.3. Results and discussion

4.3.1 Design of triple luciferase system

To choose bioluminescent reporters that can generate different colors of emission, we first screened the available luciferase-luciferin pairs that have been reported previously in literature.¹⁸ RLuc8 is able to produce intense bioluminescence in a violet wavelength range (λ_{max} : ~405 nm) when methoxy-eCoelenterazine (me-eCTZ) was used as the substrate.¹⁹ *Renilla* luciferase (RLuc) is also known to be not tolerant to C-8 chemical modifications.²⁰ We reasoned that the blue-shifted emission of me-eCTZ might be due to dihedral angle twist in the catalytic pocket caused by the bulky C-6 methoxyphenyl substitution. This twist can break the coplanar property of emitter and cause blue-shifted emission. Therefore, we synthesized a me-eCTZ analog, pyOMeCTZ (**Figure 1A**), with a pyridyl substitution on C-2 to improve the water solubility by taking advantage of the fact that pyridine-containing molecules can be readily turned into pyridinium salts. As a result, RLuc8-pyOMeCTZ pair is able to generate violet emission with λ_{max} at ~416 nm.

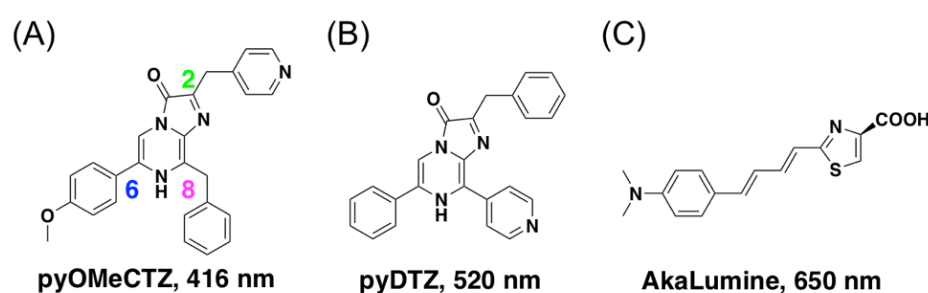


Figure 1. Chemical structures and maximum BL emission wavelength of (A) pyOMeCTZ, (B) pyDTZ, and (C) AkaLumine in the presence of its corresponding luciferase.

According to our previous result, teLuc is tolerant to a variety of C-8 chemical modifications, including both electronic and steric derivatives.¹⁷ Herein, we synthesized pyDTZ (**Figure 1B**) that can emit green to yellow photons (λ_{max} : ~530 nm) when paired with teLuc. Since the emission wavelength between RLuc8-pyOMeCTZ and teLuc-pyDTZ pairs are well resolved, they are readily available to pair with Akaluc-AkaLumine pair that produces near infrared (NIR) photons²¹ (λ_{max} : ~650 nm, **Figure 1C**) to yield a triple-color luciferase reporter system. It has been known that CTZ-utilizing murine luciferases do not have substrate cross-talk with D-luciferin-utilizing insect luciferases, so the remaining issue is the substrate selectivity between RLuc8 and teLuc to engineer a fully orthogonal triple-color luciferase system.

4.3.2 Directed evolution of luciferase to improve pyDTZ selectivity

To address this issue, we noticed that teLuc exhibited a substrate preference to pyDTZ over pyOMeCTZ by ~ 50-fold activity, suggesting that it might be feasible to engineer a mutant via directed evolution to more selectively access pyDTZ rather than pyOMeCTZ. Instead of screening the library for only enhanced bioluminescence output, we designed a method where we screened the BL activity of the mutants to both of pyDTZ (positive screening) and pyOMeCTZ (negative screening) in parallel. We selected the “hit” mutants showing not only high specific activity in positive screening but also low activity in negative screening for the next round selection (**Figure 2A**). After 8 rounds of selection, a mutant (designated OpyLuc) carried 11 mutations was obtained (**Figure 2B**, and **Figure 3**) and showed ~250-fold selectivity to pyDTZ over pyOMeCTZ (**Figure 2C**). Notably, Q20K and V21A mutations were acquired during random mutagenesis, suggesting residues nearby the catalytic site contribute to the substrate selectivity.

Collectively, we have three luciferase-luciferin pairs (RLuc8-pyOMeCTZ; λ_{max} : 416 nm, OpyLuc-pyDTZ; λ_{max} : 520 nm, and Akaluc-AkaLumine; λ_{max} : 650 nm) in hand that can access its specific luciferin and produce distinct colors of emission across the visible spectrum (**Figure 4A**). Their emission spectra are well separated and with only minimal spectra cross-talk. These features allow researcher to either initiate a specific luciferase activity by adding its corresponding luciferin substrate or scan the full spectra or use commercial filters to determine individual luciferase signals, thereby providing flexible data acquisition methods for any chosen purpose (**Figure 4B**).

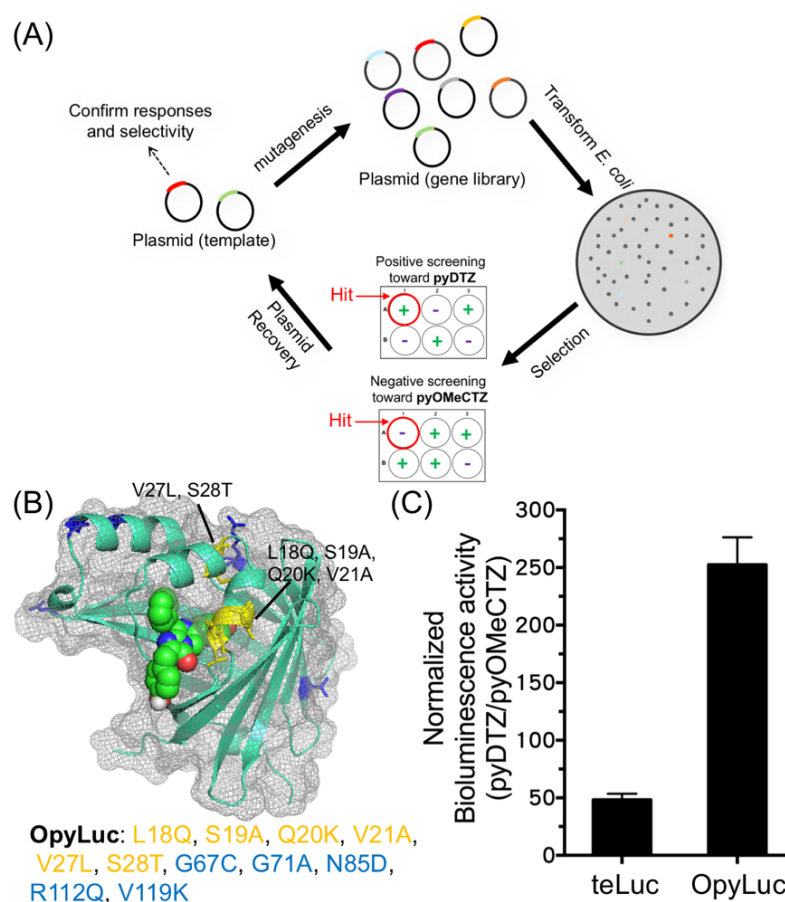


Figure 2. Engineering of OpyLuc luciferase for pyDTZ selectivity over pyOMeCTZ. (A) The schematic representation of directed evolution to derive OpyLuc. (B) Illustration of the putative substrate-binding site and OpyLuc mutations. CTZ is shown as spheres and mutated residues near the binding site are highlighted in yellow. (C) Normalized

bioluminescence activity ratio of pyCTZ/pyOMeCTZ in the presence of either teLuc or OpyLuc.

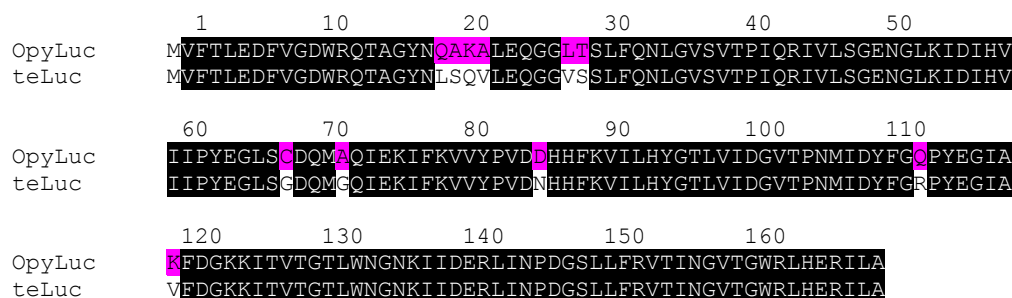


Figure 3. Alignments of primary sequences of OpyLuc and teLuc. OpyLuc mutations are highlighted in magenta background. Residues in this figure are numbered according to Protein Data Bank (PDB) ID 5B0U.

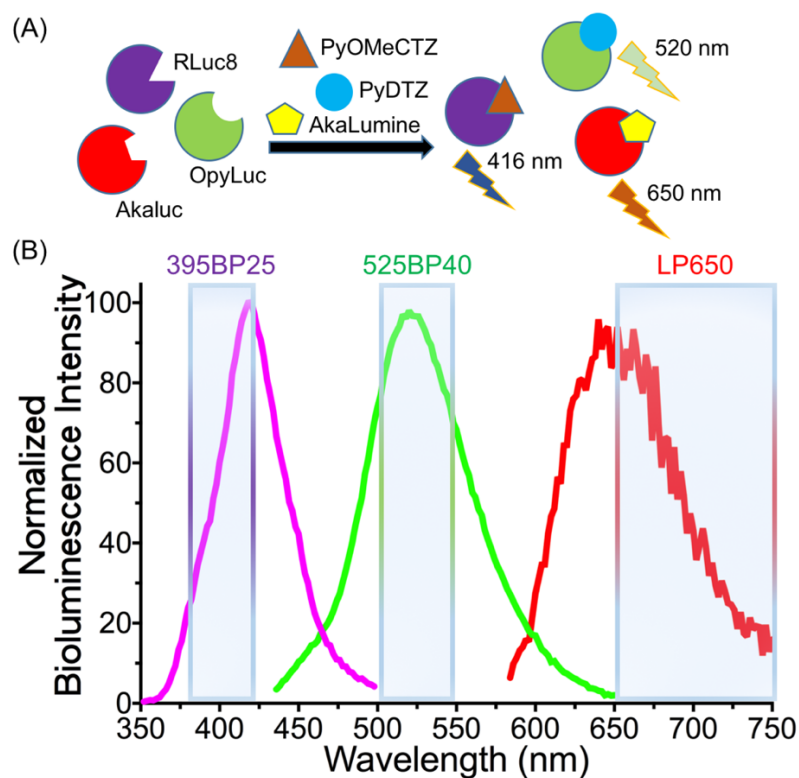


Figure 4. (A) Schematic representation of spectral-resolved and orthogonal luciferase-luciferin pairs. (B) Normalized bioluminescence emission spectra of RLuc8-pyOMeCTZ (purple), OpyLuc-pyDTZ (green), and Akaluc-AkaLumine pairs (red).

4.3.3 Triple luciferase system can produce orthogonal BL signals

To validate that the emission of these three luciferase-luciferin pairs are indeed spectrally separated, and can be resolved by filters, we first purified recombinant luciferases from *E. coli* and imaged the respective BL signals with/without 360-500 nm, 495-580 nm, or 600-700 nm bandpass filters (**Figure 5A** and **5B**). The result indicated RLuc8-pyOMeCTZ, OpyLuc-pyDTZ, and Akaluc-AkaLumine pairs all give the highest signal under the filter set-up that matches its respective emission color, suggesting their emission spectra can be well separated simultaneously by a set of commercial filters. Since these signals can be recorded in the same time, it solved the need of sequential sampling by Promega Dual-Luciferase Reporter assay.

To demonstrate that our triple luciferase system is a practical tool to monitor gene expression levels in live mammalian cells, we first evaluated the photon flux of each luciferase in the presence of a series of substrate concentrations (**Figure 6**). Ideally, we would like to explore an optimal concentration for each luciferin (pyOMeCTZ, pyDTZ, and AkaLumine) that can provide a similar level of photon flux from individual luciferase-luciferin pair. Unfortunately, the photon flux of Akaluc-AkaLumine at saturated concentration is at least 10-fold lower than that of RLuc8-pyOMeCTZ and OpyLuc-pyDTZ pairs, possibly due to its nature BL mechanism of ATP-dependency and two-step reaction. In order to at least keep the photon flux of RLuc8-pyOMeCTZ and OpyLuc-pyDTZ pairs at the same level, we selected a condition containing 25 μ M pyOMeCTZ, 10 μ M pyDTZ, and 100 μ M AkaLumine-HCl as the “Optimal Mix” for live cell imaging. By comparing Optimal Mix and only its respective substrate, only OpyLuc exhibited slightly unspecific inhibition by Optimal Mix while RLuc8 and Akaluc remained unaffected (**Figure 7**).

Next, we examined the performance of each luciferase for *in cellulo* imaging in the presence of chosen luciferin concentration. We injected the indicated luciferin

substrate solution into luciferase-expressing HEK 293T cells in a 96-well plate. As expected, pyDTZ initiated the BL emission only in the presence of OpyLuc. The excellent substrate selectivity was also observed in both Akaluc for AkaLumine and RLuc8 for pyOMeCTZ (**Figure 5C** and **5D**). Taken together, the results indicated again that each of luciferase in our triple luciferase system can process its distinct substrate and generate distinguishable emission wavelength. To briefly sum up, each luciferase can be selectively activated by its specific luciferin and the emission photons can also be distinguished by wavelength, which provided the flexibility to monitor multiple transcriptional activities specifically, stepwise, or simultaneously as a versatile experimental design. Moreover, the equations to calculate the activities of the individual luciferases by splitting emissions is not necessarily required since the spectra cross-talks are minimized.

While reporter assays are typically performed in lysates from cultured cells, we also evaluated our triple luciferase system in lysates. The results indicated that RLuc8-pyOMeCTZ and OpyLuc-pyDTZ pairs showed ~2 to 3-fold higher BL signals in lysates while Akaluc-AkaLumine exhibited decreased signal even after supplementing with additional ATP (**Figure 8**). Therefore, using lysates is not required in our triple luciferase system because all three luciferins described here are cell-permeable and work well with intact mammalian cells. This feature is beneficial to expand the real-time measurement of BL assays without lysing cultured cells.

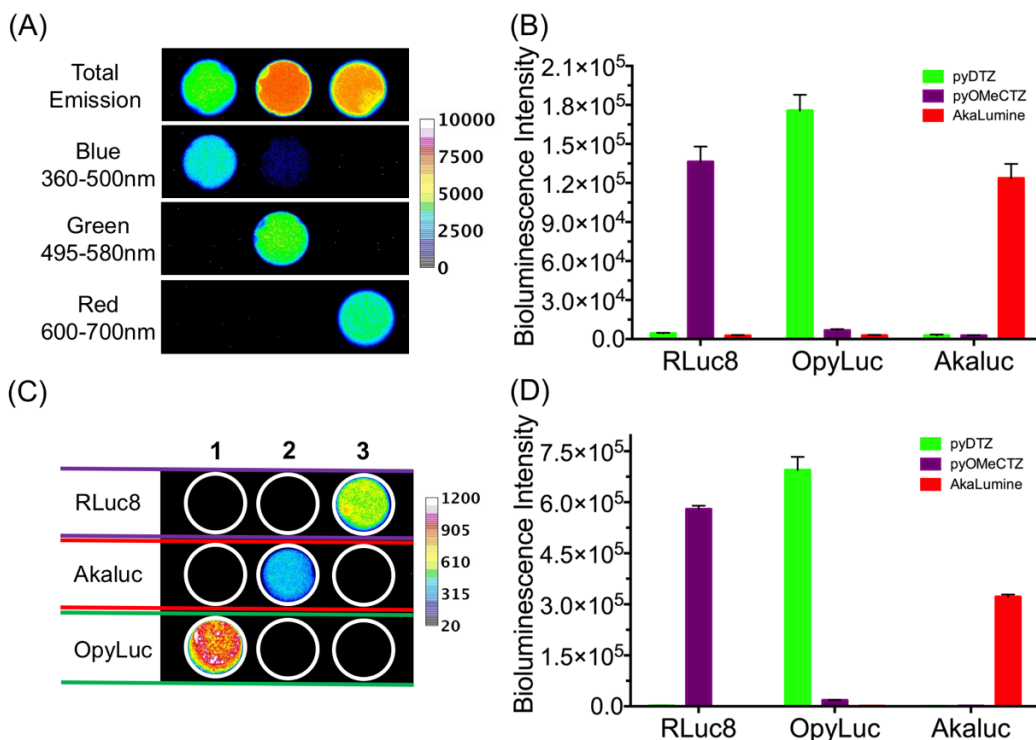


Figure 5. Bioluminescence imaging of **(AB)** purified recombinant RLuc8, OpyLuc, and Akaluc and **(CD)** luciferase-expressing HEK 293T cells. **(A)** Images were acquired without a filter or with either a 360-500 nm, 495-580 nm, or 600-700 nm bandpass filter. **(B)** Quantitative values for each tested luciferase-luciferin pair. Final concentrations were 10 nM for RLuc8 and OpyLuc; 100 nM for Akaluc; 30 μ M corresponding luciferin. **(C)** Live HEK293T cells were transfected with either RLuc8, Akaluc, or OpyLuc. 5000 cells per well for RLuc8 and OpyLuc; 30,000 cells per well for Akaluc. Images were acquired without a filter after addition of 1: 10 μ M pyDTZ, 2: 100 μ M AkaLumine, or 3: 25 μ M pyOMeCTZ. **(D)** Quantitative analysis of BL signals gained from **(C)**.

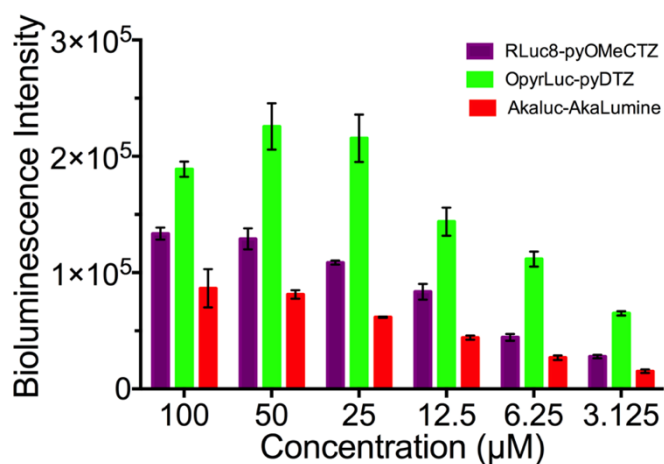


Figure 6. Bioluminescence emission of three luciferase-luciferin pairs in live mammalian cells. Measurements were performed with 2000 luciferase-expressing HEK 293T cells in PBS for RLuc8 and OpyrLuc; 20000 HEK 293T cells for Akaluc. Signals were integrated over the first 10 min post injection of substrates.

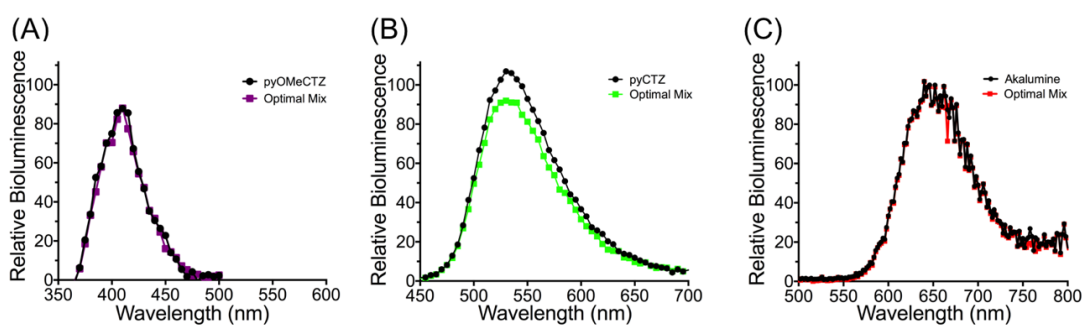


Figure 7. Bioluminescence spectra and intensity comparison of (A) RLuc8, (B) OpyrLuc, and (C) Akaluc in the presence of its corresponding substrate versus Optimal Mix containing 25 μM pyOMeCTZ, 10 μM pyDTZ, and 100 μM AkaLumine-HCl.

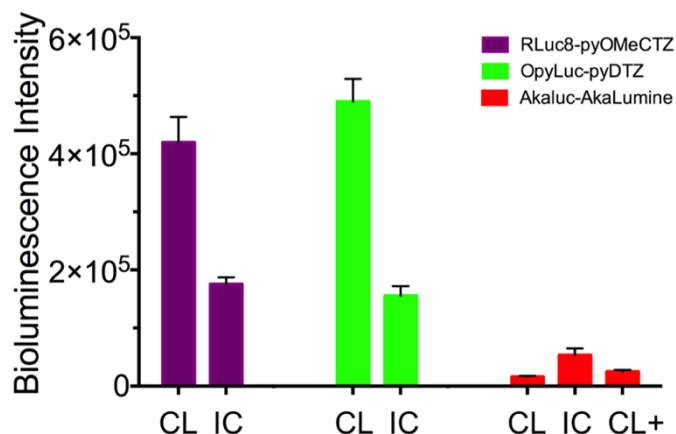


Figure 8. Comparative bioluminescence intensity detected from cell lysates (CL) and intact cells (IC) of RLuc8-pyOMeCTZ, OpyLuc-pyDTZ, and Akaluc-AkaLumine-HCl in the presence of Optimal mix containing 25 μ M pyOMeCTZ, 10 μ M pyDTZ, and 100 μ M AkaLumine-HCl.

4.3.4 Monitor serum response, antioxidant, and NF- κ B promotor activities in HEK293T cells by triple luciferase system

Subsequently, we used our triple luciferase system to monitor three signaling pathway activations in HEK293T cells where each of the luciferase expression was under control by a growth factor-regulated promoter element (serum response element, SRE),²² a Nrf2-antioxidant response element (ARE),²³ or a transcription factor–nuclear factor kappa B (NF- κ B) responsive promoter element (**Table 2**).²⁴ We designed a reporter system based on SRE promoter driving the expression of RLuc8, ARE promoter driving the expression of OpyLuc, and NF- κ B promoter driving the expression of Akaluc. The response element promoters can be specifically activated by its respective stimuli – fetal bovine serum (FBS), tert-butylhydroquinone (tBHQ), and tumor necrosis factor alpha (TNF α) (**Figure 9A**).

The basal promoter activities of all SRE, ARE, and NF- κ B response elements were low (**Figure 10B**). We measured the individual luciferase activity (RLuc8, OpyLuc, and Akaluc) by adding its corresponding luciferin (pyOMeCTZ, pyDTZ, and AkaLumine). As expected, treating with single stimuli enabled the activation of its specific pathway and drove the downstream expression of genetically encoded luciferase. Stimulating the cells with either two or three stimuli resulted in activation of multi-pathway and were reported correctly by our triple luciferase system (**Figure 9B**).

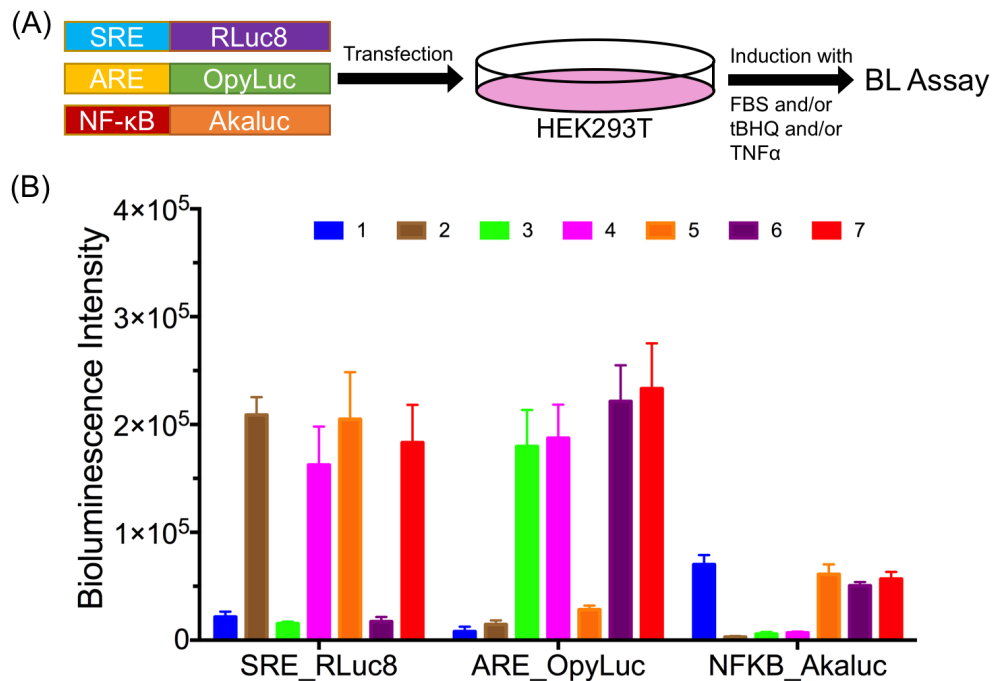


Figure 9. (A) Triple luciferase assay in live HEK293T after co-transfection of SRE-RLuc8, ARE-OpyLuc, and NF κ B-Akaluc plasmids. (B) The BL signals from each luciferase were acquired from intact cells after adding its corresponding luciferin. The cells were induced by 1: 10 ng/mL TNF α ; 2: 20% FBS; 3: 50 μ M tBHQ; 4: 20% FBS + 50 μ M tBHQ; 5: 20% FBS + 10 ng/mL TNF α ; 6: 50 μ M tBHQ + 10 ng/mL TNF α ; 7: 20% FBS + 50 μ M tBHQ + 10 ng/mL TNF α for 16 h post PEI transfection.

Next, the emission spectra were recorded after injection of Optimal Mix solution to the transfected HEK293T cells (**Figure 9B** and **Figure 10C, D, and E**). Due to the fact that all three emission spectra are well-separated, this system demonstrated a proof-of-concept of simultaneous recording of three pathway activations. Again, the results suggested that there is no cross-reactivity between each luciferase-luciferin pair, providing an advantage in future studies that require either sequential or simultaneous multicomponent monitoring.

Herein, we demonstrated the ability of our triple luciferase system to monitor the simultaneous activation of two or all three labeled pathways. Under this complexed circumstances, we cannot exclude the possible cross-talk between each signaling pathways. Therefore, we tested all three response elements under the treatment of each single stimuli (**Figure 11**). The result indicated that the up-regulation of each labeled luciferase has proportional relationship to the concentration of stimuli in a dose-dependent manner. FBS does induce the transcriptional events of NF- κ B response element and ARE, but the strength of FBS to activate SRE is ~15 to 30 times stronger than NF- κ B and ARE. tBHQ and TNF α can stimulate minimal activation of SRE, but again the cross-talk is less than 10%. To confirm that the increase of bioluminescence is indeed correlated with the corresponding expression level of luciferase after treated with respective stimuli, we will perform western blot to further quantify the up-regulation of labeled luciferases.

In addition, we observed the luciferase expression levels can vary between each sampling. It can be due to the lack of an internal control in this experiment. More quantitative and reproducible results can be obtained if an internal control is used to normalize the cell number, viability, and transfection efficiency, especially when using transiently transfected cells. Nevertheless, we were still able to qualitatively detect three signaling activation states after treating with stimuli mixtures (**Figure 10F, G, H, and I**).

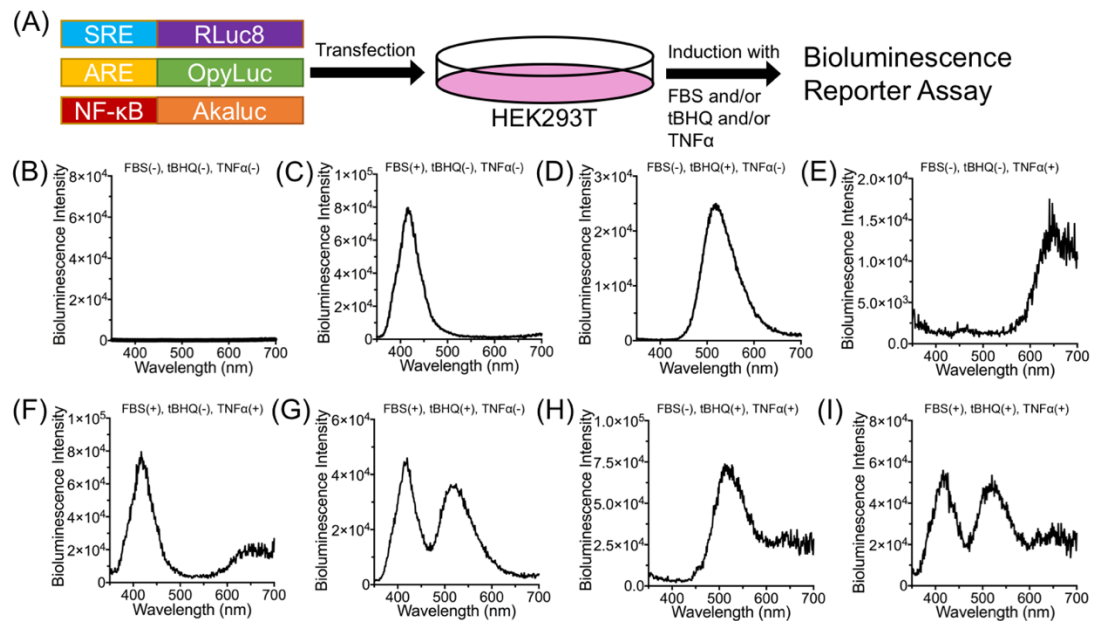


Figure 10. (A) Triple luciferase assay in live HEK293T after co-transfection of SRE-RLuc8, ARE-OpyLuc, and NFκB-Akaluc plasmids. The emission spectra were acquired from intact cells after adding Optimal Mix solution. The cells were (B) non-treated, induced by (C) 20% FBS, (D) 50 μM tBHQ, (E) 10 ng/mL TNFα, (F) 20% FBS + 10 ng/mL TNFα, (G) 20% FBS + 50 μM tBHQ, (H) 50 μM tBHQ + 10 ng/mL TNFα, (I) 20% FBS + 50 μM tBHQ 10 ng/mL + TNFα for 16 h post PEI transfection.

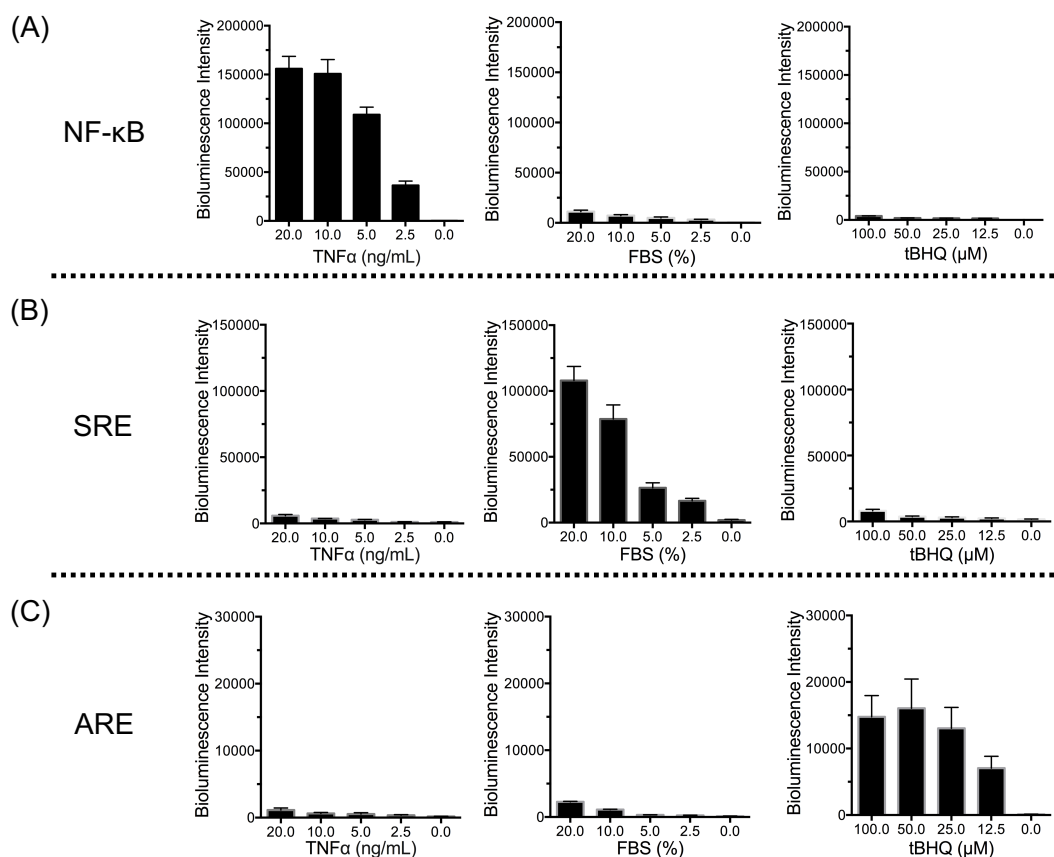


Figure 11. HEK293T cells were transfected with either (A) NF κ B-Opyluc, (B) SRE-Opyluc or (C) ARE-Opyluc plasmids and assayed in 96-well format after 16 hours stimulation with various concentrations of TNF α , FBS, and tBHQ. The bioluminescence signals were recorded by the addition of 10 μ M pyDTZ.

We next switched over the promoters to drive the downstream luciferase expression by using an alternative combination (NF- κ B-RLuc8, SRE-OpyLuc, and ARE-Akaluc). After inducing with all stimuli (TNF α , FBS, and tBHQ), the signals from RLuc8 and OpyLuc were obvious as expected, while the signal from Akaluc was overwritten by the broad emission tailing of OpyLuc (**Figure 12**). This result suggested that Akaluc is only suitable to monitor strong promoter activity when paired with the other two luciferases, because the photon flux of Akaluc is relatively lower. This is a

factor that needs to be taken into account when researchers conducting the initial experimental design.

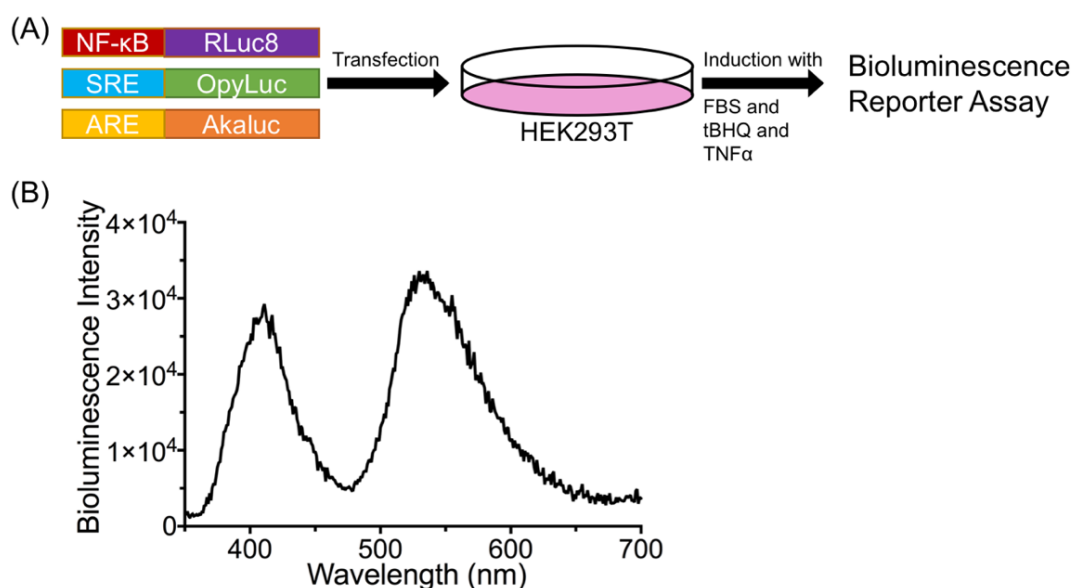


Figure 12. (A) Triple luciferase assay in live HEK293T by co-transfection of NFκB-RLuc8, SRE-OpyLuc, and ARE-Akaluc plasmids. The cells were induced by 10 ng/mL TNF α , 50 μ M tBHQ, and 20% FBS for 12 h. (B) The bioluminescence emission spectra were recorded by the addition of Optimal mix containing 25 μ M pyOMeCTZ, 10 μ M pyDTZ, and 100 μ M AkaLumine-HCl.

4.3.5 Akaluc-AkaLumine pair is more suitable as an internal control

As mentioned above, it is recommended to normalize the BL assay results by an internal control for cell number, and transfection efficiency normalizations. We prepared another set of plasmids containing NF-κB-RLuc8, SRE-OpyLuc, and a control of the constitutively active cytomegalovirus (CMV) promoter (CMV-Akaluc). We transfected the cells with all three plasmids and incubated cells with two stimuli (TNF α and FBS) for 16 h. In this case, we selectively triggered the BL signal from individual luciferase by adding its respective luciferin to intact cells (**Figure 12A**). The BL kinetics

were monitored for each luciferase after the addition of its respective luciferin (**Figure 12B**). All three luciferase generated BL signal, and the BL signal decayed by the function of time. The advantage of incorporating an internal control here is not only limited to the normalization of cell number and transfection efficiency of each sample, but also the kinetic of each BL signal can be normalized to give a more constant ratio readout, which is more amenable to high-throughput screening (**Figure 12C**). Thus, this system enabled the monitoring of two signaling activations and improved the accuracy of assay by including another orthogonal control to exclude factors such as cell number, transfection efficiency, and BL emission kinetic.

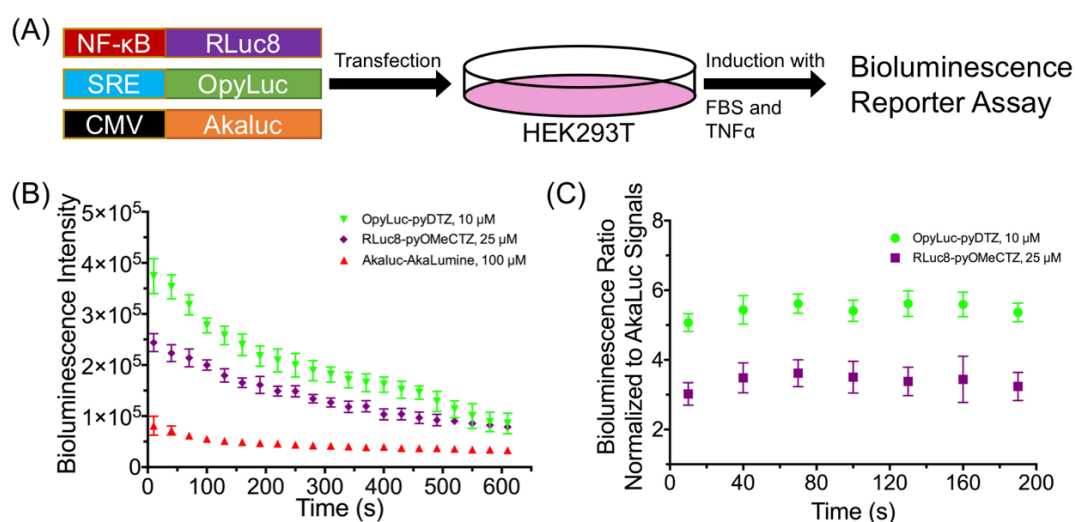


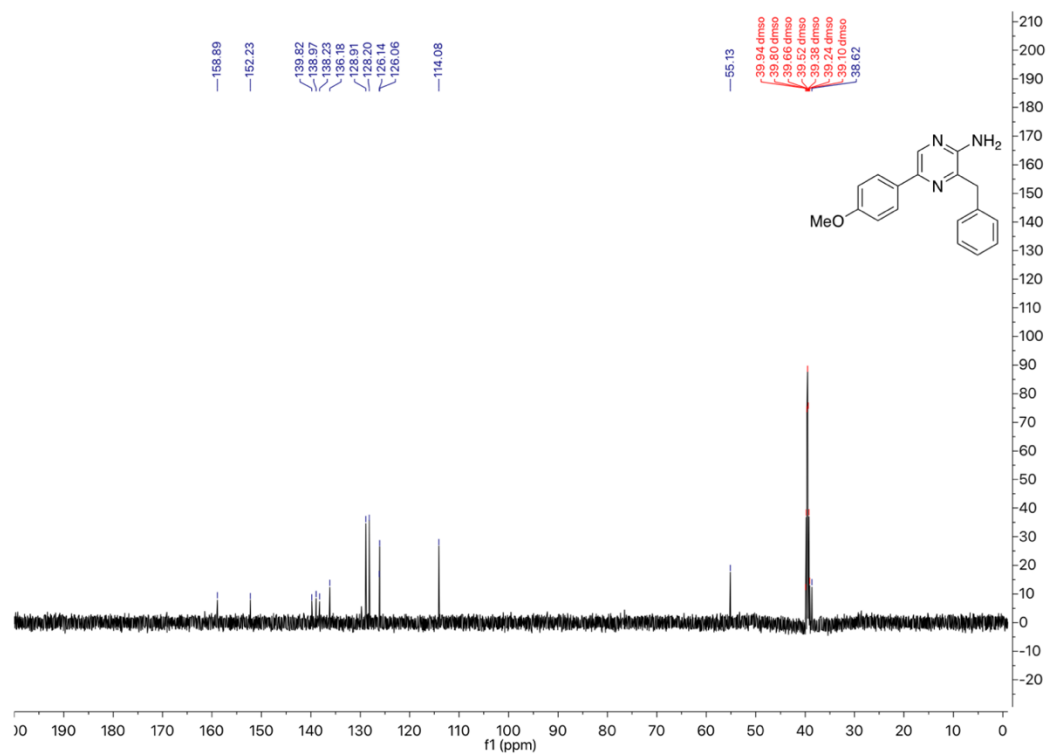
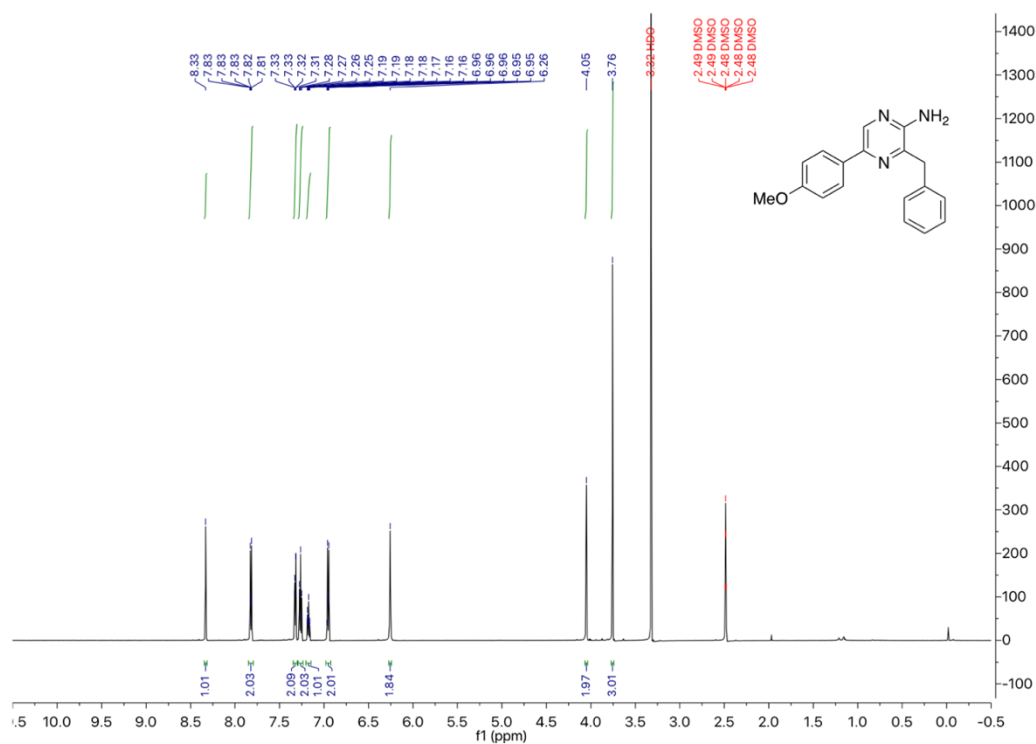
Figure 12. (A) Triple luciferase assay in live HEK293T by co-transfection of NF κ B-RLuc8, SRE-OpyLuc, and CMV-Akaluc plasmids. The cells were induced by 10 ng/mL TNF α and 20% FBS for 16 h. (B) The bioluminescence kinetics were measured by adding either 25 μ M pyOMeCTZ, 10 μ M pyDTZ, or 100 μ M AkaLumine to intact transfected HEK293T cells. (C) The BL signals from OpyLuc-pyDTZ and RLuc8-pyOMeCTZ pairs were normalized to the signal value generated by Akaluc-AkaLumine as an internal control.

4.4. Conclusion

Herein, we utilized the substrate selectivity and engineered a mutually orthogonal luciferase-luciferin pair for multiplexed cell-based BL assay. In combination with RLuc8 and Akaluc, this triple-color BL system features the selectivity of synthetic substrates and production of well separated emission spectra from 400 nm to 650 nm. We combined several advantages of previous bioluminescence technology and described a spectral-resolved triple-color BL system, which provides flexible and convenient approach to monitor multiple biological events in either qualitative or quantitative manners.

By using this triple luciferase system, we demonstrated that the activations of cell signaling can be detected simultaneously or separately from live cells in a single experiment where each individual BL signal can be distinguished from the other two luciferase-luciferin pairs. In future experimental design, it may be possible to combine newly discovered luciferase-luciferin pairs²⁵ to independently activate even more innate processes in the same sample to study the cross-talks of cellular signaling pathways. Moreover, multiplexed BL assay is compatible with modern genetically encoded fluorescent biosensors to further investigate complexed biological events via functional imaging.²⁶ We believe the development of a such versatile tool that ensures an accurate and precise analysis of signaling pathways, can be extended to study other physiologically transcriptional activation and is critical to improve the design and screening of new drugs, as well as the diagnosis and treatment of disease.

4.5. Appendix



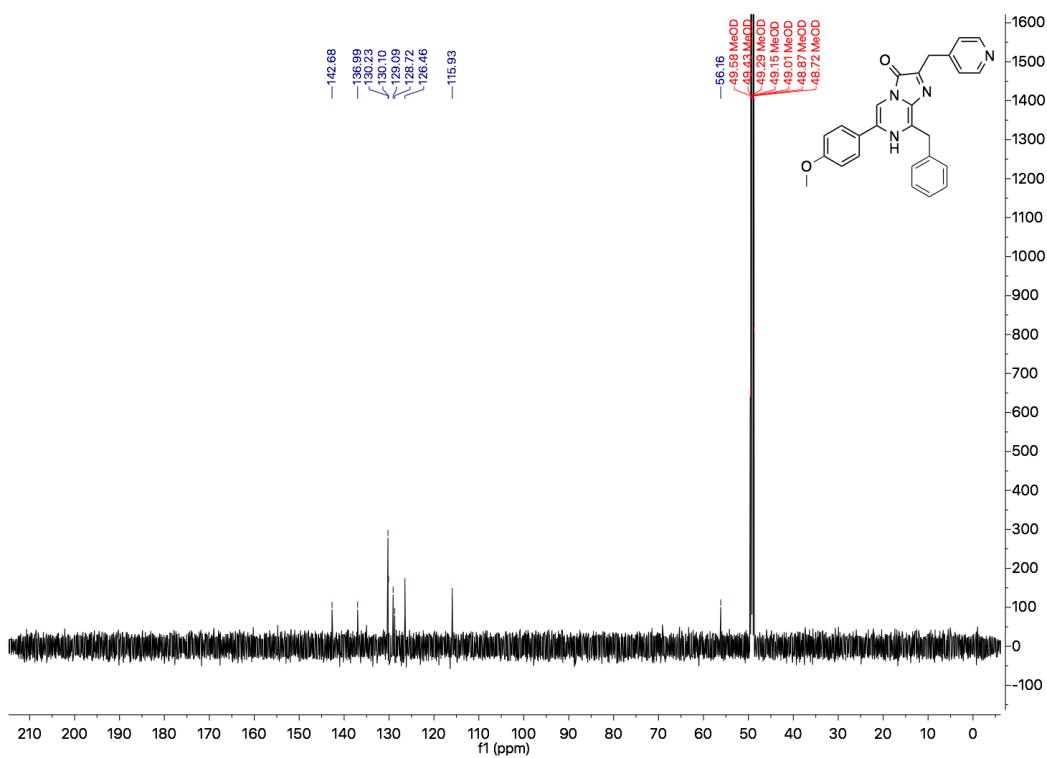
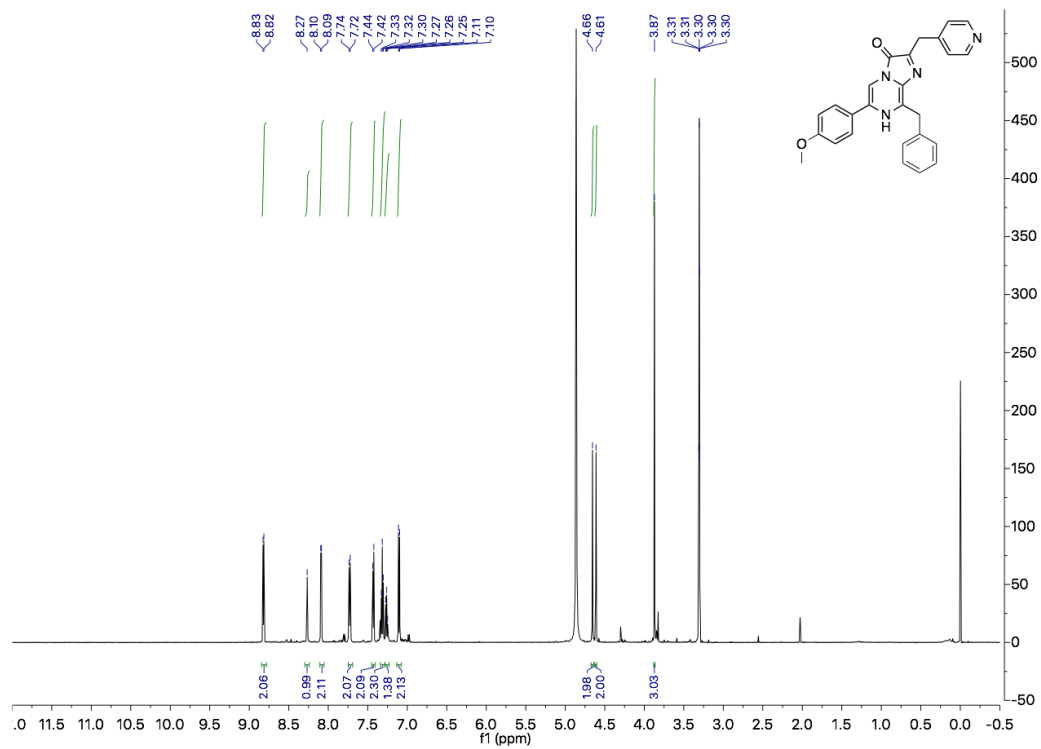


Table 1. Oligonucleotides used in this study.

Oligo name	Nucleotide sequence (5'→ 3')
pBAD-F	ATGCCATAGCATTTTTATCC
pBAD-R	GATTTAATCTGTATCAGG
NFkB_Sacl_F	TACCGAGCTCATCCAGTTTGGACTAGTGG
NFkB_BglII_R	AGCCCAGATCTCCTCTAGAGTCTAGATCTGG
opyluc_AscI_Kozak_F	AAAGCCACCGGCGCGCCGCCGCCACCATGGTCTTCACTCTCGAAGATTT TGT
opyluc_FseI_R	TCGAAGCGGCCGGCCTTACGCCAGAATGCGTTCATGCA
Akaluc_AscI_Kozak_F	AAAGCCACCGGCGCGCCGCCGCCACCATGGAAGATGCCAAAAACATTAA GA
Akaluc_FseI_R	TCGAAGCGGCCGGCCTTACACGGCGATCTTGCCGTCCTTCTT
Rluc_AscI_Kozak_F	AAAGCCACCGGCGCGCCGCCGCCACCATGGCTTCCAAGGTGTACGACC
Rluc_FseI_R	TCGAAGCGGCCGGCCTTACTGCTCGTTCTTCAGCACGCGCT

Table 2. Response element sequences used in this study.

Response Element	DNA sequence (5'→ 3')
Nuclear factor kappa-light-chain-enhancer of activated B cells (NFkB)	ATCCAGTTTGGACTAGTGGAATTTCCGGGAATTTCCGGGAATTTCCGG GAATTTCC
Serum response factor (SRE)	GCTAGCAGGATGTCCATATTAGGACATCTAGGATGTCCATATTAGGACAT CTAGGATGTCCATATTAGGACATCTAGGATGTCCATATTAGGACATCTAG GATGTCCATATTAGGACATCT
Antioxidant Nrf2 response element (ARE)	TAGCTTGGAAATGACATTGCTAATGGTGACAAAGCAACTTTTAGCTTGG AATGACATTGCTAATGGTGACAAAGCAACTTT

Table 3. Qualitative comparison of this study and commercial luciferase reporter systems.

	Promega Dual-Luciferase Assay	Promega Chroma-Glo	Pierce Cypridina-Firefly Luciferase Dual Assay	Orthogonal Triple Luciferase Assay (this work)
Number of Substrates	2	1	2	3
Types of Enzymes	2 (Rluc, FLuc)	1 (2 CBLucs)	2 (VLuc, Red FLuc)	3
Gene Identity	low	>99%	low	low
Orthogonal Signals	Yes	No	Yes	Yes
Simultaneous Detection of 2 Signals	No	Yes	Yes	Yes
Simultaneous Detection of 3 Signals	No	No	No	Yes
Data Calculations Required	No	Yes	No	Yes/No
Luminometer Filters Required	No	Yes	Yes	Yes/No
Single Reagent Solution	No (CTZ, D-luciferin)	Yes (D-luciferin)	Yes (Vargulin, D-luciferin)	Yes (pyDTZ, pyOMeCTZ, Akalumine-HCl)
Emission Signals Well-Separated	Yes	No	Yes	Yes
Cell Lysis Required	Yes	Yes	Yes	Yes/No

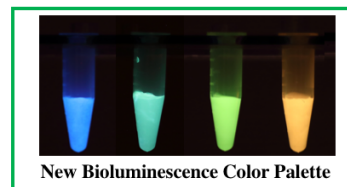
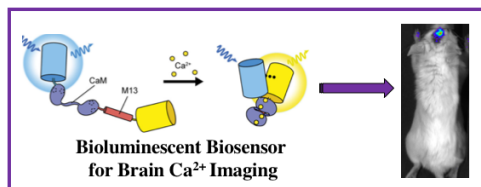
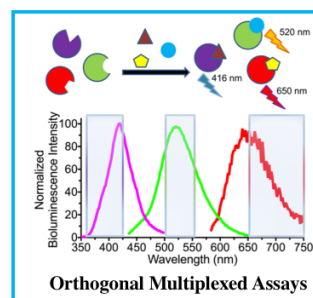
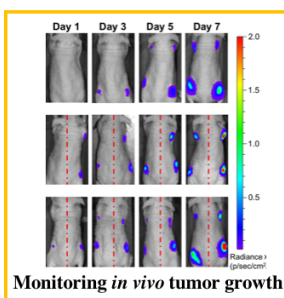
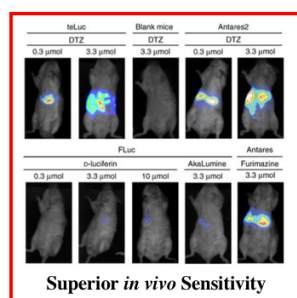
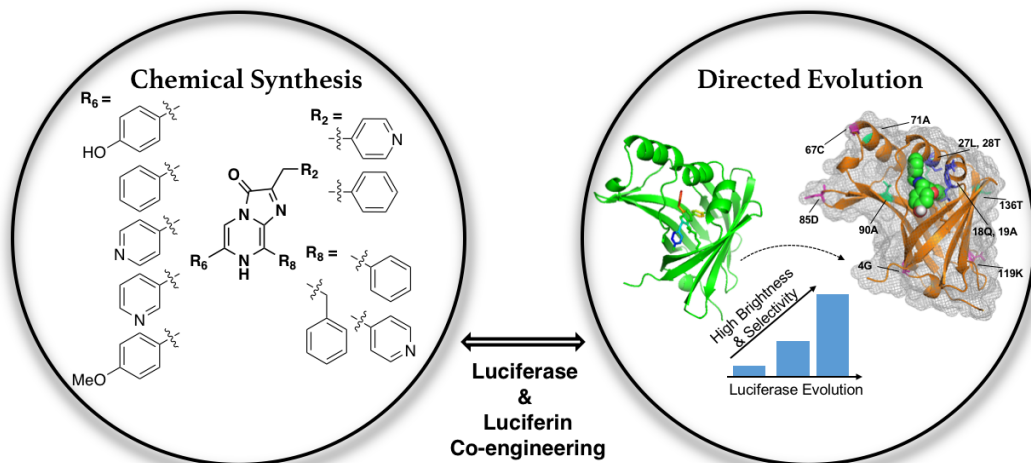
References

1. Suzuki, K.; Nagai, T., Recent progress in expanding the chemiluminescent toolbox for bioimaging. *Curr Opin Biotech* **2017**, *48*, 135-141.
2. Naylor, L. H., Reporter gene technology: the future looks bright. *Biochem Pharmacol* **1999**, *58* (5), 749-57.
3. Miraglia, L. J.; King, F. J.; Damoiseaux, R., Seeing the light: luminescent reporter gene assays. *Comb Chem High Throughput Screen* **2011**, *14* (8), 648-57.
4. Ohmiya, Y., Simultaneous multicolor luciferase reporter assays for monitoring of multiple genes expressions. *Comb Chem High Throughput Screen* **2015**, *18* (10), 937-45.
5. Michelini, E.; Cevenini, L.; Mezzanotte, L.; Coppa, A.; Roda, A., Cell-based assays: fuelling drug discovery. *Anal Bioanal Chem* **2010**, *398* (1), 227-38.
6. Thorne, N.; Inglese, J.; Auld, D. S., Illuminating Insights into Firefly Luciferase and Other Bioluminescent Reporters Used in Chemical Biology. *Chemistry & Biology* **2010**, *17* (6), 646-657.
7. Michelini, E.; Cevenini, L.; Mezzanotte, L.; Ablamsky, D.; Southworth, T.; Branchini, B.; Roda, A., Spectral-resolved gene technology for multiplexed bioluminescence and high-content screening. *Anal Chem* **2008**, *80* (1), 260-7.
8. Rathbun, C. M.; Porterfield, W. B.; Jones, K. A.; Sagoe, M. J.; Reyes, M. R.; Hua, C. T.; Prescher, J. A., Parallel Screening for Rapid Identification of Orthogonal Bioluminescent Tools. *ACS Cent Sci* **2017**, *3* (12), 1254-1261.
9. Jones, K. A.; Porterfield, W. B.; Rathbun, C. M.; McCutcheon, D. C.; Paley, M. A.; Prescher, J. A., Orthogonal luciferase-luciferin pairs for bioluminescence imaging. *Journal of the American Chemical Society* **2017**, *139*, 2351-2358.
10. Heise, K.; Oppermann, H.; Meixensberger, J.; Gebhardt, R.; Gaunitz, F., Dual Luciferase Assay for Secreted Luciferases Based on Gaussia and NanoLuc. *Assay Drug Dev Techn* **2013**, *11* (4), 244-252.
11. Mezzanotte, L.; Que, I.; Kaijzel, E.; Branchini, B.; Roda, A.; Lowik, C., Sensitive Dual Color In Vivo Bioluminescence Imaging Using a New Red Codon Optimized Firefly Luciferase and a Green Click Beetle Luciferase. *Plos One* **2011**, *6* (4).
12. Yasunaga, M.; Nakajima, Y.; Ohmiya, Y., Dual-color bioluminescence imaging assay using green- and red-emitting beetle luciferases at subcellular resolution. *Anal Bioanal Chem* **2014**, *406* (23), 5735-5742.
13. Mezzanotte, L.; An, N.; Mol, I. M.; Lowik, C. W.; Kaijzel, E. L., A new multicolor bioluminescence imaging platform to investigate NF-kappaB activity and apoptosis in human breast cancer cells. *Plos One* **2014**, *9* (1), e85550.
14. Nakajima, Y.; Kimura, T.; Sugata, K.; Enomoto, T.; Asakawa, A.; Kubota, H.; Ikeda, M.; Ohmiya, Y., Multicolor luciferase assay system: one-step monitoring of multiple gene expressions with a single substrate. *Biotechniques* **2005**, *38* (6), 891-4.
15. Branchini, B. R.; Southworth, T. L.; Fontaine, D. M.; Kohrt, D.; Florentine, C. M.; Gossel, M. J., A Firefly Luciferase Dual Color Bioluminescence Reporter Assay Using Two Substrates To Simultaneously Monitor Two Gene Expression Events. *Sci Rep-Uk* **2018**, *8*.
16. Adamczyk, M.; Akireddy, S. R.; Johnson, D. D.; Mattingly, P. G.; Pan, Y.; Reddy, R. E., Synthesis of 3,7-dihydroimidazo[1,2a]pyrazine-3-ones and their chemiluminescent properties. *Tetrahedron* **2003**, *59* (41), 8129-8142.
17. Yeh, H. W.; Karmach, O.; Ji, A.; Carter, D.; Martins-Green, M. M.; Ai, H. W., Red-shifted luciferase-luciferin pairs for enhanced bioluminescence imaging. *Nat Methods* **2017**, *14* (10), 971-974.
18. Loening, A. M.; Wu, A. M.; Gambhir, S. S., Red-shifted Renilla reniformis luciferase variants for imaging in living subjects. *Nat Methods* **2007**, *4* (8), 641-643.
19. Rummyantsev, K. A.; Turoverov, K. K.; Verkhusha, V. V., Near-infrared bioluminescent proteins for two-color multimodal imaging. *Sci Rep-Uk* **2016**, *6*, 36588.
20. Wu, C.; Nakamura, H.; Murai, A.; Shimomura, O., Chemo- and bioluminescence of coelenterazine analogues with a conjugated group at the C-8 position. *Tetrahedron Lett* **2001**, *42* (16), 2997-3000.
21. Iwano, S.; Sugiyama, M.; Hama, H.; Watakabe, A.; Hasegawa, N.; Kuchimaru, T.; Tanaka, K. Z.; Takahashi, M.; Ishida, Y.; Hata, J.; Shimozono, S.; Namiki, K.; Fukano, T.;

- Kiyama, M.; Okano, H.; Kizaka-Kondoh, S.; McHugh, T. J.; Yamamori, T.; Hioki, H.; Maki, S.; Miyawaki, A., Single-cell bioluminescence imaging of deep tissue in freely moving animals. *Science* **2018**, 359 (6378), 935-939.
22. Hill, C. S.; Treisman, R., Differential activation of c-fos promoter elements by serum, lysophosphatidic acid, G proteins and polypeptide growth factors. *Embo J* **1995**, 14 (20), 5037-47.
23. Nguyen, T.; Nioi, P.; Pickett, C. B., The Nrf2-antioxidant response element signaling pathway and its activation by oxidative stress. *J Biol Chem* **2009**, 284 (20), 13291-5.
24. Badr, C. E.; Niers, J. M.; Tjon-Kon-Fat, L. A.; Noske, D. P.; Wurdinger, T.; Tannous, B. A., Real-Time Monitoring of Nuclear Factor kappa B Activity in Cultured Cells and in Animal Models. *Molecular Imaging* **2009**, 8 (5), 278-290.
25. Kotlobay, A. A.; Sarkisyan, K. S.; Mokrushina, Y. A.; Marcet-Houben, M.; Serebrovskaya, E. O.; Markina, N. M.; Gonzalez Somermeyer, L.; Gorokhovatsky, A. Y.; Vvedensky, A.; Purtov, K. V.; Petushkov, V. N.; Rodionova, N. S.; Chepurnyh, T. V.; Fakhranurova, L. I.; Guglya, E. B.; Ziganshin, R.; Tsarkova, A. S.; Kaskova, Z. M.; Shender, V.; Abakumov, M.; Abakumova, T. O.; Povolotskaya, I. S.; Eroshkin, F. M.; Zaraisky, A. G.; Mishin, A. S.; Dolgov, S. V.; Mitouchkina, T. Y.; Kopantzev, E. P.; Waldenmaier, H. E.; Oliveira, A. G.; Oba, Y.; Barsova, E.; Bogdanova, E. A.; Gabaldon, T.; Stevani, C. V.; Lukyanov, S.; Smirnov, I. V.; Gitelson, J. I.; Kondrashov, F. A.; Yampolsky, I. V., Genetically encodable bioluminescent system from fungi. *Proceedings of the National Academy of Sciences of the United States of America* **2018**, 115, 12728-12732.
26. Greenwald, E. C.; Mehta, S.; Zhang, J., Genetically Encoded Fluorescent Biosensors Illuminate the Spatiotemporal Regulation of Signaling Networks. *Chemical reviews* **2018**, 118, 11707-11794.

Chapter 5

General Conclusions and Perspectives



In the past two decades, bioluminescence tools have shown tremendous ability and potential to reveal the mystery of biology as well as to accelerate drug discovery and development. However, bioluminescence systems found in nature are not yet ideal for what scientific community intends to do, e.g. visualizing chosen cells in living animals, molecular imaging or multiplexed assays. The vast applications of bioluminescence technology have been limited due to the following reasons. First, the blue-emissive photons of native marine luciferase do not penetrate through the biological tissue very efficiently, thus hindering their *in vivo* sensitivity. Second, the water solubility of coelenterazine (CTZ) and its analogs are poor, limiting its *in vivo* administration dosage. Third, the available choices of bioluminescence color are significantly less than the current color palette of fluorescent proteins.

An ideal bioluminescence toolkit that allows scientists to efficiently explore biology has to satisfy the following: high luminescence efficiency, red-shifted emission, thermostable, sustained light output, and proper *in vivo* luciferin biodistribution. CTZ-consuming bioluminescent reporters have several intrinsic advantages, such as small size, high catalytic turnover, high brightness, high stability, and no need of cofactors such as adenosine triphosphate (ATP). For live cell and animal imaging, ATP-dependent luciferases may consume a significant portion of intracellular ATP and disturb normal physiology. Moreover, in blood plasma, urine, and other biological fluids where the ATP level is low, ATP-dependent luciferases would not give out signals.¹ Therefore, we chose a family of ATP-independent luciferase, which was previously cloned and characterized from *Oplophorus gracilirostris* as our starting point.

In this dissertation, we have addressed several hurdles of luciferase-luciferin pairs, which were originally derived from nature. We integrated two approaches: synthetic chemistry and protein directed evolution to expand the capabilities of native bioluminescent pairs, beyond the design by nature. We synthesized coelenterazine (marine luciferin) analogs with red-shifted photophysical property and improved water

solubility, and concurrently re-engineered luciferase to maintain the high bioluminescence brightness. These newly engineered luciferase-luciferin pairs with red-shifted emission enable highly sensitive bioluminescence imaging (BLI) to non-invasively tracking biological events in live animal. Since we have also expanded the color palette of current bioluminescence toolkits, we are excited about the possibility to accelerate the drug screening process by multi-color bioluminescence assay. Meanwhile, we are enthusiastic in the development of the next generation bioluminescent biosensors on the basis of these engineered bioluminescent pairs.

With our efforts and recent advances in sharpening bioluminescence toolkits, several sets of bioluminescent pairs have provided fundamental for diverse *in vitro* to *in vivo* applications. At the cellular level, it is now possible to use multiple orthogonal bioluminescent reporters to track multiple targets. The recent development of highly bright luciferases, such as NanoLuc and teLuc also opened the door for cellular and subcellular bioluminescence microscopy. At the macro-scale level, bioluminescence imaging (BLI) has been one of the best options for *in vivo* imaging. FLuc-D-luciferin pair has already been broadly used, and the recently developed Antareas2-DTZ, LumiScarlet-8pyDTZ, and Akaluc-AkaLumine pairs are new benchmarks for *in vivo* BLI.²⁻⁴

On the other hand, CTZ-consuming bioluminescent reporters still have limitations that need to be further addressed. First, the peak emission of these reporters has not yet reached the far-red and NIR spectral region. Also, the biodistribution of CTZ seems to be dependent on the route of injection (e.g., via i.v. or i.p.).⁵ Moreover, the auto-oxidation of CTZ analogs in biological fluid may limit their use in detection of very low-abundant targets.⁶ Compare to the oxidation reaction of D-luciferin, CTZ oxidation does not involve ATP as the additional energy source. It can be reasoned that the internal energy of CTZ chemical structure is high, making the C-2 position and C-3 carbonyl group more vulnerable to molecular oxygen. In addition, it

has been known that the C-2 substitutions can alter the oxidative reaction rate of CTZ analogs, which is the primary site to determine the stability and reaction kinetics.⁷ To address abovementioned issues, we have several ongoing projects to continuously explore CTZ analogs with extended conjugation for redder emission, and we also set up further studies to investigate novel CTZ analogs that have better solubility, bioavailability, and stability. Re-engineering of luciferases for these new substrates may lead to novel luciferase-luciferin pairs that further enhance *in vivo* BLI by a few orders of magnitude. The ultimate goal of an ideal bioluminescence is to provide high spatiotemporal resolution to study the dynamic of a biological event in live animal, e.g. imaging single neuronal activity at 20 Hz acquisition rate.

Recently, the density functional theory (DFT) simulation suggested that the CTZ oxidative reaction occurs with a single electron-transfer mechanism and the emission is based on a gradually reversible charge-transfer-induced luminescence mechanism, so substitutions on C-6 and C-8 can alter the overall charge-transfer-induced luminescent intermediate, which further supports our work as a promising approach to tune the emission wavelength.⁸⁻¹⁰ Recent research also reported CTZ analogs that have peak emission up to 598 nm, but with very limited activity toward NanoLuc.¹¹ Fortunately, the low activity issue may be solved by directed evolution of luciferase to further enhance the enzymatic turnover.

Recently available fluorescent/bioluminescent reporters and their derived biosensors have allowed the visualization and probing of specific biological events, e.g. enzyme activity, metabolism, communication, and signaling.¹² To date, bioluminescence resonance energy transfer (BRET) biosensors are not as popular as many biosensors in the field of cellular imaging that have been developed by the principle of fluorescence resonance energy transfer (FRET),¹³ because luciferase generates lower photon flux, which is usually below the detection limit of common detectors at single-cell resolution. However, newly developed bioluminescence

systems are significantly brighter along with more advanced photon detection techniques,¹⁴ showing promising power for single-cell level BRET imaging. With our current effort on the development of ATP-independent bioluminescence reporters, it is expectable that more genetically encodable biosensors with molecular precision will be developed and will soon become available to facilitate further biological discoveries.

By the assist from modern gene-editing techniques, the applications of genetically encoded bioluminescent reporters and biosensors will be quickly expanded in terms of the development of bioluminescent cell lines and transgenic animals to advance the next-generation biomedical revolution. Moreover, we envision the possible elucidation of luciferin biosynthetic pathway. With the growing tools in the field of synthetic biology, it is expectable to see the development of a self-illuminated bioluminescence system other than bacterial bioluminescence in the foreseeable future.¹⁵ By then, engineered bioluminescence toolkits could even play more important roles not only in both preclinical and clinical fields,¹⁶ but also could be a clean light source toward a future powered by bioluminescence.

References

1. Yeh, H. W.; Wu, T.; Chen, M.; Ai, H. W., Identification of Factors Complicating Bioluminescence Imaging. *Biochemistry*, **2019**, *58* (12), 1689-1697.
2. Yeh, H. W.; Karmach, O.; Ji, A.; Carter, D.; Martins-Green, M. M.; Ai, H. W., Red-shifted luciferase-luciferin pairs for enhanced bioluminescence imaging. *Nat Methods* **2017**, *14* (10), 971-974.
3. Iwano, S.; Sugiyama, M.; Hama, H.; Watakabe, A.; Hasegawa, N.; Kuchimaru, T.; Tanaka, K. Z.; Takahashi, M.; Ishida, Y.; Hata, J.; Shimozono, S.; Namiki, K.; Fukano, T.; Kiyama, M.; Okano, H.; Kizaka-Kondoh, S.; McHugh, T. J.; Yamamori, T.; Hioki, H.; Maki, S.; Miyawaki, A., Single-cell bioluminescence imaging of deep tissue in freely moving animals. *Science* **2018**, *359* (6378), 935-939.
4. Yeh, H.-W.; Xiong, Y.; Wu, T.; Chen, M.; Ji, A.; Li, X.; Ai, H.-w., ATP-independent bioluminescent reporter variants to improve in vivo imaging. *ACS Chem Biol* **2019**. DOI: 10.1021/acscchembio.9b00150
5. Claes, F.; Vodnala, S. K.; van Reet, N.; Boucher, N.; Lunden-Miguel, H.; Baltz, T.; Goddeeris, B. M.; Buscher, P.; Rottenberg, M. E., Bioluminescent Imaging of Trypanosoma brucei Shows Preferential Testis Dissemination Which May Hamper Drug Efficacy in Sleeping Sickness. *Plos Neglect Trop D* **2009**, *3* (7).
6. Zhao, H.; Doyle, T. C.; Wong, R. J.; Cao, Y.; Stevenson, D. K.; Pivnicka-Worms, D.; Contag, C. H., Characterization of coelenterazine analogs for measurements of Renilla luciferase activity in live cells and living animals. *Mol Imaging* **2004**, *3* (1), 43-54.
7. Inouye, S.; Sahara-Miura, Y.; Sato, J.; Imori, R.; Yoshida, S.; Hosoya, T., Expression, purification and luminescence properties of coelenterazine-utilizing luciferases from Renilla, Oplophorus and Gaussia: comparison of substrate specificity for C2-modified coelenterazines. *Protein Expr Purif* **2013**, *88* (1), 150-156.
8. da Silva, L. P.; Magalhaes, C. M.; Crista, D. M. A.; da Silva, J. C. G. E., Theoretical modulation of singlet/triplet chemiexcitation of chemiluminescent imidazopyrazinone dioxetanone via C-8-substitution. *Photoch Photobio Sci* **2017**, *16* (6), 897-907.
9. Ding, B. W.; Liu, Y. J., Bioluminescence of Firefly Squid via Mechanism of Single Electron-Transfer Oxygenation and Charge-Transfer-Induced Luminescence. *Journal of the American Chemical Society* **2017**, *139* (3), 1106-1119.
10. Gao, M.; Liu, Y. J., Photoluminescence Rainbow From Coelenteramide - A Theoretical Study. *Photochem Photobiol* **2018**, *95* (2), 563-571.
11. Shakhmin, A.; Hall, M. P.; Machleidt, T.; Walker, J. R.; Wood, K. V.; Kirkland, T. A., Coelenterazine analogues emit red-shifted bioluminescence with NanoLuc. *Org Biomol Chem* **2017**, *15* (40), 8559-8567.
12. Greenwald, E. C.; Mehta, S.; Zhang, J., Genetically Encoded Fluorescent Biosensors Illuminate the Spatiotemporal Regulation of Signaling Networks. *Chemical reviews* **2018**, *118* (24), 11707-11794.
13. Chen, Z.; Truong, T. M.; Ai, H. W., Illuminating Brain Activities with Fluorescent Protein-Based Biosensors. *Chemosensors (Basel)* **2017**, *5* (4), 32.
14. Hattori, M.; Kawamura, G.; Kojima, R.; Kamiya, M.; Urano, Y.; Ozawa, T., Confocal Bioluminescence Imaging for Living Tissues with a Caged Substrate of Luciferin. *Anal Chem* **2016**, *88* (12), 6231-6238.
15. Kotlobay, A. A.; Sarkisyan, K. S.; Mokrushina, Y. A.; Marcet-Houben, M.; Serebrovskaya, E. O.; Markina, N. M.; Gonzalez Somermeyer, L.; Gorokhovatsky, A. Y.; Vvedensky, A.; Purtov, K. V.; Petushkov, V. N.; Rodionova, N. S.; Chepurnyh, T. V.; Fakhranurova, L. I.; Guglya, E. B.; Ziganshin, R.; Tsarkova, A. S.; Kaskova, Z. M.; Shender, V.; Abakumov, M.; Abakumova, T. O.; Povolotskaya, I. S.; Eroshkin, F. M.; Zaraisky, A. G.; Mishin, A. S.; Dolgov, S. V.; Mitiouchkina, T. Y.; Kopantzev, E. P.; Waldenmaier, H. E.; Oliveira, A. G.; Oba, Y.; Barsova, E.; Bogdanova, E. A.; Gabaldon, T.; Stevani, C. V.; Lukyanov, S.; Smirnov, I. V.; Gitelson, J. I.; Kondrashov, F. A.; Yampolsky, I. V., Genetically encodable bioluminescent system from fungi. *Proceedings of the National Academy of Sciences of the United States of America* **2018**, *115* (50), 12728-12732.
16. Yu, Q. Y.; Xue, L.; Hiblot, J.; Griss, R.; Fabritz, S.; Roux, C.; Binz, P. A.; Haas, D.; Okun, J. G.; Johnsson, K., Semisynthetic sensor proteins enable metabolic assays at the point of care. *Science* **2018**, *361* (6407), 1122-1125.